

# FINAL REPORT

## A Systems Approach to High Performance Buildings: A Computational Systems Engineering R&D Program to Increase DoD Energy Efficiency

SERDP Project EW-1709

FEBRUARY 2012

Satish Narayanan  
Niranjan Desai  
Slaven Peles  
Russell Taylor  
**United Technologies Research Center**

Sunil Ahuja  
Zheng O'Neill  
Amit Surana  
Shui Yuan

Bryan Eisenhower  
Igor Mezić  
Vladimir Fonoberov  
**AimDyn, Inc.**

Kevin Otto  
**Researchers Organization**

Eugene Cliff  
John Burns  
Jeff Borggaard  
**Virginia Tech**

Angela Lewis  
Paul Ehrlich  
Jeff Seewald  
**Building Intelligence Group LLC**

*This document has been cleared for public release*



This report was prepared under contract to the Department of Defense Strategic Environmental Research and Development Program (SERDP). The publication of this report does not indicate endorsement by the Department of Defense, nor should the contents be construed as reflecting the official policy or position of the Department of Defense. Reference herein to any specific commercial product, process, or service by trade name, trademark, manufacturer, or otherwise, does not necessarily constitute or imply its endorsement, recommendation, or favoring by the Department of Defense.

<b>REPORT DOCUMENTATION PAGE</b>				<i>Form Approved</i> <i>OMB No. 0704-0188</i>	
The public reporting burden for this collection of information is estimated to average 1 hour per response, including the time for reviewing instructions, searching existing data sources, gathering and maintaining the data needed, and completing and reviewing the collection of information. Send comments regarding this burden estimate or any other aspect of this collection of information, including suggestions for reducing the burden, to the Department of Defense, Executive Services and Communications Directorate (0704-0188). Respondents should be aware that notwithstanding any other provision of law, no person shall be subject to any penalty for failing to comply with a collection of information if it does not display a currently valid OMB control number.					
<b>PLEASE DO NOT RETURN YOUR FORM TO THE ABOVE ORGANIZATION.</b>					
<b>1. REPORT DATE (DD-MM-YYYY)</b> 02/29/2012		<b>2. REPORT TYPE</b> Final Report		<b>3. DATES COVERED (From - To)</b> Sep. 2009-Feb. 2012	
<b>4. TITLE AND SUBTITLE</b> A Systems Approach to High Performance Buildings: A Computational Systems Engineering R&D Program to Increase DoD Energy Efficiency				<b>5a. CONTRACT NUMBER</b> W912HQ-09-C-0054	
				<b>5b. GRANT NUMBER</b>	
				<b>5c. PROGRAM ELEMENT NUMBER</b>	
<b>6. AUTHOR(S)</b> Narayanan, S., Ahuja, S., Desai, N., O'Neill, Z.O., Peles, S., Surana, A., Taylor, R.D., Yuan, S., Eisenhower, B., Fonoberov, V., Mezic, I., Otto, K., Cliff, E., Borgaard, J., Burns, J.A., Lewis, A., Seewald, J., and Ehrlich, P.				<b>5d. PROJECT NUMBER</b> EW-1709	
				<b>5e. TASK NUMBER</b>	
				<b>5f. WORK UNIT NUMBER</b>	
<b>7. PERFORMING ORGANIZATION NAME(S) AND ADDRESS(ES)</b> United Technologies Research Center 411 Silver Lane East Hartford, CT 06108				<b>8. PERFORMING ORGANIZATION REPORT NUMBER</b>	
<b>9. SPONSORING/MONITORING AGENCY NAME(S) AND ADDRESS(ES)</b> SERDP/ESTCP Office 901 North Stuart Street, Suite 303 Arlington, VA 22203				<b>10. SPONSOR/MONITOR'S ACRONYM(S)</b> SERDP/ESTCP	
				<b>11. SPONSOR/MONITOR'S REPORT NUMBER(S)</b>	
<b>12. DISTRIBUTION/AVAILABILITY STATEMENT</b>					
<b>13. SUPPLEMENTARY NOTES</b>					
<b>14. ABSTRACT</b> Retrofitting the existing building stock represents the largest and fastest way to reduce energy consumption for the DoD. However the current retrofit delivery process is manually intensive and expensive, focused on equipment selection for initial cost and not energy performance, and the design tools are not amenable to systems solutions that have the potential for substantially reducing energy consumption in buildings. Systems methodology and tools are necessary to deliver deep retrofits, i.e. significantly higher energy performance in existing buildings than is achievable by the current retrofit process. The report describes newly developed screening methodology and tools for early assessment of deep retrofit potential across the entire DoD stock of 250,000 buildings, use of sensitivity and uncertainty analysis tools to isolate critical design parameters and establish performance bounds during design, and reduced-order modeling tools for highly energy efficient building system control design. Validated tools were developed, and retrofit system options that can reduce energy consumption by 30-50% have been identified with existing DoD building use cases.					
<b>15. SUBJECT TERMS</b> Existing buildings, Deep retrofits, Energy efficiency, Systems solutions and integration, Uncertainty analysis, Dynamic and reduced-order modeling, Robust design and failure mechanisms					
<b>16. SECURITY CLASSIFICATION OF:</b>			<b>17. LIMITATION OF ABSTRACT</b> SAR	<b>18. NUMBER OF PAGES</b> 191	<b>19a. NAME OF RESPONSIBLE PERSON</b> Satish Narayanan
<b>a. REPORT</b> U	<b>b. ABSTRACT</b> U	<b>c. THIS PAGE</b> U			<b>19b. TELEPHONE NUMBER (Include area code)</b> (860)610-7412

Reset

## Table of Contents

1.	Abstract.....	20
2.	Background, Objectives and Overall Approach .....	20
3.	Detailed Technical Approach, Results and Discussion .....	22
3.1	DoD Building Stock Modeling and Low Energy Use Retrofit Screening .....	22
3.1.1	Objectives and Background .....	22
3.1.2	Problem Formulation.....	24
3.1.3	DoD Case Studies Results and Discussion.....	29
3.1.4	Summary and Recommendations.....	48
3.2	DoD Building Audit and Energy Efficient Retrofit Measure Identification.....	49
3.2.1	Overview .....	49
3.2.2	Process.....	49
3.2.3	Case Studies .....	51
3.2.4	Overall Results and Conclusions.....	57
3.2.5	Common Observations and Challenges .....	57
3.2.6	Lessons Learned.....	58
3.3	Whole Building Energy Performance Simulation.....	58
3.3.1	Modeling Procedure .....	59
3.3.2	DoD Case Studies: Results and Discussion .....	60
3.3.3	Modelica-Based Building Energy Simulation and Dynamic Modeling Assessment .....	66
3.4	Uncertainty and Sensitivity Decomposition of Building Energy Models.....	71
3.4.1	Objective .....	71
3.4.2	Introduction and Background.....	71
3.4.3	DoD Case Studies.....	74
3.4.4	Discussion .....	89
3.5	Model-Based Failure Modes and Effects Analysis for Robust Building Design.....	90
3.5.1	Introduction and Background.....	90
3.5.2	Technical Approach .....	91
3.5.3	DoD Case Studies.....	99
	DoD/Ft. Carson Building 1225: Standard Configuration- Critical Failure Modes .....	99
	DoD/Ft. Carson Building 1225: Advanced Design - Critical Failure Modes .....	103
3.5.4	Summary .....	107
3.6	Reduced-Order Modeling and Control Design for Low Energy Building Ventilation and Space Conditioning Systems .....	107
3.6.1	Current Practices in Modeling Building Indoor Environment .....	108



3.6.2 Model Reduction .....	108
3.6.3 Section Outline.....	109
3.6.4 Problem Statement and Formulation .....	110
3.6.5 DoD Case Study: Atlantic Fleet Drill Hall.....	111
3.6.6 Summary and Next Steps .....	134
<b>4. References.....</b>	<b>134</b>
APPENDIX A.....	141
Building Load and Energy Performance Model.....	141
HVAC and Central Plant Model and Assumptions .....	142
Low Energy Design Principles and Models .....	143
Comparison of Stock Tool Calculation Results with Reported CBECS Data .....	145
APPENDIX B: Whole Building Energy Performance Simulations .....	155
Whole Building Simulation Tool Selection .....	155
Whole Building Simulation Tool Assessment .....	158
APPENDIX C: Uncertainty and Sensitivity Decomposition of Building Energy Models .....	162
APPENDIX D: Reduced-Order Modeling and Control Design for Low Energy Building Systems ....	172
D.1 Model Reduction Techniques.....	172
D.1.1 Eigensystem Realization Algorithm (ERA) .....	172
D.1.2 Proper Orthogonal Decomposition (POD) .....	173
D.2 Control Design .....	174
D.3 Case Study 1: DOE Benchmark Building Model.....	176
D.4 Case Study 2: Room with Displacement Ventilation and Chilled Ceiling .....	179
D.4.3 Reduced Order Modeling .....	181
D.4.4 Controller Design and Performance .....	186
APPENDIX E: List of Scientific/Technical Publications Resulting From Project.....	190

## **List of Tables**

Table 3.1.1: Energy Efficient Design Principles.

Table 3.1.2: Packages with increasing cost and complexity.

Table 3.1.3: DOD real property database attributes.

Table 3.1.4: Comparison of estimated DOD total and average EUI with that reported across all of DoD stock.

Table 3.1.5: Usage and Climate categories for clustering.

Table 3.1.6: Clustering based on usage and climate zones (Number of Buildings).

Table 3.1.7: Energy Use Intensity (EUI) of Median Building (KBTU/ft<sup>2</sup>).

Table 3.1.8: Extrapolation of energy savings for DOD stock based on savings for median EUI buildings.

Table 3.1.9: Comparison of Stock Tool savings with EnergyPlus results.

Table 3.1.10: Comparison of energy savings broken by end use type based on Stock tool and TRNSYS model.

Table 3.2.1: Energy and engineering audit/study process.

Table 3.2.2: Key tasks and work content.

Table 3.2.3: Buildings overview.

Table 3.2.4: Building systems.

Table 3.2.5: Potential energy conservation measures by building.

Table 3.2.6: Summary of projected improvement by building.

Table 3.3.1 2 Modeled Buildings in DoD bases.

Table 3.3.2 Comparisons of building systems between baseline and advanced EnergyPlus model for Building 26.

Table 3.3.3 3 Energy consumption comparisons between baseline and advanced EnergyPlus model for Building 26.

Table 3.4.1. Analysis performed on different energy models (baseline is the actual building, energy efficient retrofit design with high performance attributes). Abbreviations are described in the bulleted list above.

Table 3.4.2. Parameter group types.

Table 3.4.3 Variables for the nodes of the sensitivity decomposition of Facility Electricity (Figure 8).

Table 3.4.4 The twenty most influential parameters on both comfort and energy consumption.

Table 3.5.1 Probability of Occurrence for Various FMEA Occurrence Ratings.

Table 3.5.2 Baseline Energy Intensity for Building 1225 (kBtu/ft<sup>2</sup>/yr).

Table 3.5.3 Distribution of Failure Modes.

Table 3.5.4 Baseline Energy Intensity for Building 1225 (kWhr/m<sup>2</sup>/yr).

Table 3.6.1: Boundary conditions used in the model of airflow in the drill-deck, for the baseline case served by overhead diffusers. The temperature values are shown for both heating and cooling operations.

Table 3.6.2: Estimated of energy savings in different HVAC components, over with a baseline system modeled in EnergyPlus, for a period of 3 months (June-August).

Table 3.6.3: Boundary conditions for the drill-deck retrofitted with radiant heated floor and DV.

Table 3.6.4: Estimated of energy savings in different HVAC components, over with a baseline system modeled in EnergyPlus, for a period of 2 months (January and February).

Table 3.6.5: Boundary conditions for the conference room; cooling mode operation.

Table 3.6.6: Input-output decomposition.

Table 3.6.7: Boundary conditions for the conference room, for a heating-mode operation.

Table A.1: Efficient system lighting power density for various building types (ASHRAE recommended).

Table A.2: Lighting and Equipment Retrofits.

Table A.3: Envelope Related Retrofits.

Table A.4: Temperature setpoints and setbacks used in energy efficient strategy implementation.

Table A.5: HVAC Terminal Side Retrofits.

Table A.6: HVAC Supply Side Retrofits.

Table B. 1 Electricity End Use Breakdown.

Table C. 1. Electricity usage comparison, nominal versus high performance model.

Table C.2 Parameter group types.

Table C.3 Consumption outputs chosen for the analysis.

Table D.1: Boundary conditions for one room in the DOE medium-office building approximated using inputs from EnergyPlus simulations.

## List of Figures

Figure 2.1 Illustration of methodology for rapid energy efficient retrofit selection and design.

Figure 3.1.1 Typical facility retrofit procedure and key steps.

Figure 3.1.2 Overall DoD stock modeling approach.

Figure 3.1.3 HVAC and Central plant model in Stock Tool.

Figure 3.1.4: Sensitivity Analysis approach in the Stock Tool.

Figure 3.1.5 DOD Site energy (Btu Billions) based on building usage. Here Healthcare includes outpatient and inpatient services, and Pub/POS/RelW stands for Public Assembly, Public Order and Safety, and Religious Worship.

Figure 3.1.6 EUI distribution for top three DOD usage sectors. The red triangle indicates median EUI for each sector.

Figure 3.1.7 % Site Energy Savings due to few selected ECMs for the median DoD building for each climate zone and building use category.

Figure 3.1.8 % Site Energy Savings due to few selected ECMs for the median DoD buildings for each climate zone and building use category.

Figure 3.1.9 % Site Energy Savings from different package applications for the median DoD buildings for each climate zone and building use category.

Figure 3.1.10 % Source Energy Savings from different package applications for the median DoD buildings for each climate zone and building use category.

Figure 3.1.11: Comparison of EUI for different DOD facilities.

Figure 3.1.12: Site energy savings for different ECM's. ECMs marked with red circles are used to assemble a package.

Figure 3.1.13: On left is shown site energy savings from assembled package broken by end use type. On right are shown results of UQ/SA for the building with the baseline and packaged system.

Figure 3.1.14: Site energy savings for different ECM's. ECMs marked with red circles are used to assemble a package.

Figure 3.1.15: On left is shown site energy savings from assembled package broken by end use type. On right are shown results of UQ/SA for the building with the baseline and packaged system.

Figure 3.1.16: Site energy savings for different ECM's. ECMs marked with red circles are used to assemble a package.

Figure 3.1.17: On left is shown site energy savings from assembled package broken by end use type. On right are shown results of UQ/SA for the building with the baseline and packaged system.

Figure 3.1.18: On left is EUI distribution in the cluster (Office-,) to which Fort Carson belongs. On right is the distribution of site energy savings resulting from packaged system chosen for the Ft. Carson building.

Figure 3.1.19: Site energy savings for different ECM's. ECMs marked with red circles are used to assemble a package.

Figure 3.1.20: On left is shown site energy savings from assembled package broken by end use type. On right are shown results of UQ/SA for the building with the baseline and packaged system.

Figure 3.1.21: Site energy savings for different ECM's. ECMs marked with red circles are used to assemble a package.

Figure 3.1.22: On left is shown site energy savings from assembled package broken by end use type. On right are shown results of UQ/SA for the building with the baseline and packaged system.

Figure 3.1.23: Site energy savings for different ECM's. ECMs marked with red circles are used to assemble a package.

Figure 3.1.24: On left is shown site energy savings from assembled package broken by end use type. On right are shown results of UQ/SA for the building with the baseline and packaged system.

Figure 3.1.25: Summary of accomplishments in this program and proposal for enhancements in next phase.

Figure 3.2.1 EUI improvements projected by the energy engineering studies.

Figure 3.3.1 Schematics for Modeling Evaluation.

Figure 3.3.2 Drill Hall building at the Navy Station Great Lakes.

Figure 3.3.3 Comparisons of 2009 utility bill and energy prediction with EnergyPlus model in Drill Hall.

Figure 3.3.4 Building 26 outlook.

Figure 3.3.5 Comparisons of 2010 utility electricity bill and predictions with EnergyPlus model in Building 26.

Figure 3.3.6 BLDG 26 high efficient system concepts chosen by stock analysis tool.

Figure 3.3.7 Building 1225 in Ft. Carson.

Figure 3.3.8 TRNSYS baseline model of Building 1225.

Figure 3.3.9 A diagram of the advanced system.

Figure 3.3.10: Simulation results for temperatures in zones 1-6 as obtained from Matlab R-C model and Dymola/Buildings Library.

Figure 3.3.11: Dymola model of the office space on the second floor of Great Lakes Drill Hall Building.

Figure 3.3.12 Temperatures in Zones 1, 4 and 5 and heat demand for Air Handling Unit 3 as simulated by EnergyPlus and Dymola/Buildings Library.

Figure 3.4.1 Schematic of the different analysis techniques that are performed on the building energy models.

Figure 3.4.2 Convergence properties of the 10 outputs. The mean and standard deviation, with respect to the value after 5000 simulations is presented for both peak usage and annual consumption.

Figure 3.4.3 Uncertainty in 10 energy consumption variables when varying input parameters by 10% or 20%.

Figure 3.4.4 Example distributions for cooling(top) and heating (bottom) when varying the input parameters by either 10% or 20%. The black dot is the nominal simulation results.

Figure 3.4.5 Sensitivity indices for two facility consumption variables.

Figure 3.4.6 Sensitivity decomposition of electricity consumed by the facility (sum over summer months). Labels on the vertical axis describe the nodes of the 4<sup>th</sup> level, while the other node/levels of this plot are tabulated in Table 7.

Figure 3.4.7 Sensitivity indices for both PMV and total facility energy for the 1009 uncertain parameters. Some of the parameter classes are grouped by color in this figure.

Figure 3.4.8 Optimization results for energy consumption using the 8 meta-models, and one case using the EnergyPlus model. Each data point in this figure for the meta-model optimization was generated by inserting the optimal parameter values into EnergyPlus and simulated.

Figure 3.4.9 Optimization results for thermal comfort using the 8 meta-models, and one case using the EnergyPlus model. Each data point in this figure for the meta-model optimization was generated by inserting the optimal parameter values into EnergyPlus and simulated.

Figure 3.4.10 Uncertainty ranges for the baseline Fort Carson design and a re-design with high performance features.

Figure 3.4.11 Results of sensitivity analysis for the Fort Carson building 1225 (baseline and advanced building designs).

Figure 3.4.12 Uncertainty in energy consumption for the total facility (left) and only electricity (right) for the DoD Building 26.

Figure 3.4.13 Critical parameter results for Building 26.

Figure 3.4.14. Raw sensor data taken from 2010 used for calibration of the EnergyPlus Model.

Figure 3.4.15 Calibration results for Building 26.

Figure 3.4.16 Verification results for Building 26.

Figure 3.5.1 Overall process flow for analyzing effects of failure modes on building energy.

Figure 3.5.2 Block Diagram of a constant volume air handling unit.

Figure 3.5.3 FMEA worksheet.

Figure 3.5.4 Example map types of failure mode to building energy simulation inputs.

Figure 3.5.5: Failure Mode Participation Probability Density Function.

Figure 3.5.6 Distribution of Overall Building Energy Consumption over the Failure Modes.

Figure 3.5.7 Distribution of Subsystem Building Energy Consumption over the Failure Modes.

Figure 3.5.8 Sensitivity of Overall Building Energy Consumption to the top 10 contributing Failure Modes.

Figure 3.5.9 Sensitivity of Subsystem Building Energy Consumption to the top 20 contributing Failure Modes.



Figure 3.5.10 Distribution of Overall Building Energy Consumption over the Failure Modes.

Figure 3.5.11 Distribution of Subsystem Building Energy Consumption over the Failure Modes.

Figure 3.5.12 Sensitivity of Overall Building Energy Consumption to the top 10 contributing Failure Modes.

Figure 3.5.13 Sensitivity of Subsystem Building Energy Consumption to the top 10 contributing Failure Modes.

Figure 3.6.1: Schematic of model-based feedback-control, for rejecting disturbances solar radiation and occupant loads. The control goal is to maintain the comfort measure within specified limits, while minimizing energy consumption.

Figure 3.6.2: Plan view of the first floor Atlantic Fleet Drill Hall, showing the drill-deck and the conference room, which are the DoD cases undertaken for developing models of airflow and control design.

Figure 3.6.3: Model of the drill-hall, with dimensions, boundary conditions, and a resultant thermo-fluid field. The vertical slices show temperature contours for a summer case, depicting uniform temperature up to the diffuser locations. Also shown are z-velocity iso-surfaces (in blue), to point out the supply diffuser locations. The figure on the right shows an interior view of the drill-deck, which is a large open space in the building.

Figure 3.6.4: Grid G3 (fine) at the central cross-section of the drill-hall. The maximum grid-spacing in the x, y and z directions are 0.2m, 0.2m and 0.1m. The number of grid-points is 1,284,072.

Figure 3.6.5: Logger horizontal locations, marked in plan view (center) and the vertical locations, marked with yellow circles. Also shown is the location of diffusers as modeled in CFD simulations.

Figure 3.6.6: Measurement data, shown for May 15.

Figure 3.6.7: (Left) Temperature contours along vertical slices and iso-surfaces of the z-component of the velocity field, for a winter simulation, depicting an adverse stratification with colder temperature near the floor. (Right) Stratification during heating, computed using G3. Measurement data is shown in circles.

Figure 3.6.8: Retrofits using displacement vents, running along the length of the drill-deck. Six equi-spaced vents, of dimension 1m x 1.25m, are provided along the walls perpendicular to the x-axis. The figure also illustrates the volumes used to define occupant comfort. Finally, the slices of temperature contours at a steady state along two vertical planes illustrate significant temperature stratification along the height.

Figure 3.6.9: (Left) Floor-plan of the building, illustrating the two occupied zones (blue rectangles, north and south) used to define a comfort metric, and the two controls  $u_1$  and  $u_2$ , each representing either the supply flow rate or supply air humidity to a set of six diffusers (arrows, north and south). (Right) Model of the disturbance due to solar radiation or occupants flux; both are modeled as heat-fluxes through the floor, with contours shown in the top figure.

Figure 3.6.10: Outputs of the system to step changes in the supply velocity (left) and supply air humidity (right). The curves show the filtered CFD responses (blue) and a 50-mode ERA model prediction (red, dashed lines). The inputs are stepped from their baseline values over 15 minutes, starting at  $t=0$ .

Figure 3.6.11: The response of the system to a step change in occupants from 0 to 100 in the southern zone (left); each occupant is assumed contribute 100W of sensible load and 200W of latent load. The latent load is modeled as a vapor source, uniformly distributed over the occupied volume.

Figure 3.6.12: Realistic disturbances from solar radiation and occupants, shown in the left plot. The right plot shows the system responses, with and without control.

Figure 3.6.13(a): (Left) Zone temperatures in the systems served by overhead diffusers (black) and displacement ventilation (red). (Right) Mass flow rate of air supplied by the two systems; in both cases, the minimum flow is constrained by the same outdoor air (ventilation) requirement.

Figure 3.6.13(b): Whole building energy consumption. (Left) Energy consumption by components, obtained from a model calibrated against measurement data. (Right) Energy consumed by fans, obtained from measurements during a week in May. The drill-deck is served by AHU 1 and 2, which consume more than 90% of the total fan energy.

Figure 3.6.14: Comparison of the proposed LQR control design vs. the currently practiced PI control design. Shown is the time-integral of the square error (deviation from the set-point) vs. that of cost. Each point in the plot is obtained from a 6-hour simulation using the same disturbance profile, but with different control gains. For a given error (say,  $\text{error}=0.2$ ), the PI controller shows a wider variation in the potential cost as compared to LQR.

Figure 3.6.15: Temperature contours at a steady state, in the drill-deck retrofitted for a heating mode operation. The contours are shown along two vertical planes, and illustrate that air is well-mixed in the zone for the heating operation, and the velocity contours indicate a Rayleigh-Benard like airflow pattern.

Figure 3.6.16: Outputs of the system to step changes in the floor-flux (left) and ambient air temperature (right). The curves show the filtered CFD responses (blue) and a 50-mode ERA model prediction (red, dashed lines). The inputs are stepped from their baseline values over 15 minutes, starting at  $t=0$ .

Figure 3.6.17: Realistic disturbances from changes in the ambient air temperature and occupancy, shown in the left plot. The right plot shows the system responses, with and without control.

Figure 3.6.18: (Left) Zone temperatures in the systems heated using overhead diffusers (black) and using radiant floors (red). (Right) Mass flow rate of air supplied by the two systems; in both cases, the minimum flow is constrained by the same minimum ventilation requirement; the low-energy system has considerably lower supply air flow rate, due to primary heating by the radiant floors.

Figure 3.6.19: Conference Room Geometry, illustrating the boundary conditions. On the right is shown an initial transient response of the volume-averaged and exhaust temperature, starting from a uniform initial condition. The flow evolved to a “steady” state, with minimal fluctuations on temperature or velocity fields.

Figure 3.6.20: Responses of the system to a step change in the supply velocity. Both the temperature and humidity drop with increasing supply; an 88-mode model accurately predicts the response of the full system.

Figure 3.6.21: Responses to a step in the disturbance inputs; plots similar to those shown in Figure 3.6.20.

Figure 3.6.22: Simulink diagram of the closed-loop conference room cooling.

Figure 3.6.23(a): Controlled temperature and humidity responses.

Figure 3.6.23(b): Control inputs, for two different choices of gain, chosen such that the weights on the temperature and humidity control are 8-times larger (blue) or 8-times smaller (red) than that on the velocity input.

Figure 3.6.24: Startup temperature transients (left) and steady h2o field (right).

Figure 3.6.25: Response of the volume-averaged temperature to a step in the floor flux (left) and window temperature (right).

Figure 3.6.22: Simulink diagram of the closed-loop conference room cooling.

Figure 3.6.23(a): Controlled temperature and humidity responses.

Figure 3.6.23(b): Control inputs, for two different choices of gain, chosen such that the weights on the temperature and humidity control are 8-times larger (blue) or 8-times smaller (red) than that on the velocity input.

Figure 3.6.24: Startup temperature transients (left) and steady h2o field (right).

Figure 3.6.25: Response of the volume-averaged temperature to a step in the floor flux (left) and window temperature (right).

Figure A.1 Air and water loop schematic for the building, HVAC air and central plant model.

Figure A.2 Window selection based on CBECS climate zone.

Figure A.3: CBECS total site reported energy use and component fractional use.

Figure A.4: Stock tool total site reported energy use and component fractional use.

Figure A.5: Comparison of reported and stock tool energy use.

Figure A.6: Differences in stock tool calculated and CBECS reported energy use for CBECS building stock.

Figure A.7: Reported vs. computed electricity EUI for buildings in the CBECS database.

Figure A.8: Reported vs. computed EUI for buildings in the CBECS database.

Figure A.9: Normalized standard deviation of CBECS reported total energy consumption values.

Figure A.10: Distribution of error in total energy consumption between reported and calculated values.

Figure A.11: Distribution of error in non-heating/cooling energy consumption between reported and calculated values.

Figure A.12: Distribution of error in cooling energy consumption between reported and calculated values.

Figure A.13: Distribution of error in heating energy consumption between reported and calculated values.

Figure B.1 Rendered Geometry for DOE Medium Office Building.

Figure B.2 Schematic Ductwork and Controls for Air Loop in DOE Medium Office Building.

Figure B.3 Schematic Ductwork and Controls for Water Loop in DOE Medium Office Building.

Figure B. 4 HVAC System Schematic Diagram for High Performance Building.

Figure B.5 Schematic Ductwork and Controls for Air Loop in High Performance Building.

Figure B.6 Energy Consumption Comparisons between DOE Baseline Case and High Performance Case.

Figure B.7 Electricity End Use Breakdown Comparisons.

Figure C.1 Standard deviation for the seven outputs of the two models (nominal model and high performance design).

Figure C.2 Coefficient of variation for the seven outputs of the two models (nominal model and high performance design).

Figure C.3 Example histograms of the two main facility wide outputs.

Figure C.4 Aggregated influence coefficients for yearly peak energy consumption (nominal and high performance models).

Figure C.5 Aggregated influence coefficients for yearly sum energy consumption (nominal and high performance models).

Figure C.6 Sum of the total influence coefficients for peak consumption in the TRNSYS model.

Figure C.7 Sum of the influence coefficients for annual consumption in the TRNSYS model.

Figure D.1: (a,b) Sensed temperatures: T1, Tmid, (c) Control flux and (d) Tcore.

Figure D.2: DOE Energyplus benchmark model: (a) 3-D geometry (b) Plan/top view. (c) Solar heat flux (in  $\text{W/m}^2$ ) transmitted through the window facing West, for one design day in summer.

Figure D.3: Schematic of a chilled beam (left). Model used in CFD (right), showing supply ducts and a return duct, which models the airflow induced by a low-pressure region formed near the central part of the beam.

Figure D.4: Flow and temperature fields in a room equipped with active chilled beams. The plots show the temperature fields and projected streamlines at a few vertical cross-sections. The slices on the right show velocity streamlines on the central slice, perpendicular to the z-axis. The counter-rotating vortices persist in the presence of solar radiation.

Figure D.5: Flow and temperature fields in the presence of a passive radiant ceiling and displacement ventilation. The slices on the right show velocity streamlines on the central slice, perpendicular to the z-axis. The streamlines considerably drift away from the window when subject to solar radiation.

Figure D.6: Room equipped with a displacement vent, a chilled ceiling, a window and an internal load modeled as a floor-mat, with the boundary conditions as shown in the figure. The slices represent the steady-state temperature field and projected stream-lines, obtained from a FLUENT simulation. The right plot shows a slightly modified geometry used (by Virginia Tech) for developing POD/Galerkin model.

Figure D.7: (a) Hankel singular values of the system in a log-scale; these decay sharply, indicating that the system is low-dimensional. These also quantify the approximation error and provide a guideline for truncation. Response of the full system (black, solid line) and a 10-mode reduced-order model (red, dashed line, crosses) to (b)  $-10\text{W/m}^2$  step in the chilled ceiling flux (c)

40W/m<sup>2</sup> step in the floor-mat flux. Plots compare the controlled outputs  $z_k$ , that is, perturbations from the steady state temperature averaged over the occupied region  $D_o$ .

Figure D.8: Startup transient for volume-averaged temperature (left), outflow temperature (center) and the temperature field at  $t = 5400$ s (right).

Figure D.9: Volume-averaged temperature; relaxation from  $T = 28$  C (left). Reduced-order model prediction of the outflow-averaged temperature (right).

Figure D.10: Applied input fluxes at the ceiling (left), floor (center) and the window (right).

Figure D.11: Responses of the volume-averaged temperature to the inputs shown in Figure 3.62.

Figure D.12: Cumulative POD energy (left), first (center) and second (right) POD modes.

Figure D.13: Predicted outflow average temperatures, in response to the perturbed (a) ceiling (b) floor and (c) window fluxes. Initial condition used is  $T(5400, x) = T_{ss}(x)$ .

Figure D.14: Predicted outflow average temperatures, in response to the perturbed (a) ceiling (b) floor and (c) window fluxes. Initial condition used is  $T(5400; x) = T_{startup}(5400; x)$ .

Figure D.15: Schematic of controller implementation in the full simulation.

Figure D.16: (a) Disturbance input (floor heat flux, in W/m<sup>2</sup>) as a function of time, and (b) the flow-field resulting when the disturbance reaches its maximum value.

Figure D.17: (a) The controlled outputs  $z_k$  (temperature, averaged over the occupied zone), in the presence of the disturbance shown in Figure D.16a, for different control gains obtained using  $q = 5, 50$ . Also shown is the response when the control is off. The response of the full simulation (black, solid line) is compared with the observer reconstruction (red, dashed line). (b) Control inputs (chilled ceiling flux in W/m<sup>2</sup>) required to reject the disturbance, for the two control gains.

Figure D.18: (Left) Functional Gain for  $Re=4800$ ; advection field. (Right) Functional Gain for  $Re=100$ .

Figure D.19: Feedback functional gain.

## **List of Acronyms and Keywords**

AHU – Air Handling Unit

ANOVA – Analysis of Variance

ASHRAE – American Society of Heating, Refrigeration and Air-conditioning Engineers

BMS – Building Management System

BTU – British Thermal Units

CBECS – Commercial Buildings Energy Consumption Survey

CFD – Computational Fluid Dynamics

COP – Coefficient of Performance

DoD – Department of Defense

DDC – Direct Digital Control

DHW – District Hot Water

DOE – Department of Energy

DV – Displacement Ventilation

ECM - Energy Conservation Measure

ERA – Eigensystem Realization Algorithm

EUI – Energy Use Intensity

FMEA – Failure Mode Effects and Analysis

GSHP – Ground Source Heat Pump

HSV – Hankel Singular Values

IP – Interior Point

HVAC – Heating, Ventilation and Air Conditioning

LED – Light Emitting Diode



LEED – Leadership in Energy and Environmental Design

NREL – National Renewable Energy Laboratory

PMV – Perceived Mean Vote

POD – Proper Orthogonal Decomposition

RPAD – Real Property Asset Database

RTS – Radiant Time Series

SVD – Singular Value Decomposition

TMY – Typical Meteorological Year

TRNSYS – Transient System Simulation Program

UDF – User Defined Function

VAV – Variable Area Volume

VFD – Variable Frequency Drive



## Acknowledgements

The team and authors gratefully acknowledge the financial support and technical guidance provided by the SERDP/ESTCP Office under the leadership of leadership Drs. Jeff Marqusee and Jim Galvin as well as the support provided by Mr. Jonathan Thigpen (HGL) throughout the project period of performance. The team is very thankful to the support provided by various DoD installations that provided data for the project, including Mrs. Peter Behrens (Navy Great Lakes, Chicago, IL), Scott Clark (Ft. Carson, CO), Tom Santiovanni (Navy Base Ventura County, CA), Jim Peedin (Ft. Bragg), and Mark Zangara (Ft. Detrick, MD). The team is grateful for the leadership support, encouragement and guidance provided by Drs. J. Michael McQuade (Senior VP, Science & Technology, UTC) and Clas Jacobson (Chief Scientist Controls, UTC), and Mr. Craig Walker (Director, Energy Systems Program Office, UTRC) well before the initiation of the project and throughout the project performance period.

## 1. Abstract

Retrofitting the existing building stock represents the largest and fastest way to reduce energy consumption for the DoD. However the current retrofit delivery process is manually intensive and expensive, focused on equipment selection for initial cost and not energy performance, and the design tools are not amenable to systems solutions that have the potential for substantially reducing energy consumption in buildings. Systems methodology and tools are necessary to deliver deep retrofits, i.e. significantly higher energy performance in existing buildings than is achievable by the current retrofit process. The report describes newly developed screening methodology and tools for early assessment of deep retrofit potential across the entire DoD stock of 250,000 buildings, use of sensitivity and uncertainty analysis tools to isolate critical design parameters and establish performance bounds during design, and reduced-order modeling tools for highly energy efficient building system control design. Validated tools were developed, and retrofit system options that can reduce energy consumption by 30-50% have been identified with existing DoD building use cases.

## 2. Background, Objectives and Overall Approach

Retrofitting the existing building stock represents the largest and fastest way to reduce energy consumption for the Department of Defense (DoD). However, the current retrofit process is manually intensive, focused on equipment selection for initial cost and not energy performance, and not amenable to systems solutions with potential for substantially reducing energy consumption in buildings. Systems approaches have been demonstrated in a number of "one-off" new construction projects, but significant challenges exist in being able to reproduce the energy savings in a cost-effective, timely, and reliable manner, particularly for the constrained problem of retrofitting existing buildings. The systems approach is based on the observation that a building is a multi-scale, heterogeneous, complex dynamic system with considerable uncertainty. Existing modeling and simulation tools cannot accurately capture the dynamic coupling among building subsystems, especially as it relates to control, and therefore represent a barrier to robust and scalable deployment of technologies that require low levels of energy consumption.

The project objective is to develop the required systems methodology and building physics and dynamics-based analysis tool set to deliver significantly higher energy performance in existing buildings than is achievable by the current retrofit process. The methodology consists of tools for rapid survey, audit, retrofit option analysis, and selection to ensure robust design and operation of buildings. Use of this methodology and associated tools to design building systems with energy efficiency gains of 50% or more is projected to be applicable to major retrofits of medium- to large-sized buildings, representing a nominal portion of the DoD building stock. Once these designs are piloted and demonstrated at DoD sites and the process and tool set is standardized for broader dissemination, impact on the larger building stock is anticipated. A 50% reduction in energy utilization across all DoD facilities would yield \$1.75 billion in energy cost savings.

The two-year program is being executed in two phases: 1) Assessment and Classification and 2) Retrofit Design (illustrated in Figure 2.1). The assessment phase involves model and data based representations of the DoD existing building stock energy performance, classified by different building usage types and climates. This is followed by evaluation of the energy use reduction

potential of low energy design principles (e.g. insulation, daylighting and ground source heat pumps) and their combinations, resulting in system configurations for a class or cluster of buildings (i.e. representative of a particular combination of building usage type and climate). Building clusters with the largest potential for energy use reduction are then identified and full system (thermo-fluid) simulations are performed to establish baseline energy performance and to evaluate energy use reductions achievable with the best available system solutions screened in the previous step. This constitutes the second phase of the project for energy efficient retrofit design. Analytical tools for sensitivity and uncertainty analysis are used to reveal system couplings and interactions that underlie the baseline building energy performance and isolate critical failures and opportunities for the energy efficiency improvements. Reduced-order models are used to evaluate the robustness of the energy efficient system designs and for optimization. The use of reduced-order models and new analysis tools for concept synthesis enables rapid progression from a baseline building to a ranked set of retrofitable alternatives with quantified energy performance gains within known bounds of uncertainty.

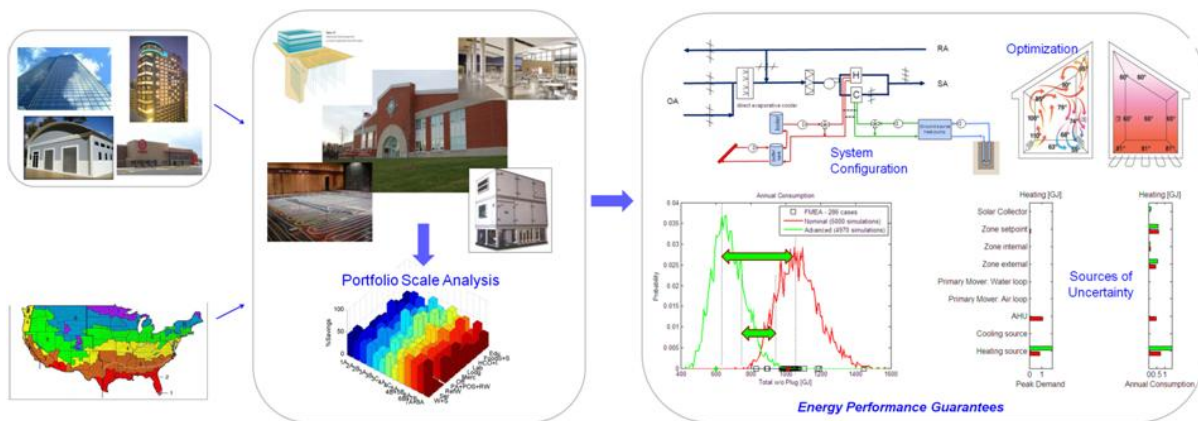


Figure 2.1 Illustration of methodology for rapid energy efficient retrofit selection and design.

For the Assessment and Classification phase, the objectives are to:

1. Evaluate existing DoD building stock surveys and provide classification by critical characteristics and associated energy efficiency design principles.
2. Gather extensive data on a few representative building types including design data, energy information, operations processes, and conduct a series of conventional energy audits and evaluations.
3. Use the collected data on the sample building types and building simulations to develop system models and tools that reveal system interactions underlying building performance problems.

For the Retrofit Design phase, the objectives are to:

1. Develop computational and analytical tools for the synthesis, design, control and optimization of dynamic building systems. This includes computational tools for sensitivity and uncertainty analysis, for model reduction of complex thermo-fluid building phenomena, and for extracting key dynamic features underlying very low energy consumption building systems;
2. Use computational tools to conduct system architecture trade studies that identify and rank design alternatives for energy efficient building retrofit solutions.

3. Develop and apply Critical Parameter Management tools (CPM) to articulate to Facility Managers how to maintain energy efficiency gains.
4. Assess building performance results against the baseline data gathered in phase I.

Details on the methodologies and tools developed and results from their application are provided in the following sections. The focus of this interim report is on: the building stock energy performance analysis and energy efficient retrofit screening tools, whole building energy performance simulation tools, sensitivity and uncertainty analysis tools, and reduced-order model-based energy efficient building control design. Results from audits the first of five DoD sites are also presented.

### **3. Detailed Technical Approach, Results and Discussion**

#### **3.1 DoD Building Stock Modeling and Low Energy Use Retrofit Screening**

##### **3.1.1 Objectives and Background**

###### **3.1.1a) Background: Building Energy Efficiency Retrofit Process**

The key steps (see Figure 3.1.1) in the current building energy efficiency retrofit, include

- 1) Facility Audit to collect building information such as:
  - Building type (climate, usage characteristics, systems...)
  - Detailed architecture & mechanical drawings
  - Available/metered utility & energy use data
  - Establish baseline performance
  - Identify constraints for implementation of energy efficiency measures
- 2) Energy Efficiency Measure Identification based on
  - Expert system-based screening and ranking of energy efficiency measures & economic analysis
  - Rough estimates of achievable performance
  - No-/low- medium- and high-cost measure ID
- 3) Retrofit System Selection and Specification for
  - Detailed sizing and cost assessment of selected energy efficiency measures
  - Refined estimates (simulation-based) of achievable performance
  - Post-retrofit measurement & verification of performance (optional)



Figure 3.1.1 Typical facility retrofit procedure and key steps.

The main limitation of the current practice are:

- Screening is limited to conservative energy efficiency measures (< 30% reduction)

- Detailed simulations are required for energy performance assessment and limited to few configurations
- Critical parameters for retrofit system concept design are not well understood prior to installation and commissioning

### 3.1.1b) Objectives

In order to rapidly explore larger design space for system solutions, and enable performance and robustness guarantees for system solution, we propose development of:

- Automated screening tools for deep energy efficient retrofit measures based on calibrated low order building models.
- Analytical toolset for design and performance verification of energy efficient solutions.

The task objective is a statistical analysis of the technical suitability and potential of DoD buildings for deep energy efficiency retrofits. The approach is outlined in Figure 3.1.2, where the current energy consumption of each building is estimated, and then the impact of individual energy conservation measures is estimated individually and in combination, for each individual building. Details will be explained in subsequent sections.

Overall, the objectives are to:

1. Assess how low the DOD stock can become through deep energy retrofits using known technology,
2. Determine which energy conservation measures offer the best potential for DOD,
3. Determine which whole-building retrofit solutions integrating the different building system's operation to provide the most synergistic energy conservation,
4. Determine standard packages of whole-building retrofit solutions for the various DOD building climactic and use categories,
5. Determine standard packages for increasing energy reduction classes for the DOD building various climactic and use categories.

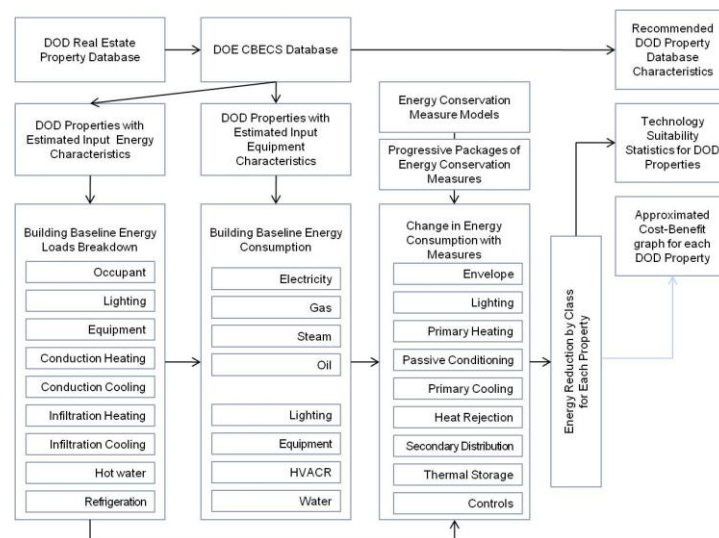


Figure 3.1.2 Overall DoD stock modeling approach.

### 3.1.2 Problem Formulation

#### 3.1.2-1 Building Data Requirements for Energy Modeling

Below is a list key building attributes which are required for energy modeling in stock tool:

- Building location
  - Geographical coordinates
  - Address
  - Time zone
  - Weather
- Building geometry
  - Floor Area, number of floors, building exterior shape and floorplan, or Exterior dimensions, overall height or floor-to-floor height, glazing fractions
- Construction materials
  - Wall and roof thermal conductance, capacitance, thickness and mass density
  - Glazing thermal conductance, solar heat gain coefficient (SHGC, spectral average) and visible transmittance
- Equipment configurations
  - HVAC system type
  - Fan and pump power
  - Primary cooling equipment type and COP
  - Primary heating equipment type and efficiency
  - Heat rejection (condenser) type and efficiency
- Peak occupancy rate and time varying schedule Fuel type use
- Peak end use loads (e.g. plug loads or type/number of equipment, lighting power density, service hot water usage, refrigeration power density) and associated time varying schedules

While several of these attributes can be determined during a Level 1 audit, other parameters can be filled from standard sources like ASHRAE Handbook, DOE Glass Library, NREL Report [Griffith et al. 2008]. For weather data we used 30 year average available in TMY3 files for 1024 weather station locations.

#### Approach to Filling Missing Information from CBECS Database

In several instances building data required for energy performance modeling (as outlined in previous section) may not be available. In order to estimate the missing building information, we use CBECS database which is relatively richer in the reported building attributes. For a given building we find a closest CBECS building match based on climate zone, usage and size. The closest match is then used to augment the building with the missing attributes. We used this procedure to fill in the missing building attributes in the DOD Real Property Database (RPAD), see section 3.1.3.

#### 3.1.2-2 Building Load and Energy Performance Model

A building load and energy performance model was created to calculate the annual energy consumption of the buildings for which attributes outlined in section 3.1.2-1 are available. The model was designed to quickly perform an 8760 hour annual load and energy calculation from this limited building attributes. The model assumptions were as follows:

- The building could be represented by a single, well mixed zone (i.e. single inside air temperature node).
- The thermal capacitance of building structure and furnishings could be represented by a single lumped mass.
- Wall surface temperatures were assumed to be uniform and therefore that heat transfer processes are 1-D.
- The combination of direct and diffuse solar radiation heat gains and convective heat gains to exterior surfaces can be represented by the interaction of the wall with an effective sol-air temperature.
- The sol-air temperature method allows wall and roof conduction processes to be modeled using the ASHRAE Radiant Time Series (RTS) method, which accounts for the thermal resistance and capacitance effects of exterior surfaces.
- The building heating/cooling load can be calculated from a quasi-steady energy balance on the zone air node as follows:

$$\begin{aligned} \dot{Q}_{LOAD} = & \dot{Q}_{People,sensible} + \dot{Q}_{Equip,sensible} + \dot{Q}_{Fenestration} \left( T_{Sol-Air}, \dot{Q}_{Solar\ Radiation}, T_{Zone} \right) \\ & + \sum_{All\ Surfaces} \dot{Q}_{Conduction} \left( T_{Sol-Air}, T_{Zone} \right) + \dot{Q}_{Infiltration} \left( T_{Outside\ Air}, T_{Zone} \right) \\ & + \dot{Q}_{Internal\ Mass} \left( T_{Zone}, T_{Internal\ Mass} \right) \end{aligned}$$

The details of how each of above term is computed are described in appendix A.2.

### 3.1.2-3 HVAC and Central Plant Model and Assumptions

HVAC system and central plant performance was calculated using hourly load data to drive the system response. In keeping with the simplicity of the load model, the air side of the primary HVAC system was modeled as a single loop serving the single building thermal zone as shown in Figure 3.1.3. In appendix A.3 we describe in detail the model of each component in the loop.

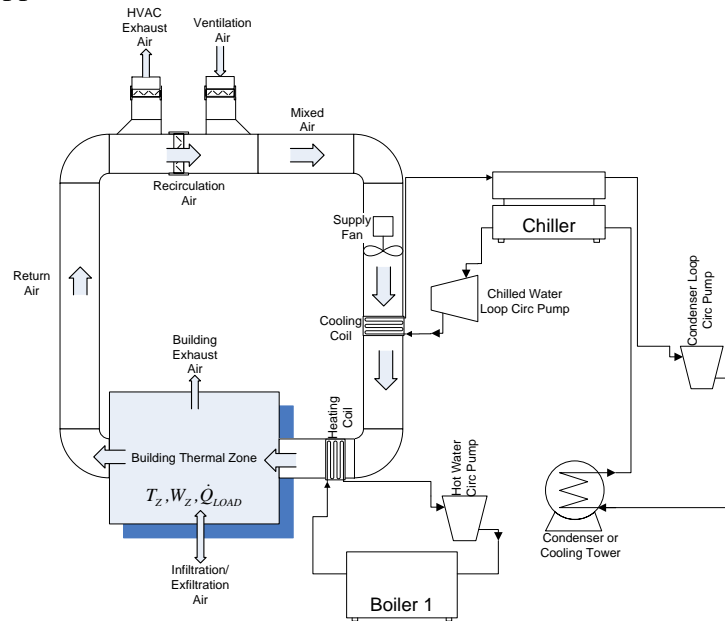


Figure 3.1.3 HVAC and Central plant model in Stock Tool



### 3.1.2-4 Energy Conservation Measures, Models and Packages

In this section we list various low energy design principles, or energy conservation measures (ECMs) which have been modeled in the Stock Tool. These measures have been categorized based on how they affect the building: Lighting and equipment, Envelope, HVAC terminal side and HVAC supply side (see Table 3.1.1 for the list of measures in each category). The approach to modeling these measures vary from simple changes in building model parameters (e.g. related to COP, envelope properties, set points etc.) based on engineering judgments to more detailed physics based models. One unique aspect of our approach is that while modeling each measure the interaction of that measure with the others is captured to the level of detail which is consistent with the fidelity of energy performance and HVAC model described in the previous sections. Detailed models for each ECM are described in the appendix A.4.

Table 3.1.4: Energy Efficient Design Principles

<i>Lighting and Equipment</i>	<i>HVAC (Terminal side)</i>	<i>HVAC (Supply side)</i>
Light Scheduling	Air Side Economizer	CAV to VAV
Occupancy Based Lighting Sensors	Fan Assisted Precooling	VAV & Control Retrofit
Daylight Based Dimming	Modified Setpoint & Setback	Chiller Plant Optimization
Upgraded Lighting/ Delamping	Supply Air Temperature Reset	Heating Plant Optimization
Plug Load Control	Supply Static Pressure Reset	On Demand Service Hot Water
Efficient Equipment (Plug Loads Only)	Water Side Economizer (used in combination with Energy Recovery/ DOAS)	Solar Waste Heat Absorption Chiller
Light Shelves	Demand Control Ventilation	Condensing Boiler
Day Lighting (Solar Tubes, Sky lights)	Displacement Ventilation + Radiant Cooling/Heating	Hybrid Ground Source Heat Pump
<i>Envelope</i>	Under Floor Air Ventilation (UFAD) with Personal Supply Temp Control	Energy Recovery
Weatherization	Mixed Mode Ventilation	Indirect Evaporative Cooling
Trees	NV for night-time pre-cooling	Direct Evaporative Cooling
Cool Roof	HVAC Equipment Upgrade	Solar Thermal
Upgraded Windows		Desiccant Dehumidification (used only with Solar Thermal)
Increased Insulation		DOAS (Used in conjunction with DV +Radiant Systems)
Green Roof		
Active External Shading		

### Assembling Retrofit Systems and Packages

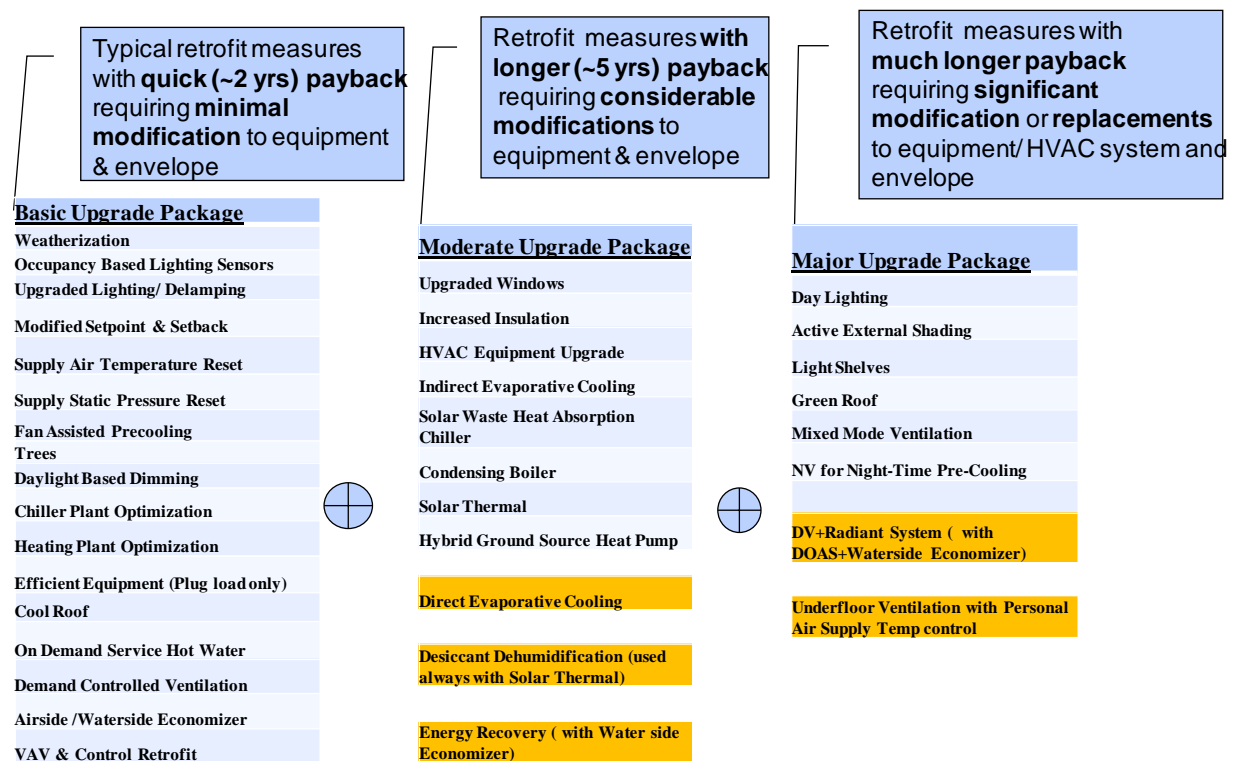
In order to achieve desired reduction in energy consumption for a given building, typically several retrofit measures need to be applied in conjunction, leading to a packaged retrofit solution. While the best (for e.g. in terms of minimum economic cost leading to desired energy savings) packages solution will vary across buildings, one can pre-assemble packages which are expected to give similar performance across similar buildings. For example, one can consider usage and/or climate adaptive packages which are tailored to give best performance for a class of buildings with similar usage and/or in similar climate zone. Alternatively, packages can be constructed with consideration to the cost (in terms of payback) and complexity (in terms of amount of building infrastructure modification), as described below:



- **Basic Upgrade Package:** Consists of typical retrofit measures with quick (~2years) payback requiring minimal modification to equipment and envelope.
- **Moderate Upgrade Package:** Consists of retrofit measures with longer (~5 years) payback requiring considerable modifications to equipment and envelope.
- **Major Upgrade Package:** Consists of retrofit measures with much longer payback and require significant modifications or replacements to equipment/HVAC system and envelope.

Table 3.1.2 shows an example the breakup of the energy conservation measures discussed in previous section into groups with increasing cost and complexity. While assembling the packages one has to be careful, that principles which are incompatible with each other or provide similar functionality are not considered in the same package. For example, in the moderate package direct evaporative cooling, desiccant dehumidification, and energy recovery with waterside economizer should never be used together, since they can lead to detrimental effects on each other's performance. On the hand in major upgrade category, either DV and radiant system, or under floor ventilation should be considered, since they provide similar functionality. Also, note that moderate upgrade package includes the basic package, and similarly major package includes both moderate and basic package. Thus, there is 1 basic package, 3 possible moderate packages and 6 major packages, leading to a total of 10 possible packages.

Table 3.1.2: Packages with increasing cost and complexity



### 3.1.2-5 Uncertainty Quantification and Sensitivity Analysis

In order to establish the robustness of building's energy consumption, both with baseline system and particular ECM or packaged retrofit solution, we developed an uncertainty quantification and sensitivity analysis tool. Figure 3.1.4 shows the schematic of our overall approach. As indi-

cated our approach can handle both parametric (e.g. envelope related parameters, setpoints etc.) and time varying uncertainty (e.g. internal heat gains, external weather conditions etc.). Time varying uncertainty is transformed into parametric uncertainty by using Karhunen Loeve expansion, see Surana et al. (2012) for details. A Quasi Monte Carlo method is employed to sample uncertain inputs parameter space, and the output distribution obtained is used for computing the ANOVA (Analysis of Variance) decomposition and corresponding first order Sobol indices (see [Li,Sobol] and references there in for details of this method). The Sobol indices represent the sensitivity of output of interest (e.g. energy usage) with respect to the input uncertain parameters. Details of a related approach employed in UQ/SA using high fidelity models are described in section 3.4.

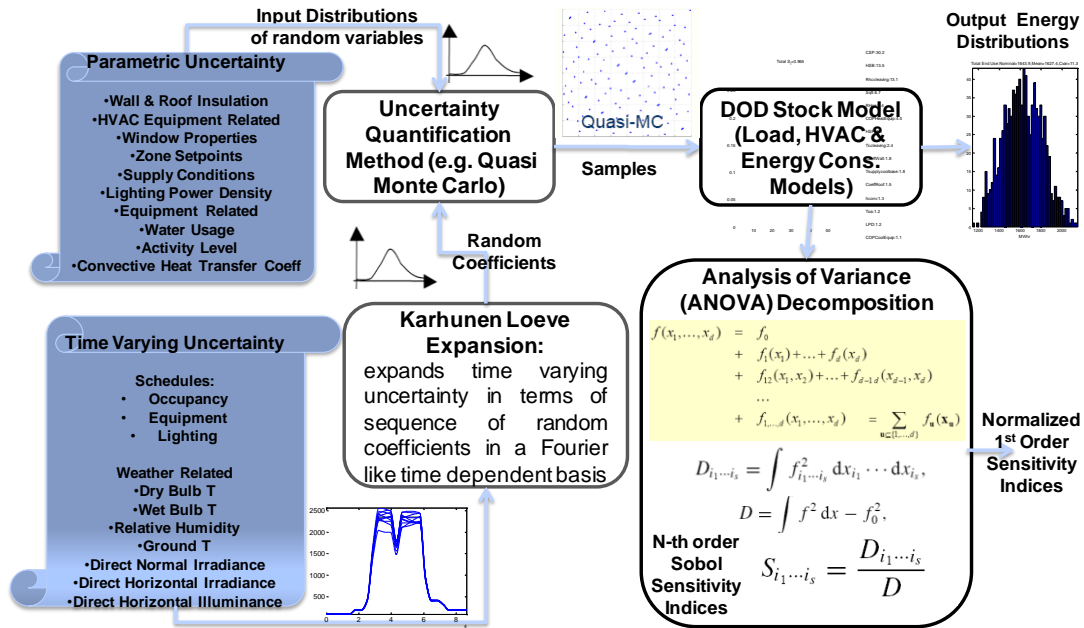


Figure 3.1.4: Sensitivity Analysis approach in the Stock Tool

### 3.1.2-6 Energy Related Operating Cost Analysis

In addition to site-energy consumption estimates for whole buildings, the tools developed and described above provide annual energy cost estimates (i.e. building operating costs) by using a cost function. The cost function depends on rates and tariff structures for energy sources (such as electricity, natural gas, propane, etc.) typically utilized at several geographical locations in the U.S. For example, the energy cost function of a building at Fort Carson (a DoD use case considered in the present study) will include average energy rates (\$/kWh) for natural gas, propane, and fuel oil in the Fort Carson (CO) area. Average energy (\$/kWh) and demand (\$/kWmax) rates for electricity in the specific area will also be a part of the cost function. Tariffs (\$ or %) and taxes (%) are included to calculate the total energy costs (\$) for a whole building at the specified location. Once the energy costs for the baseline and the retrofit solutions are obtained based on the site-energy consumption and the cost function, the energy cost savings potential for system retrofit solutions can be evaluated. This annual energy cost analysis capability developed is a subset of total life-cycle energy cost analysis of whole buildings.

For the DoD case studies discussed in this report, source-energy consumption estimates are provided (based on source-energy multipliers) that can be interpreted as a proxy for energy costs.

The cost function capability described above was not utilized to perform energy cost analysis for the DoD case studies.

### 3.1.3 DoD Case Studies Results and Discussion

In this section we demonstrate the application of the Stock Tool for which we consider two types of case studies: 1) DoD RPAD Portfolio Retrofit Analysis and 2) Specific DOD building Retrofit Analysis. For the first use case we employ CBECS database to fill in the missing building attributes in the RPAD, establish the baseline for each building in the RPAD and compare the overall stock tool EUI predictions with the reported energy data in 2009 US DoD Annual Energy Management Report. We then cluster the RPAD by CBECS primary usage categories and ASHRAE climate zones. For each cluster we select a representative building based on energy usage, square footage, number of floors and average envelope properties. We then apply ECM analysis for each of these representative buildings to identify potential energy savings. Based on this analysis, we extrapolate potential energy savings potential for different ECM's at portfolio level. For the second use case, Stock tool is applied to 6 selected DoD building for which detailed building information is available. For each building we first establish the Stock tool baseline and compare it metered or simulated data from high fidelity simulation environment (e.g. EPlus , TRNSYS), apply ECM analysis, manually assemble packages which give 40% or higher savings. We also apply UQ/SA analysis to compute output distributions in energy consumptions and identify key factors (e.g. building attributes, parameters, external/internal loads etc) to which the building energy consumption is most sensitive to.

#### 3.1.3-1 DoD RPAD Analysis

##### 3.1.3-1a) DoD Building Stock Repository Data and Filling Missing Information

The U.S. DoD real property database made available consists of 247,205 building with a total of 1.72 Billion . Below is a list of building attributes (see Table 3.1.3) available in this database:

- Property Unique Identity Number
- Site Unique Identity Name
- State
- County
- City
- Zipcode
- Building Description
- Operational Status
- Current Use
- Building Total Area (sq ft)
- Building Height (# floors above grade)
- Floors below grade
- Construction Type
- Construction Material

Table3.1.3: DOD real property database attributes.

RPUID	RPSUID	State	County	City	ZIP	Census Division	Building Description	Operational Status	Current Use	Building Total Area	Building Height	Floors Below Grade	Construction Type	Construction Material
100000	CSO HUNTERS POINT AN	California	San Francis	San Francis	94066	West-Pacif	STANDBY G	Caretaker	- Utility Bldg	616	1	0	Permanent	Does Not A
100001	CSO HUNTERS POINT AN	California	San Francis	San Francis	94066	West-Pacif	GARAGE	Caretaker	- Family Hou	240	1	0	Semi-perm	Does Not A
100002	CSO HUNTERS POINT AN	California	San Francis	San Francis	94066	West-Pacif	GARAGE	Caretaker	- Family Hou	286	1	0	Semi-perm	Does Not A
100003	CSO HUNTERS POINT AN	California	San Francis	San Francis	94066	West-Pacif	OFFICERS Q	Caretaker	- Family Hou	2133	1	1	Semi-perm	Does Not A
100032	DAVISVILLE R/CBC CSO	Rhode Isla	Washingto	Davisville	02852	Northeast-	GEN WAREH	Caretaker	- Covered Stc	30400	1	0	Semi-perm	Does Not A
100033	DAVISVILLE R/CBC CSO	Rhode Isla	Washingto	Davisville	02852	Northeast-	STOREHOU	Caretaker	- Covered Stc	4000	1	0	Semi-perm	Does Not A
100034	CSO NASALAMEDA CA	California	Alameda	Alameda	94501	West-Pacif	GATE HOU	Caretaker	- Police Stat	5196	2	0	Permanent	Does Not A

The information available in the DOD stock repository is not sufficient for energy modeling and subsequent retrofit analysis. In order to estimate the missing information in the DOD stock repository, we use CBECS database which is relatively richer in the reported building attributes. For each DoD building we find a closest CBECS building match based on climate zone, usage and size (as described in section 3.1.2-1 and appendix A.1). However, before applying this mapping procedure to the DOD stock, we pruned the stock repository, as follows:

- 1) DOD buildings with \_\_\_\_\_ and CBECS primary usage type=“Other”, were removed, which constitute around 12% of the DOD stock.
- 2) DOD buildings duplicates were removed with a remaining total of 161,988 buildings.

For each DoD building in the pruned stock repository, steps 1-4 (see appendix A.1 for detail) were applied. During this process we found that around:

- 1) 5% DOD stock could not be matched based on CBECS census division
- 2) 15% DOD stock could not be matched based on CBECS detailed usage category
- 3) 5% DOD stock could not be matched based on CBECS primary usage category

However, by relaxing some of the constraints in the matching process as described in Steps 1 and 2, 99.98% of DOD buildings in the pruned stock could be matched to buildings in the CBECS database. For subsequent energy modeling and retrofit analysis, we used this CBECS updated stock DOD repository.

### 3.1.3-1b) DoD Energy Consumption Stock Characteristics

In this section we report the US DOD real property energy consumption estimated based on the energy performance modeling described in section 3.1.2. For each building in the CBECS augmented DoD database, we compute the site energy consumption. Table 3.1.4 shows that the total model based estimate of site energy consumption to be 135,580 billion Btu for the 1.72 billion GSF US DoD real property database we have, with an average EUI of 78,736 Btu/GSF. In the table we also list the reported worldwide DoD GSF, site BTU and EUI obtained from 2009 US DoD Annual Energy Management Report. Using this we estimate the US DoD site Btu and EUI to be 186,932 billion and 108,560 Btu/GSF, respectively. Hence, our energy model underestimates the total US DoD site Btu by around 30%. Given that the key DoD stock attributes were estimated from CBECS database, and our energy performance model simplifies the building to a single zone, this estimation accuracy is reasonable. Moreover, the underestimation can be most likely attributed to the idealized energy performance and HVAC model assumed in our study.

Table 3.1.4: Comparison of estimated DOD total and average EUI with that reported across all of DoD stock

	GSF (Billion)	Site Btu (Billion)	Avg. EUI Btu/GSF
Worldwide	1.93	209,789	108,560
US (Estimated)	1.72	186,932	108,560
Model Results	1.72	135,580	78,736

Figure 3.1.5 shows the site energy consumption breakup for the DoD stock based on the building usage. The top three building usage sectors are: Lodging, Office, and Warehouse and Storage. Figure 3.1.6 shows the EUI distribution for these sectors, along with the median EUI.

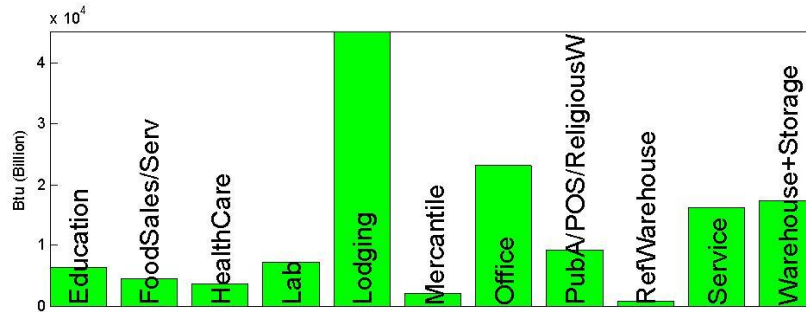


Figure 3.1.5 DOD Site energy (Btu Billions) based on building usage. Here Healthcare includes outpatient and inpatient services, and Pub/POS/RelW stands for Public Assembly, Public Order and Safety, and Religious Worship.

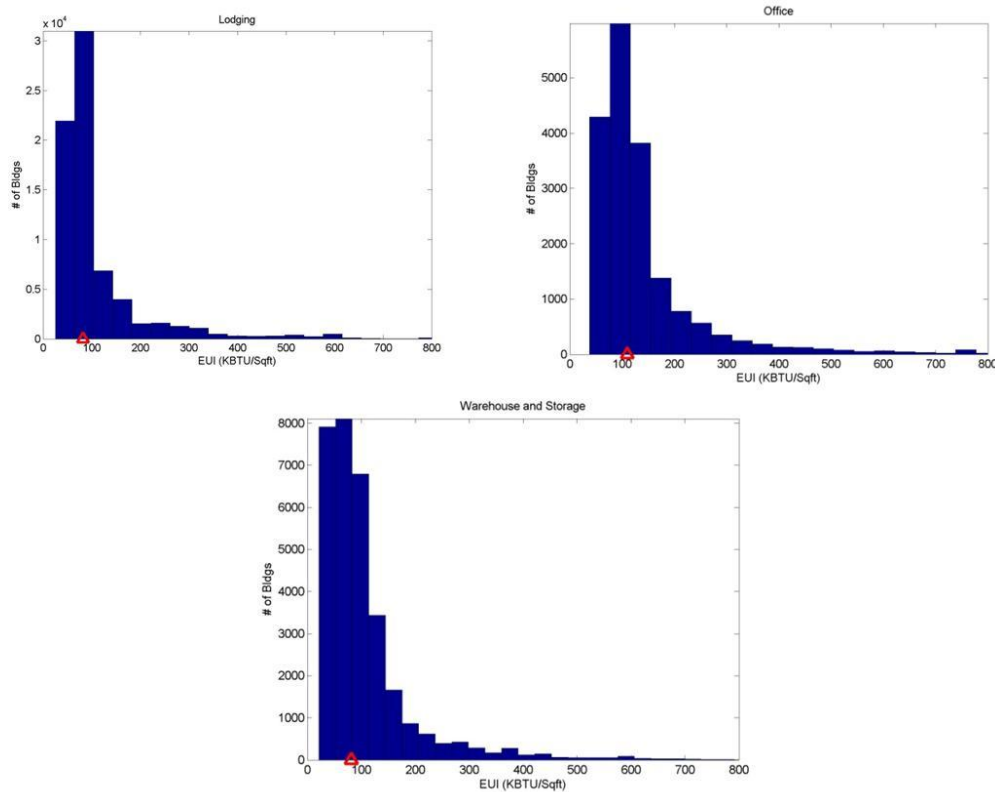


Figure 3.1.6 EUI distribution for top three DOD usage sectors. The red triangle indicates median EUI for each sector.

### 3.1.3-1c) Composition of Median EUI Building

In this section we cluster the DoD stock based on CBECS primary usage types and ASHRAE climate zones, and determine a representative building for each cluster. Since, some usage categories and climate zones have negligible number of DoD building, we regrouped some of the similar usage categories and climate zones, respectively. Table 3.1.5 below list the combined CBECS primary usage and combined ASHRAE climate zones, used in the clustering, leading to total of 110 clusters. Table 3.1.6 shows the number of DoD buildings in each of these clusters; note that three clusters (DoD refrigerated warehouses in Seattle, Duluth and Helena, and Fairbanks) have no buildings.

The procedure for selecting the representative building in each cluster is described below. For each building in the cluster, we first select a feature vector which comprises of following attributes: energy use, square footage, number of floors and average envelope properties. The average envelope property is characterized in terms of area weighted average of conduction values of roof, ceiling and the fenestration. This feature vector is then normalized in each dimension with the normalization constant being the maximum value attained by the attributes (i.e. energy use, square footage, number of floors and average envelope properties) in the cluster. A weighted mean is then computed, where the weight given to each building is computed based on the inverse of sum of the Euclidean distance between feature vector representing the building and the feature vector of all other buildings in the cluster. Hence, more weight is given to buildings which fall in high density feature vector space. Finally, the closest building (again in terms of Euclidean distance between feature vectors) from the computed weighted mean is determined and is taken to be a representative building for the cluster.

Table 3.1.7 shows the EUI of the representative building in each cluster. The percent EUI variability within a cluster from its median, across all clusters was found to be no more than 37%. The last two columns in Table 3.1.7 compare the model based DoD median EUI with the estimated CBECS EUI (estimated from the reported site energy consumption in the CBECS database) across different usage categories.

Table 3.1.5: Usage and Climate categories for clustering

<b>Usage Categories (Based on CBECS Primary Usage Types)</b>	<b>Climate Zones (Based on ASHRAE Zones)</b>
<b>Education</b>	<b>1A+2A=Miami, FL+Houston, TX</b>
<b>Food Service + Sales</b>	<b>2B+3B=Phoenix, AZ+Las Vegas, NV</b>
<b>Health Care (Outpatient), Health Care (Inpatient)</b>	<b>3A=Atlanta, GA</b>
<b>Laboratory</b>	<b>3C=San Francisco, CA</b>
<b>Lodging</b>	<b>4A=Baltimore, MD</b>
<b>Mercantile (Retail other than mall)</b>	<b>4C=Seattle, WA</b>
<b>Office</b>	<b>5A+6A=Chicago, IL+Minneapolis, MN</b>
<b>Public Assembly, Public Order and Safety, Religious Worship</b>	<b>4B + 5B= Albuquerque, NM +Denver, CO</b>
<b>Refrigerated Warehouse</b>	<b>6B + 7B= Helena, MT +Duluth, MN</b>
<b>Service</b>	<b>7A+8A=Fairbanks, AK</b>
<b>Warehouse and Storage</b>	



Table 3.1.6: Clustering based on usage and climate zones (Number of Buildings)

	Miami, Houston	Phoenix, Las Vegas	Atlanta	San Francisco	Baltimore	Seattle	Chicago, Minneapolis	Albuquerque, Denver	Helena, Duluth	Fairbanks	
	1A+2A	2B+3B	3A	3C	4A	4C	5A+6A	4B+5B	6B+7B	7A+8A	Total
Education	724	626	1091	196	954	72	465	199	32	55	4414
Food Service + Sales	372	271	371	122	408	67	309	157	16	36	2129
Health Care (Outpatient), Health Care (Inpatient)	269	215	265	27	275	68	126	70	9	27	1351
Laboratory	160	1424	235	286	1515	53	533	111	9	11	4337
Lodging	18845	18143	20190	3556	16206	3785	9993	4803	1100	2867	99488
Mercantile (Retail other than mall)	353	319	405	43	372	52	191	106	17	45	1903
Office	3248	3218	4052	560	4146	502	2235	1140	165	527	19793
Public Assembly, Public Order and Safety, Religious Worship	1626	1225	1627	267	1645	250	1610	509	92	322	9173
Refrigerated Warehouse	77	81	85	67	70	0	146	64	0	0	590
Service	2681	2868	3040	415	2817	512	2040	1197	118	419	16107
Warehouse and Storage	7815	5552	10899	1017	12453	1436	7541	9436	550	1001	57700
Total	36170	33942	42260	6556	40861	6797	25189	17792	2108	5310	216,985

Table 3.1.7: Energy Use Intensity (EUI) of Median Building (KBTU/ft<sup>2</sup>)

Median EUI (KBTU/Sqft)	Miami, Houston	Phoenix, Las Vegas	Atlanta	San Francisco	Baltimore	Seattle	Chicago, Minneapolis	Albuquerque, Denver	Helena, Duluth	Fairbanks	Average EUI by Usage	CBECS Average EUI
	1A+2A	2B+3B	3A	3C	4A	4C	5A+6A	4B+5B	6B+7B	7A+8A		
Education	88.9	91.1	103.8	72.0	72.5	46.0	85.4	78.5	108.5	99.5	76.7	85.1
Food Service + Sales	140.0	138.8	138.1	309.1	144.7	271.7	156.3	150.0	147.5	158.9	136.2	294.5
Health Care (Outpatient), Health Care (Inpatient)	81.2	84.8	73.9	64.9	71.0	151.9	99.8	84.1	105.4	90.2	71.6	193.7
Laboratory	245.2	175.4	157.2	155.8	129.7	110.1	129.6	117.9	329.5	172.5	115.3	283.8
Lodging	70.2	68.7	76.3	65.0	97.0	93.3	95.3	122.9	122.0	106.4	86.1	94.2
Mercantile (Retail other than mall)	97.9	101.2	80.9	82.8	90.7	86.3	90.4	115.5	140.5	105.4	76.7	115.1
Office	132.9	111.7	110.3	125.0	96.5	126.1	97.5	108.9	111.9	128.5	89.8	93.6
Public Assembly, Public Order and Safety, Religious Worship	87.9	78.2	84.1	68.0	71.8	58.5	82.2	76.7	74.0	125.2	79.8	74.8
Refrigerated Warehouse	49.2	85.2	37.2	29.9	116.3	0.0	64.3	96.7	0.0	0.0	42.5	117.6
Service	71.4	75.0	66.8	61.9	83.5	80.2	88.7	82.2	86.8	97.5	71.11	84.1
Warehouse and Storage	86.2	95.7	53.9	74.3	79.6	115.5	78.1	93.7	132.0	90.9	53.79	33.6

### 3.1.3-1d) Energy Efficient Concept Screening

In this section we describe preliminary retrofit screening results. Figures 3.1.7-3.1.8 show the savings from a few individually applied energy efficient design principles for DoD representative buildings in each cluster. Figure 3.1.9 shows site energy savings (similarly Figure 3.1.10 shows source energy savings) with three self assembled packages: basic package, moderate package, and major package. Note that the energy saving impact of these packages is more or less similar, despite variation in usage and climate. Table 3.1.8 summarizes the implications for DoD stock, extrapolated from representative building savings. Here we assume that within each cluster, different buildings will exhibit similar savings as that of the representative building. Based on this, we can estimate %DoD stock space (in sqft) for which savings will be greater than a given thre-

shold. Thus, the way to interpret the table is following: due to upgraded lighting, 48% of DoD space can save more than 10%. Similarly, one can make following estimates: 98% DoD space can save more than 20% with basic package, 97% DoD space can save more than 40% with moderate package, and 63% DoD space can save more than 60% with the major package.

Table 3.1.8: Extrapolation of energy savings for DOD stock based on savings for median EUI buildings

Principle	Threshold	% DOD Sqft
Occupancy based lighting sensors	2	9.1
Upgraded lighting and Delamping	10	48.3
Upgraded windows	5	68.2
Daylight based dimming	10	0.0
Daylighting	10	27.6
Light shelves	10	7.1
Weatherization	5	15.0
Modified Setpoint and Setback	10	5.6
Supply Static Pressure Reset	10	4.6
Trees	5	29.0
Active External Shading	5	0.0
Cool roof	2	3.1
Heating plant optimization	2	14.3
Chiller plant optimization	2	7.5
Condensing boiler	5	0.4
1 Stage Abs Chillers + Solar Thermal	5	93.2
Solar thermal	5	9.6
Indirect evaporative cooling	10	1.5
Direct Evaporative cooling	10	17.5
Mixed mode ventilation	5	8.6
Hybrid GSHP	20	71.2
Underfloor + Personal Air Supply temp control	10	50.3
Displacement RHRC + DOAS + WSE	10	75.3
NV Night-Time Pre-Cooling	5	2.5
Desiccant Dehumid + Solar Thermal	5	12.4
Supply Air Temp Reset	5	6.3
Variable flow VFD	2	4.7
Airside Economizer	5	44.5
Green Roof	5	4.1
Increased Insulation	5	40.0
Efficient Equipment	5	10.0
VAV + Control Retrofit	5	7.6
Basic	20	98.0
Moderate	40	97.5
Major	60	62.9



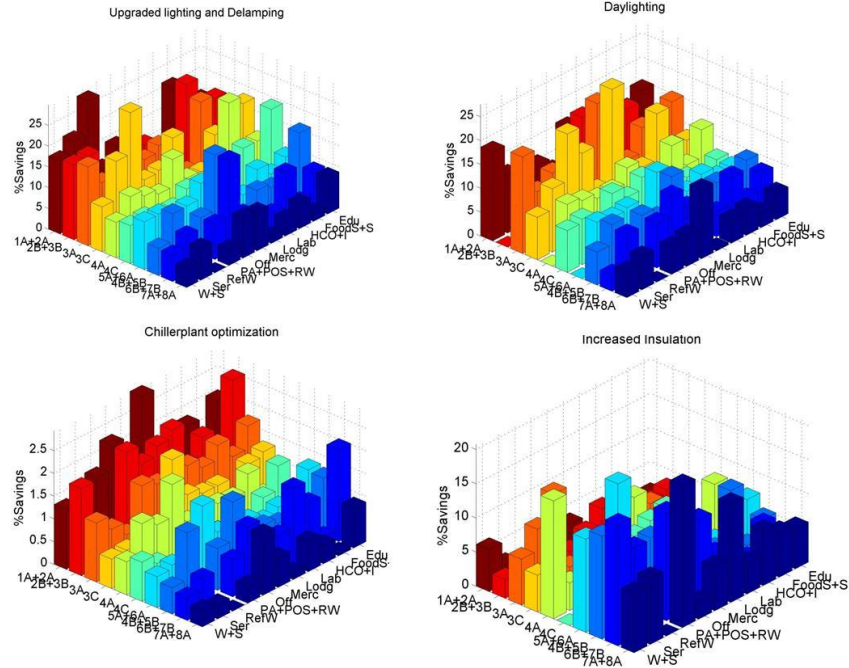


Figure 3.1.7 % Site Energy Savings due to few selected ECMs for the median DoD building for each climate zone and building use category.

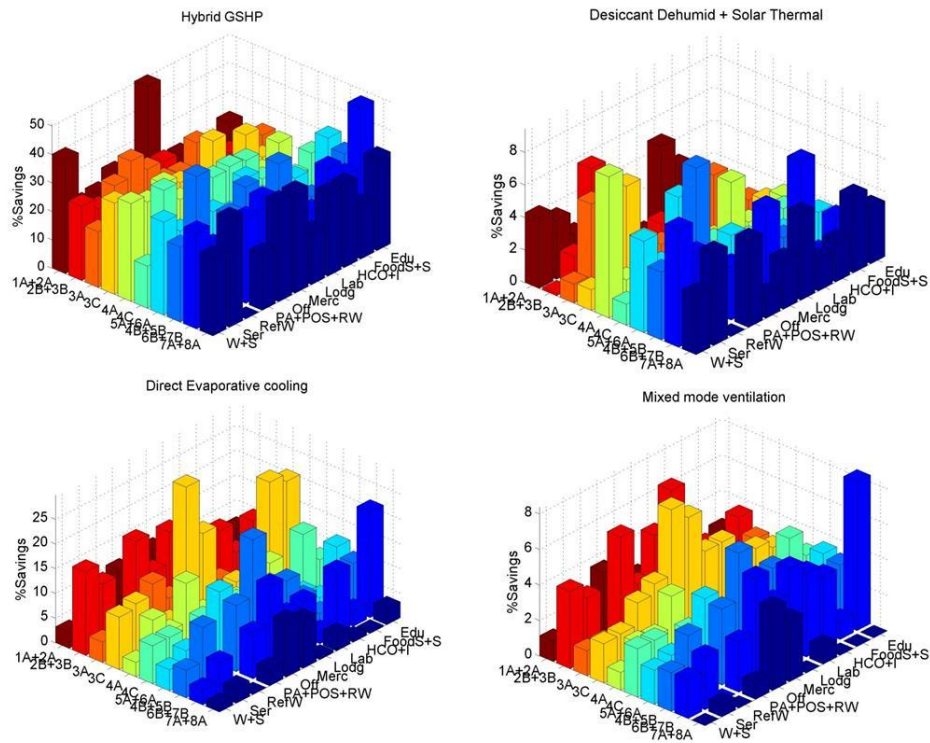


Figure 3.1.8 % Site Energy Savings due to few selected ECMs for the median DoD buildings for each climate zone and building use category.

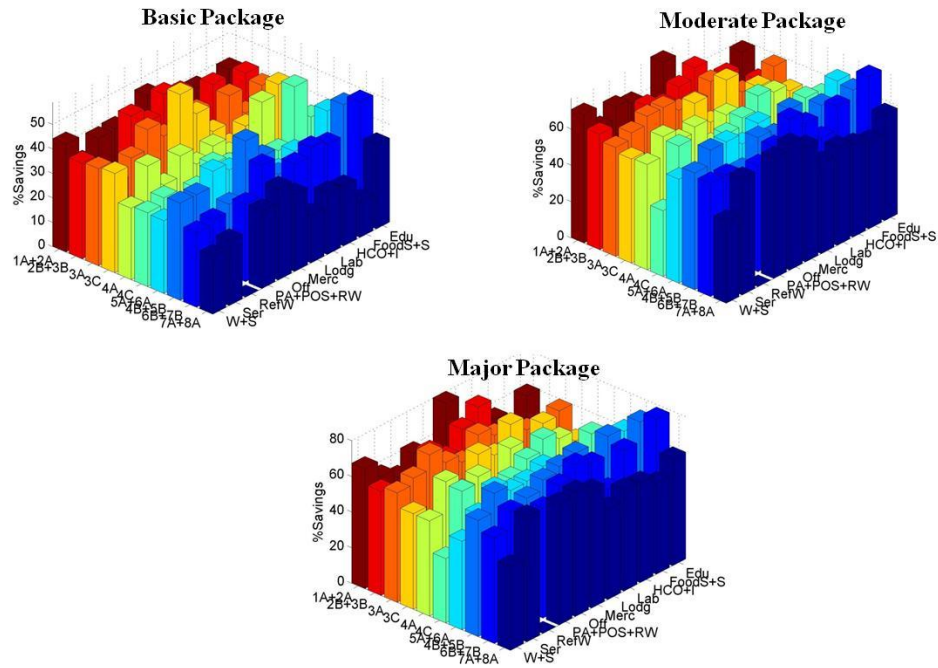


Figure 3.1.9 % Site Energy Savings from different package applications for the median DoD buildings for each climate zone and building use category.

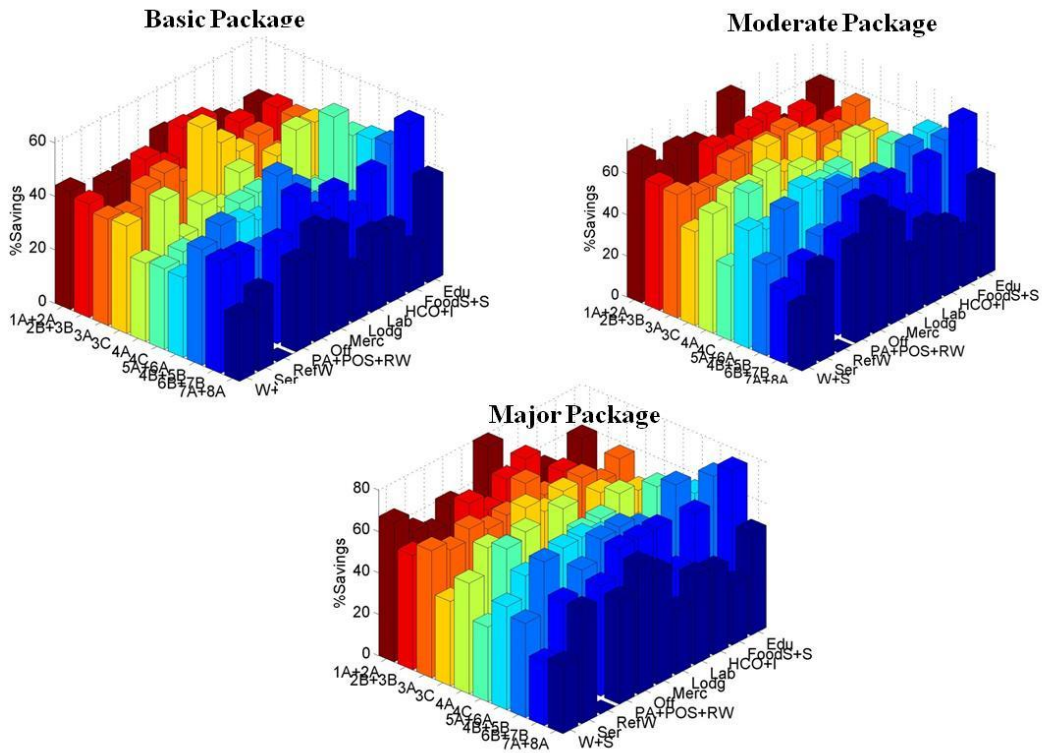


Figure 3.1.10 % Source Energy Savings from different package applications for the median DoD buildings for each climate zone and building use category.

### 3.1.3-2 Specific DOD Building Retrofit Analysis

DoD facility audits in multiple sites (climates, building types) – Naval Station Great Lakes (IL), Ft. Carson (CO), Ft. Detrick (MD), Ft. Bragg (NC) and Ventura Naval Base (CA) was conducted during the program. With the availability of more detailed information, there was no need to extrapolate the data from CBECS database for establishing the baseline EUI and ECM analysis. Figure 3.1.11 below shows the comparison of estimated EUI based on the stock tool with either metered data (Drill Hall, Bldg26 and Ventura) or simulation results from high fidelity tools like TRNSYS (Ft. Carson and Bragg). As can be seen, the Stock tool estimated EUI values are within 10-15%.

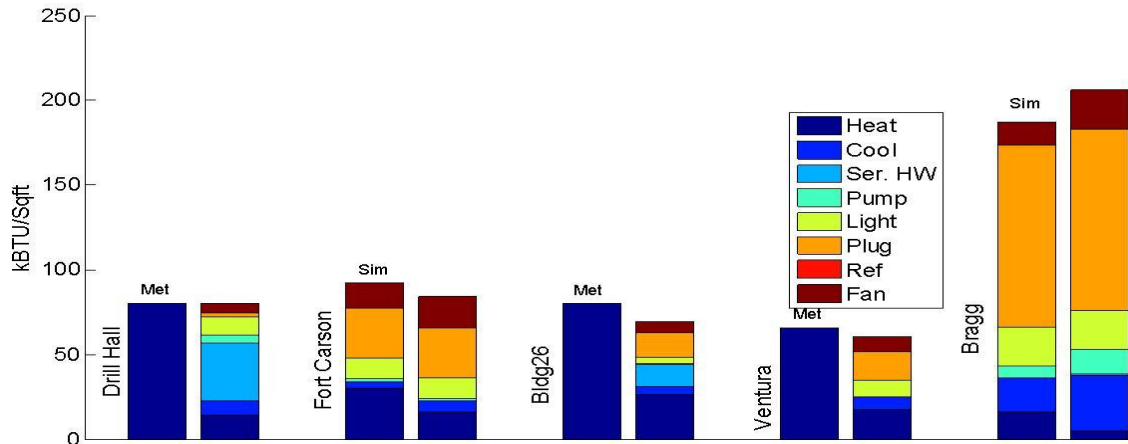


Figure 3.1.11: Comparison of EUI for different DOD facilities

#### 3.1.3-2a) Drill Hall, Great Lakes Naval facility

The first location was a Drill hall at the Great Lakes Naval facility near Chicago, IL. It is a military training facility with primary use being physical training and graduation rehearsal. The building has air-cooled chillers, four VAV air handling units: Each with demand control ventilation, full economizer and VFDs, and heat is supplied by district steam. The building has been certified as LEED Gold.

Figure 3.1.12 shows the site energy saving reduction due to application of different ECM's. The basic, moderate and major package on an average saves 19%, 58% and 64%, respectively. A package comprising of *On demand service hot water, Demand controlled ventilation, Solar thermal, Increased Insulation, Day-lighting and Displacement ventilation with radiant heating and cooling* (marked in Figure 3.1.13 with red circles) was chosen for this facility. Figure .1.14 on left shows the site energy savings of 45.6% that results from application of this assembled package. The source energy savings turns out to be similar around 42.8%. Figure 3.1.13 on right also shows the distribution of total energy consumption for the facility with the baseline and the packaged system. The mean site EUI for baseline was 78kBTU/ft<sup>2</sup>/year (nominal value being 80kBTU/ft<sup>2</sup>/year) with a standard deviation of 9kBTU/ft<sup>2</sup>/year, while with the packaged system the building mean site EUI reduced to 44kBTU/ft<sup>2</sup>/year with a standard deviation of



Usage	Public assembly
Climate	Cold/Humid
Square Footage	69788
#Floors	1
Peak Occupancy	550
Schedule	80hrs, Open only WD
Glass	13.4%, Single layer glass, Not tinted, Not Reflective
Wall	Concrete Block
Roof	Metal Deck
HVAC Type	•VAV Multizone •Electric Chillers •District Steam

3kBtu/ft<sup>2</sup>/year. For these computations, the uncertainty in input variables was assumed to be uniform with 20% variation about nominal values. Energy use in this building with baseline system is found to be most sensitive to parameters such as internal heating and cooling set-points/setbacks, supply temperature, envelope (roof/wall conduction and infiltration rate) & fenestration related, and external weather conditions. With the packaged system, the facility remains sensitive to most of these parameters with some change in order. Envelope related parameters become less influential, while parameters related to service hot water, peak occupancy and sensible heat gain per occupant become more dominant.

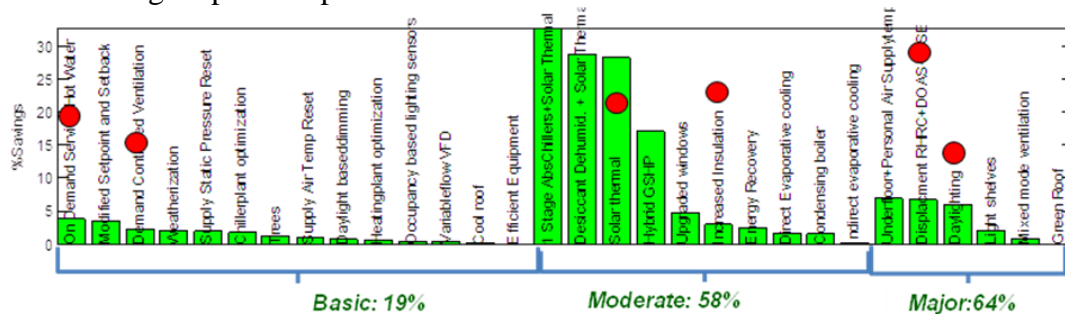


Figure 3.1.12: Site energy savings for different ECM's. ECMs marked with red circles are used to assemble a package.

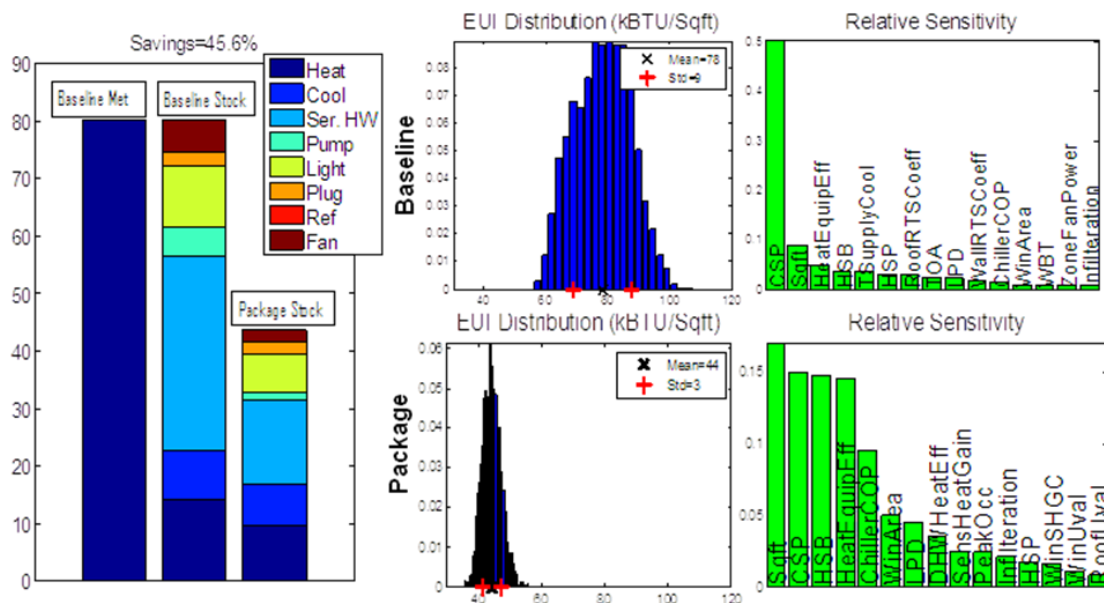


Figure 3.1.13: On left is shown site energy savings from assembled package broken by end use type. On right are shown results of UQ/SA for the building with the baseline and packaged system.

### 3.1.3-2b) Building 26, Great Lakes Naval facility

Building 26 is another facility located in the Great Lakes area. It is a 3 storey office building with electric cooling and district heating. Other key attributes of the building are listed in the table on the side.



Figure 3.1.14 shows the site energy saving reduction due to application of different ECM's. The basic, moderate and major package on an average saves 27%, 57% and 62%, respectively. A package comprising of *Efficient equipment*, *Modified set-point and set –back*, *Hybrid GSHP*, *Solar thermal* and *Upgraded windows* was chosen for this building. Figure 3.1.15 on the left shows the site energy savings of 49.4% that results from application of this assembled package. The source energy savings is much smaller, around 27.8%. On right in Figure 3.1.16 is also shown the distribution of total energy consumption for the facility with baseline and packaged system. The mean site EUI for baseline was 70kBtu/ft<sup>2</sup>/year (nominal value being 69kBtu/ft<sup>2</sup>/year) with a standard deviation of 6kBtu/ft<sup>2</sup>/year, while with the packaged system the building mean site EUI reduced to 35kBtu/ft<sup>2</sup>/year with a standard deviation of 3kBtu/ft<sup>2</sup>/year. Energy use in this building with the baseline system is found to be most sensitive to parameters such as internal heating and cooling setpoints/setbacks, heating equipment COP, service hot water requirement per occupant, infiltration rate, equipment related. With packaged system the building remains sensitive to most of these parameters but shows increased sensitivity to parameters related to equipment, and lesser to setpoints and infiltration.



Usage	Office
Climate	Cold/Humid
Square Footage	29555 (Effective)
#Floors	3 ( with Basement)
Peak Occupancy	93
Schedule	55 hrs, Open WD & WE
Glass	18%, Multi layer, Not tinted, Not reflective
Wall	Brick, stone, or stucco
Roof	Asphalt/fiberglass/other shingles
HVAC Type	•VAV •Electric Cooling •District Heating

Table 3.1.9 shows a comparison of the stock model results to EnergyPlus simulation results for the baseline building and for advanced building with the package of retrofits shown in figure 3.1.15. The stock model and EnergyPlus cooling energies match within 6% but the stock model heating energy is substantially less than that computed by the EnergyPlus model. This is likely a consequence of the single zone assumption in the EnergyPlus model. The other major discrepancy is the difference between fan energy computed by the two models. The cause of this difference is likely a result of the simplification of the fan system configuration and part-load models required to simulate the HVAC system in the stock model. Both models predict that the major components of energy savings can be obtained from reductions in heating and cooling energy.

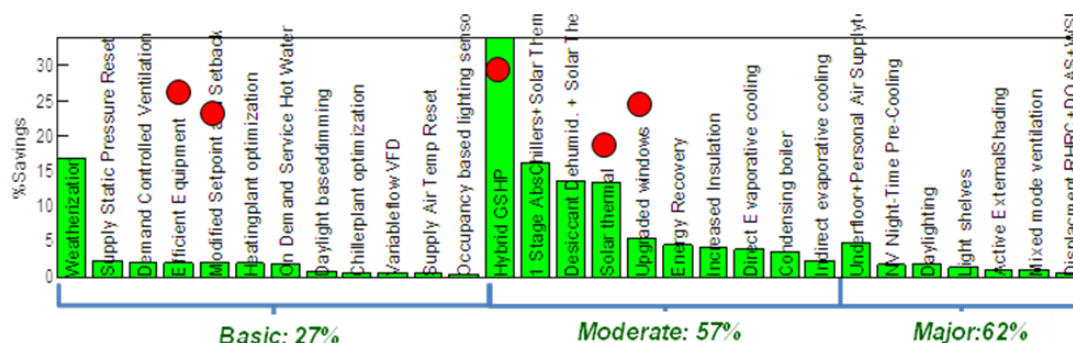


Figure 3.1.14: Site energy savings for different ECM's. ECMs marked with red circles are used to assemble a package.

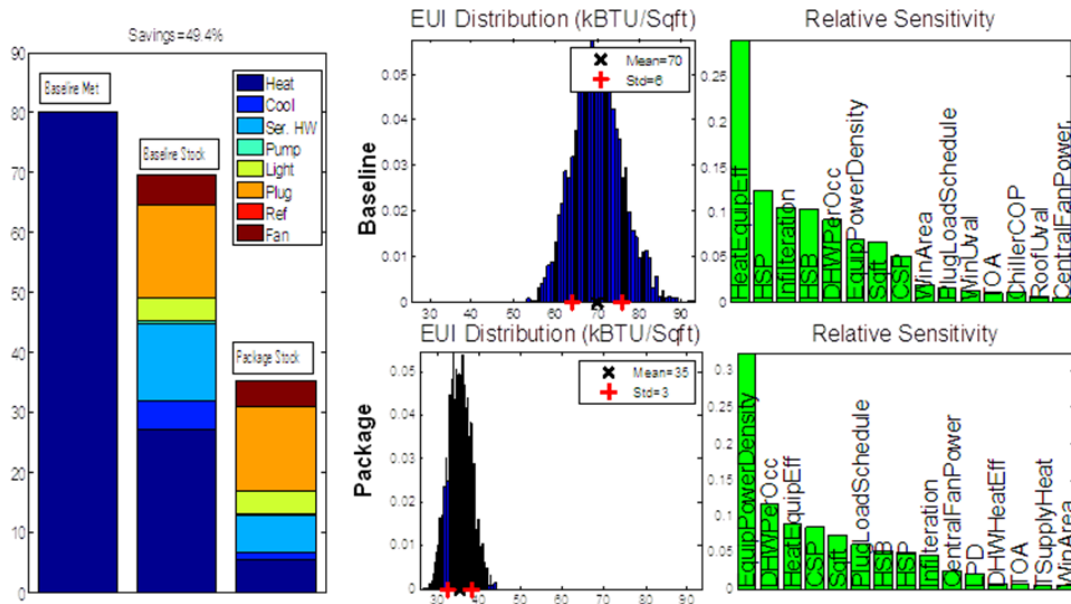


Figure 3.1.15: On left is shown site energy savings from assembled package broken by end use type. On right are shown results of UQ/SA for the building with the baseline and packaged system.

Table3.1.9: Comparison of Stock Tool savings with EnergyPlus results.

	Stock Baseline (GJ)	Stock Advanced Building	Stock %Energy Reduction	EPlus Baseline (GJ)	EPlus Advanced Building	Eplus % Energy Reduction
Heating	813.8	212.5	73.8	1258	580.6	53.8
Cooling	155.4	34.8	77.6	164.3	70.0	57.4
Pump	12.6	11.5	8.4	40.4	44.5	-11.2
Fan	210.6	131.7	37.4	62.6	127.4	-103.6
Lighting	115.4	115.4	0	127.4	123.4	3.1
Plug	441.7	397.8	10	502.1	454.9	9.4
EUI (MJ/m2 conditioned area)	875.6	452.3	48.3	1078	701	35.0

### 3.1.3-2c) Building 1225, Fort Carson

Building 1225 is a single-story office building constructed in late 1980's. The building is mixed use office type and is heavily used (limited access). A single central fan room contains two constant volume multi-zone units. Controls are pneumatic converted to DDC (Williams) with the pneumatic actuators and zone controls still in place. Gas-fired boilers in the building provide the primary heating, and uses chilled water from the base chiller plant provides cooling. Lighting is primarily T8 32W fluorescent. Other key attributes of the facility are listed in the table on the side.

Figure 3.1.16 shows the site energy saving reduction due to application of different ECM's. The basic, moderate and major package on an average saves 23%, 54% and 61%, respectively. A package comprising of *Upgraded lighting*, *VAV control retrofit*, *Direct evaporative cooling* and *Solar thermal* was chosen for this building. Figure 3.1.18 on left shows the site energy saving of 23.3% with assembled package. The source energy savings turns was around 31.7%. Figure 3.1.17 on right also shows the distribution of total energy consumption for the facility with baseline and packaged system. The mean site EUI was 87kBTU/ft<sup>2</sup>/year (nominal value being 84kBTU/ft<sup>2</sup>/year) with a standard deviation of 10kBTU/ft<sup>2</sup>/year for the baseline, while with the packaged solution the mean site EUI reduced to 66kBTU/ft<sup>2</sup>/year with a standard deviation of 7kBTU/ft<sup>2</sup>/year. Energy use in this building with baseline system is found to be most sensitive to parameters such as equipment related, internal heating and cooling setpoints/setbacks, supply temperature, envelope parameters such as roof/wall conduction, and heating and cooling equipment COPs. With the packaged system the building exhibits similar sensitivity behavior.



Usage	Mixed Office
Climate	Cold/Dry
Square Footage	18631
#Floors	1
Peak Occupancy	152
Schedule	45hrs, Open only WD
Glass	4%, Multi layer, Tinted, Non reflective
Wall	Brick Walls
Roof	Metal Deck Roofs
HVAC Type	<ul style="list-style-type: none"> <li>•CAV Multi Zone</li> <li>•District Cooling (Electric Chiller)</li> <li>•Gas Heating</li> </ul>

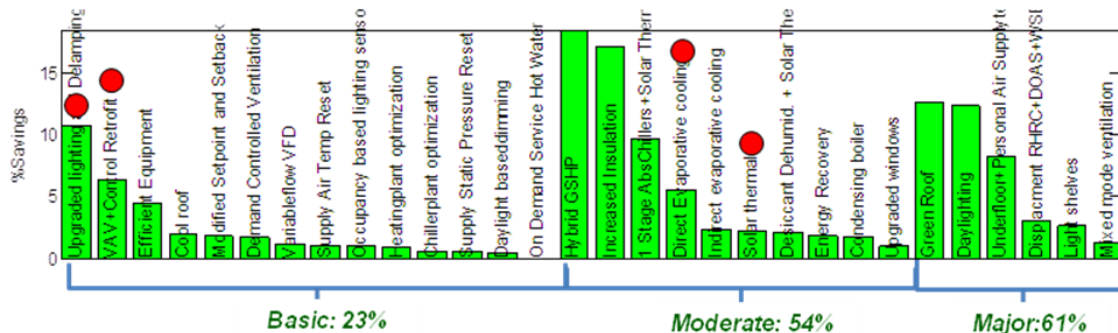


Figure 3.1.16: Site energy savings for different ECM's. ECMs marked with red circles are used to assemble a package.

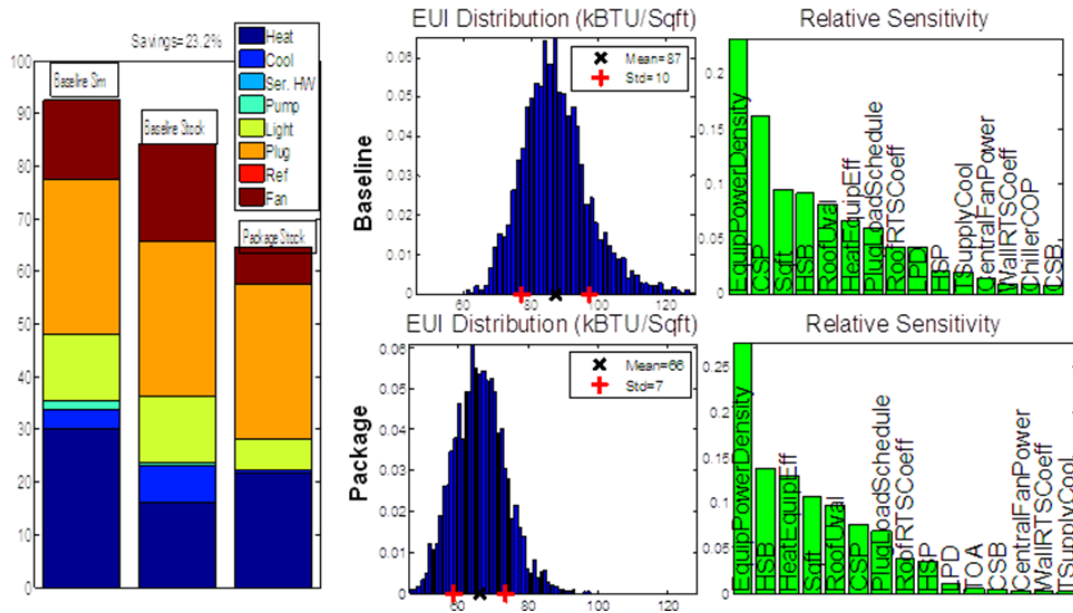


Figure 3.1.17: On left is shown site energy savings from assembled package broken by end use type. On right are shown results of UQ/SA for the building with the baseline and packaged system

Table 3.1.10 shows the component-by-component breakdown of the energy reduction resulting from packaged system as predicted by the Stock tool. For comparison, also shown in the right columns, are predictions based on a high fidelity TRNSYS model (described further in sec. 3.3). As can be seen the two models predict very similar overall energy savings, however at an individual end use level, there are differences. Except for the heating energy, the general trend is similar. In the TRNSYS model, the baseline total annual heating energy consumption is 590.8 GJ compared to 314.8 GJ in the stock tool model. The bulk of this difference is likely due to the single zone assumption in the stock tool, the implications of which were previously discussed. The trend in heating consumption from baseline to advanced system is also different, with the stock tool model showing an increase in heating energy of 110 GJ annually versus an annual reduction in heating energy of 140 GJ for the TRNSYS model. In the stock tool results, the total reduction in fan and lighting energy is 360 GJ. Assuming half of this reduction can be ascribed to the heating season, we should expect heating energy to increase by about 180 GJ. The actual increase is 110 GJ, with the difference being offset primarily by heat gained from solar thermal.

In the TRNSYS model, the fan and lighting annual energy consumption reduction totals approximately 210GJ, of which we can ascribe about 110 GJ to the heating season. This would increase heating energy to approximately 700 GJ but for a contribution from solar thermal of 250 GJ. This results in a real heating energy reduction to 448 GJ of heating energy annually.



Table 3.1.10: Comparison of energy savings broken by end use type based on Stock tool and TRNSYS model.

	Stock Baseline (GJ)	Stock Adv	Stock %Energy Reduction	TRNSYS Baseline (GJ)	TRNSYS Adv	TRNSYS % Energy Reduction
Heating	314.8	425.3	35.1%	590.8	448.4	-24%
Cooling	135.0	9.2	-93.1%	74.7	39.7	-46.9%
Pump	11.8	3.4	-70.1%	28.1	6.3	-78%
Fan	361.1	140.0	-61.2%	294.0	185.8	-36.8%
Lighting	249.2	110.7	-55.1%	249.2	141.9	-43%
Plug	580.5	580.5	0%	580.5	580.5	0%
EUI	84	64.5	-23.2%	92.4	71.4	-22.8%

Figure 3.1.18 shows the EUI distribution for all DOD facilities (in RPAD) in the cluster (Office-, see section for definition of clusters) to which Ft. Carson belongs. Note that the mean EUI of the cluster is very close to the nominal EUI value of Ft. Carson. Also shown are distribution of energy savings in the cluster which results from application of assembled package chosen for Ft. Carson building above. The average savings are around 32% with a standard deviation of 9%, and Ft. Carson savings of 23% falls in the one-sigma range. These results indicate that in buildings with similar usage and climate zone,

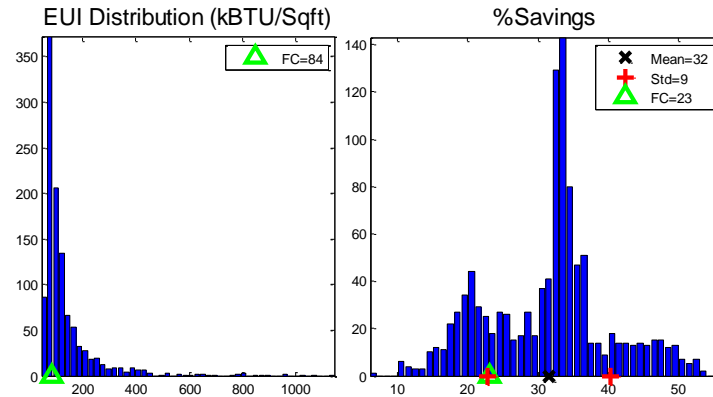


Figure 3.1.18: On left is EUI distribution in the cluster (Office-,) to which Fort Carson belongs. On right is the distribution of site energy savings resulting from packaged system chosen for the Ft. Carson building.

### 3.1.3-2d) Building 1000, Navy Base Ventura County

Building PH1000 is a two-story office building located at Port Hueneme, California. The building uses energy primarily for lighting, plug load, and ventilation. Heating and cooling loads are relatively minimal as the building resides in a mild climate. HVAC primarily serves to ventilate and heat the building. Only three rooms and the computer room are air-conditioned. Operable windows allow for natural ventilation. A 25 kW PV array on the roof generates power for the building with excess feeding back into the grid. This facility is part of a demand response program administered by EnerNOC. Other key attributes of the building are listed in the table on the side.

Figure 3.1.19 shows the site energy saving reduction due to application of different ECM's. Note that the *Mixed mode ventilation* (3%) and *Night time precooling* (1%) do not show much promise, as significant stack effect cannot be attained due to small height (2-story) of the building. The basic, moderate and major package on an average saves 23%, 50% and 63%, respectively. A package comprising of *Weatherization, Upgraded lighting and delamping, Modified set-points/setbacks, Hybrid GSHP, Upgraded windows and Daylighting* (marked in Figure 3.1.19

with red circles) was chosen for this building. Figure 3.1.20 on the left shows the site energy savings of 47.8% that results from application of this assembled package. The source energy savings is much smaller, around 35.8%. Figure 3.1.21 on right also shows the distribution of total energy consumption for the facility with baseline and packaged system. The mean site EUI for baseline was 60kBTU/ft<sup>2</sup>/year (nominal value being also 60kBTU/ft<sup>2</sup>/year) with a standard deviation of 9kBTU/ft<sup>2</sup>/year, while with the packaged system the building mean site EUI reduced to 31kBTU/ft<sup>2</sup>/year with a standard deviation of 5kBTU/ft<sup>2</sup>/year. Energy use in this building with the baseline system is found to be most sensitive to parameters such as internal heating and cooling setpoints/setbacks, equipment and lighting schedules, LPD and equipment power density, and envelope and heating equipment related parameters. With the packaged system the building there is change in relative sensitivities with respect to these dominant parameters, most notable change being increased sensitivity to equipment/lighting related parameters while becoming insensitive to heating equipment efficiency.



Usage	Office
Climate	Warm/Dry
Square Footage	68400
#Floors	2
Peak Occupancy	342 (Guess)
Schedule	250hrs, Open only WD
Glass	10% (Guess), Single Layer, Not tinted, Not Reflective
Wall	Brick, stone, or stucco
Roof	Metal surfacing
HVAC Type	•Fan Coil •Electric Chillers •Gas Heating

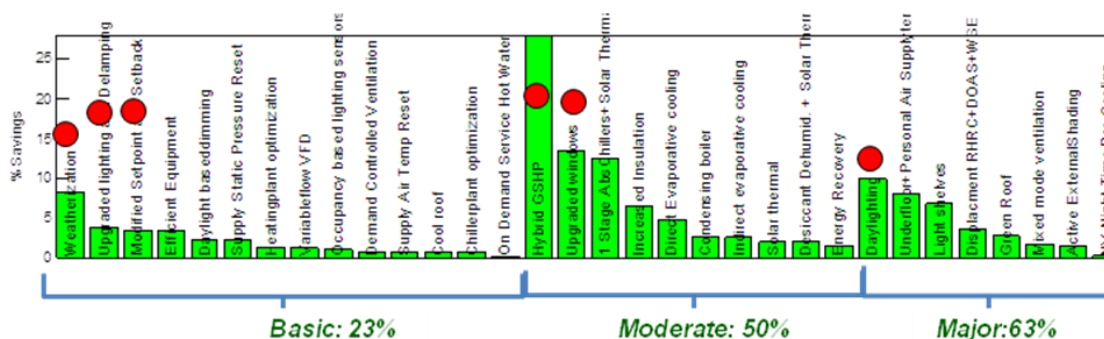


Figure 3.1.19: Site energy savings for different ECM's. ECMs marked with red circles are used to assemble a package.

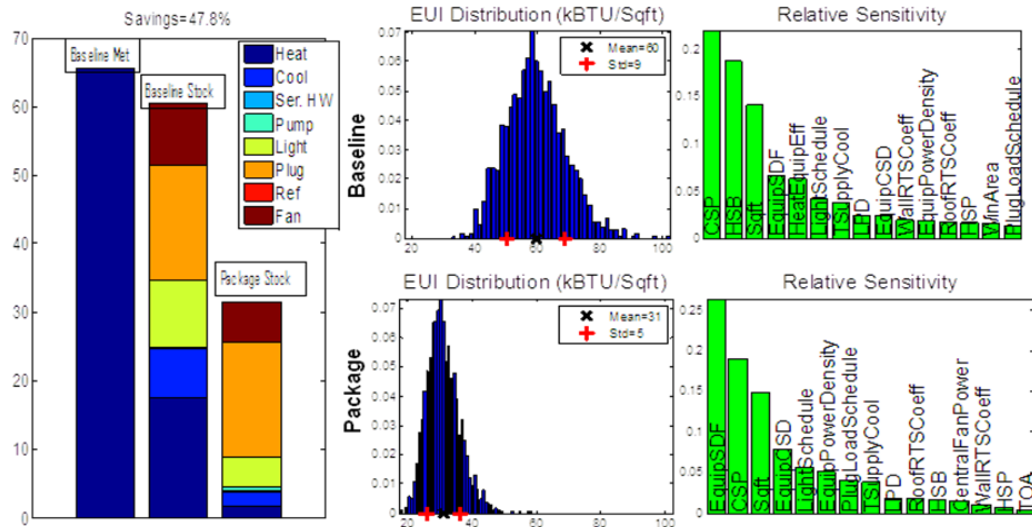


Figure 3.1.20: On left is shown site energy savings from assembled package broken by end use type. On right are shown results of UQ/SA for the building with the baseline and packaged system

### 3.1.3-2e) Building C-2040, Fort Bragg

Building C-2040 is a dining facility including kitchens and was constructed in early 1990's. The building uses natural gas for cooking and for heating make up air. Chilled water, hot water and domestic hot water all come from a central plant. Other key attributes of the building are listed in the table on the side.



Figure 3.1.21 shows the site energy saving reduction due to application of different ECM's. The basic, moderate and major package on an average saves 26%, 35% and 38%, respectively. A package comprising of VAV control, Efficient equipment, Supply air temperature reset, Chillerplant optimization, VFD, Hybrid GSHO and Daylighting was chosen for this building. Figure 3.1.23 on left shows the site energy saving of 30.5% with assembled package. The source energy savings was around 29.4%. Figure 3.1.22 on right also shows the distribution of total energy consumption for the facility with baseline and packaged system. The mean site EUI was 209kBTU/ft<sup>2</sup>/year (nominal value being 206kBTU/ft<sup>2</sup>/year) with a standard deviation of 25kBTU/ft<sup>2</sup>/year for the baseline, while with the packaged solution the mean site EUI reduced to 139kBTU/ft<sup>2</sup>/year with a standard deviation of 19kBTU/ft<sup>2</sup>/year. Energy use in this building with baseline system is found to be most sensitive to parameters related to equipment load and schedules, lighting power density and occupancy schedule, supply conditions, cooling equipment efficiency, fan power, and wall/roof thermal properties. With the packaged system the building shows different order of sensitivity to most of these parameter, and becomes additionally more sensitive to external weather conditions.

Usage	Cafeteria
Climate	Mild/Humid
Square Footage	27800
#Floors	1
Peak Occupancy	300
Schedule	98hrs, Open WD & WE
Glass	4%, Multi layer, Not reflective, not tinted
Wall	rick, air layer, rigid insulation, CMU, air layer, gypsum
Roof	shingle, felt underlayment, plywood, nailbase insulation, steel
HVAC Type	<ul style="list-style-type: none"> <li>•CAV Multizone</li> <li>•Air-cooled Electric Chillers</li> <li>•Gas Heating</li> </ul>

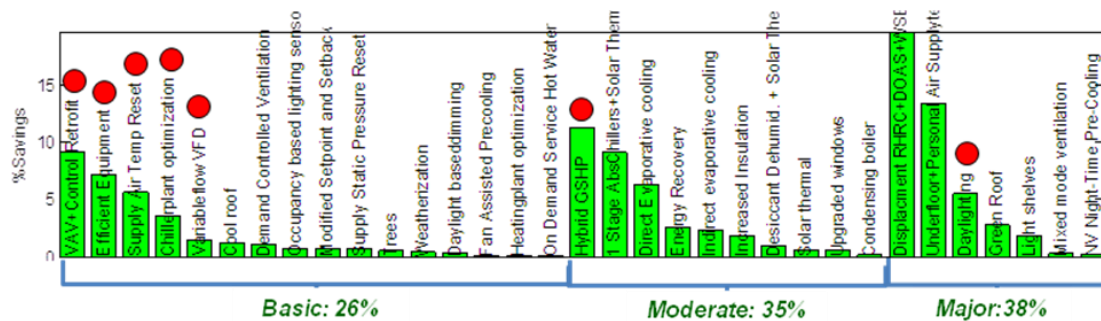


Figure 3.1.21: Site energy savings for different ECM's. ECMs marked with red circles are used to assemble a package.

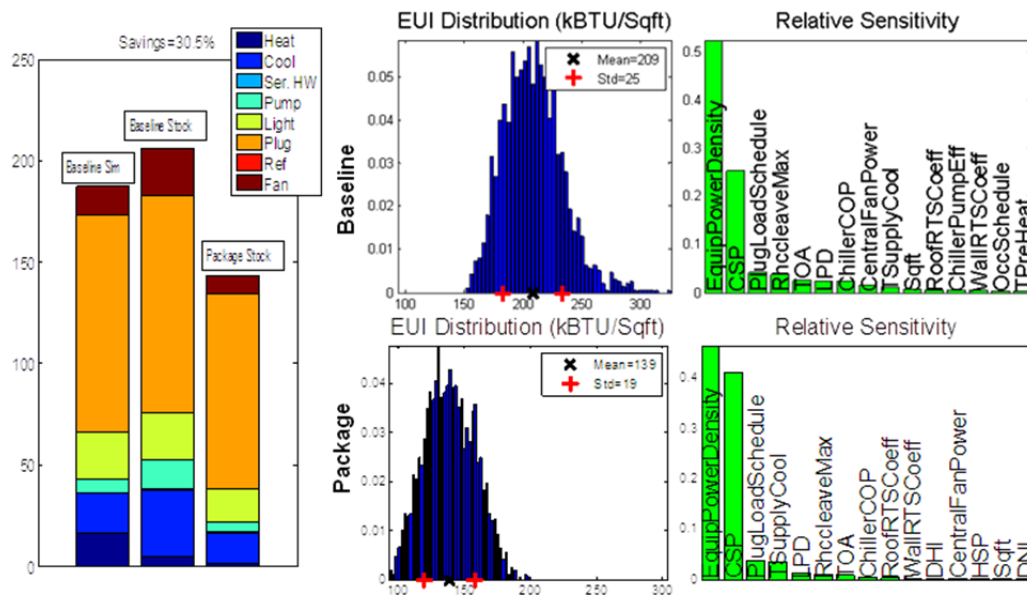


Figure 3.1.22: On left is shown site energy savings from assembled package broken by end use type. On right are shown results of UQ/SA for the building with the baseline and packaged system

### 3.1.3-2f) Building 1520, Fort Detrick

Building 1520 two-story building constructed in the 1990's at Fort Detrick which is an Army base located in central Maryland in Fredrick. The building originally had mixed use: Classroom, training center (with computers), assembly space, administrative office, library, café credit union and tenant space for local Goodwill. Initially built as a commissary (a store for solders that provides goods such as groceries and household supplies), it was later converted to an administrative office space. Based on the data collected during the audit (see section 3.2), overall, it cannot be overstated that the energy consumption in building 1520 is much greater than buildings of similar type and size. During the site visit, the root cause of the excessive energy consumption was not determined. Therefore, we did could validate the stock model in this case.

Figure 3.1.23 shows the site energy saving reduction due to application of different ECM's. The basic, moderate and major package on an average saves 42%, 63% and 78%, respectively. A package comprising of *Upgraded lighting and delamping*, *Modified setpoints/setback*, *Weatherization*, *Supply static pressure reset*, *Occupancy based lighting sensor*, *Hybrid GSHP* and *Daylighting* was chosen for this building. Figure 3.1.24 on left shows the site energy saving of 64.3% with assembled package. The source energy savings was around 54.9%. Figure 3.1.24 on right also shows the distribution of total energy consumption for the facility with baseline and packaged system. The mean site EUI was 61kBTU/ft<sup>2</sup>/year (nominal value being also 61kBTU/ft<sup>2</sup>/year) with a standard deviation of 12kBTU/ft<sup>2</sup>/year for the baseline, while with the packaged solution the mean site EUI reduced to 23kBTU/ft<sup>2</sup>/year with a standard deviation of 5kBTU/ft<sup>2</sup>/year. Energy use in this building with baseline system is found to be most sensitive to parameters such as internal heating and cooling setpoints/setbacks, heating equipment efficiency, lighting and equipment loads, fan power and envelope parameters such as roof/wall conduction and infiltration rate. With the packaged system the building shows sensitivity to similar parameters but in different order.



Usage	Office
Climate	Mild/Humid
Square Footage	21277
#Floors	2
Peak Occupancy	107 (Guess)
Schedule	66hrs, Open WD & WE
Glass	5% Multi Layer, Not tinted, Not reflective (Guess)
Wall	Brick, stone, or stucco
Roof	Plastic/rubber/synthetic sheeting
HVAC Type	<ul style="list-style-type: none"> <li>•Package VAV</li> <li>•Electric DX Air to Air</li> <li>•Gas Heating</li> </ul>

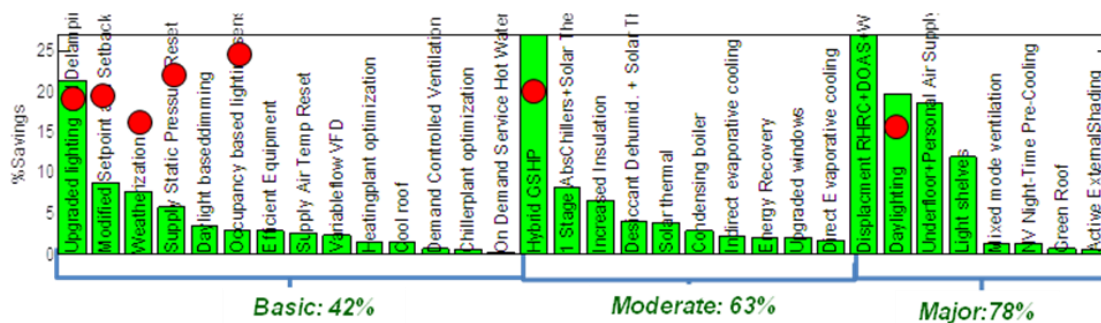


Figure 3.1.23: Site energy savings for different ECM's. ECMs marked with red circles are used to assemble a package.



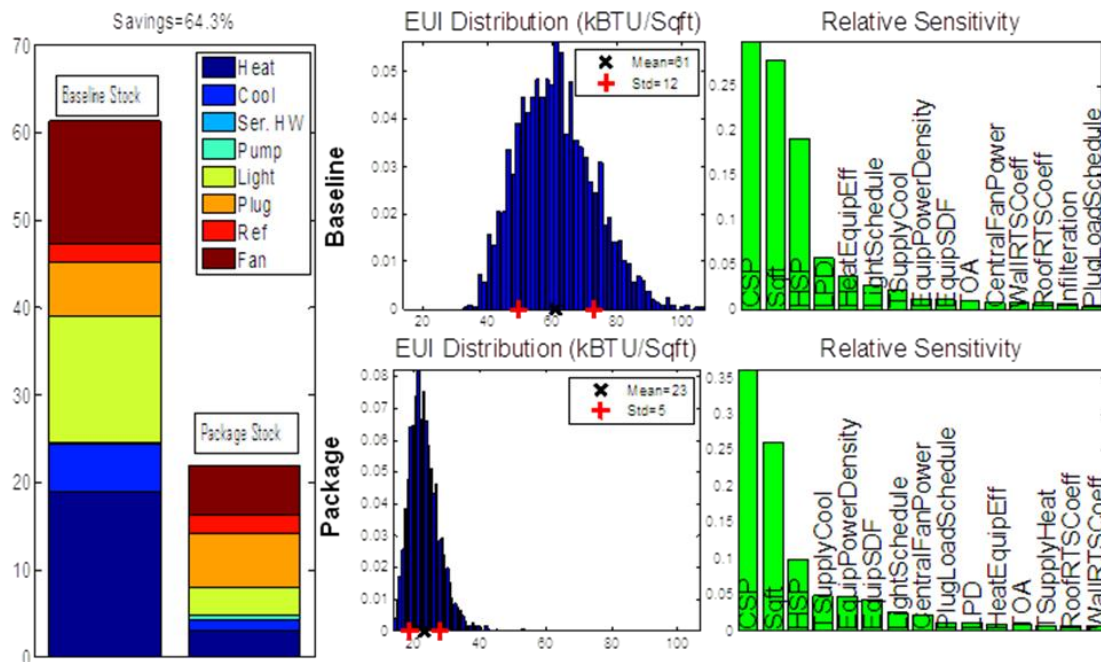


Figure 3.1.24: On left is shown site energy savings from assembled package broken by end use type. On right are shown results of UQ/SA for the building with the baseline and packaged system

### 3.1.4 Summary and Recommendations

We have summarized the tool chain for energy modeling and low energy retrofit screening. This tool chain addresses several gaps in current retrofit procedure. We also presented results demonstrating the use of the tool chain in predicting potential retrofit energy savings for the DOD stock. We also demonstrated the stock tool for multiple specific sites, where detailed building data was available, representing a range of building types and climates, i.e. Naval Station Great Lakes (IL), Ft. Carson (CO), Ft. Detrick (MD), Ft. Bragg (NC) and Ventura Naval Base (CA).

The key next steps are described below (shown schematically in Figure 3.1.25):

- **Installation and Building Survey and Audit**
  - Field surveys and energy use data gathering in a larger number of buildings spanning diverse use types in DoD stock
  - Metered data from a larger sample of buildings
- **Stock Tool Enhancement and Validation**
  - Replace estimates of several model inputs with actual values from surveys
  - Improve system thermal and energy performance modeling
  - Integrate analytical tools for uncertainty and sensitivity analysis
  - Validate models with monthly, annual energy consumption data from installation(s)
  - Integrate a user interface to analyze applicability of different system configurations prioritized by energy performance as well as economic parameters

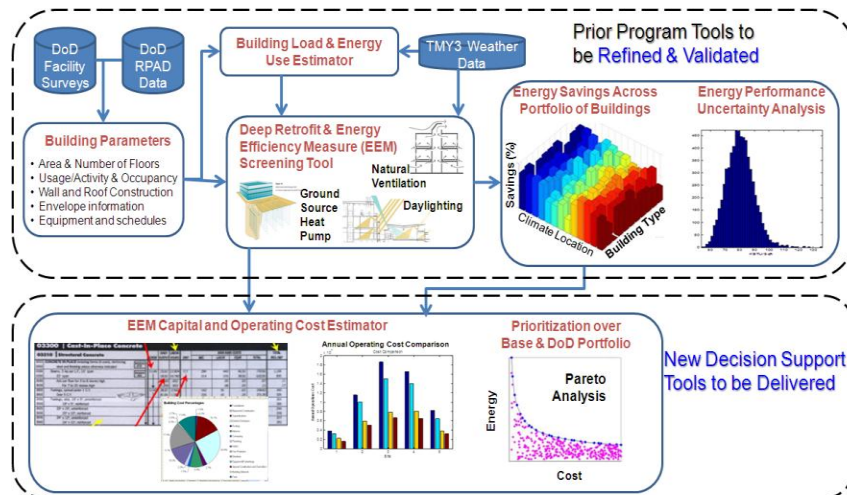


Figure 3.1.25: Summary of accomplishments in this program and proposal for enhancements in next phase

- Economics Modeling and Analysis**
  - Provide baseline building model first and non-energy operating cost parameters by mapping model to those in other relevant DoD cost tools
  - For ECM's found in available costing tool, create a mapping to provide first and non-energy operating cost parameters for implementation of the measures
- Portfolio Planner Tool Implementation and Prototyping**
  - Exercise process and toolchain in DoD installation(s)
  - Assess energy and economic benefits of various energy conservation measures for each building across the entire installation or subset of buildings
  - Provide a capital planning priority for economically attractive projects with positive NPV, while fulfilling compliance with energy mandates
  - Benchmark tool with other existing tools with similar functionality (e.g., FEDS) and identify opportunities for continuous improvement
  - Gather stakeholder feedback early and late in program with a prototype tool

## 3.2 DoD Building Audit and Energy Efficient Retrofit Measure Identification

### 3.2.1 Overview

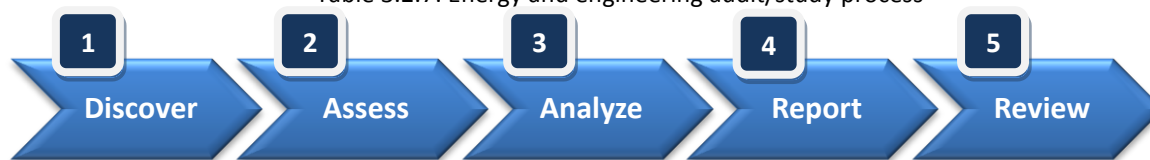
A series of energy audits and engineering studies on selected DoD (Department of Defense) facilities support a research program focused on devising tools and processes to effect large-scale comprehensive energy efficiency improvements across the DoD facilities portfolio. Each study assesses the current energy performance of the selected building(s) at a military base, identifies opportunities to improve performance, and estimates the potential impact as well as the cost required to implement the improvements.

### 3.2.2 Process

The general process applied is depicted in the table below and involved a series of activities focused on discovery and analysis. Discovery involved the collection of detailed building attributes

and information. This was followed by analysis to identify, develop and quantify energy performance improvements.

Table 3.2.7: Energy and engineering audit/study process



Stage	Activity
<b>1 Discover</b>	<ul style="list-style-type: none"> <li>Collect information on the site/building and its mechanical and electrical systems</li> <li>Collect and review project information including as-built drawings, submittals, control sequences, submittals, and utility bills</li> </ul>
<b>2 Assess</b>	<ul style="list-style-type: none"> <li>Engineering walk-through and audit, including survey and inspection of all building systems</li> <li>Interview building operator(s), energy manager, and/or facility manager</li> <li>Site observations, notes and photography</li> <li>Deployment of data loggers to collect data on space conditions and system and equipment operation</li> </ul>
<b>3 Analyze</b>	<ul style="list-style-type: none"> <li>Energy performance benchmarking</li> <li>Identification and development of potential energy conservation measures</li> <li>Further on-site engineering study if required</li> <li>Energy performance improvement and economic analysis</li> </ul>
<b>4 Report</b>	<ul style="list-style-type: none"> <li>Report development and submittal</li> </ul>
<b>5 Review</b>	<ul style="list-style-type: none"> <li>Evaluation of results</li> <li>Review and revision of analysis and report</li> </ul>

Assessment was typically a multi-step iterative process with incrementally deeper rounds of on-site surveys. Not all information could be practically gathered at the first visit, and most sites required two to three on-site visits. To develop a more detailed understanding the work content, key tasks are described further.

**Initial Study/Assessment:** Initial assessment involved a day of on-site walk-through and observation with some follow-up work to document the project. The most important aspects of the initial assessment were to establish a basic understanding of the building and its systems as well as its potential for energy performance improvements.

**Benchmarking:** Energy performance benchmarking, while not very time consuming, is a keystone task because it establishes the basis for quantification of energy performance improvements. Multiple years of historical utility data for all energy sources is necessary to establish baseline energy performance.

**Energy and Engineering Study:** The most time and labor-intensive part of the process is the energy and engineering study. Sub-tasks include detailed survey of the building and its systems, deployment of data loggers, identification and analysis of energy conservation measures, and report development.

Table 3.2.8: Key tasks and work content

Task	Time Required	Work Content
<b>Initial Assessment</b>	<ul style="list-style-type: none"> <li>1 day on site</li> <li>2-4 days follow up work</li> <li>Typically, 40 to 60 hours</li> </ul>	<ul style="list-style-type: none"> <li>Gathering facility information</li> <li>On-site interview and walk-through</li> <li>Compilation of notes and observations</li> </ul>






	<ul style="list-style-type: none"> <li>• Calendar time: 10 days</li> </ul>	
<b>Benchmarking</b>	<ul style="list-style-type: none"> <li>• Typically, 8 hours</li> </ul>	<ul style="list-style-type: none"> <li>• Gathering utility bills and data</li> <li>• Analysis and comparison to benchmark</li> </ul>
<b>Engineering Study</b>	<ul style="list-style-type: none"> <li>• 1-2 days on site</li> <li>• 4-6 weeks follow up work</li> <li>• Typically, 130 to 250 hours</li> <li>• Calendar time: 4-6 weeks</li> </ul>	<ul style="list-style-type: none"> <li>• Gathering detailed facility information</li> <li>• On-site detailed survey</li> <li>• Installation of data loggers</li> <li>• Extensive observations, including notes and photography</li> <li>• Compilation of notes and observations</li> <li>• ECM identification and analysis</li> <li>• Report development</li> </ul>

### 3.2.3 Case Studies

The five projects studied using the process described above are listed in the table below. Subsequent tables summarize the existing systems in place and the energy efficiency measures proposed for each project.

Table 3.2.9: Buildings overview

Building		Location	Floor Space (square feet)
<b>Naval Station Great Lakes Atlantic Fleet Drill Hall Building 7230</b>		Naval Station Great Lakes, Illinois	69,218
<b>Fort Carson Building 1225</b>		Fort Carson, Colorado	22,175
<b>Fort Detrick Building 1520 Community Assembly Center</b>		Fort Detrick, Maryland	21,277

Building		Location	Floor Space (square feet)
Fort Bragg 3 <sup>rd</sup> Brigade Combat Team Dining Facility		Fort Bragg, North Carolina	30,000
Naval Base Ventura County Building PH1000		Port Hueneme, California	68,400

Table 3.2.10: Building systems

Building	Mechanical (HVAC)	Electrical (Lighting)	Controls
<b>Naval Station Great Lakes Atlantic Fleet Drill Hall Building 7230</b>	<ul style="list-style-type: none"> <li>• Air-cooled chillers</li> <li>• Four VAV air handling units               <ul style="list-style-type: none"> <li>○ Each with demand control ventilation, full economizer and VFDs</li> <li>○ Only two or three are in regular use</li> </ul> </li> <li>• Heat supplied by district steam</li> </ul>	<ul style="list-style-type: none"> <li>• High bay metal halide lighting for the drill deck, 400 Watts per fixture</li> <li>• Light levels average 40 FC</li> <li>• T5 / T8 fluorescent lighting in offices and classrooms</li> <li>• Lighting levels average 50 FC</li> <li>• Motion sensors in large restrooms, and switches for all other lighting</li> </ul>	<ul style="list-style-type: none"> <li>• Siemens Apogee building automation system</li> </ul>
<b>Fort Carson Building 1225</b>	<ul style="list-style-type: none"> <li>• AHUs: Most of the building is heated and cooled by two constant-volume multi-zone AHUs.</li> <li>• Cooling: District chilled water</li> <li>• Heating: Hot water heating provided by stand-alone gas-fired boilers with constant volume pumping</li> <li>• Auxiliary heating and cooling               <ul style="list-style-type: none"> <li>○ Unit heaters provide auxiliary heat in the entry vestibules</li> <li>○ Three split systems serve computer rooms and meeting spaces</li> </ul> </li> </ul>	<ul style="list-style-type: none"> <li>• Lighting is primarily T8 32W fluorescent.</li> </ul>	<ul style="list-style-type: none"> <li>• Limited building automation</li> <li>• DDC control overlaid on pneumatic actuators</li> </ul>
<b>Fort Detrick Building 1520</b>	<ul style="list-style-type: none"> <li>• Multiple VAV air handling units with DX cooling.</li> <li>• One constant volume air handling unit.</li> <li>• Three rooftop units with DX cooling.</li> <li>• Hot water boilers provide heating.</li> </ul>	<ul style="list-style-type: none"> <li>• Lighting is primarily T8 32W fluorescent.</li> </ul>	<ul style="list-style-type: none"> <li>• Johnson Controls Metasys (first floor)</li> <li>• Invensys (second floor)</li> </ul>
<b>Fort Bragg 3<sup>rd</sup> Brigade Combat Team Dining Facility</b>	<ul style="list-style-type: none"> <li>• Multiple constant volume air handling units</li> <li>• Plus, one multi-zone air handling unit</li> <li>• Kitchen ventilation exhaust fans with make-up air units</li> <li>• Air-cooled chiller supplies chilled water</li> </ul>	<ul style="list-style-type: none"> <li>• Lighting is primarily T8 fluorescent.</li> </ul>	

Building	Mechanical (HVAC)	Electrical (Lighting)	Controls
<b>Naval Base Ventura County Building PH1000</b>	<ul style="list-style-type: none"> <li>Boiler supplies hot water</li> <li>A large industrial-type air handling unit serves interior zones.</li> <li>Fan coils serve offices and many perimeter areas.</li> <li>All fan coils have heating coils.</li> <li>Only three rooms in the building have mechanical cooling where fan coils have chilled water coils, including:</li> <li>Air-cooled chiller supplies chilled water.</li> <li>Two boilers provide hot water.</li> </ul>	<ul style="list-style-type: none"> <li>Office lighting fixtures are parabolic 18-cell with 3 30 Watt lamps each.</li> <li>Down lights are fitted with 2 18 Watt CFLs.</li> <li>Lobby lighting fixtures are refitted with LED (LR24, 54 Watts each).</li> <li>Some lighting is on occupancy sensors.</li> </ul>	<ul style="list-style-type: none"> <li>Barber-Coleman Network 8000 system</li> <li>Limited to monitoring only at the operator's station.</li> </ul>

Table 3.2.11: Potential energy conservation measures by building

Building	Mechanical (Envelope, HVAC)	Electrical (Lighting)	Controls
<b>Naval Station Great Lakes Atlantic Fleet Drill Hall Building 7230</b>	<ul style="list-style-type: none"> <li>Enforcement of base setpoints: 68°F winter and 78°F summer.</li> <li>Interlock overhead doors to AHU operation allowing doors to be opened for natural ventilation and disabling of mechanical cooling.</li> <li>Revise or replace the steam meter for accurate measurement of usage. Network-enable and connect power and steam meters and deploy a program for regular data collection and analysis.</li> <li>Replace the current steam domestic hot water heating system with an electric water heater, which would be scheduled based on occupancy. Domestic hot water usage in the building is low</li> </ul>	<ul style="list-style-type: none"> <li>Retrofit arena lighting from metal halide to high bay fluorescent.</li> <li>Deploy lighting control in the arena for both daylight harvesting (variable light levels) and occupancy sensing. Split the drill deck into zones and allow them to be controlled and run independently.</li> <li>Reprogram or disable blind controls in the arena to maximize daylight and minimize solar gain.</li> <li>Eliminate halogen lighting in the entry area for the display cases.</li> <li>Utilize occupancy-based control for the arena allowing the unit(s) to go into unoccupied mode when space is not in use. Evaluate options to split the hall</li> </ul>	

Building	Mechanical (Envelope, HVAC)	Electrical (Lighting)	Controls
	<p>and this option would allow for steam to be shut off during warm weather.</p> <ul style="list-style-type: none"> <li>• Properly schedule office areas and conference room based on actual occupancy or use occupancy-based controls.</li> <li>• Evaluate the control system for improvements. Areas to focus on may include reset schedules, ventilation strategy using demand-control ventilation, static pressure reset for office areas, and chiller plant optimization.</li> </ul>	<p>into north and south zones (using existing isolation dampers) and only condition the one that is in use.</p> <ul style="list-style-type: none"> <li>• Add occupancy sensors for lights in the offices and other spaces. Occupancy sensors are currently only in place in the recruit heads (or bathrooms).</li> <li>• Use daylight harvesting in the head entry areas, which have windows.</li> </ul>	
<b>Fort Carson Building 1225</b>	<ul style="list-style-type: none"> <li>• Convert multi-zone AHUs to VAV</li> <li>• Space temperature control per zone</li> <li>• Variable chilled water flow</li> <li>• Schedule domestic hot water pumping</li> </ul>	<ul style="list-style-type: none"> <li>• Occupancy-based control of lighting</li> <li>• Re-lamp where necessary to 28W T5 bulbs</li> </ul>	<ul style="list-style-type: none"> <li>• Overlay existing controls, or retrofit fully to DDC controls, including electronic actuators and valves</li> </ul>
<b>Fort Detrick Building 1520</b>	<ul style="list-style-type: none"> <li>• Retro-commission constant volume unit.</li> <li>• Retro-commission boilers</li> <li>• Schedule domestic water heater operation</li> </ul>	<ul style="list-style-type: none"> <li>• Control ancillary loads (snack machines)</li> <li>• Standardize number and type of lamps and ballasts throughout building.</li> <li>• De-lamp first floor corridors to reduce lighting level to meet code minimum.</li> <li>• Install daylighting sensors and/or dimmable fixtures near the windows in library.</li> <li>• Schedule and/or reduce exterior lighting.</li> </ul>	<ul style="list-style-type: none"> <li>• Replace controls for three air handler and VAV boxes and commission HVAC and control systems.</li> </ul>
<b>Fort Bragg 3<sup>rd</sup> Brigade Combat Team Dining Facility</b>			
<b>Naval Base Ventura County Building PH1000</b>	<ul style="list-style-type: none"> <li>• Conversion of the constant volume AHU to variable-air-volume with variable speed drives.</li> <li>• Application of window interlocks to deactivate fan coils when windows are</li> </ul>	<ul style="list-style-type: none"> <li>• Lighting retrofit and lighting controls.</li> </ul>	

Building	Mechanical (Envelope, HVAC)	Electrical (Lighting)	Controls
	open.		
<b>Notes:</b>			

Table 3.2.12: Summary of projected improvement by building

Building	Current EUI (kBtu/ft <sup>2</sup> )	Projected EUI (kBtu/ft <sup>2</sup> )	Improvement (%)	Estimated Savings (\$)	Estimated Cost (\$)	Payback (Years)
Naval Station Great Lakes Atlantic Fleet Drill Hall Building 7230	97.1	78.3	19.4%	\$22,394	\$34,450	1.5
Fort Carson Building 1225	100.9	90.0	10.8%	\$3,328	\$63,528	19.1
Fort Detrick Building 1520						
Fort Bragg 3 <sup>rd</sup> Brigade Combat Team Dining Facility						
Naval Base Ventura County Building PH1000	65.6	53.4	18.7%	\$34,799	\$225,850	6.5
<b>Notes:</b>						

### 3.2.4 Overall Results and Conclusions

The energy audit and engineering study process demonstrated potential energy usage reductions ranging from 11% to nearly 20% on the three projects that yielded final results. For relatively small and simple facilities with conventional mechanical and electrical systems, this is a reasonable range of energy performance improvement employing standard practical techniques and available technologies. Corresponding economics of the various energy performance improvements spanned a wide range of paybacks depending on the complexity and effectiveness of the proposed improvements. Table 3.2.6 above tabulates energy performance improvements and the associated savings, cost and payback.

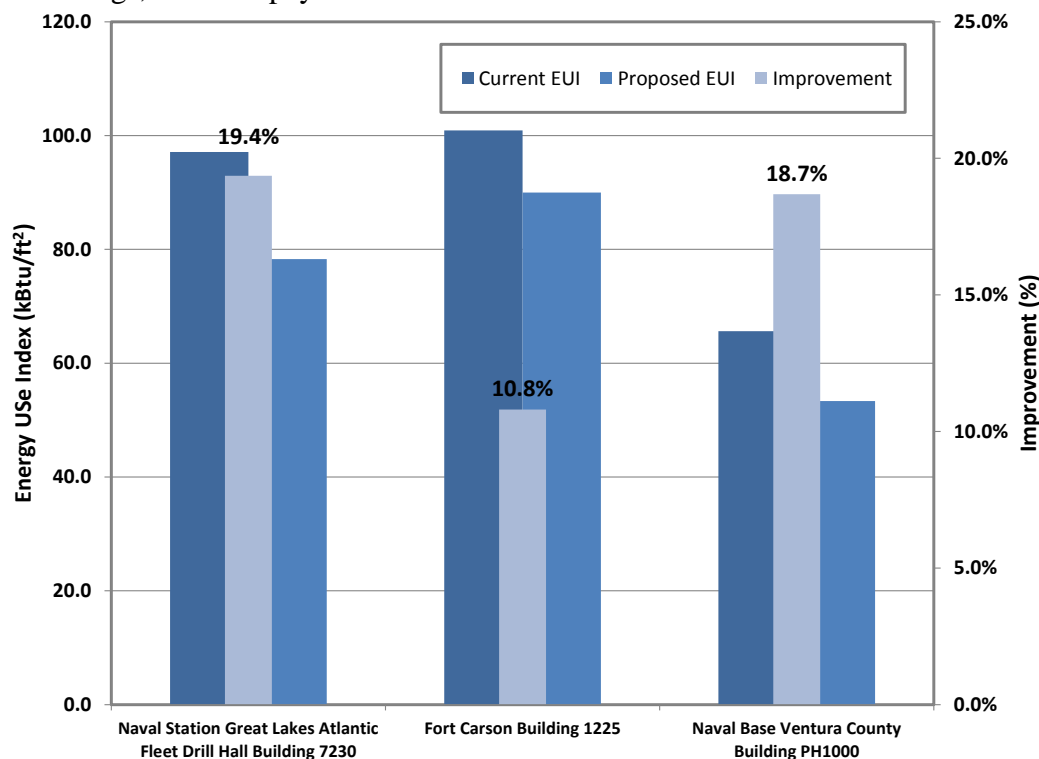


Figure 3.2.2 EUI improvements projected by the energy engineering studies

### 3.2.5 Common Observations and Challenges

Common observations and challenges across the five projects illustrate issues that may apply on a large scale to many DoD facilities.

**Documentation:** Obtaining complete documentation was frequently a challenge, but generally could be achieved with persistent efforts. However, documentation was often not up to date and had to be reconciled with the facility in its current state of operation.

**Systems in disrepair:** On some of the sites, systems in disrepair or non-functional states were obstacles to completion of the study. For example, at the Fort Bragg dining facility, non-functional kitchen ventilation systems did not allow for the building to be studied as it would normally operate. During on-site visits, it was also not clear for how long the system was not working, who had ownership of its repair, or when it might actually be repaired.

**Ownership of facilities:** For some of the facilities, there was no clear ownership of the facility from a facilities management perspective. While our contact was typically through energy management, the energy manager often did not have any ownership or responsibility for the facility itself. In commercial and institutional facilities (outside of the military), a facility manager, building operator, or similar role, is often responsible for the building. They also typically have some knowledge of the building's history, systems, and operation that can be tapped. Such a resource did not generally exist for the facilities studied as part of this research effort.

### 3.2.6 Lessons Learned

Lessons learned include considerations that would improve the effectiveness of the energy study and engineering process.

**Site selection:** In some cases, site selection was not properly reviewed prior to proceeding with site survey work. The absence of energy data with which to establish a benchmark, or whole systems in a state of disrepair were obstacles encountered that could have been avoided through more careful site selection.

**On-site effectiveness:** Over the course of conduct of the five site studies, it became increasingly evident that much of each study's success hinged on the effectiveness and completeness of on-site work. This consisted of thorough interviews of staff combined with detailed site survey work focused on capturing a complete and detailed picture of the facilities current state and operation. Through the experience gained on the five projects, optimized on-site practices could be developed and standardized for future work.

### 3.3 Whole Building Energy Performance Simulation

The objective of this task is to create whole building energy models for selected DoD buildings. These energy models are used as: 1) the baseline for validating the stock analysis tool, 2) a platform for evaluating performance of low-energy retrofit options provided by the stock analysis tool, and 3) computational backbones to generate data for UA/SA and FMEA study.

Criteria and guidelines for the assessment of simulation tools for low energy (high performance) building systems were developed and are described in Appendix B. The suitability of available energy simulation tools for the project was evaluated using EnergyPlus, TRNSYS and Dymola/Modelica. A medium-sized office building from DOE benchmarks was modeled in EnergyPlus and TRNSYS. Low energy systems including radiant heating, ground source heat pump and chilled beams were modeled and analyzed; details provided in Appendix B. The schematic for modeling evaluation is depicted in Figure 3.3.1. Whole building energy simulations for the DoD use cases considered were performed using EnergyPlus and TRNSYS due to their relative ease of use and flexibility for the analysis required. TRNSYS enables the required flexible use of component models and controls and EnergyPlus has a comprehensive library for both building envelope and HVAC component/system.



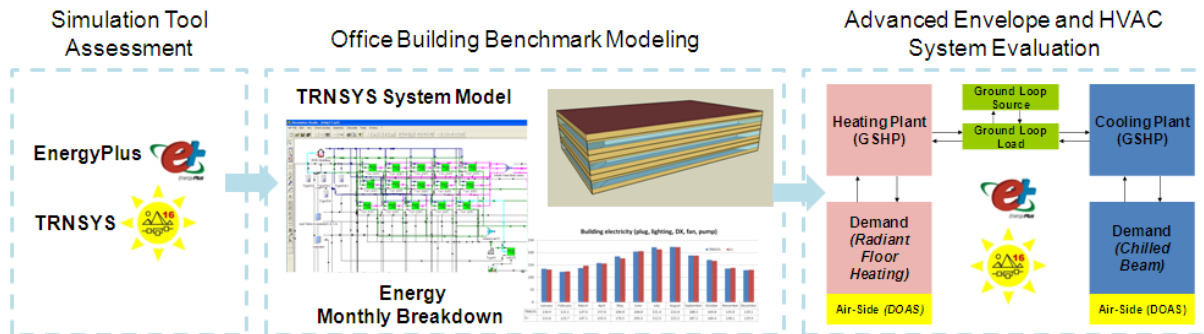


Figure 3.3.10 Schematics for Modeling Evaluation

EnergyPlus is a whole-building simulation program developed by the U.S. Department of Energy (Crawley et al., 2000). It models heating, cooling, lighting, and ventilating processes, as well as water usage in buildings, and includes many innovative simulation capabilities such as time steps of less than one hour, modular systems, multizone airflow, thermal comfort, water use, and natural ventilation. An EnergyPlus model takes as inputs a description of the building (e.g., geometry, materials, roof type, window type, shading geometry, location, orientation), its usage and internal heat gains (as a scheduled function of time), and the HVAC equipment and system description (e.g., chiller performance, air and water loop specifications), and then computes the energy flows, zonal temperatures, airflows, and comfort levels on sub-hourly intervals for periods of days to years.

TRNSYS is an energy simulation program whose modular system approach makes it one of the most flexible tools available. TRNSYS (TRaNsient SYstem Simulation Program) includes a graphical interface, a simulation engine, and a library of components that range from various building models to standard HVAC equipment to renewable energy and emerging technologies. TRNSYS also includes a method for creating new components that do not exist in the standard package. This simulation package has been used for more than 30 years for HVAC analysis and sizing, multizone airflow analyses, electric power simulation, solar design, building thermal performance, analysis of control schemes, etc.

### 3.3.1 Modeling Procedure

- Target building

The modeling process starts with selecting a representative building in a DoD base. The audit team worked with Facility department of a base to identify a building, which is typical in terms of usage and building/HVAC configuration.

- Design and as-built information

Design information, including design drawings and manufacturers' catalogs, are collected as much as possible. The data will be used for creating models. A walk-through energy audit is conducted to acquire operation data such as monthly utility bills if available, ground-truth information that are different from the design documents such as the number of light fixtures and type of indoor equipment.

- Data acquisition

Additional sensors may be deployed to capture more operation data that are not available from the existing building energy management system, such as plug power, actual lighting schedule,

fan power, etc. The data will be used to determine time-based internal heat gains, and to validate a baseline model.

- Models

There are two types of models: baseline and an advanced building system with multiple low-energy features.

The acquired information above is used mainly for creating and validating a baseline building model, which simulates the energy performance of a target building in as-built conditions. The parameters in the baseline model are tuned to have the predicted monthly energy usage match the measured data as close as possible. The uncertainty and sensitivity study plays a key role in this validation process. Simulations are set to run 8760-hours with a sub-hour time step. Note that a baseline model may not be validated due to lack of operation data.

The advanced building system model is built upon the baseline. The stock analysis tool is run first to identify a set of low-energy feature candidates, which are able to significantly reduce energy consumption. Then the baseline model is revised to accommodate these candidates.

Table 3.3.1 below lists the modeled buildings.

Table 3.3.4 5 Modeled Buildings in DoD bases

	Building 7230	Building 26	Building 1225
Location	Great Lakes	Great Lakes	Ft. Carson
Modeling tool	EnergyPlus	EnergyPlus	TRNSYS
Validation of baseline	Yes	Yes	No
Advanced system	No	Yes	Yes

### 3.3.2 DoD Case Studies: Results and Discussion

#### EnergyPlus modeling of Drill Hall

Building 7230 (Atlantic Fleet Drill Hall) at the Naval Station Great Lakes, Great Lakes, Illinois was modeled in EnergyPlus. The Drill Hall is a two-storey facility with a drill deck, offices, and administrative rooms. The gross area of this building is approximately 69,218 ft<sup>2</sup>. Figure 3.3.2 shows the exterior and interior outlook for this building.

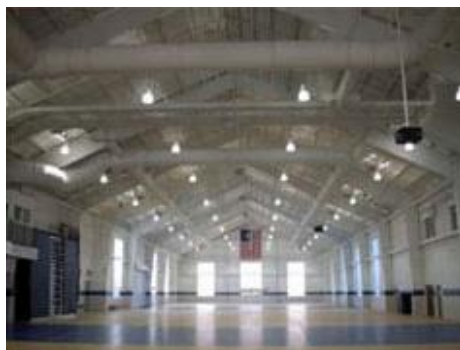


Figure 3.3.11 Drill Hall building at the Navy Station Great Lakes

The Drill Hall HVAC system consists of four airside subsystems and two separate waterside subsystems. The Drill deck is supplied by two variable-air volume (VAV) air handling units (AHU) with heating and cooling capability, and a classroom on the second floor is served by one VAV

air handling unit. Operation of these units depends on the occupancy of the Drill deck space. Double-walled sheet metal ductwork with a perforated liner and drum louvers distribute the air throughout the space. The office and administrative area is served by one VAV air handling unit with VAV terminal units (with hot water reheat). The chilled water system consists of two 110-ton air-cooled rotary-screw type chillers with fixed-speed primary pumping and variable-speed secondary pumping. Heating is supplied from the existing campus-wide steam system through a steam-to-water heat exchanger. The hot water serves unit heaters, VAV box reheating coils, and air handling unit heating coils. There is an instantaneous steam-to-domestic hot water generator for domestic hot water service. The server room and communication service room are served by dedicated duct free split systems. A distributed Direct Digital Control (DDC) control system is installed in this building which monitors all major environmental systems. Building electric and water meters are also read by the DDC system. Operator workstations provide graphics with real-time status for all DDC input and output connections. An EnergyPlus baseline energy model on the Drill Hall was developed. Comparisons between the 2009 utility bill and calibrated EnergyPlus energy predictions are shown in the barcharts below. The plot on the left-hand side of Figure 3.3.3 is steam consumption, the right is electricity. The cases are presented here – using TMY3 weather data and using real-time measured weather data (except solar data).

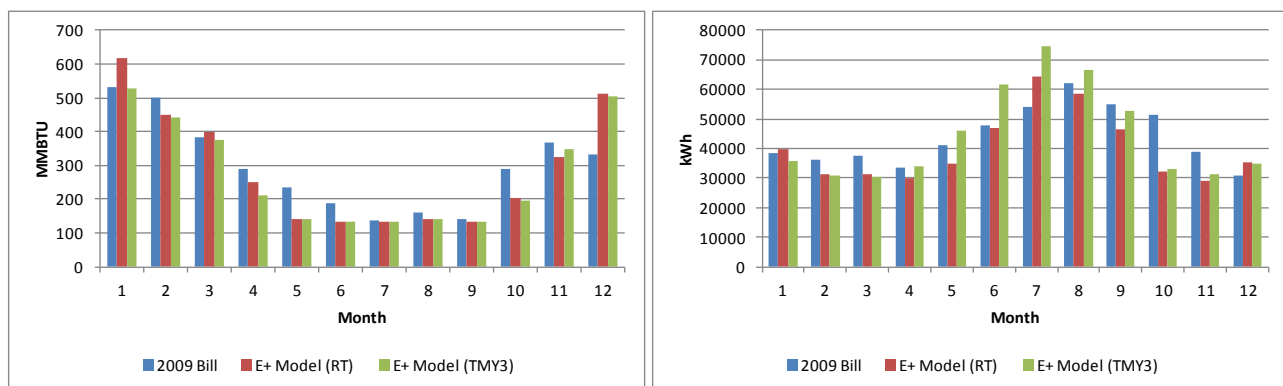


Figure 3.3.12 Comparisons of 2009 utility bill and energy prediction with EnergyPlus model in Drill Hall

### EnergyPlus modeling of Building 26

#### **Baseline case**

Building 26, Fleet and Family Support Center (FFSC)/Navy Marine Corps Relief Society (NMCRS), is located at Naval Training Center, Great Lakes, IL. It is a two-storey office building with basement. The gross area of this building is approximately 37,000 ft<sup>2</sup>. Figure 3.3.4 shows the outlook of this building.



Figure 3.3.13 Building 26 outlook

The Building 26 HVAC system consists of two airside systems and two separate waterside systems. The office and administrative area on the first and second floors is served by two variable-air volume (VAV) Air Handling Units (AHU) with VAV terminal unit (with hot water reheat) heating and cooling capability. These AHUs have both heating and cooling capability. Operation of these units depends on the occupancy of the building. The chilled water system consists of one 54.5-ton air-cooled rotary-screw type chillers with fixed-speed primary pumping. Heating is supplied from the existing base-wide steam system through a steam-to-water heat exchanger. The hot water serves unit heaters, VAV box reheating coils, and air handling unit heating coils. The communication service room is served by one dedicated split system. Electric unit heater and baseboard are used to provide heating to stairwells and restrooms. Comparisons between the 2010 utility electricity bill and calibrated EnergyPlus energy predictions are shown in the bar charts below. The plot on the left-hand side of Figure 3.3.5 is plug electricity consumption, the right is total building electricity. The cases are presented here –using real-time measured weather data.

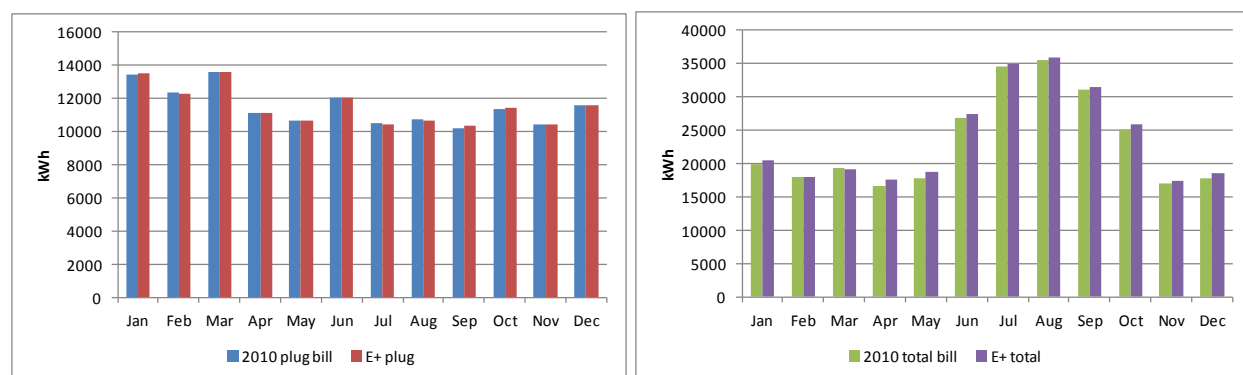


Figure 3.3.14 Comparisons of 2010 utility electricity bill and predictions with EnergyPlus model in Building 26.

### Advanced system

The stock analysis tool developed in this project was used to pre-select the high efficient system concepts, which are illustrated in the pareto plot below.

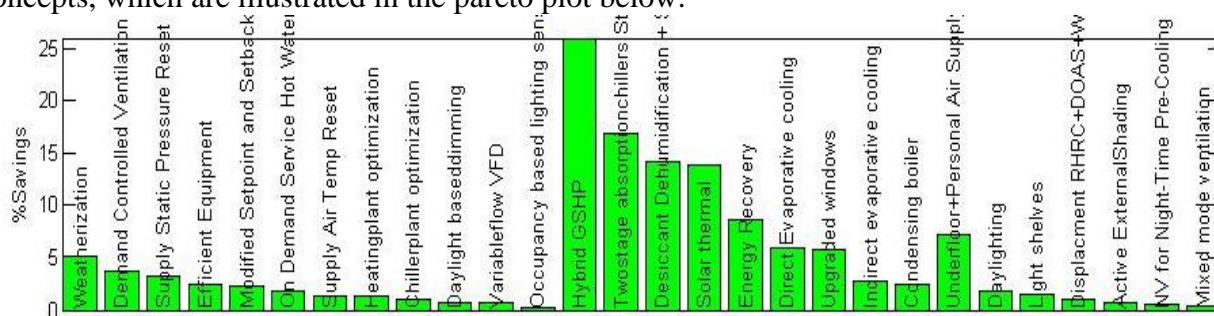


Figure 3.3.15 BLDG 26 high efficient system concepts chosen by stock analysis tool

The selected high efficient concepts include ground source heat pump systems, solar thermal heating for domestic hot water (DHW), efficient electrical equipment (plug), zone setpoint reset. The concepts modeled in baseline and the advanced systems are presented in Table 3.3.2.

Table 3.3.5 Comparisons of building systems between baseline and advanced EnergyPlus model for Building 26

Building System	Baseline	Advanced
Central VAV system	Y	Y
Air-cooled chiller	Y	-
District heating	Y	-
GSHP with supplemental district heat	-	Y
Single-pane windows	Y	-
Double-pane low-e windows with argon fill	-	Y
District heating DHW	Y	-
Solar thermal DHW with supplemental district heat	-	Y
Modified zone temperature setpoints	-	Y
Efficient electrical equipment	-	Y

The energy usage from different end use in both baseline and advanced systems is listed in Table 3.3.3. The energy savings is also presented in the last column. In summary, the energy usage index (EUI) is reduced by 35% by applying selected energy efficient concepts in Building 26.

Table 3.3.6 6 Energy consumption comparisons between baseline and advanced EnergyPlus model for Building 26

End use	Unit	Baseline	Advanced	$(ad-ba)/ba*100\%$
Heating	GJ	1258.	580.6	-53.8%
Cooling	GJ	164.3	69.95	-56.2%
Pump	GJ	40.04	123.4	228%
Fan	GJ	62.55	44.51	-30.1%
Lighting	GJ	127.4	127.4	0.0%
Plug	GJ	502.1	454.9	-9.4%
Total	GJ	2154	1400.	-35%
EUI	kBTU/ft2/year	55.2	35.9	-35%

#### TRNSYS modeling of Building 1225

Building 1225, as shown in Fig 3.3.7, is an administration and training facility selected by the audit team in Ft. Carson in Colorado Springs, CO.





Figure 3.3.16 Building 1225 in Ft. Carson

A partial set of design drawings were obtained from the base's facility department. As-built information was collected during an on-site audit. The building has one floor with an area of ~23000 ft<sup>2</sup>. It was originally built in 1970's, and has been through a few retrofits since then, for instance, docking areas on both ends of the building were remodeled to office space, and pneumatic controls were converted to DDC controls with pneumatic actuators. Two constant-air-volume multi-zone units serve the building for heating and cooling. The chilled water is supplied from a central plant in the base, and available between May and October. The hot water is provided by a gas-fired boiler in the building, and available between November and April, but can be turned on manually any time if heating is required. Domestic hot water is generated with a separate gas-fired boiler in the building. All the water pumps are of constant-speed, and 3-way valves are used to modulate the water flow rate through coils. The temperature of hot water for heating is adjusted based on ambient air temperature. The boiler is off when ambient temperature is above 70°F. The chilled water temperature is 48°F, and is off when ambient temperature is below 70°F. The air-side economizer is enabled when ambient temperature is below 70°F. The cold deck temperature is between 78°F and 55°F based on the warmest space temperature, the hot deck temperature is between 68°F and 120°F based on the coldest space temperature. Zones have a heating set point of 70°F and a cooling set point of 77°F. The night setback heating is set to 55°F. The building has auxiliary heating and cooling - unit heaters provide auxiliary heat in entry vestibules, and three split systems serve computer rooms and meeting spaces. The building is occupied between 6AM and 5PM Monday to Friday. The lighting is primarily T8 32W fluorescent. The audit team counted the number of lighting fixtures in each accessible room during the visit, and some missing information on lighting fixtures was retrieved from the available floor plan drawings. The peak lighting heat gain for each zone is then determined. The audit team measured the instantaneous plug and lighting loads of selected zones on the electrical panels, which showed the plug load was roughly 2 times of the lighting load. Thus the zonal plug loads in the models (both the baseline and the advanced system) are set to 200% of the baseline's zonal lighting load.

The design information on the building envelope is missing. Thus the envelope data representing typical buildings built in 1970's from a DoE's database were used in the model. The building geometry was measured during the on-site audit. Since the usage of the three split-systems is not scheduled, it is difficult to estimate its energy consumption. So they are not considered in the model. The chilled water usage is not metered and lacks historic data, so the model of this build-

ing cannot be validated. It was also noticed by the audit team that there are HVAC equipment on the roof of this building, which are neither shown in the available drawings nor known by our point of contact. Thus they are out of the scope of our modeling work. The baseline model in TRNSYS is shown in Fig 3.3.8.

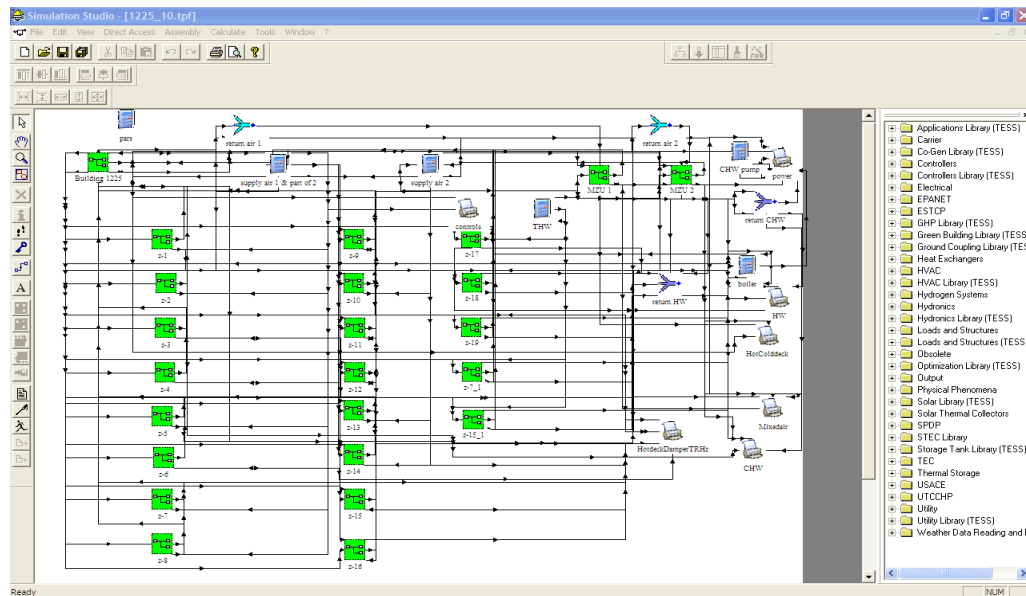


Figure 3.3.17 TRNSYS baseline model of Building 1225

Table 3.3.4 lists the simulated annual energy consumption of the baseline.

Table 3.3.7 Annual energy consumption of the baseline

Heating	GJ	403.9
Cooling	GJ	63.7
Pump	GJ	25.8
Fan	GJ	267.0
Lighting	GJ	249.2
Plug	GJ	580.5
total	GJ	1590.2
EUI	kBTU/ft <sup>2</sup> /year	80.9

The benchmark office buildings in CBECS have an average total energy consumption of 80.9 kBTU/ft<sup>2</sup>/year.

An advanced system for Building 1225 was built upon the baseline model with the low-energy features selected by running the stock analysis tool, which are:

- A direct evaporative cooler installed in each multi-zone unit.
- Replacing the constant-speed fans/pumps with variable-speed fans/pumps.
- A solar thermal collector installed on the roof to generate hot water for heating.

- Replacing T8 light fixture with T5, and lowering lighting power density from 1.58W/ft<sup>2</sup> to 0.8 W/ft<sup>2</sup>.
- Raising zonal cooling set point by 1.8°F, lowering heating set point by 1.8°F, and heating set back by 3.6°F.

Fig 3.3.9 shows the diagram of advanced HVAC system.

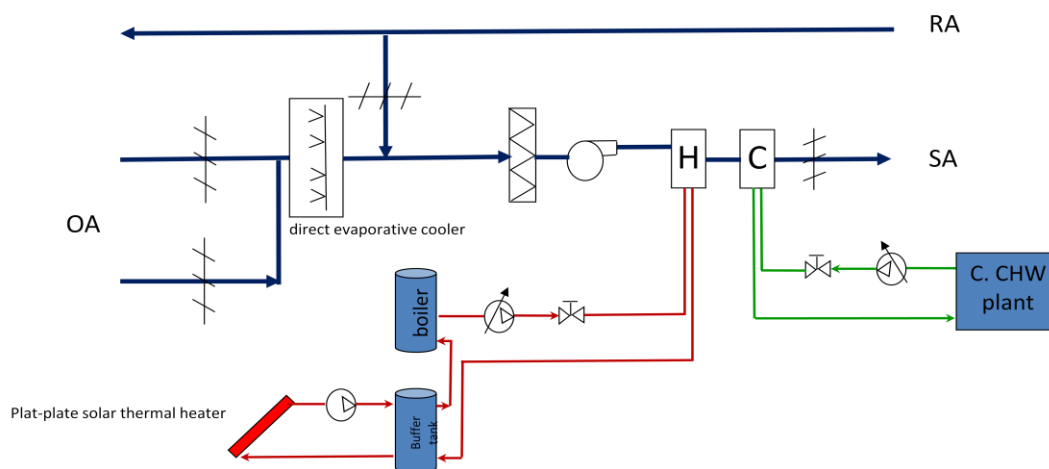


Figure 3.3.18 A diagram of the advanced system

Table 3.3.5 compares the annual energy consumption between the baseline and the advanced system. The advanced system can save 27.2% energy over the baseline.

		baseline	adv	(ad-ba)/ba*100%
Heating	GJ	403.9	234.7	-42%
Cooling	GJ	63.7	36.3	-43.0%
Pump	GJ	25.8	5.3	-80%
Fan	GJ	267.0	113.2	-57.6%
Lighting	GJ	249.2	167.0	-33%
Plug	GJ	580.5	580.5	0%
total	GJ	1590.2	1136.9	-28.5%
EUI	kBTU/ft2/year	80.9	57.8	-28.5%

In summary, the building simulation models are able to provide detailed energy consumption information, which enables studies in this project, for instance, the FMEA analysis, without costly physical experiments on a real building. The comparison between the baseline and advanced system reveals the impacts of low-energy features, and their strength and limitations.

### 3.3.3 Modelica-Based Building Energy Simulation and Dynamic Modeling Assessment

Current state of the art tools for simulating buildings, such as TRNSYS or EnergyPlus have some serious design flows. In particular, these tools often use models with a solver (or part of it) em-



bedded within. Adding new solvers to such tools requires rewriting entire component model library and it is not feasible for any practical purposes. Furthermore, having solver embedded in the component model implies certain assumptions on the coupling strength between the component and the rest of the system, and those assumptions may not be valid for every system configuration. This all raises concern whether present tools are good long term solutions for building simulations. Because of that, we investigated an alternative platform for buildings simulation based on Modelica programming language.

Modelica is an equation-based object-oriented language, which is particularly suitable for physics based modeling and simulations. The platform we tested consists of Dymola integrated development environment that has Modelica compiler, graphic user interface, and visualization tools; Modelica Standard Library and Modelica Buildings Library. The key advantage of this platform is that models can be developed independently of solvers that are used for simulations and vice versa – new solvers can be added and used with existing models. Modelica based tools have been successfully used for modeling electrical and HVAC systems, as well as for component design in automotive industry.

The objective of this investigation was to:

- Assess suitability of Modelica-based toolchain for buildings modeling and simulations, in particular
  - Modeling capability
  - Computational reliability
  - Available component model library (e.g. models for windows, construction materials, HVAC equipment, etc.)
- Assess efficiency of Modelica-based toolchain when used to develop whole building models and perform simulations, with emphasis on
  - Computational efficiency
  - Training time required
  - Total simulation turnaround time

#### Preliminary results with legacy Buildings library

Legacy Buildings library was originally developed at UTRC and donated to Lawrence Berkley National Laboratories (LBNL). The improved library was later released by LBNL under open source license to general public. The legacy library has some significant limitations. Most notably there are no models for windows and no ability to calculate solar radiation on inclined surfaces. Furthermore, fluid port in the room model is intended for setting and reading air properties in the room only. It does not allow for connecting physics based HVAC equipment models.

The legacy library was used for preliminary assessment of suitability of Modelica-based tools for building simulations. Tests were run for a model of the office space and classroom on the second floor of Great Lakes Drill Hall building. The simulation results were compared with an equivalent R-C model coded in Matlab. Because of limitations of the legacy library, only building envelope without windows was modeled. Matlab model was modified accordingly so that a meaningful comparison could be made. At the time when these tests were performed, the new version of Modelica Buildings Library was still under heavy development and a stable version was not available.

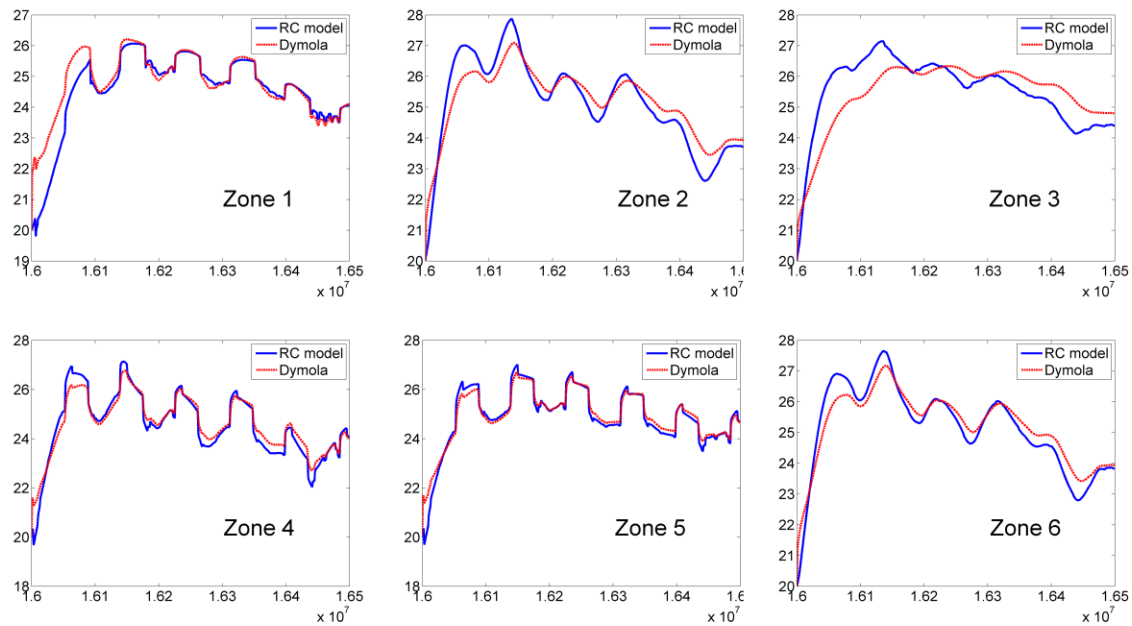


Figure 3.3.10: Simulation results for temperatures in zones 1-6 as obtained from Matlab R-C model and Dymola/Buildings Library.

These preliminary tests showed good agreement between Modelica and Matlab models (Figure 3.3.10), suggesting that the new toolchain may be a promising long term solution for buildings simulations.

#### Developing model with new Buildings library

The new and improved Modelica Buildings Library was released early in 2011. Most notable improvements were addition of glazing surface models, which allowed for modeling any type of windows, and the new interface, which allows zone model to be connected to Modelica HVAC equipment models of any complexity. Still, there are some important pieces missing from the library, such as models for window overhangs.

We developed model of the office space at Great Lakes building using the new library, which included building envelop with windows and HVAC equipment (Figure 3.3.11). All of our tests were performed using Buildings Library version 0.10.0 and Dymola version 7.2.

The envelope model consists of 6 zones as before. Mechanical equipment includes two air handling units and two VAV boxes. One air handling unit is connected directly to the classroom (Zone 1), while the other one is connected to Zones 4 and 5 through the two VAV boxes. The equipment has thermostat controls with different settings for day and night.

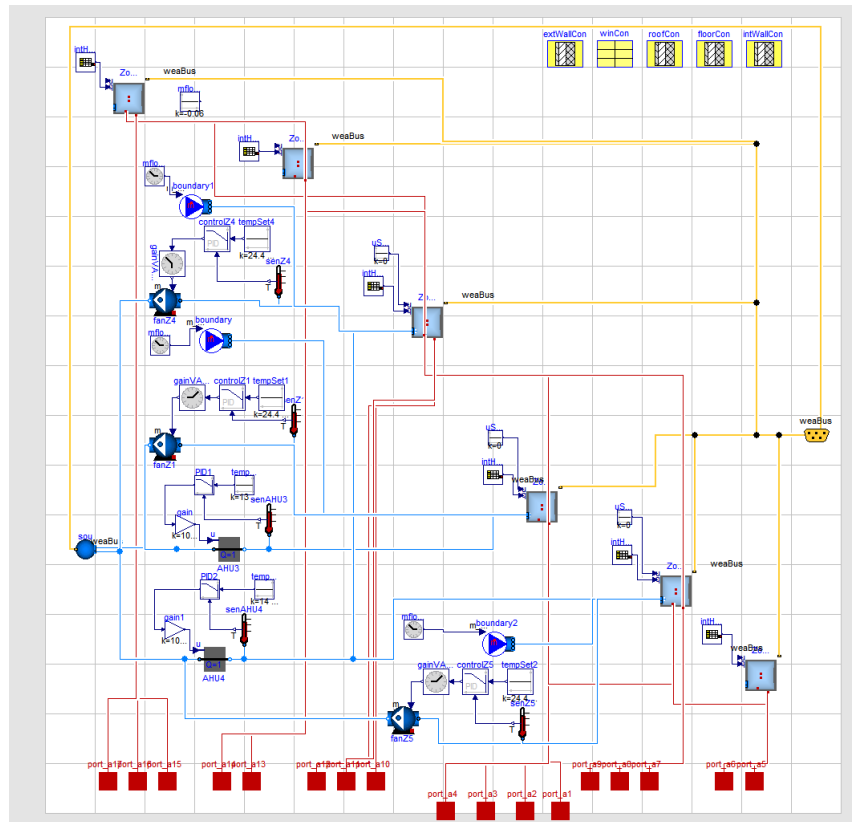


Figure 3.3.11: Dymola model of the office space on the second floor of Great Lakes Drill Hall Building.

While building envelope only simulations were quite robust, simulations of building envelope together with HVAC equipment were plagued by serious convergence problems. Interestingly enough, simulations for standalone equipment model for the building had much less problems running. To be able to run simulations at all, a series of simplifications needed to be made to HVAC equipment. For example, heat exchangers were modeled as a simple heat transfer from one flow to another, parasitic heat from fans was not modeled, dampers were modeled as ideal flow control, etc.

Even with all of these simplifications, simulations were not running smoothly. Checking simulation log files revealed that every third integration steps failed, what caused simulations to take unusually long time to execute. At this time it is unclear what causes these convergence issues. The root cause analysis of numerical convergence problems was outside of the scope of this activity.

In addition to convergence issues we discovered several bugs in the Buildings Library. Most serious of them were incorrect calculation for the diffuse solar radiation, incorrect air convection model and a bug in the graphic user interface for glazing surfaces, which caused incorrect parameter values to be passed to the solver. These problems were quickly resolved in collaboration with the library developers at LBNL. We compared numerical results obtained using Modelica Buildings Library with results obtained simulating an equivalent model in EnergyPlus and we found a good agreement between the two. Figure 3.3.12 shows simulation results for EnergyPlus and Buildings library, before and after bug fixes.

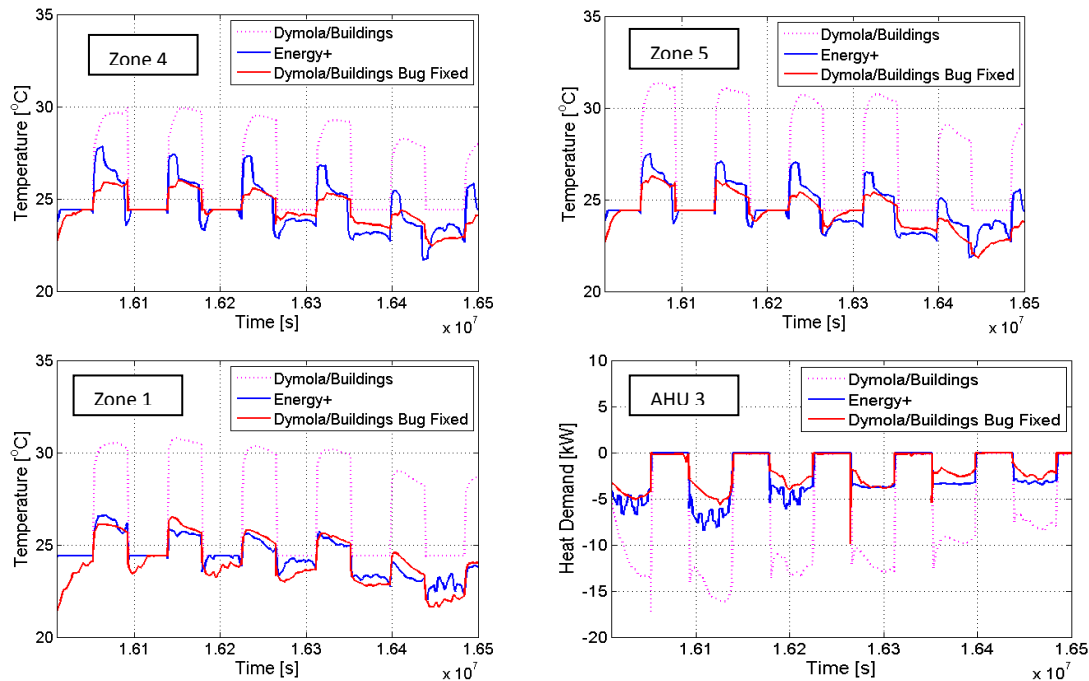


Figure 3.3.12 Temperatures in Zones 1, 4 and 5 and heat demand for Air Handling Unit 3 as simulated by EnergyPlus and Dymola/Buildings Library.

In addition to comparisons with EnergyPlus results for Great Lakes Building model, we performed a comprehensive accuracy testing of Buildings Library following ASHRAE 140 Standard. Out of 155 tests we ran, 51 failed. We repeated 9 of those 51 failed tests after corrections (bug fixes) were made to the Buildings Library. Six of repeated tests passed, while three failed again. This suggests that there are still some bugs in the library that we have not been able to isolate. This information was passed to the library developers at LBNL.

### Future prospects

Overall conclusion is that the Modelica based toolchain for buildings simulations is not mature enough for production use, given unresolved convergence issues and failed ASHRAE 140 tests. However, we do believe that this is a promising new technology that may have a significant impact on building design in the future. The promise lies in the architecture of the Modelica based platform which allows for adding new numerical solvers seamlessly, without affecting modeling aspects of the platform. This makes Modelica an environment where not only new models can be built, but also new analysis methods can be implemented. Built as such highly extensible environment, Modelica is better suited to meet future challenges in buildings design than currently dominant tools, such as TRNSYS and EnergyPlus. Another reason to seriously consider Modelica based tools is rapid development of Modelica Buildings Library. At the beginning of this activity in Q3 2010 the Buildings Library was at early development stage and mostly nonfunctional. Only 6 months later it grew into a full featured suite of building component models for high fidelity simulations. Computational accuracy issues were resolved promptly as they appeared, and currently an intensive investigation of numerical convergence problems is underway. If such development pace is sustained over next 1-2 years, the Modelica based toolchain may become a feasible alternative to the current state of the art tools.

### 3.4 Uncertainty and Sensitivity Decomposition of Building Energy Models

Because of the highly coupled nature inherent in building dynamics, optimized design requires an *integrated* and *system-wide* solution that considers interaction between all components of a building (e.g. HVAC equipment and scheduling, envelope design and material properties, occupants). In this part of the project, a tool chain was developed to support decision making involved in specifying and selecting *system-wide* and *integrated* solutions for deep retrofits that considers uncertainty or variation in performance of all the subcomponents and contributors of the design. In this framework, critical parameters of the design and operation of a building are identified and leveraged in order to propose leading efficient retrofit cases.

#### 3.4.1 Objective

As illustrated in the previous section, whole building energy models are adequate for calculating energy consumption and comfort for a specified design and operation strategy of a particular building exposed to typical yearly weather and internal load profiles. Because of the complexity of these models, analysis that considers uncertainty in their prediction or optimization of either the design or operation strategy is typically limited to studying only subcomponents of a building. In this part of the project, model-based analysis is performed to identify parametric sensitivities of a building that influence both energy consumption and comfort at the entire building level. With an understanding of these sensitivities, trade studies can be performed and optimal designs can be generated in rapid succession. The challenge in model-based analysis of building systems lies in the mathematical complexity of the models (e.g. discontinuities), computation time, and the enormous numbers of parameters within these models. The techniques developed in this project which are described below address these three concerns by applying advanced mathematical tools to efficiently manage the vast number of parameters as well as approximate characteristics of the model at discontinuities in a numerically efficient way.

#### 3.4.2 Introduction and Background

In our approach, uncertainty and sensitivity analysis is thoroughly integrated into the analysis of a design of a building (e.g. selection of internal systems). As an outcome, methods have been developed for model-based optimization and model calibration that considers thousands of partially known model parameters. These different technologies are tested on three different DoD buildings (modeled as-built and with high performance upgrades). Below is a list of the different analysis technologies followed by a table that describes which building model each technology is tested on.

- **Uncertainty and sensitivity analysis (UA/SA):** In this work, all parameters of a building system design (from material properties and equipment selection, to operational strategies) are treated as uncertain with a pre-defined range (typically about +/- 25%) around their estimated nominal value. On the order of 5000 annual simulations are then performed to generate energy and comfort information based on each of these design and operation scenarios and statistical analysis is performed on the outputs to quantify uncertainty in predictions. Sensitivity analysis is then performed to identify which of the 1000's of uncertain parameters drive changes in the outputs the most. Often an engineer must make educated guesses for parameter values in an energy model and sensitivity analysis offers insight into which parameters are critical and should receive more attention for these estimates.

- **Sensitivity decomposition (Decomp):** Traditional sensitivity analysis investigates the influence of input parameters on the output of a given model. In sensitivity decomposition, we further this study by investigating influences of intermediate variables. For instance, in studying energy consumption, we may investigate which subsystems influence electrical energy consumption the most (e.g. fans, HVAC, lights, plug loads, etc.) and then further study which of these groups (e.g. lighted zones) carry the most uncertainty. A network tree is developed in this way and a flow of uncertainty is calculated through this tree that highlights pathways where uncertainty passes or accumulates the model. This analysis is useful to identify which equipment in a building provides robustness by blocking the pathway of uncertainty, or which components further amplify uncertainty as it passes from the building design, construction and operation to the meters (and therefore should receive more engineering attention).
- **Meta-model based optimization (Optim):** State of the art optimization in the building energy modeling community utilizes either very simple sub system building models, or optimization experiments with only a few optimization parameters (Djuric, et al, 2007, Kampf et al, 2010, and Diakaki et al, 2008). This approach is used because full order energy models (e.g. TRNSYS, EnergyPlus) are typically computationally expensive (minutes to hours for each function evaluation), and are often discontinuous in their cost function (Wetter and Wright, 2003, Wetter and Wright 2003b, and Wetter and Polak 2004). In this part of the work, we develop an approach that utilizes data generated from the uncertainty and sensitivity analysis to develop a model of the full energy model (meta-model) with which rapid optimization can be performed. Meta-modeling has been previously used in the buildings community to a limited extent but not yet for optimization. Using this approach, optimization can be performed on thousands of parameters as well as a subset of the full list of parameters (chosen by parameter type or by the most influential for instance).
- **Model calibration (Calib):** In the optimization work, a cost function is defined that balances energy use and comfort and seeks a parameter combination that minimizes energy while maximizing comfort. Other cost functions can be defined in order to obtain a different objective as desired. For example, in model calibration, we define the objective to be the error between the prediction of the model and data captured from sensors in a real building. An optimization is then performed to identify parameter combinations that drive this error to a minimum which results in the model output matching sensor data. This type of work has been performed manually in other projects (O'Neill et al., 2011), while the focus of this part of the work was to automate it to some extent.

Table 3.4.1. Analysis performed on different energy models (baseline is the actual building, energy efficient retrofit design with high performance attributes). Abbreviations are described in the bulleted list above.

Building Name	Modeling Tool	UA/SA	Decomp	Optim	Calib
Drill Hall Baseline	EnergyPlus	☑	☑	☑	
Fort Carson Baseline	TRNSYS	☑			
Fort Carson Energy efficient retrofit design	TRNSYS	☑			
Building 26 Baseline	EnergyPlus	☑			☑
Building 26 Energy efficient retrofit design	EnergyPlus	☑			

A schematic of the procedure for each of these technologies is presented in Figure 3.4.1 and each element of this figure will be discussed in further detail in the sections below. All of the algorithmic functions in Figure 3.4.1 have been integrated into a software analysis package (Aimdyn, 2011).

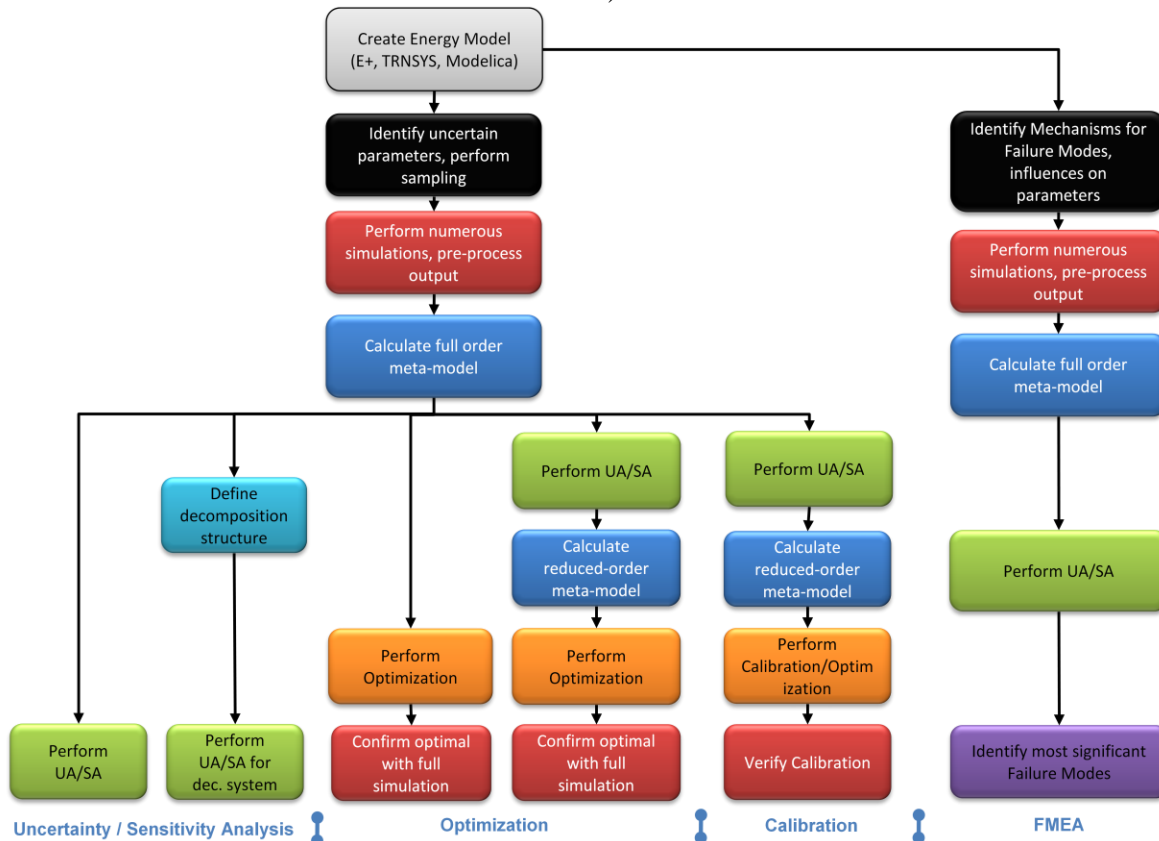


Figure 3.4.1 Schematic of the different analysis techniques that are performed on the building energy models.



### 3.4.3 DoD Case Studies

The following sections describe specific results for uncertainty and sensitivity analysis, optimization, and model calibration for three Department of Defense buildings. A detailed description of the analysis methods is described in Appendix C and the papers referenced therein. Further details of the buildings themselves and their models can be found in Section 3.3.2.

#### 3.4.3.1 *Atlantic Fleet Drill Hall*

The Atlantic Fleet Drill Hall building was used as a case study to test the uncertainty and sensitivity analysis, system decomposition, and numerical optimization tools developed on this project. This DOD building (number 7230), which is situated at the Naval Station Great Lakes, is approximately 6430 m<sup>2</sup> (69 K ft<sup>2</sup>) and contains a large gymnasium as well as offices and administrative areas.

The building is conditioned using four air handling units (AHUs) and has variable area volume (VAV) boxes as terminal units in the occupied zones. The gymnasium uses two AHUs, a classroom uses one AHU and the offices use the final AHU. Cooling comes from two 110-ton air cooled chillers and heating is from a district supply (which also provides the domestic hot water). An EnergyPlus model was generated for this building (using version 4.0.0.024), and TMY3 (typical meteorological year) weather data for Chicago, O'Hare airport was used for environmental reference (see Section 3.3.2). To keep the size of the model manageable, 30 conditioned zones were considered (12 for the gymnasium, and 18 for the conditioned office spaces). The model takes about 15 minutes to simulate on a standard desktop computer with 2.8 GHz CPU.

#### Uncertainty and Sensitivity Analysis

To perform uncertainty analysis, almost all numeric parameters in the EnergyPlus model were selected as uncertain, a few of the parameters were chosen to be held constant in the analysis like architectural parameters (size, shape and orientation of the building). Text-based parameters (e.g. whether certain equipment is auto-sized, or other calculation methods), as well as the weather data were also not changed. The nominal values for parameters were chosen from (1) as-built architectural, mechanical and control drawings (e.g. thermal properties of envelope and windows); (2) actual building operation (e.g. lighting and AHU operation schedules); (3) manufacturer's catalog data (e.g. chiller coefficient of performance COP)).

The resulting 1009 parameters were varied  $\pm 20\%$  of their nominal value (we also include data illustrating how uncertainty is influenced when this range is  $\pm 10\%$ ). For nonzero parameters, a uniform distribution was imposed, while for parameters with zero nominal value (and constrained to be positive), an exponential distribution was used to keep the mean of the sampled values closer to nominal. Many of the parameters were constrained; for instance, fractional parameters with a nominal of 0.9 would be varied between 0.72 and 1.0. The heating and cooling setpoints are limited to 6.5% variation because otherwise they would overlap, which created conflict in the dual-setpoint management. All parameters were varied concurrently using a quasi-random approach. In this way, 5000 models were created which were ultimately parallelized and simulated on a 184-CPU Linux cluster.

Ten energy consumption outputs were investigated for this part of the study, and convergence behavior for these outputs is presented in Figure 3.4.2 (when parameters were varied by +20%).

The trends in this figure were obtained by calculating the percent difference between the mean at the  $i^{\text{th}}$  simulation and the mean after 5000 simulations. The percentage of absolute value of the error for each of the 10 annual consumption and peak demand outputs were then averaged to create two convergence response curves. In this figure, the slope at which the error converges is calculated using a least squares fit and included in the legend. Note that the exponent of the line fit for the annual consumption and peak demand variables is on the order of -0.7 (using the quasi-MC approach). This same exponent for a — convergence rate, which is common for standard MC methods, would be -0.5.

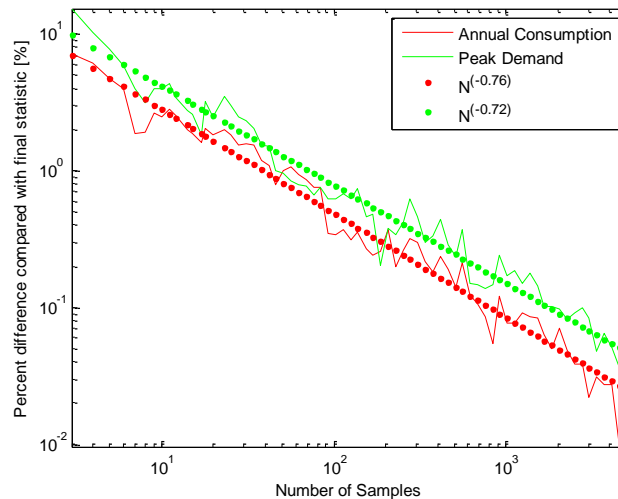


Figure 3.4.2 Convergence properties of the 10 outputs. The mean and standard deviation, with respect to the value after 5000 simulations is presented for both peak usage and annual consumption.

Figure 3.4.3 illustrates statistical analysis for the ten outputs considering both peak demand and annual energy consumption (for reference, Figure 3.4.4 presents actual probability distributions of two of the outputs) when the uncertain parameters are varied by either 10% or 20%. As is evident in Figure 3.4.3, the variance and coefficient of variation increases by increasing the uncertainty in the input parameters. Specifically, in most cases, the increase in a factor of two on the input parameter standard deviation amplifies the uncertainty in the output by a factor of two as well, indicating linearity in the dynamics. It is also clear that cooling electricity is always amplified the most. The uncertainty in energy use from both interior equipment and interior lights is attenuated by about a factor of two. All other output variables have uncertainty which is on the order of the input uncertainty.

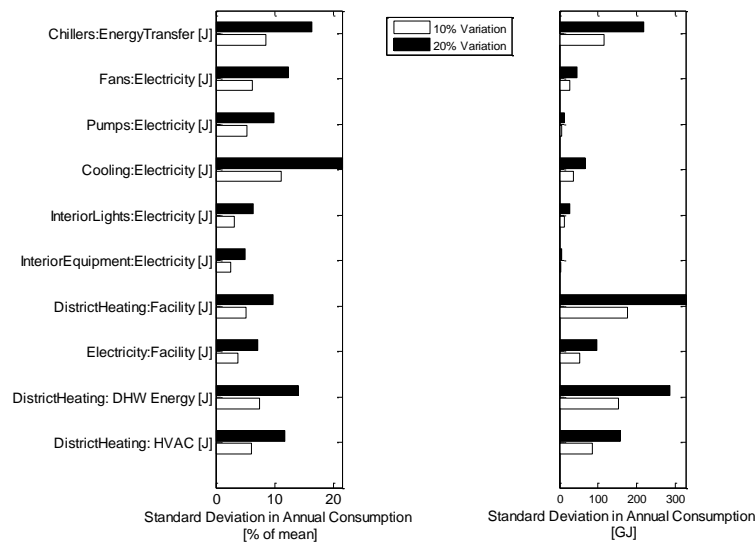


Figure 3.4.3 Uncertainty in 10 energy consumption variables when varying input parameters by 10% or 20%.

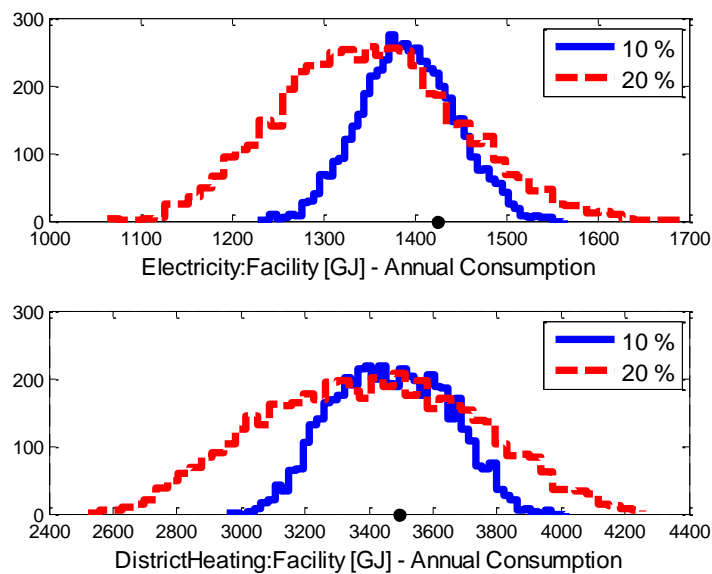


Figure 3.4.4 Example distributions for cooling(top) and heating (bottom) when varying the input parameters by either 10% or 20%. The black dot is the nominal simulation results.

The sensitivity indices for the two main seasonal outputs of the model; the district hot water consumption in winter (October 15 to April 14), and the facility electricity in summer (April 15 to October 14) are presented in Figure 3.4.5. To generate this figure, the individual sensitivity indices were added using 10 parameter groups in Table 3. 4.2. It should be noted that since we are using derivative based sensitivities, the summation may be larger than 1.0.

Table 3.4.2. Parameter group types.

Number	Type	Note: examples in this Drill Hall system 1
1	Heating source	District heating system (normal capacity, maximum hot water system temperature, loop flow rate, etc.)
2	Cooling source	Air cooled chiller (chiller reference capacity, reference COP, reference leaving chilled water temperature, etc.)
3	AHU	AHU (supply air temperature setpoint, cooling coil design flow rate, design inlet water temperature, design inlet air temperature, etc.)
4	Primary Mover: Air loop	Fans (efficiency, pressure rise, etc.)
5	Primary Mover: Water loop	Pumps (rated flow rate, rated head, rated power consumption, etc.)
6	Terminal unit	VAV boxes (maximum air flow rate, minimum air flow fraction, etc.), maximum zonal flow rates
7	Zone external	Building envelope(material thermal properties such as conductivity, density, and specific heat, window thermal and optic properties, etc.), outdoor conditions (ground temperature, ground reflectance, etc.)
8	Zone internal	Internal heat gains design level (lighting load, number of people, people activity level, etc.), schedules
9	Zone setpoint	Zone temperature setpoint (space cooling and heating set-points)
10	Domestic hot water	Domestic hot water usage (peak flow rate, target temperature, etc.)

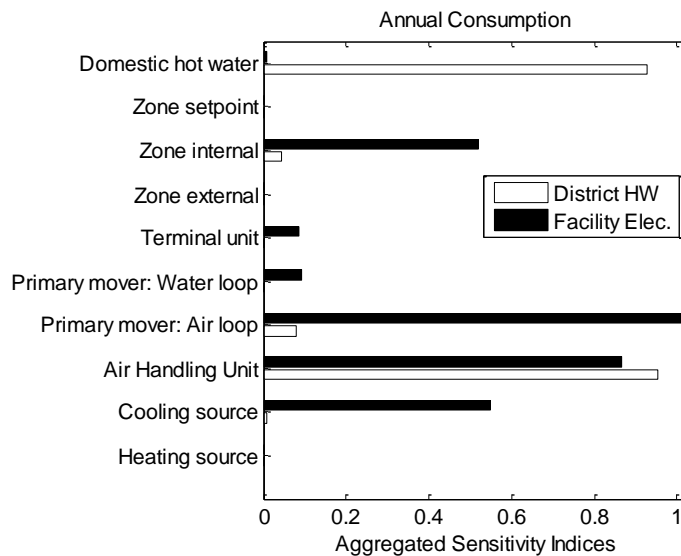


Figure 3.4.5 Sensitivity indices for two facility consumption variables.

Starting from the bottom of Figure 3.4.5, we highlight the parameters which contribute most to the parameter type for those outputs.

- For the Heating Source parameter type, two parameters are influential, but one parameter stands out as dominant: HW loop max temperature (hot water loop maximum temperature).
- For the Cooling Source parameter group, out of nine total, two parameters stand out the most: Chiller on at OAT (chiller is on when outside temperature reaches a threshold) and CW loop temp schedule (chilled supply water temperature setpoint schedule).
- The Air Handling Unit parameter type is comprised of 22 parameters in this case, but is predominately defined by Min OA schedule fraction (minimal outside air fraction) and SAT reset temp (AHU supply air temperature setpoint).

- The Primary Mover: Air Loop parameter group contains 20 parameters, but are dominated by AHUS1 and AHUS2 fan parameters (fan efficiency and pressure rise).
- The Primary Mover: Water Loop parameter type only has five significant parameters in it. The most dominant of these parameters are the Rated pump consumption parameters, while one pump efficiency, from the primary chilled water pump does play a small role.
- The Terminal Unit parameter type is comprised of nine parameters, with approximately equal contributions from Zone max flow rate (drill deck) and VAV max flow rate (office area) parameters.
- The Zone external parameter type has 14 significant parameters in it. There is no small set of parameters which stand out in this set. The contributions come from material types in building construction as well as ground surface temperature and ground reflectance.
- The parameter type zone internal contains 48 significant parameters, with People schedule (fraction of number of people) and Lighting Schedule (fraction of lighting load) parameters dominating this group.
- The zone setpoint parameter group has 3 significant parameters. These are associated with high-use time periods of the Zone cooling setpoint and one Zone heating setpoint schedules. They influence the facility electricity and district hot water respectively.
- The Domestic hot water parameter type has 6 significant parameters. The Water equipment target temperature is a large contributor, followed closely by four parameters that define the domestic hot water use fraction.

Figure 3.4.5 also shows that 1) summer electricity is mainly influenced by the air loop primary mover (i.e. supply and return fans); and 2) winter district heating is mainly influenced by domestic hot water (i.e., water usage) and the AHU (i.e., AHU heating coils, and the AHU supply air temperature setpoints).

**Sensitivity Decomposition:** The standard input-output sensitivity analysis described above is useful to identify which parameter type influences the two facility-wide consumption variables the most. In this section, we further break this down to illustrate how uncertainty in the input parameters influence intermediate consumption variables which eventually make up the total usage (either district hot water, or building electricity). In Figure 3.4.6, the sensitivity decomposition for facility electricity is presented. In this plot, the nodes are subsystem energy variables, which are described in Table 3.4.3, and the connecting wires are sensitivity indices. For instance, in Figure 3.4.6, the right most node is the electricity use at the building level. The 5 nodes to the left of this are the 5 major electrical subsystems in the building (lighting, interior equipment, fan total, pump total, and cooling). To the left of this, an even greater decomposition is presented for electrical consumers (individual fans and pumps, etc.). The left-most axis contains the input parameter types which influence the entire dynamics of the model (as in Table 3.4.2). For each node, a circle is drawn around it which represents the coefficient of variation. There is no appropriate scale for these circles, they are intended to be viewed relative to other circles in the figure.

The thickness of the wires corresponds to the magnitude of the sensitivity index. Where there is no wire, the sensitivity index is negligible, and the thickest wires represent the strongest influence between the variables.

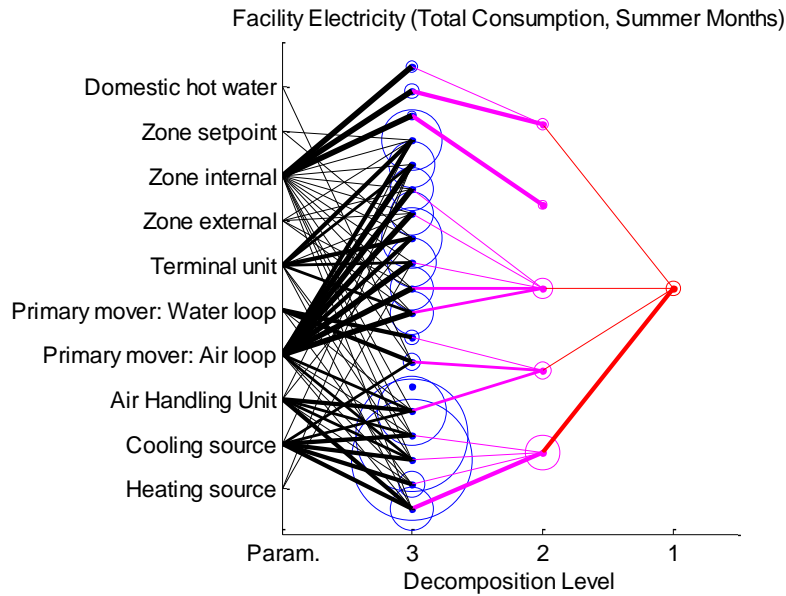


Figure 3.4.6 Sensitivity decomposition of electricity consumed by the facility (sum over summer months). Labels on the vertical axis describe the nodes of the 4<sup>th</sup> level, while the other node/levels of this plot are tabulated in Table 7.

As seen in the decomposition of facility electricity consumption, the uncertainty in facility electricity is driven mostly by uncertainty in fan and cooling source (chillers) electricity consumption. These in turn are influenced mostly by AHU1S and AHU2S fan consumption, and CHILLER1 electricity consumption respectively. This makes sense because 1) AHU1 and AHU2 are serving all the zones in the drill deck which is the largest area in the building (80%), and 2) CHILLER1 was set as the primary chiller in the model.

Table 3.4.3 Variables for the nodes of the sensitivity decomposition of Facility Electricity (Figure 8).

Level 3	Level 2	Level 1
Equipment: Office area [J] Equipment: Drill Deck [J] Lights: Office area [J] AHU4RFAN:Fan Elec. Cons. [J] AHU3RFAN:Fan Elec. Cons. [J] AHU2RFAN:Fan Elec. Cons. [J] AHU1RFAN:Fan Elec. Cons. [J] AHU4SFAN:Fan Elec. Cons. [J] AHU3SFAN:Fan Elec. Cons. [J] AHU2SFAN:Fan Elec. Cons. [J] AHU1SFAN:Fan Elec. Cons. [J] DHWPUMP:Pump Elec. Cons. [J] PRIMARY-PUMP:Pump Elec. Cons. [J] HWPUMP:Pump Elec. Cons. [J] SECONDARYPUMP:Pump Elec. Cons. [J] CHILLER2:Chiller Cond Fan Elec. Cons. [J] CHILLER2:Chiller Elec. Cons. [J] CHILLER1:Chiller Cond Fan Elec. Cons. [J] CHILLER1:Chiller Elec. Cons. [J]	InteriorLights:Elec. [J] Int.Equip.:Elec. [J] Fans:Elec. [J] Pumps:Elec. [J] Cooling:Elec. [J]	Facility Elec. [J]

Similar analysis has been performed on other facility-level quantities like district heating (Eisenhower, 2011a).

**Optimization** The next part of this study leverages the uncertainty and sensitivity analysis (and the creation of the meta-model) to perform numerical optimization. The analytic meta-model that was calculated for sensitivity analysis provides a means for rapid and accurate optimization

that otherwise would be hampered by the computational cost of the full energy model. In this part of the study, optimization was performed on the Drill Hall model using a cost function that balances the influences of both comfort and energy consumption. The cost function was defined as

$$(Eq\ 3.4.1)$$

where PMV (which is an indicator of thermal comfort (Fanger, 1970)) was squared to drive it towards zero without taking the absolute value (continuous cost functions have better mathematical properties than discontinuous ones in this case). Since PMV is on the order of 1.0, the energy was normalized to vary between 0.0 and 1.0. The cost was broken up into two parts to identify the best possible comfort or energy solution and then a solution that balances both.

Optimization results are presented in Figures 3.4.8 and 3.4.9 for many different test cases which investigate the optimal solution based on all parameters as well as reduced models that use different subsets of the whole parameter set. These subsets are chosen in two ways: 1) physical grouping by parameter type (e.g. all schedule parameters, or material properties), and 2) parameters chosen from rank-ordering by their influence on the output.

**Sensitivity Analysis:** To guide in parameter selection for model reduction, sensitivity analysis was performed to identify which parameters are critical to optimizing a certain cost. Figure 3.4.7 illustrates the total sensitivity indices for both PMV and total facility energy for the 1009 parameters.

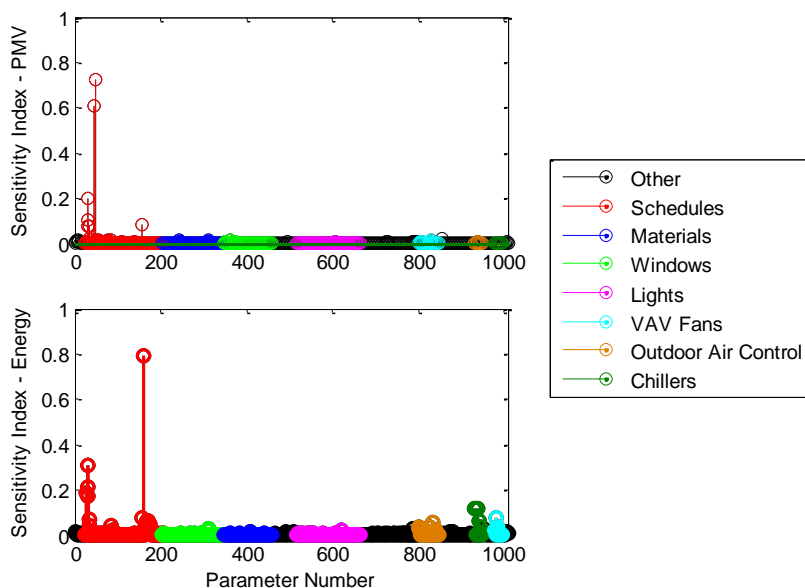


Figure 3.4.7 Sensitivity indices for both PMV and total facility energy for the 1009 uncertain parameters. Some of the parameter classes are grouped by color in this figure.



As illustrated in Figure 3.4.7, there are only tens of parameters that significantly influence either energy or comfort in this model. This suggests that an optimized solution may be achieved without necessarily changing all parameters of the building energy model.

**Model Reduction** Optimized performance using seven different reduced order models (as well as the full EnergyPlus model) will now be considered. The first four reduced models are generated by selecting a subset of parameters based on class: 1) All schedule parameters (180 parameters), 2) All envelope material properties (142 parameters), 3) Outdoor air controller properties (16 parameters), and 4) AHU fan parameters (48 parameters).

The second subset of parameters were selected based on their influence as calculated from sensitivity analysis. To identify the most influential parameters, the parameters that were presented in Figure 3.4.7 are ordered in terms of their importance and three more reduced order meta-models are created that contain: 5) the top 20 most influential parameters (see Table 3.4.4), 6) the top 7 most influential parameters (labeled B in Table 3.4.4), and 7) 5 of the top 20 parameters that influence both comfort and energy simultaneously (labeled C in Table 3.4.4). This last category was selected because many of the top 20 parameters influence *only* comfort *or* energy.

Table 3.4.4 The twenty most influential parameters on both comfort and energy consumption.

Reduced Parameter Number	Label	Parameter Description
1	B	Minimum outside fraction in occupied hours
2	B,C	AHU1/2 winter (1/1 to 4/15) supply air temp. setpoint
3	B,C	AHU1/2 summer (4/16 to 8/15) supply air temp. setpoint
4	B,C	AHU1/2 winter (8/16 to 12/31) supply air temp. setpoint
5	B,C	Hot water supply temperature setpoint
6	C	Weekday zone temp. setpoint from 12:00am to 6:00am
7	B	People activity level (in W) in office area
8	B	People activity level (in W) in Drill Deck
9		AHU4 summer (4/16 to 8/15) supply air temp. setpoint
10		Domestic hot water supply temperature setpoint
11	B	Water equipment target temperature setpoint
12		Domestic hot water usage fraction from 11:00 to 12:00
13		Domestic hot water usage fraction from 12:00 to 13:00
14		Domestic hot water usage fraction from 13:00 to 14:00
15		Domestic hot water usage fraction from 16:00 to 17:00
16		AHU2 return fan maximum flow rate
17		AHU1 minimum outside flow rate
18		AHU2 minimum outside flow rate
19		AHU3 minimum outside flow rate
20		Chiller reference COP (coefficient of performance)

**Optimization** To obtain optimization results, the single full order model and seven reduced order meta-models were integrated with both Interior Point (IP) (IPOPT (Wachter and Biegler, 2006)) and Derivative Free (DF) (NOMAD (LeDigabel, 2011)) optimization algorithms. Many

different cost functions and weighted combinations of the cost in the three Equations of Eq 3.4.1 were investigated. For brevity we present results when using the cost function  $C_3$  for all models, and cost functions  $C_1$  and  $C_2$  for the full model (with all 1009 parameters).

The results of the optimization for all these meta-models are illustrated in Figures 3.4.8 and 3.4.9, and compared to one case where the full EnergyPlus model was used instead of the meta-model (see *Top 7 [7,C3] E+ in the Loop*).

For each of the optimization cases, the optimizer was executed and an optimal solution was calculated using the meta-model in seconds (for the interior point method) and in minutes (using the derivative free method). To ensure a proper comparison of all optimization cases, the optimal parameter choices for each case were substituted into the baseline EnergyPlus model and a single simulation was performed to calculate energy usage and average comfort over the year.

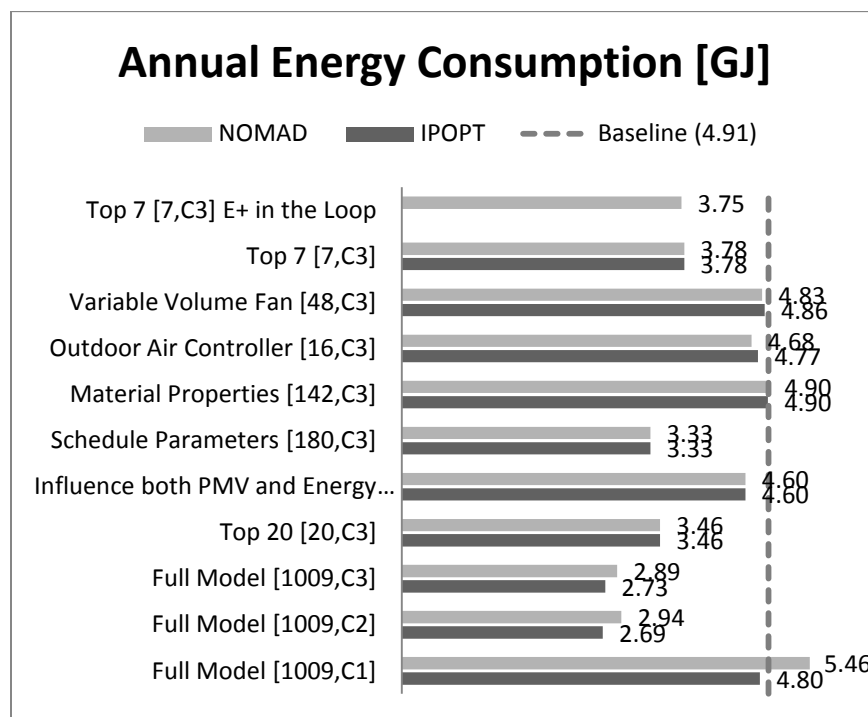


Figure 3.4.8 Optimization results for energy consumption using the 8 meta-models, and one case using the EnergyPlus model. Each data point in this figure for the meta-model optimization was generated by inserting the optimal parameter values into EnergyPlus and simulated.

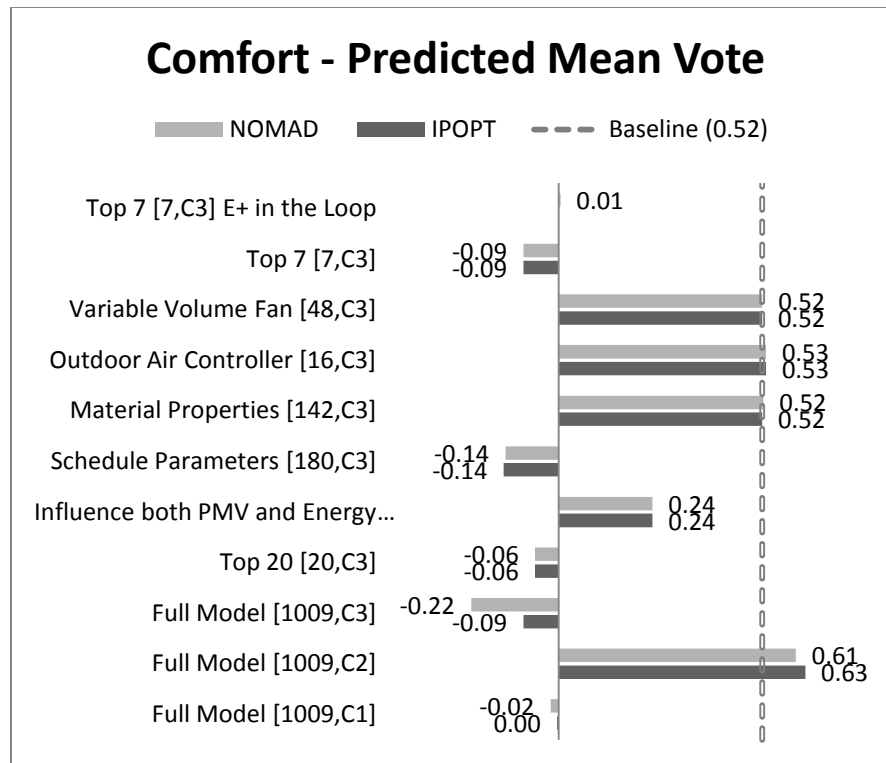


Figure 3.4.9 Optimization results for thermal comfort using the 8 meta-models, and one case using the EnergyPlus model. Each data point in this figure for the meta-model optimization was generated by inserting the optimal parameter values into EnergyPlus and simulated.

As seen in Figures 3.4.8 and 3.4.9, when penalizing only comfort (using  $C_1$ ), the optimization drives comfort to nearly neutral (0.0). Similarly, when penalizing only energy (using  $C_2$ , the derivative free and interior point methods reduce the energy consumption to 40% and 45% respectively). These cases show the best possible isolated comfort optimization or energy reduction while the more appropriate case of considering both (using  $C_3$ ) offers energy reduction of 45% for the IP method and 41% for DF optimization. In this combinatorial case, the comfort is also optimized as well. The comfort index is reduced to -0.09 and -0.22 using the IP and DF approaches respectively.

**Discussion** In terms of discussing the results presented in Figures 3.4.8 and 3.4.9, there are five topics that are worth emphasizing; the importance of sensitivity analysis in the optimization process, a comparison of numerical quality using a meta-model or the full EnergyPlus model, a comparison between the two optimization algorithms, a discussion on optimization seeds, and a brief discussion of computation time. These topics are itemized below.

- By comparing all of the different optimization cases which use a different number of parameters, it is evident that optimizing over even a very small subset of parameters, if chosen appropriately, will offer respectable results compared to optimizing over all parameters (by comparing *Top 7 [7,C3]*, and *Top 7 [7,C3] E+ in the Loop* with *Full Model [1009,C3]*). The key is performing sensitivity analysis which highlights which parameters influence the cost function the most.

- This notion highlights the need to integrate other analytical tools (like uncertainty and sensitivity analysis) into any optimization experiment. Rigorous parameter selection based on sensitivity analysis allows the designer to choose parameters, which may otherwise not be intuitively obvious, and rank them as to those which will have the most impact on the optimization process.
- By comparing the optimization experiments *Top 7 [7,C3]*, and *Top 7 [7,C3] E+ in the Loop*, it is evident that the optimization using the meta-model offers nearly equivalent results to those obtained by performing DF optimization with EnergyPlus in the loop (in terms of numerical quality).
- In almost all cases, it is apparent that the gradient-based method IPOPT performs similarly to the derivative free method (NOMAD), with the exception when the number of function evaluations were limited to 1,000,000. Beyond the optimization accuracy, there is a large difference in the number of function evaluations between the two methods. This is not a significant issue when using a meta-model as we have constructed (its evaluations are very rapid), but may become a concern in other situations.
- One traditional concern that has not been mentioned until now is the choice of the seed (or initial condition) for each optimization experiment. That is, both the gradient-based and DF optimization approaches produce different (even if only slightly) results based on initial guesses of the optimization parameters. We found this variation to be so small that we do not report it for each case. For example, in the case where the optimization is performed with EnergyPlus in the loop (*Top 7 [7,C3] E+ in the Loop*), four experiments were performed resulting in a variance in optimized energy of 0.00057% of mean in [GJ], and 0.28% of mean in PMV. The total number of function evaluations (15 minute simulations) for these four experiments was 4688 (1172 CPU hours of simulation). Thankfully, the NOMAD algorithm is parallelized, and is run on many CPU's at once, but this series of experiments in itself (using only 7 parameters) was computationally expensive. Optimization using a gradient based-method (IPOPT) coupled to the full EnergyPlus model was not performed because expected discontinuities would have resulted in poor performance (see (Wetter and Wright, 2003b)).

It is challenging to make a direct comparison of computational cost between the traditional optimization approach (full EnergyPlus model in the loop) and the meta-model approach because the latter offers different possibilities than the former. To be specific, one optimization experiment on the EnergyPlus model with 7 parameters (*Top 7 [7,C3] E+ in the Loop*) took on average 1000 simulations. Creating the meta-model took 5000 simulations which is much larger, but once the meta-model is calculated, more optimization experiments can be performed. In other words, the meta-modeling approach becomes more computationally efficient as more optimization experiments are introduced. Given that the weighting or form of a particular cost function, or parameters of the optimization algorithm that one may be using are not always well known prior to testing (which means more than one optimization experiment is almost always needed), the meta-modeling approach becomes very attractive as a time saving measure when the entire design cycle is considered.

#### 3.4.3.2 Fort Carson

Building 1225 at Fort Carson is a single storey administrative and training facility built in the 1970's with approximately 24K ft<sup>2</sup> floor area. Two TRNSYS models were generated to describe the as-built (baseline) design and a hypothetical advanced design with efficient energy systems

(described in Section 3.3.2). These models were used to study both uncertainty and sensitivity analysis and failure mode effect analysis.

To perform uncertainty and sensitivity analysis, the parameter sampling using deterministic samples was performed as described in Appendix C. There were only 316 uncertain parameters in the baseline building design and 323 for advanced design. The number of parameters were much smaller in these models because the size of the building and complexity was smaller than the Drill Hall, and because the modeling paradigm in TRNSYS is such that fewer parameters are used to describe the same processes. The results from uncertainty analysis are presented in Figure 3.4.10 where probability distributions for annual energy consumption and peak demand for the entire building is presented. There is an obvious decrease in the mean probability of annual energy consumption (from 1664 GJ to 1264 GJ). On the other hand, the coefficient of variation (standard deviation divided by the mean) remains fairly constant at 0.08 for the baseline building and 0.09 for the advanced design.

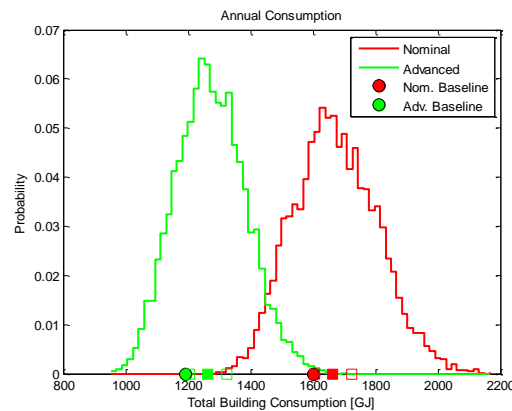


Figure 3.4.10 Uncertainty ranges for the baseline Fort Carson design and a re-design with high performance features.

Sensitivity analysis was performed on the data generated for the uncertainty analysis that was described above. For presentation purposes, once a subset of the parameters were identified as being influential, these parameters were classified by parameter type and the sensitivity indices were summed for each parameter type (as listed in Table 3.4.2) and presented in Figure 3.4.11.

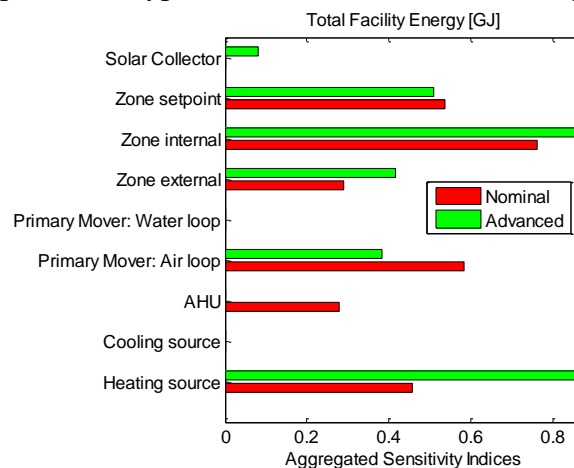


Figure 3.4.11 Results of sensitivity analysis for the Fort Carson building 1225 (baseline and advanced building designs).

Figure 3.4.11, are attributed to 2 factors: 1) the advanced system reducing energy consumption; 2) different HVAC configurations. Due to reduced total facility energy, the advanced system is more sensitive to the same amount of variations in a parameter. Thus more parameters stand out in terms of energy impact, which contribute to the aggregated sensitivity. For instance, the high-impact parameter of heating source in the baseline is the boiler efficiency, while the advanced system has parameters of hot-water set point and heating coil heat transfer coefficients, in addition to boiler efficiency. In the category zonal external, the advanced system has one high-impact parameter more than the baseline, which is thermal conductivity of insulation layer of external wall. The different configuration is the other cause of differences. For instance, the advanced system has solar thermal collectors, and it has no economizer since it employs direct evaporative coolers. Therefore the baseline has nothing to do with the category of solar collector, and no parameter in AHU of the advanced system shows up. In addition, the advanced system uses variable-speed fans while the baseline has constant-speed ones, so the parameters in the category of air-loop primary mover, such as fan efficiency, have a higher-impact on the total energy of the baseline than that of the advanced system.

#### **3.4.3.3 Building 26**

Our third case study investigated energy models of Building 26, the Fleet and Family Support Center (FFSC)/Navy Marine Corps Relief Society (NMCRS), at the Naval Training Center, Great Lakes, IL. This is a two-storey office building with basement and a gross area of approximately 37,000 ft<sup>2</sup>. The Building 26 HVAC system consists of two airside systems and two separated waterside systems. The office and administrative area on the first and second floors is served by two variable-air volume (VAV) Air Handling Units (AHU) with a VAV terminal unit (with hot water reheat) heating and cooling capability. These AHUs have both heating and cooling capability and the operation of these units depends on the occupancy of the building. The chilled water system consists of one 54.5-ton air-cooled rotary-screw type chillers with fixed-speed primary pumping. Heating is supplied from the existing base-wide steam system through a steam-to-water heat exchanger. The hot water serves unit heaters, VAV box reheating coils, and air handling unit heating coils. The communication service room is served by one dedicated split system and electric unit heater and baseboards are used to provide heating to stairwells and restrooms. The conditioning of this building is primarily provided through two variable air volume air handling units served by a 54.5 ton air-cooled chiller and district steam. An EnergyPlus model for the as-built design of the building and a high-performance re-design were constructed as discussed in Section 3.3.2. For this case study, both uncertainty and sensitivity analysis as well as model calibration was investigated using the methods described in Appendix C.

**Uncertainty and Sensitivity Analysis:** The uncertainty and sensitivity analysis for this case study was performed exactly the same way as in the previous studies outlined above. Selecting all numerical parameters in each EnergyPlus model revealed 2063 parameters for the baseline building design and 2197 for the advanced design model. Because the number of parameters were larger than in the previous cases, a total of 6500 concurrent parameter samples were computed for each model (in each case there was also a number of unsuccessful simulations due to incompatibility of parameter choices).

The uncertainty in the computed annual consumption for both cases is presented in Figure 3.4.12. These uncertainty distributions help the designer better understand building performance

bounds. The advanced design is about 30% more efficient compared with the baseline design (solid square in Figure 3.4.12). With uncertainty in thousands of parameters, if we look at the distribution within  $\pm 1\sigma$  (standard deviation, hollow square in Figure 3.4.12), the advanced design can achieve at most 50% and at least 20% improvement.

The bimodal behavior for facility electricity in advanced system is due to the fact that ground source heat pump (GSHP) heating (using electricity) is turned on only when heating demand is less than a given number. When the heating demand is high, only district heating is available and GSHP heating is turned off.

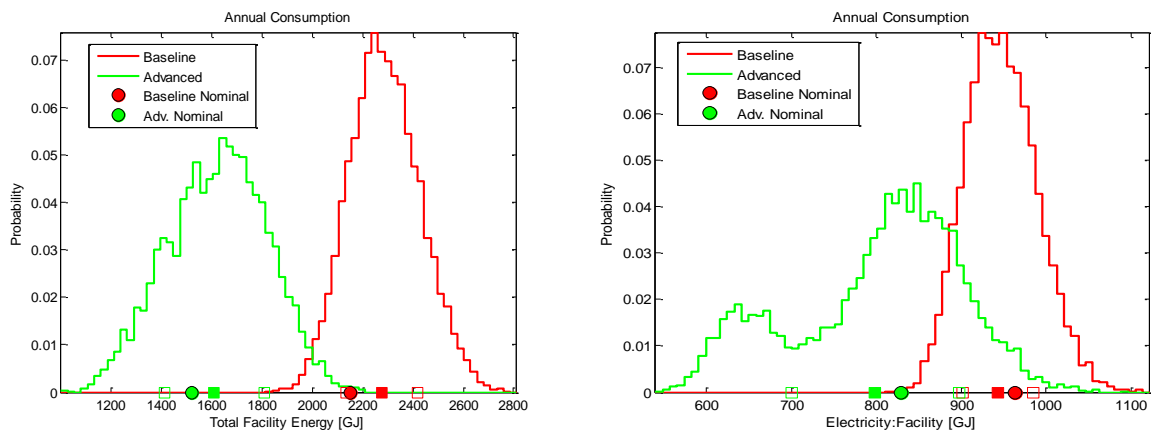


Figure 3.4.12 Uncertainty in energy consumption for the total facility (left) and only electricity (right) for the DoD Building 26.

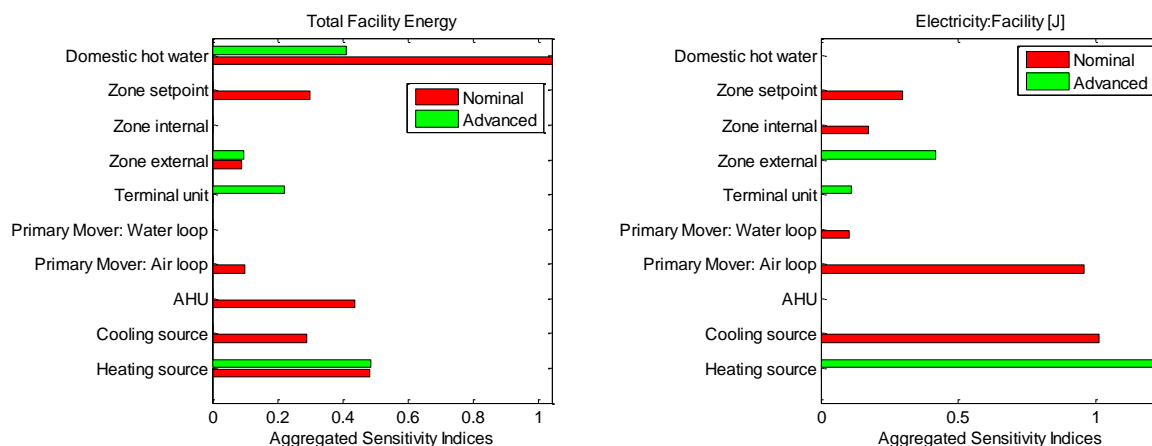


Figure 3.4.13 Critical parameter results for Building 26

In both baseline and advanced systems, the total building annual energy consumption are most sensitive to parameters related to domestic hot water and heating source due to the fact that heating is dominant in Chicago area (Figure 3.4.13). For the total building annual electricity consumption, the most influential parameters in advanced system are from heat source type while from cooling source type in baseline system. This makes sense because air cooled electric chiller is the only cooling source for summer while district heating provides heating for winter in baseline case. In the advanced system, high efficient electric GSHPs are used for both heating and cooling. Cooling end use from air cooled chiller is about 18% of total electricity consumption



and cooling end use from GSHP is about 10% of total electricity. This is why the total electricity consumption in baseline system is more sensitive to cooling source.

**Model Calibration:** In this case study, there was sensor data that was available from a separate ESTCP project (ESTCP SI-0929), and therefore we sought to use the uncertainty and sensitivity analysis methods, along with parameter optimization to identify which parameters would be best to tune the response of the model closer to data. The optimization algorithm was then used to perform this calibration process automatically.

For the calibration process, data was used which included utility meters for total building electricity and plug load electricity in 2010 (it was found that the steam meter data was unreliable for this task). Using the 2010 data in Figure 3.4.14, the model was tuned on a month-by-month basis, and after this calibration was performed, the prediction capability of the model was tested on for a few months in early 2011.

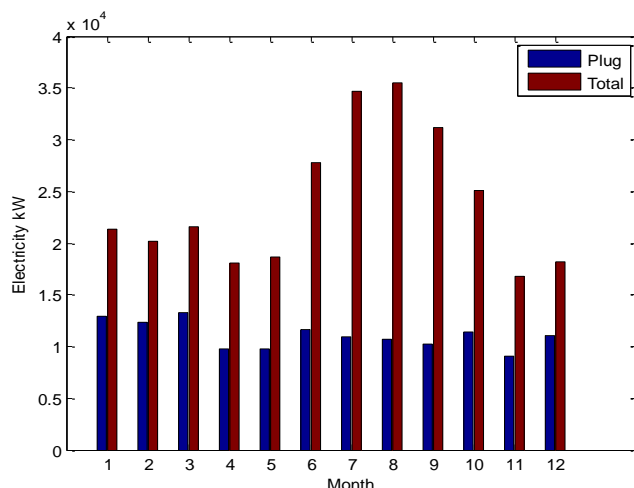


Figure 3.4.14. Raw sensor data taken from 2010 used for calibration of the EnergyPlus Model

The baseline Building 26 EnergyPlus model contained 2063 uncertain parameters, and in order for the calibration process to be tractable, model reduction was necessary. In order to perform model reduction, the top 20 critical parameters were identified for each month of sensor data. Once these were identified, optimization was performed using a cost function defined as  $\sqrt{\text{monthly or annual energy consumption}}$  where the two variables under the radical are either monthly or annual energy consumption.

The optimization results for monthly energy consumption are presented in Figure 3.4.15 where it can be seen that significant improvement with respect to the ability of the model to represent sensor data after calibration. It should be noted that these results are from optimization with output constraints and the error can be reduced if these constraints are lifted. The constraints were needed because the meta-model that was used for the optimization was only valid in regions where the output histograms fell. In many cases, these histograms did not encompass the sensor data points. Therefore, these constraints can be lifted by moving the cloud of sampled data (with which the meta-model is derived) closer to the sensor data. This can be done by either larger perturbations on the sampled input, or by moving the nominal value closer to the sensor data.

Parameters	Nominal	Calibrated
FL2 Zone5 plug load power density W/m <sup>2</sup>	20	17.513
FL2 Zone15 plug load power density W/m <sup>2</sup>	14	17.083
Hot water pump rated power consumption W	2238	2797.498
FL2 Zone11 plug load power density W/m <sup>2</sup>	14	17.335
FL1 Zone4 plug load power density W/m <sup>2</sup>	14.5	18.118
FL1 Zone1 plug load power density W/m <sup>2</sup>	14.5	18.106
FL0 Zone5 plug load power density W	600	652.766
Hot water loop max water temperature C	100	85.758
FL1 Zone11 plug load power density W/m <sup>2</sup>	14	17.500
Office lighting schedule fraction weekend	0.26	0.250

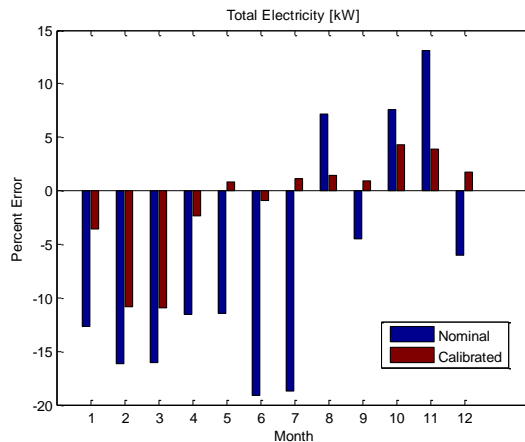


Figure 3.4.15 Calibration results for Building 26

The above calibration process illustrates how well a model can be tuned to fit a pre-described sensor data set. Once the model is calibrated it is desirable for the model to have prediction capability for future data. This validation process was performed using three months of data from 2011 (recall that the model was calibrated for 2010 data) and presented in Figure 3.4.16. This image illustrates that the error in prediction using the calibrated model (*Verification with 2011 weather* in the figure) is respectable and better than the un-calibrated model (*Nominal with 2011 weather* in the figure). There is a significant error in the month of May which is due to a chiller failure, which did not occur when the model was calibrated. In a sense, this verification test for this month illustrated an unexpected excursion in the data due to an equipment fault which is predicted by the validated model.

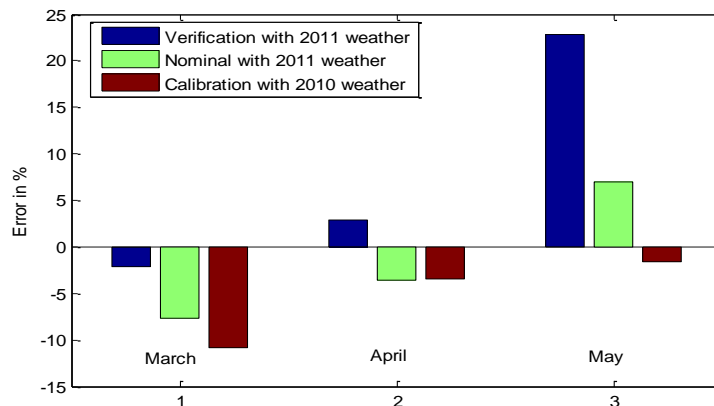


Figure 3.4.16 Verification results for Building 26

### 3.4.4 Discussion

In this part of the project, advances in parameter sampling integrated into a process to rapidly quantify uncertainty in building energy performance assessments and identify critical parameters during retrofit design were developed. This was accomplished by embedding existing building energy modeling tools into new methodology for analysis of these tools using state of the art advances in uncertainty quantification, sensitivity analysis, and optimization. The tools that were

integrated with the existing energy modeling software were able to efficiently manage thousands of parameters (2 orders of magnitude greater than in previous work).

A new process and tool chain was developed to automate analysis of energy performance failures from whole building energy models during design which was enabled by parametric sensitivity and uncertainty analysis. Because of the integrated and holistic nature of the analysis tools, failure modes at the building level can be identified in the design stage and avoided in the final design of the building. To further benefit the performance of the building, tools were developed for tractable design optimization which trades off building energy efficiency and indoor comfort.

The uncertainty and sensitivity analysis methods were tested in three case studies on DoD buildings (two of which had deep retrofits of their system configurations). In each case, uncertainty analysis offered insight into how high performance building design impacts uncertainty in this design. The sensitivity analysis illustrated which of the operation or design parameters of the building are critical to the energy consumption or comfort of the building.

### **3.5 Model-Based Failure Modes and Effects Analysis for Robust Building Design**

#### **3.5.1 Introduction and Background**

In the building retrofit design-build process, it is of benefit to understand not the simulation inputs which are critical, but rather what building failure modes are critical. These are often not the same thing. Design engineers and facility managers think of proper building operation in terms of how things can operate incorrectly, or *failure modes*. We assert that whole building energy simulation models can be effectively used to assess the risk and criticality of failure modes, as outlined here.

To do this, we use optimal sampling based methods over the domain of failure modes to then evaluate whole building energy consumptions, to determine a sensitivity analysis and thereby determine criticality of the failure modes. This can then be used, for example, to redesign the systems to create mitigations to the critical failure modes. Further, the results can be used to define requirements for any additionally necessary monitoring and controls.

We demonstrated our approach on an office building on the Fort Carson Colorado campus. We found the approach highlighted both expected as well as several unexpected non-linear interactions. Expected critical failure modes included lights being left on or night setbacks not being implemented. Non-obvious included the high sensitivity to degradation of circulating flows including chilled or hot water. We also find efficiency benefits having one standard work approach to both parametric uncertainty studies on building simulation inputs (described in section 3.4) integrated with the failure mode analysis described here. Both can make simultaneous use of the same whole building simulation sampling.

### 3.5.2 Technical Approach

To capture the energy loss impact of failure modes in buildings, it is important to capture the effects of not just one failure mode occurring in isolation, but of multiple failure modes occurring simultaneously. Interactions and compounding effects can create situations that cause large energy loss. Rather than exploring these multi-way modes through brute-force enumeration, our process flow makes use of modern probabilistic methods to explore combinations of failure modes.

Our overall process flow is depicted in Figure 3.5.1, consisting of 11 basic process steps. We start with the existing building walk-through analysis, to establish basic building parameters and existing systems configuration. With then establish alternative retrofit configurations, and from this we analyze the configurations for energy loss failure modes. With these defined, we map their effects into the simulation input variables. We then sample the failure modes for combinations to simultaneously simulate, using optimal sampling based methods. With these failure mode samples, we compute a set of whole building energy simulation input decks, each slightly different in input variable values, according to the failure modes of each sample. We execute these decks to compute a set of whole building simulation output decks. We then extract from these decks the relevant output parameter values of interest, namely the energy consumption and hourly peak power demand loads. We then complete an uncertainty analysis and sensitivity analysis (using the methodology described in section 3.4), but here we relate the sensitivity all the way back to the input failure modes. We now discuss each of these steps.

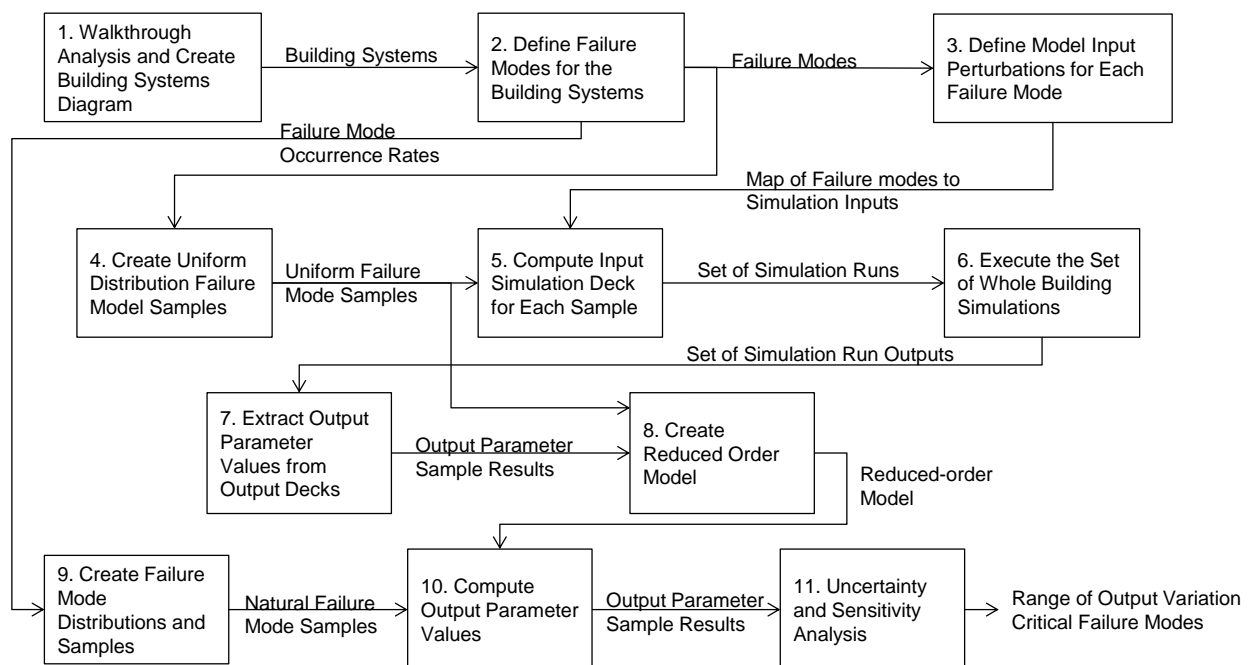


Figure 3.5.1 Overall process flow for analyzing effects of failure modes on building energy.

#### Step 1: Walkthrough Analysis and Create Building Systems Diagrams.

We begin by defining the systems in the building to analyze for energy loss failure modes. This includes establishing basic building parameters such as layout, floor plans, zones, schedules, and material construction. It also includes the different equipment selections for different scenarios

to analyze. Typically this includes a baseline design of the existing equipment, and one or more alternative designs with higher energy efficiency equipment.

The first result of this work for modeling purposes is a set of block diagrams depicting the building systems, the set of which describes graphically all energy related systems in the building. An example is shown in Figure 3.5.2, for a constant volume air handling unit portion of the HVAC equipment in a building. Constructing a block diagram is an exercise of diagramming all energy related components in the building and their interconnections. Generally this is a connected set of functional components and their interactions at end points of occupancy zones.

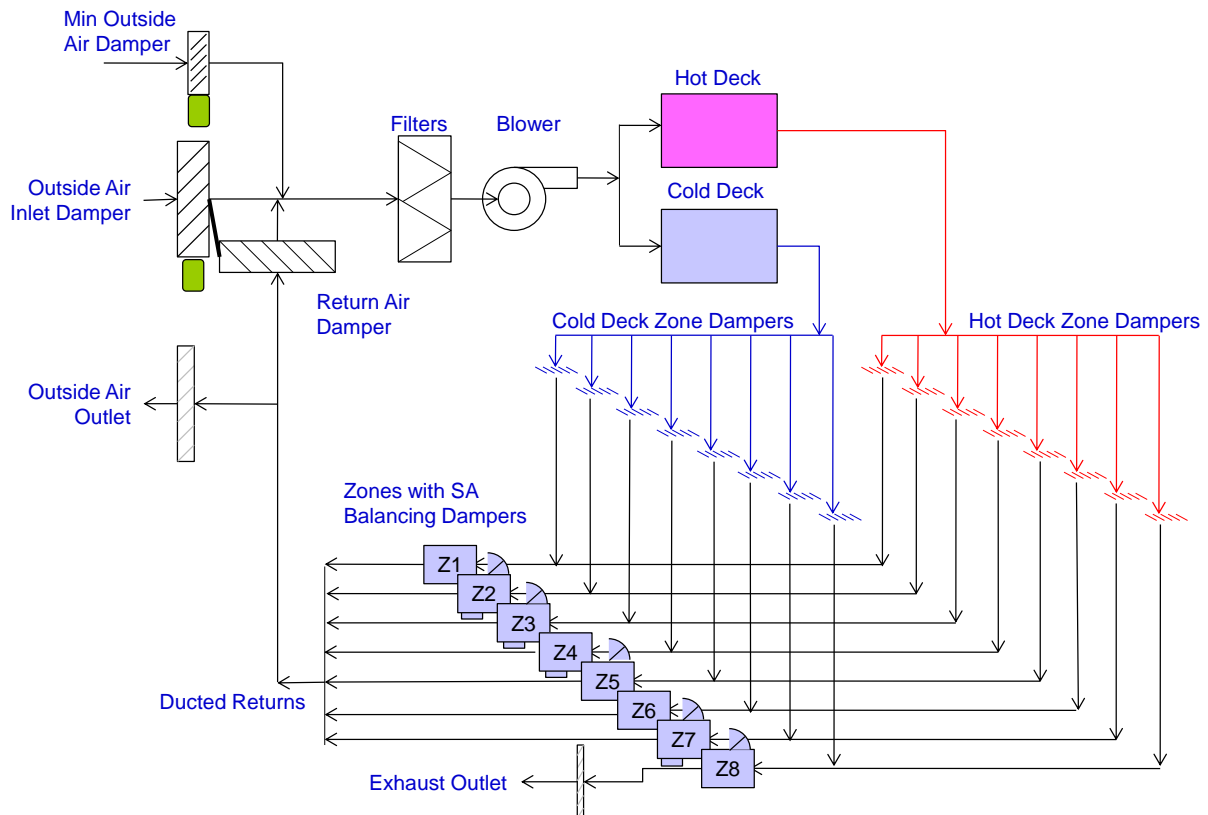


Figure 3.5.2 Block Diagram of a constant volume air handing unit.

The second result of this step is a complete while building energy simulation, generally an EnergyPlus or TRNSYS model. All building parameters and operational schedules are entered into the model descriptions of the building and its use cases as loads. All building systems are entered into the model descriptions of equipment. Typically this includes a model of the baseline design of the existing building envelope and equipment, and additional models for one or more alternative designs with higher energy efficiency equipment.

These two steps are not entirely separate. It is desirable to ensure the system block diagrams are aligned with the elements in the building energy simulation model. EnergyPlus and TRNSYS generally have modular code blocks representing the actual modular building systems. Therefore, the graphical block diagram representing the building systems should match the simulation code blocks. This is typically not an issue, but useful to mistake-proof the analysis.



Similarly, the detectability rating common to an FMEA is also not necessary here, since we seek to design the building monitoring and controls to be robust against the high severity commonly occurring failure modes. The purpose of the failure mode analysis is in part to design in sufficient detectability. Nonetheless, we do partition all failure modes into two categories, those that will need monitoring to detect, and those that will be naturally observed and corrected if they occur due to functionality. For example, if the boiler fails, there will be no heat, and the failure mode will be fixed. On the other, an economizer failing may mean 100% outside air is always drawn in, gets heated, and the occupants remain comfortable yet the energy consumption is far in excess of its design intent. In our work, we focus on the energy loss failure mode causes.

### Step 3: Define Model Input Perturbations for Each Failure Mode.

The next step is to map each failure mode to an associated set of inputs to the whole building energy simulation model. It is often not a simple mapping of considering each input individually, the mapping can be anything from many-to-one to one-to-many. For example, a typical building energy model variable is the leakage rate in a zone, often expressed as a percent of the air exchange rate. Failure modes of duct leakage or open windows, for example, could both contribute to variations in the simulation variable of leakage rate. On the hand, a controls system failure mode of the building lights being incorrectly forced on and left on 24-7 can affect the zone lighting schedule variables, one variable for each zone.

Nonetheless, one can create a mapping from each failure mode the set of associated building energy simulation model. The next step of this is to define the associate between each failure mode and the range of perturbation on each associated simulation variable. We do this by defining the *participation level* of any failure mode as a zero to one variable. When a failure mode is not active, we say its participation level is zero. When a failure mode is active, we say its participation level is one. We can define intermediate levels of failure mode participation as a value between zero and one.

Mathematically, the failure modes must be mapped to the building energy simulation input variables. Practically, there are three types of failure mode mappings to simulation input variables, as shown in Figure 3.5.4, unilateral, bilateral, and discrete, where the x-axis is a building energy simulation input variable, and the y-axis is a failure mode probability distribution.

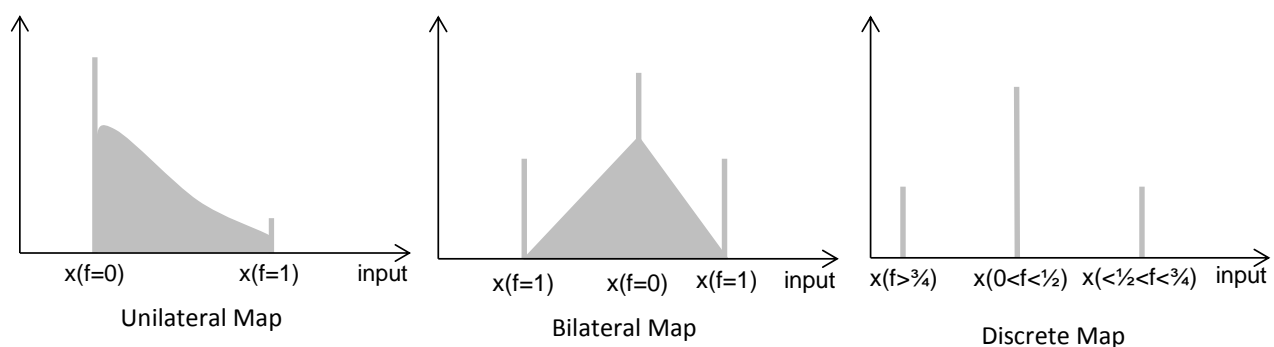


Figure 3.5.4 Example map types of failure mode to building energy simulation inputs.

The unilateral map is easiest to model and map, the upper and lower range of a building energy simulation input variable is defined for the zero and full participation levels of the failure mode.



For example, a dirty economizer failure mode can prevent complete closure, and so is mapped to the economizer air flow rate from zero to 5% of the nominal economizer full flow level.

The bilateral map is slightly more complex, since a zero value of the failure mode participation means the building energy simulation input variable is at nominal, and then as the failure mode increases in participation to one, the building simulation input variable value increases or decreases to the max or min. For example, consider the failure mode of an economizer improperly commissioned slightly high or low from the desired outdoor air flow rate. This can be mapped to plus or minus 2% of the nominal outdoor air refresh rate.

Finally, the discrete mapping is the nominal discrete value at zero failure mode participation, and then can take on any of the other values according to a discrete map from the failure mode participation variable. Generally this map is constructed by providing each discrete value an associate range of participation such that it has the desired level of probability of occurring. For example, an economizer control failure mode may incorrectly command the economizer to be open when it should be closed. This can be mapped to “on” or “off” over-ride to the economizer set point variable, each with a probability of occurrence.

Having defined each failure mode’s mapping to the building energy simulation inputs, one can turn each failure mode “on” one at a time, and compare the results with no failure modes active. This would provide an indication of the impact of a failure mode occurring in isolation, with all other failure modes not active and their related building systems operating perfectly at design intent. This ignores interactions. For example, an economizer and a chilled water supply valve both stuck partially open will cause much more energy loss than either failing alone or compared to their linear addition.

To explore this, simultaneous failure modes need to be explored. However, to do this, multiple failure modes can impact the same variable. For example, there are several failure modes associated with the single building energy simulation input representing the fraction of outside air, as discussed above.

To capture this, the next step is to define how multiple failure modes interact, and any precedence relations. Many failure modes simply add, particularly the unilateral and bilateral failure modes (Figure 3.5.4). A dirty economizer and an economizer setpoint error simply add in their impact on the economizer flowrate. However, an economizer controls error such as setting the economizer fully closed when it should be open is a failure mode that does not add with the previous; rather, it over-rides the economizer setpoint value to zero. This logic amongst the failure mode mappings to building energy simulation input variables must be defined and modeled.

Fortunately, these problems are easily detected. One must examine each building energy simulation input variable individually, and back identify all failure modes associated with the variable. Then, for this small set, the logic to establish the input value from the combined failure modes defined. Typically, this is simple addition with some special over-ride failure modes. The economizer setpoint variable provides a descriptive example.

With these tasks complete, a mapping from all the failure modes to the building simulation inputs is complete. All failure modes are defined in terms of  $[0,1]$  participation levels, and as each failure mode varies from zero to one in participation, an associated mapped set of building energy simulation inputs change as a dependent variable mapping.

#### **Step 4: Compute Failure Mode Uniform Distribution Samples.**

The next step is to sample the failure mode participation level space, an  $n$ -dimensional  $[0,1]$  compact space, to represent the domain with a finite sample set. Ultimately, we do the sampling according to the probability distributions defined on the failure mode participation levels discussed earlier (Figure 3.5.4). However, it is impractical to do this sampling against the whole building energy simulations.

That is, some failure modes have very low occurrence rates, reducing their risk levels in actual practice, compared to their sensitivity. If a failure rate only occurs once every ten years, it is perhaps of less concern than another failure mode that occurs monthly, if they have the same energy impact. To have a distribution sampling rate sufficient to capture very rare events, however, requires very high sampling rates, particularly to ascertain compounding interactions with other failure modes.

There, we apply a two-step approach to sampling, as shown in Figure 3.5.1. First, we ignore the occurrence rates from the FMEA, and sample all failure modes uniformly. We compute the energy results using the whole building simulation at each sample point, which is computationally intensive. This approach clarifies each failure mode's contribution to energy consumption and how they interact with other failure modes. We fit the results to a reduced order model, to easily and quickly indicate how all failure modes individual and together affect energy consumption.

We then separately compute actual risk, incorporating the occurrence rates of the failure modes. To do this, we sample a second time the failure modes, but this time using their actual occurrence rates. We then compute actual expected energy consumption levels from the failure modes. We can do this for rare failure modes by using very large sampling rates, since the reduced order model computes much more quickly.

To do the sampling, we make use of advanced optimal spaced sampling techniques (described in section 3.4). This provides a minimal sample set that can cover the failure mode participation distributions.

The result is a matrix of samples, where each failure mode is a column and each sample is row. Each sample has a  $[0,1]$  value for each failure mode, representing the participation level of each failure mode in the failure mode scenario represented by the row sample.

#### **Step 5: Compute the Input Simulation Deck for Each Sample.**

The next step is to map the matrix of failure mode participation level samples to building energy simulation inputs. Practically, this means creating a slightly varied building simulation input deck for each row of the failure mode participation sample matrix. For each row in the matrix, a separate building simulation input deck is created.

**Step 6: Execute the Set of Whole Building Simulations.**

The next step is to execute the set of input decks on a high performance computing cluster, to quickly compute each simulation. This computation is intense, but can be highly parallelized. The result is a set of building energy simulation output decks, each slightly different in values according to the varied performance impacts of the different participation levels of the failure modes occurring simultaneously.

**Step 7: Extract the Output Parameter Values from the Output Decks.**

Once all sample runs are complete, the set of output decks is parsed and the desired energy and power figures are extracted. Typically, this involves summing the energy data over the 8760 hours of simulated building operation over a simulated year, as well as recording the peak hourly consumption figures.

The result is an output matrix with columns of the output energy and peak power metrics, and rows of the number of samples.

**Step 8: Create Reduced Order Model.**

With this matrix of input and output samples, we compute a rapid reduced order model, making use of reduced order model surface fitting techniques described in section 3.4. The result is equations that represent how each failure impacts energy consumption, and further how each interacts with others to impact energy consumption together. These equations are independent of the actual occurrence levels and associated probability distributions of the failure modes. The next step is to modulate the risk levels of each failure mode energy sensitivity according to how likely each is to occur.

**Step 9: Create Failure Mode Distributions and Samples.**

Most failure modes are not active at any given moment, or only slightly active. For example, a duct can be blocked and cause a high pressure loss as a failure mode. More likely is the failure mode is only partially participating and contributes a slight pressure loss. We capture this character using a failure mode participation probability function, where over the [0,1] domain of the failure mode, we define a probability distribution. Generally, we use a distribution biased toward zero participation, according to the expected probability of occurrence associated with the occurrence rate defined in the FMEA, as shown in Table 3.5.1.

Table 3.5.1 Probability of Occurrence for Various FMEA Occurrence Ratings.

Occurrence Table		Fraction View		Downtime View		Part Life View	
Occurrence	Probability	%	Description	Hours/Yr	Description	Hrs to Fail	Description
0	0.000000	0%	Never	0	Never	0	Never
1	0.000002	0.0002%	2 per million	0.017	1 min/yr	525,600	60 yr part
2	0.000010	0.001%	1 per 100,000	0.08	5 min/yr	105,120	10 yr part
3	0.000114	0.01%	1 per 10,000	1	1 hr/yr	8,760	Fails once / yr
4	0.000913	0.1%	1 per 1000	8	1 workday/yr	1,095	Fails every month
5	0.002740	0.3%	3 per 1000	24	1 fullday/yr	365	Fails every 2 wks
6	0.005479	0.5%	5 per 1000	48	2 days/yr	183	Fails every week
7	0.013699	1.4%	1 in 75	120	1 wk/yr	73	Fails every 3 days
8	0.083333	8%	1 in 10	730	1 mo/yr	12	12 hourly
9	0.500000	50%	Half	4380	6 mo/yr	2	2 hourly
10	1.000000	100%	All	8760	Entire year	1	> Hourly failure

From the expected probability of occurrence, a participation level probability distribution is defined such as shown in Figure 3.5.5. As shown, the cumulative probability out to the expected value of a failure mode's participation distribution should equal the probability of the occurrence rate, as listed in Table 3.5.1. This rule constrains the probability distribution, which with a desired shape definition such as a long tail, exponential, or Weibull distribution, provides sufficient information to define the failure mode distribution.

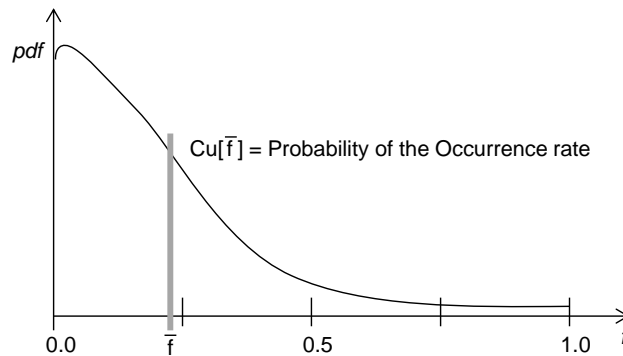


Figure 3.5.5: Failure Mode Participation Probability Density Function.

We define these distributions on each failure mode according to the FMEA occurrence rates, and then we sample these distributions, similar to Step 4, but not using uniform distributions. With the actual distributions, some of which can be highly skewed, we sample at much higher rates.

#### Step 10: Compute Output Parameter Values.

Using the very rapid reduced order model, we compute output energy consumption levels for each sample point of failure mode participation levels. This is a very rapid calculation set over many sample points, as compared to Step 4.

### Step 11: Uncertainty and Sensitivity Analysis.

The next step is to analyze the output matrix data as sampled values of distributions, for each output metric. The shape of the distribution is of interest, to determine any bias from nominal operating conditions, large outliers, etc.

Finally, the last step is to correlate the inputs failure mode participation levels with output energy consumption and peak power metrics. Through correlation, regression, and variance decomposition techniques, we determine which failure modes drive excess energy and peak power consumption above the as-designed condition. This step is using the same methodology and approach depicted in section 3.4

### 3.5.3 DoD Case Studies

To demonstrate the methodology, consider a mid-sized office building on the Fort Carson Colorado campus. As shown in Figure 3.3.7 in section 3.3.2, the building is single floor, long, flat building with two separate wings, 22,300 square feet total with 18,631 square feet occupied, two separate constant volume air handling units, and 18 separate zones. In the baseline condition, the Energy Use Intensity has been modeled at 80.9 kBTU/ft<sup>2</sup>/year, putting it at a rating of 24 in the EnergyStar Portfolio Manager database, or that it is in the bottom 24% of buildings in it's class of usage and climate.

The building was also instrumented and measured over a limited duration. Based on this, the building was measured with an Energy Use Intensity at 101 kBTU/ft<sup>2</sup>/year as operated in a 24-7 capacity. Accounting for the differences in operating schedule at the time of measurement, the energy use is comparable.

The breakout of the energy consumption is shown in Table 3.5.2. The vast majority is going into plug loads, followed by heating, air circulation and lighting loads.

Table 3.5.2 Baseline Energy Intensity for Building 1225 (kBTU/ft<sup>2</sup>/yr)

Heating	Cooling	Pumps	Fans	Lighting	Plug	Total - Plug	Total
20.5	3.2	1.3	13.6	12.7	29.5	51.4	80.9

These results suggest we can understand, quantify, and simulate failure modes that cause energy efficiency degradation. For this baseline building configuration, the next step is to consider not only the observed failure modes in the particular state of maintenance and equipment replacement at the time, but all possible failure modes at any future state, to determine what failure modes are most critical to manage.

### DoD/Ft. Carson Building 1225: Standard Configuration- Critical Failure Modes

The baseline existing systems in the building were diagrammed into a set of block diagrams representing all energy related systems and interconnections in the building. This was then analyzed for all failure modes of all components and their interconnections. There were 38 systems and zones with 89 critical components to analyze, and 533 failure modes in the building energy systems (lighting, HVAC, power, and controls, etc.).

The distribution of failure modes are shown in Table 3.5.3. There are three columns, indicating the need or ability to model the failure mode. The rows indicate general categories of building

systems. The “Alarmed” column indicates failure modes that, should they occur, will generate an immediate response from occupant complaints. For example, if the boiler fails, there will be no heat, occupants will complain and the failure will be fixed. These failure modes are not necessary to model here, where we are concerned with energy loss failure modes that do not necessarily cause a sufficient comfort complaint. Such energy loss failure modes are represented in the “Modeled” column of Table 3.5.3. These are failure modes such as missing insulation, stuck economizers, etc. Finally, there are failure modes that can exist in the building, but cannot be directly modeled in whole building simulation tools, and so must be estimated outside the model. These are typically pressurized flow of air between zones, control system feedback dynamics, or other short cycle dynamics.

Table 3.5.3 Distribution of Failure Modes.

	Alarmed	Modeled	Outside Model	Total
Envelope	0	26	10	36
HVAC Equipment	10	42	12	64
HVAC Controls	29	173	192	394
Internal Gains	0	1	2	3
Internal Gain Controls	0	35	1	36
Total	39	277	215	533

The modeled impact of failure modes on the energy consumption for the system is substantial, with the deviations operating at 15% higher energy consumption rate than when all systems operating perfectly at the nominal as-designed conditions. The distribution of total energy consumption is shown in Figure 3.5.6, indicating the spread of energy consumption across the failure modes.

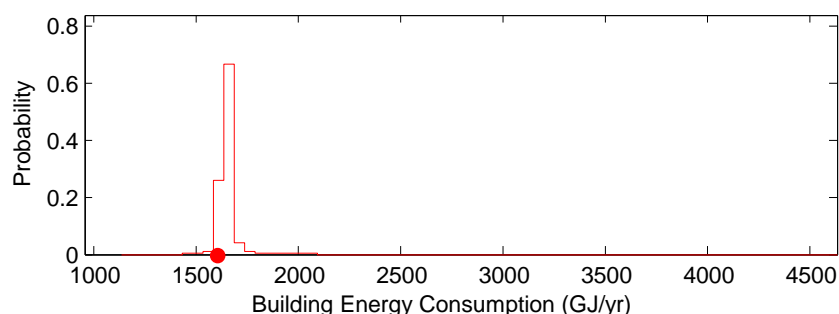


Figure 3.5.6 Distribution of Overall Building Energy Consumption over the Failure Modes.

This uncertainty breaks down into Heating, Cooling, Pumps, Fans, Lighting and Plug loads as shown in Figure 3.5.7. While the range is similar by subsystem, note the effects of the failure mode result in different probability shapes for the different building subsystems. The failure modes affect the energy consumption differently by subsystem.

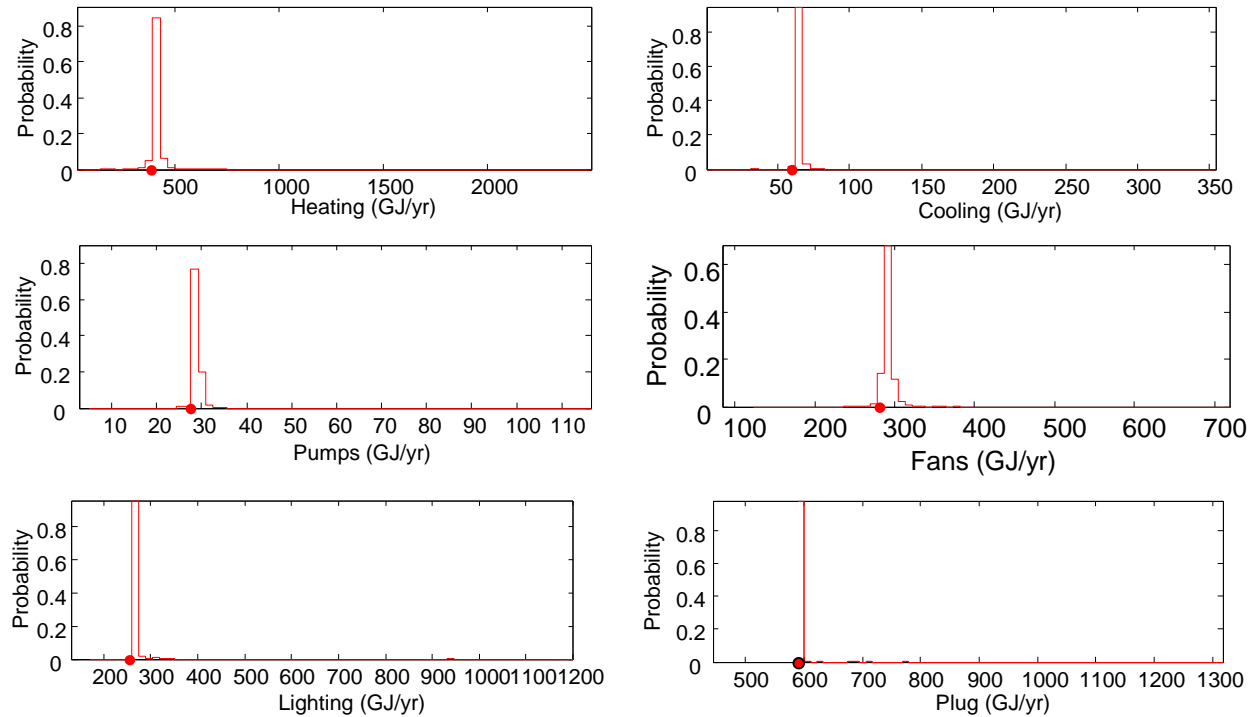


Figure 3.5.7 Distribution of Subsystem Building Energy Consumption over the Failure Modes.

Given the distribution of energy consumption from all of the various failure modes, some contribute more than others. The primary largest contributing failure mode causes were identified as outlined in Figure 3.5.8, as determined by the sensitivity analysis described in Figure 3.5.1. The largest contributing failure modes to overall energy consumption included the lights being left on all night and the night temperature setback not being used. Assuming these occur and happen every day, these double the energy consumption. On the other hand, such occurrence rates are not expected, and so the predicted energy distribution is smaller as shown in Figure 3.5.9.

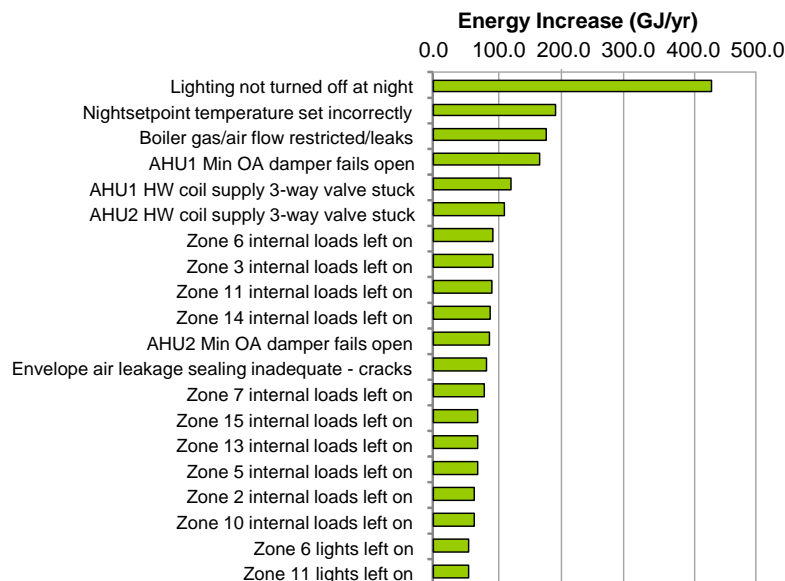


Figure 3.5.8 Sensitivity of Overall Building Energy Consumption to the top 10 contributing Failure Modes.



Similarly, the distributions of subsystem energy consumption from all of the various failure modes can be analyzed for contributors using the same sensitivity analysis approach described in Figure 3.5.1. The primary largest contributing failure mode causes were identified for each subsystem as outlined in Figure 3.5.9. Notice the largest contributing failure modes to each subsystem's energy consumption are not the same as the largest contributors to overall energy consumption. For example, the failure mode that contributes highest to overall energy consumption is the lights left on at night, but for the cooling system, it is the chilled water supply valve partially stuck shut thereby reducing cooling flow (and causing discomfort). This reflects the refinement of analysis by subsystem.

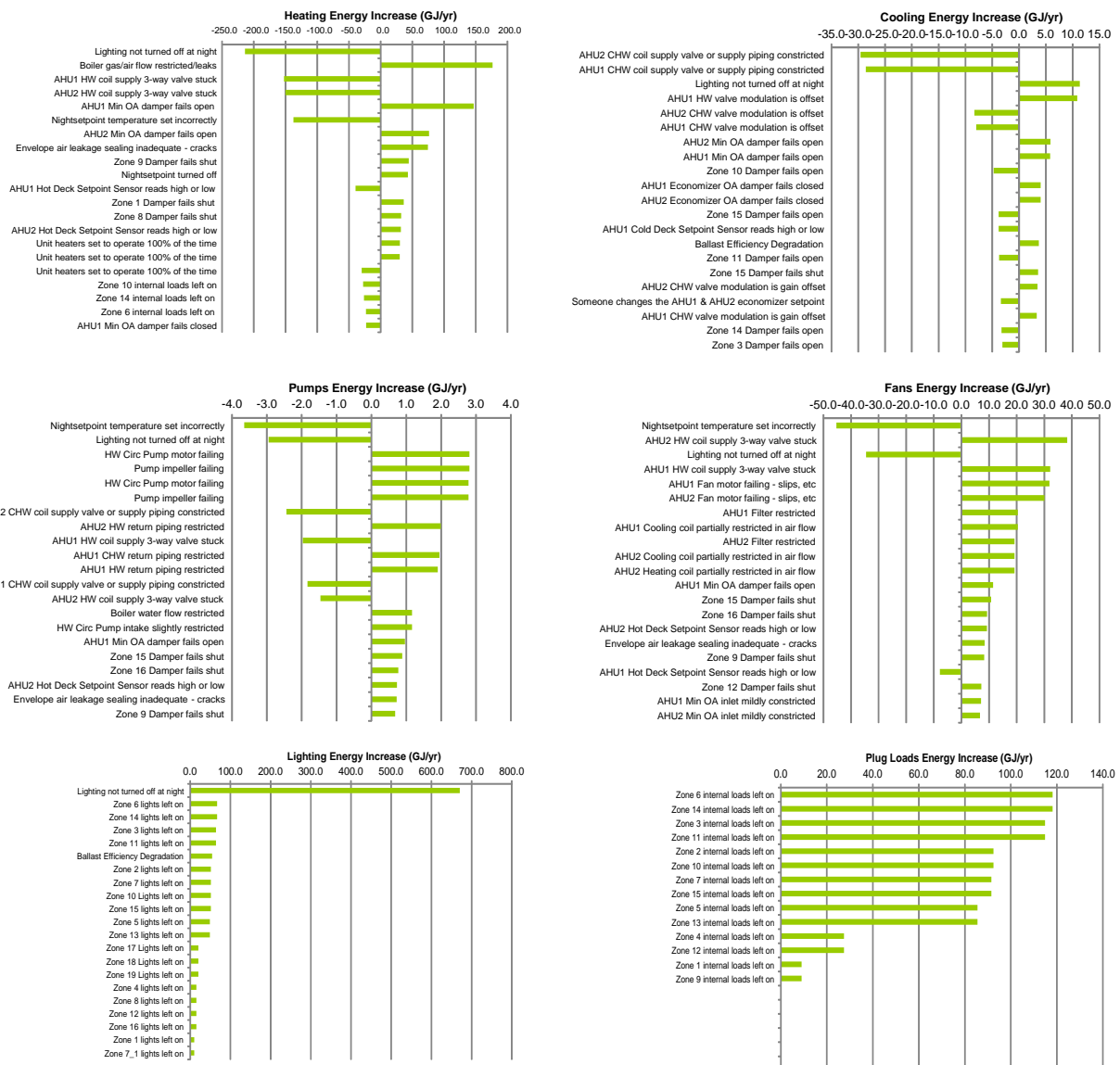


Figure 3.5.9 Sensitivity of Subsystem Building Energy Consumption to the top 20 contributing Failure Modes.

Overall, the standard, traditional baseline system configuration of building 1225 shows a design intent of 80.9 kBtu/ft<sup>2</sup> energy intensity. When considering failure modes and their expected occurrence rates with reasonable maintenance, this increases by 15%. If any of several failure modes occur continuously throughout the year, the energy increase can be much more substantial and easily double the energy consumption of the building.

Given these results, next a low energy design retrofit concept was explored for Building 1225, discussed next.

### **DoD/Ft. Carson Building 1225: Advanced Design - Critical Failure Modes**

The systems in Building 1225 were explored as retrofits for increased energy efficiency. The HVAC system was explored as a high efficiency solar thermal system retrofit with the campus steam as backup. The cooling system was explored with an evaporative cooling system retrofit with the campus chilled water system as backup. The constant air volume systems were retrofitted with VAV distribution for higher efficiency. High efficiency fluorescent lighting was considered. No advanced occupancy based controls were considered, given the building has a high 24-7 occupancy. Also, the only envelope measures considered were double pane windows. Nonetheless, this retrofit solution upgrades Building 1225 to a design intent of 58 kBtu/ft<sup>2</sup>/year, a 28% overall reduction with rather modest interventions and places the building at an EnergyStar Portfolio Manager rating of 54, a 100% improvement. The low rating is entirely due to the unusually high internal computing loads and unusually high occupancy rate and schedule.

The breakout of the energy consumption is shown in Table 3.5.4. The vast majority is going into plug loads, followed by heating, air circulation and lighting loads.

Table 3.5.4 Baseline Energy Intensity for Building 1225 (kWhr/m<sup>2</sup>/yr)

Heating	Cooling	Pumps	Fans	Lighting	Plug	Total - Plug	Total
11.9	1.8	0.3	5.8	8.5	29.5	28.3	57.8
-38%	-41%	-79%	-50%	-33%	0%	-41%	-26%

Similar to the baseline existing building systems configuration, the advanced systems in the building were diagrammed into a set of block diagrams representing all energy related systems and interconnections in the building. This was then analyzed for all failure modes of all components and their interconnections. There were 43 systems and zones with 98 critical components to analyze, and 565 failure modes in the building energy systems (lighting, HVAC, power, and controls, etc.).

Similar to the baseline existing configuration, the advanced system modeled impact of failure modes on the energy consumption for the system is substantial, with the expected average operation at 20% higher energy consumption rate than the operation with all systems operating perfectly at the nominal as-designed conditions. The distribution of total energy consumption is shown in Figure 3.5.10, indicating the spread of energy consumption across the failure modes. Notice the range of uncertainty is slightly larger the baseline configuration. But with the decrease in nominal energy consumption, the percent uncertainty is larger.

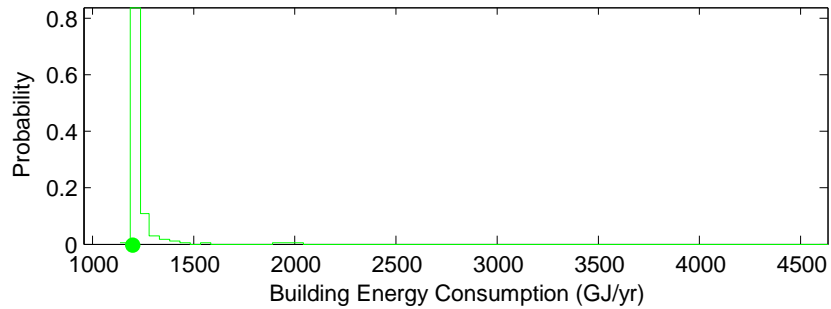


Figure 3.5.10 Distribution of Overall Building Energy Consumption over the Failure Modes.

This uncertainty breaks down into Heating, Cooling, Pumps, Fans, Lighting and Plug loads as shown in Figure 3.5.11. While the range is similar by subsystem, note the effects of the failure mode result in different probability shapes for the different building subsystems. The failure modes affect the energy consumption differently by subsystem.

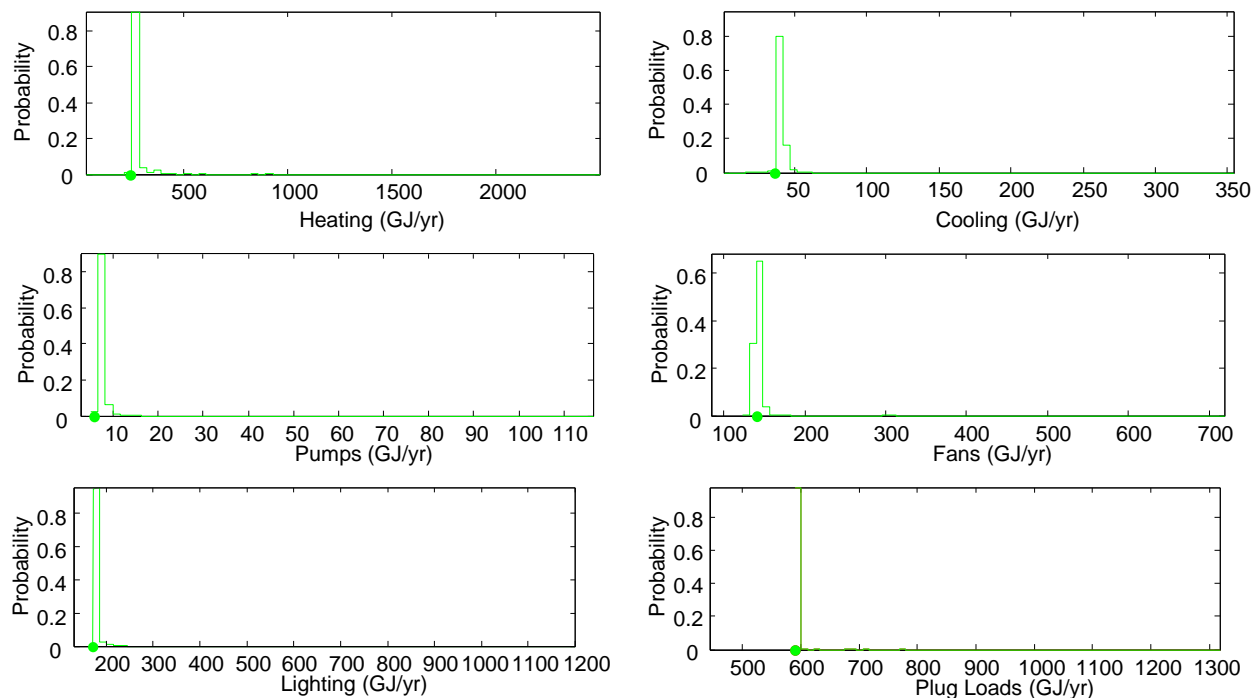


Figure 3.5.11 Distribution of Subsystem Building Energy Consumption over the Failure Modes.

Given the distribution of energy consumption from all of the various failure modes, some contribute more than others. The primary largest contributing failure mode causes were identified as outlined in Figure 3.5.12, as determined by the sensitivity analysis described in Figure 3.5.1. The largest contributing failure modes to overall energy consumption included the lights not turned off at night, and the night temperature setback not operating. These failures are shared with the nominal baseline system, though in different order of sensitivity. The similarity is due to the design changes made being mostly robust, such as lighting upgrades that cannot be defeated. The failure modes that are present, similar to the baseline design, generally account for

an increase of 15% energy consumption rate than when all systems operating perfectly at the nominal as-designed conditions.

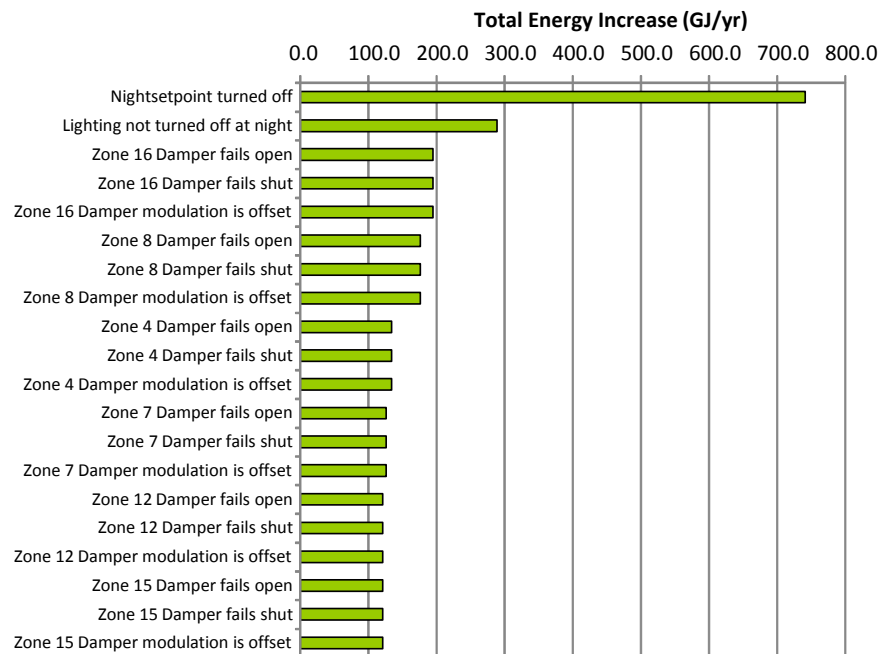


Figure 3.5.12 Sensitivity of Overall Building Energy Consumption to the top 10 contributing Failure Modes.

Similarly, the distributions of subsystem energy consumption from all of the various failure modes can be analyzed for contributors using the same sensitivity analysis approach described in Figure 3.5.1. The primary largest contributing failure mode causes were identified for each subsystem as outlined in Figure 3.5.13. Notice the largest contributing failure modes to each subsystem energy consumption are not the same as the largest contributors to overall energy consumption. For example, the failure mode that contributes highest to overall energy consumption is a controls failure turning off the night temperature setback, but for the cooling system, it is a controls failure blocking the economizer mode operation. This reflects the refinement of analysis by subsystem.



Figure 3.5.13 Sensitivity of Subsystem Building Energy Consumption to the top 10 contributing Failure Modes.

Overall, the advanced retrofit design configuration of building 1225 shows a design intent of 57.8 kBTU/ft<sup>2</sup>/year energy intensity. When considering failure modes, this increases by an expected 15%. If any of several failure modes occur continuously throughout the year, the energy increase can be much more substantial and easily double the energy consumption of the building.

### 3.5.4 Summary

Analysis of building energy overconsumption due to building system failure modes is possible through whole building simulation tools. We define the failure modes, relate these to the whole building energy simulation inputs, and then use sample based methods to evaluate energy performance at each sample of failure mode combinations. Performing a sensitivity analysis on the results can indicate which failure modes are more significant than others in contributing to energy consumption.

### 3.6 Reduced-Order Modeling and Control Design for Low Energy Building Ventilation and Space Conditioning Systems

This section focuses on the modeling and control of airflow in buildings equipped with low-energy HVAC systems. The air in rooms or spaces equipped with terminal units such as displacement or under-floor vents and radiant floors or ceilings, are often characterized by buoyancy and vertical temperature stratification. Such systems tend to be sensitive to disturbances, and careful control design is needed to maintain comfort, while achieving the potential energy savings. The treatment of airflow in current simulation tools such as EnergyPlus, TrnSys, Modelica, and others, tends to be inadequate to accurately represent the actual physics, and this section demonstrates techniques that fill some of these gaps. The main objectives are:

1. Develop low-order models of airflow in rooms or zones equipped (or retrofitted) with low-energy terminal HVAC units, starting with high-fidelity CFD simulations.
2. Develop controllers that reject disturbances (solar radiation, occupant, etc.), maintain comfort, while minimizing energy consumption.
3. Test the performance of model-based controllers by performing closed-loop simulations in the original high-fidelity CFD models; this is schematically shown in
4. Figure3.6.1.
5. Evaluate energy savings over conventional HVAC system

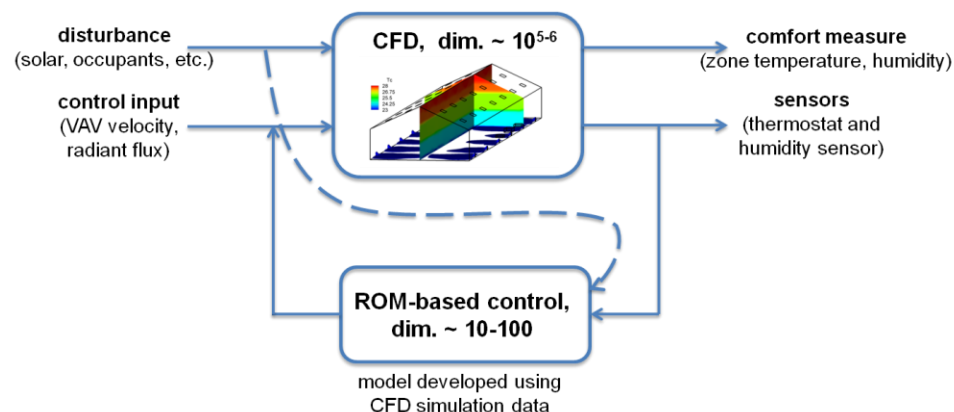


Figure3.6.1: Schematic of model-based feedback-control, for rejecting disturbances solar radiation and occupant loads. The control goal is to maintain the comfort measure within specified limits, while minimizing energy consumption.

### 3.6.1 Current Practices in Modeling Building Indoor Environment

The standard approach in the buildings community for modeling airflow is to use lumped models, typically based on energy balance over a large control volume; see (Griffith, Long, Torcellini, & Judkoff, 2008) for examples. These models essentially represent the air in a zone using a single node, and hence are inadequate for resolving spatial in-homogeneity. Other approaches are nodal models, which represent indoor air using multiple nodes to capture stratification, or zonal models which divide the control volume into smaller parts, and derive models based on energy balance over each of the sub-volumes. The models resulting from these approaches typically have parameters that need to be obtained empirically from experiments of high-fidelity simulations. On the other extreme, computational fluid dynamic (CFD) simulations have been used to study stratification in passive systems (Lee et al., 2009; Kobayashi & Chen, 2003), but are too complex and intractable for practical design, optimization or control.

In this work, we apply model reduction techniques to extract dynamics at temporal and spatial scales suitable for analysis and control design of low-energy HVAC systems. The models that we develop here are of the input-output dynamics, built-in with control inputs, thus allowing control design.

### 3.6.2 Model Reduction

Model reduction involves finding low-dimensional models that approximate the full high-dimensional dynamics (here, the Boussinesq partial differential equations). These methods have been developed by the fluid mechanics community through extensive research aimed at understanding complex flow physics and flow control. Most of these methods involve post-processing data obtained from carefully designed experiments or simulations, to result in low-order representations. One of the first methods was that of proper orthogonal decomposition (POD) and Galerkin projection, developed by Lumley (1970) to develop models of turbulence. In this method, empirical data is first used to develop a set of basis called POD modes, which optimally capture the energy-content of the given data-set. The governing equations are then projected onto a subset of POD modes, using Galerkin projection, to develop low-order models. In the context of building airflows, this method has been applied for real-time estimation of airflows in buildings (Surana et al., 2008; Borggaard et al., 2009a,b). In Surana et al. (2008), a Lagrangian Coherent Structure based metric was employed to enhance conventional POD based models by identifying mode shapes that have relevance to transport of passive contaminants in building airflows.

The standard POD/Galerkin approach suffers from several limitations. In general, the POD/Galerkin method can yield unpredictable results, and it is sensitive to details such as the empirical data used, and the choice of inner product (Rowley et al., 2004). POD/Galerkin models near stable equilibrium points can even be unstable (Rowley, 2005; Ilak & Rowley, 2008). An alternate snapshot-based approach, inspired from control theory, is the approximate balanced truncation developed in Rowley (2005); it is particularly suitable for control design since it accurately captures input-output dynamics of the full system. This method is applicable to stable linear input-output systems, and results in balanced models, with guaranteed error bounds; extensions have been developed for unstable (Ahuja & Rowley, 2010) and periodic systems (Ma et al., 2010b). The resulting models are superior as compared to POD/Galerkin, in the sense that they



preserve stability of the original system and fewer modes are required to capture the original dynamics. However, compared to POD, this approach is only applicable to linear systems (or linearized dynamics) and requires solution of the associated adjoint system. Recently, it was shown that for a discrete time input-output system, a system identification method known as eigensystem realization algorithm (ERA) is equivalent to the balanced POD (Juang & Pappa, 1985; Ma et al., 2010a). The advantage of ERA is that it has a significantly lower computational cost, and it does not require adjoint simulations, thus making it applicable for model reduction using experimental data and simulation data from commercial software. The main disadvantage of ERA as compared to balanced POD is that it does not provide modes for projecting the full dynamics; the modes are desirable as they could guide actuator and sensor placement, provide insight into the flow physics, and also be used to obtain nonlinear models by projecting the full nonlinear equations.

In this work, we use both the model reduction techniques described above – ERA and POD/Galerkin – to determine input-output dynamics of airflow in buildings, and compare the models developed using the two techniques. Using these models, we design an optimal controller for rejecting disturbances such as solar radiation and occupant heat gains. The resulting controllers are used to perform closed-loop simulations in CFD, and are shown to be effective in maintaining comfort. Finally, the resulting models are used to evaluate energy savings over the baseline system, for a period of a few months, which would otherwise not be possible in the high-fidelity simulations.

### **3.6.3 Section Outline**

The remainder of this section is organized as follows: a general problem formulation and control objective is described in section 3.6.4. The DoD case-studies presented in sections 3.6.5, where we consider the Atlantic Fleet Drill Hall located in Great Lakes, Illinois. We consider models of airflow in rooms of two different spatial scales – one, a drill-deck of dimensions 138m x 26m x 14m, which is a large open area, and second, a smaller conference room of dimensions 14m x 8m x 3m. For the drill-deck, high-fidelity CFD models of the baseline overhead supply system are validated against field measurements. Retrofits are proposed for the two rooms: displacement ventilation (DV) for a cooling mode operation, and radiant floors combined with DV for a heating mode operation. Low-order models are developed using ERA, and controllers are developed to reject disturbances from solar radiation and occupant heat gains. The models and controllers are tested by comparing their predictions against CFD simulations, with feedback control. The models are also used to provide estimates of energy savings in different HVAC components over the baseline system. Finally, conclusions are provided in section 3.6.6 along with some future plans.

In appendix D, the model reduction and control design techniques used in this project are described. The appendix also details two additional case-studies that were used to develop the tool-chain applied to the DoD case-studies. The first case-study of airflow in one room of a medium office building taken from the United States Department of Energy (DOE) EnergyPlus Benchmark Model Suite is considered, mainly to test robustness of airflows in systems served by low-energy HVAC units. The second case-study is a model problem of airflow in a room with a dis-

placement vent supplying conditioned air at the occupant level and a passive chilled ceiling, and is used to develop and test the model reduction and control design tool-chain.

### 3.6.4 Problem Statement and Formulation

For airflows in building applications, the coupled Navier-Stokes and energy equations can be approximated by the Boussinesq equations (1-3), where temperature introduces a buoyancy force (Kundu, 1990):

$$\frac{\partial \mathbf{v}}{\partial t} = -\mathbf{v} \cdot \nabla \mathbf{v} - \frac{1}{\rho_0} \nabla p' - \beta T \mathbf{g} + \nu \nabla^2 \mathbf{v}, \quad (1)$$

$$\frac{\partial T}{\partial t} = -\mathbf{v} \cdot \nabla T + \frac{\kappa}{\rho_0 C_p} \nabla^2 T, \quad (2)$$

$$\nabla \cdot \mathbf{v} = 0. \quad (3)$$

Here, the three-dimensional velocity field  $\mathbf{v} = \mathbf{v}(\mathbf{Z}, t)$ , temperature field  $T = T(\mathbf{Z}, t)$ , and pressure distribution  $p_0(\mathbf{Z}; t)$  are the unknowns,  $\mathbf{Z} = (X, Y, Z)^T$  is the spatial coordinate vector defined over a region,  $\mathbf{g}$  is acceleration due to gravity,  $\rho_0$  is reference air density,  $\beta$  is its thermal coefficient of expansion,  $\nu$  is kinematic viscosity,  $C_p$  is thermal capacitance and  $\kappa$  is the thermal conductivity. For well-posedness, the equations (1-3) need to be supplemented with an initial condition and boundary conditions for the velocity and temperature fields. For airflows in buildings, these are typically in the form of control inputs, such as the supply air temperature and velocity from diffusers or heat flux through a radiant component (ceiling or floor), or in the form of disturbances, such as solar heat flux through a window or internal heat gains from people or equipment. Mathematically, we can abstract some of these conditions as:

$$\mathbf{v}(\mathbf{Z}, t) = \mathbf{u}_v(\mathbf{Z}), \quad \text{for } \mathbf{Z} \in \partial\Omega_1 \quad (4)$$

$$T(\mathbf{Z}, t) = u_T(\mathbf{Z}), \quad \text{for } \mathbf{Z} \in \partial\Omega_2 \quad (5)$$

$$\nabla T(\mathbf{Z}, t) \cdot \mathbf{n} = u_q(\mathbf{Z}), \quad \text{for } \mathbf{Z} \in \partial\Omega_3. \quad (6)$$

The system of equations (1-3) along with the boundary conditions (4-6) are approximated by numerical discretization of the domain and a time interval  $[0, t_f]$ , and are solved using a commercial CFD solver, which in our case is ANSYS FLUENT. Our goal is to determine control inputs that reject the disturbances in the building, while maintaining comfort and minimizing the required control effort. An example of a control objective can be stated as follows: given a disturbance  $d(t)$  over a region of the boundary, determine a control input  $u(t)$  (that depends on the choice of HVAC component), over another region of the boundary that maintains the average temperature in the occupied region of the room at a certain desired value of  $T_{avg}$ , while minimizing a quadratic cost function:

$$J[T, u] = \int_0^{t_f} \left[ \int_{\Omega_{occ}} Q(T - T_{avg})^2 d\mathbf{Z} + u^T R u \right] dt, \quad (7)$$

where  $Q$  and  $R$  are positive-definite,  $\Omega_{occ}$  is the occupied region of the building, and  $u^T$  is the transpose of  $u$ .

Now, this control problem involves solutions of Riccati equations, and becomes intractable with increasing number of grid points. For instance, the number of equations resulting involved in a CFD simulation can be on the order of  $n \sim 10^{5-8}$ , while the dimension of the corresponding Riccati equations is  $n^2$ . For  $n = 10^5$ , this corresponds to more than 37 GB for simply storing one vector

(floating-point on a 32-bit machine). Thus, model reduction is a key enabler for designing controllers for fluid flows. In this work, we explore two different techniques for model reduction. First, eigensystem realization algorithm (ERA) is used to develop models valid in the linear neighborhood of steady states. The method results in input-output balanced models and provides guaranteed error bounds. The main disadvantage of the method is that it does not provide modes for projecting the full dynamics. Hence, we next use POD/Galerkin method, which is applicable to full nonlinear systems as well. The models resulting from the two techniques are used to develop controllers, which are finally implemented in the full CFD simulations.

The control goal in this work is disturbance rejection, where the disturbances can be thought of those from solar radiation, ambient temperature, and internal heat gains from occupants, lights and plug loads. For that purpose, we also explore two different control designs: first, we assume that future disturbances are known and design an optimal controller that minimizes quadratic a cost function, balancing comfort and cost. The assumption that the disturbance is known in future is not unrealistic: for example, it may be known a-priori that there is a meeting in the room with an expected attendance. Next, we relax this assumption and develop a robust controller that estimates the disturbance magnitude using the reduced-order model.

### **3.6.5 DoD Case Study: Atlantic Fleet Drill Hall**

In this section, we describe the application of modeling and control design tools to a DoD facility located at Great Lakes, Illinois. The building under consideration is Building 7230 (Atlantic Fleet Drill Hall) at the Naval Station Great Lakes, Great Lakes, Illinois. We model airflow in rooms/zones at two different spatial scales, shown in Figure 3.6.2:

1. A drill deck, which is a large open space, with floor dimensions 138m x 26m, and the floor-to-ceiling height of 14m at the center.
2. A conference room, which is much smaller, with floor dimensions 9m x 6m, and the floor-to-ceiling height of 3m.

We model the dynamics of air taking into account both sensible and latent loads or disturbances, and also allowing control of both temperature and humidity.

#### **3.6.5.1 Existing HVAC system and proposed retrofits**

The current HVAC terminal units are overhead diffusers equipped with VAVs (only in the conference room), used throughout the year for conditioning zones. Such systems typically result in zones with well-mixed air at uniform temperatures and simple lumped models suffice. The retrofits proposed for these zones are:

1. Displacement ventilation (DV), to supply conditioned air at the floor-level directly to the occupied zone, for summer or during periods when cooling load dominates. This system is characterized by strong temperature stratification and has potential for reducing zone loads by conditioning only the occupied volume.
2. Radiant heated floors, with DV to supply ventilation air, for winter or when heating load dominates. The radiant systems have the advantage of enabling lower set-points, due to increased comfort from higher mean radiant temperatures.

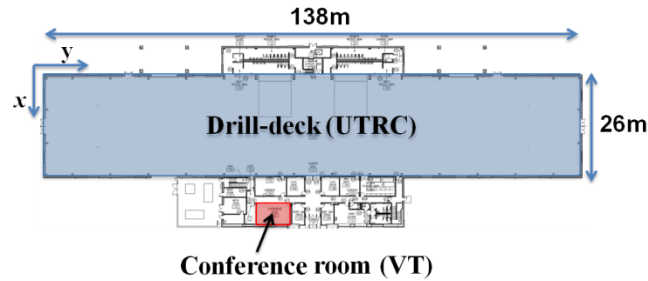


Figure 3.6.2: Plan view of the first floor Atlantic Fleet Drill Hall, showing the drill-deck and the conference room, which are the DoD cases undertaken for developing models of airflow and control design.

### 3.6.5.2 High-fidelity CFD Model (Baseline)

The drill-hall is conditioned by two rows of diffuser-pairs located at a height of approximately 10m, and equally spaced along the length of the drill-hall. The primary loads are due to lighting, occupants, and solar radiation through the windows, shown schematically. An interior 3D-view of the drill-deck and a model developed in Airpak are illustrated with details in Figure 3.6.3. For simplifying the geometry, some of the diffusers were aggregated along the length (y-axis) of the region, from fifteen to six diffusers, while maintaining the total face-area a constant.

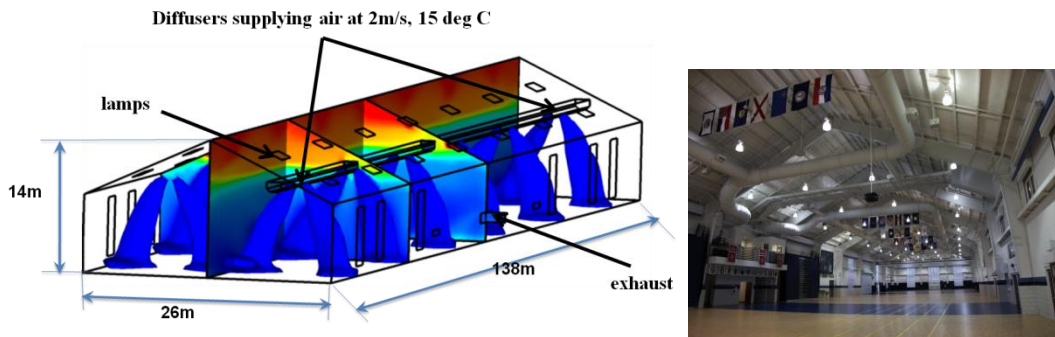


Figure 3.6.3: Model of the drill-hall, with dimensions, boundary conditions, and a resultant thermo-fluid field. The vertical slices show temperature contours for a summer case, depicting uniform temperature up to the diffuser locations. Also shown are z-velocity iso-surfaces (in blue), to point out the supply diffuser locations. The figure on the right shows an interior view of the drill-deck, which is a large open space in the building.

Both the supply air and return air locations are marked schematically in Figure 3.6.3 and Figure 3.6.4. All the walls are modeled as solid surfaces, with their thickness and properties obtained from the drawings; a mesh is not generated for the thickness of the walls, but the conduction through the walls is modeled using an equivalent resistance, computed using the wall material properties. The roof is modeled similar to the walls, while the floor is modeled as adiabatic. The lights are modeled as rectangular patches of heat sources on the ceiling, with specified energy flux boundary condition. The windows are similarly modeled with a specified heat flux; this simplification was used due to a limitation of the solver in computing solar radiation in parallel simulations.

The models invoked in the numerical solver are the Boussinesq approximation, surface-to-surface radiative heat transfer, and shell conduction through the walls. The detailed boundary

conditions used are specified in table 2 below, for a heating case. Although species boundary conditions are shown in the table, the species models were not invoked for the validation study. The species transportation equations were invoked in Fluent for developing models, in order to take into account both, sensible and latent loads.

The simulations were validated against temperature measurements obtained from sensors that were installed (for a period of one week in May 2010) during an audit of the facility by Building Intelligence Group (BIG). The grids were successively refined till convergence, which was achieved, with 1,284,072 grid-points. A vertical cross-section of the grid along the central plane perpendicular to the y-axis is shown in Figure 3.6.4.

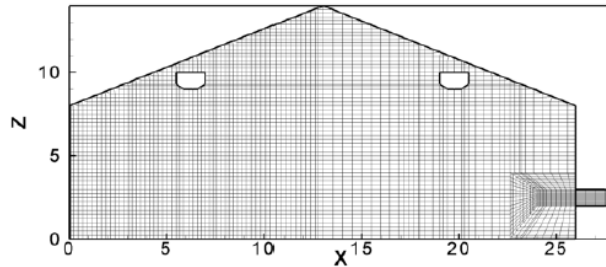


Figure 3.6.4: Grid G3 (fine) at the central cross-section of the drill-hall. The maximum grid-spacing in the x, y and z directions are 0.2m, 0.2m and 0.1m. The number of grid-points is 1,284,072.

Boundary	Momentum boundary condition	Energy boundary condition	Species (water-vapor) boundary condition
Diffusers (total area = 4.2 m <sup>2</sup> )	Velocity magnitude = 1.8 m/s	Supply temperature = 33 deg C (heating)/ 15 deg C (cooling)	Supply air humidity ratio = 10 g/kg of vapor/dry air
Exhaust	Ambient pressure	-	-
Walls and ceilings	No-slip	Isothermal, T <sub>ambient</sub> = 12 deg C (heating) / 27 deg C (cooling)	Zero normal gradient
Floor	No-slip	Adiabatic or specified heat-flux (to model occupants)	Zero normal gradient
Lights (total area = 160 m <sup>2</sup> )	No-slip	160 W/m <sup>2</sup>	Zero normal gradient

Table 3.6.1: Boundary conditions used in the model of airflow in the drill-deck, for the baseline case served by overhead diffusers. The temperature values are shown for both heating and cooling operations.

### 3.6.5.3 High Fidelity Simulation Validation

**Field Experiments.** During an audit of the facility, HOBO sensors were installed at various locations in the drill-deck, and at various heights, and data was collected for a period of one week, May 12-19, 2010. The sensors logged temperature and humidity, at an interval of 5 minutes. The sensor locations are shown in Figure 3.6.5: at each of locations 1, 3, 4 and 7, four sensors were



installed along heights of 12, 16, 25 and 30 feet, to capture vertical stratification. The locations were chosen to capture temperature stratification and spatial inhomogeneity that might be present in the space. We note that these locations were limited to heights above the occupied zone (height > 10 feet), due to restrictions imposed by the facility, which was used for performing drills. However, two sensors were placed at location 7, at heights of 2 and 8 feet, which were used as a representative for the occupied zone temperature. Finally, sensors at three heights were also placed close to the windows on walls of different orientations (locations 1W, 2W and 3W), to capture the effect of solar load on the indoor air temperature. However, due to the limitation of the CFD solver in modeling solar radiation, these data points were not used for validation.

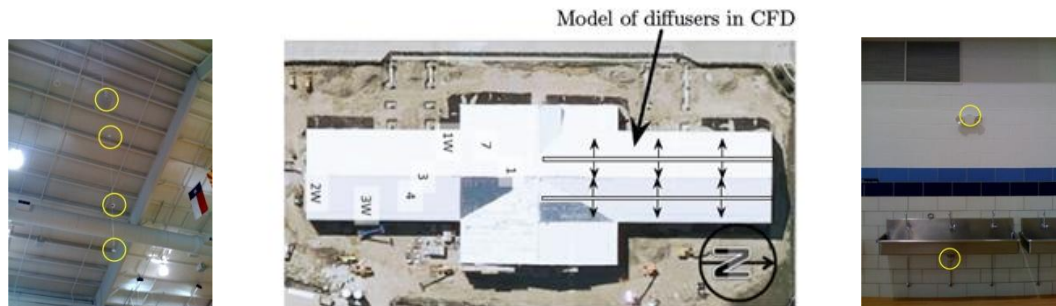


Figure 3.6.5: Logger horizontal locations, marked in plan view (center) and the vertical locations, marked with yellow circles. Also shown is the location of diffusers as modeled in CFD simulations.

Other boundary conditions needed to develop CFD models were the supply air temperature, flow rate, and ambient air temperature. These data were gathered from the building measurement system (BMS) for an accompanying ESTCP project. The measurements for one representative day during the period are summarized in Figure. The figure shows plots of temperature at locations 1 and 7 (in red, with height increasing from bottom to top). The plot of the supply air temperature (black, dashed line) shows that the system switched from cooling mode to heating mode around noon, and then back to cooling mode around 6pm. The temperature is uniform along the height during the cooling mode, implying that air is well-mixed in bulk of the region. However, significant *adverse* stratification occurs during the heating mode, with temperatures higher at increasing heights. The CFD model was developed and validated against the data obtained during the heating mode. The ambient air temperature and the supply air flow rate varied slowly during this period, and were treated as constants in the model.

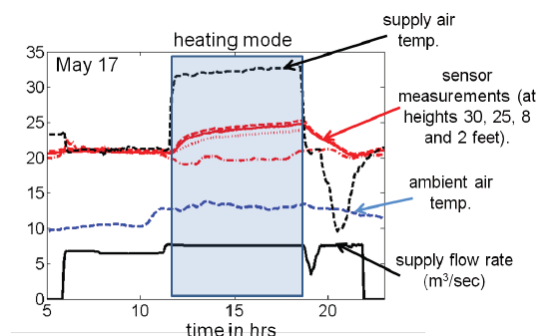


Figure 3.6.6: Measurement data, shown for May 15.

**CFD simulation validation.** For convergence study, three different grids are generated in AIR-PAK with 286,561 (G1), 452,865 (G2) and 1,284,072 (G3) cells. The cross-section of the finest

grid G3, through the center of the domain and parallel to the XZ plane is shown in Figure 3.6.4. The results of the simulations using grid G3 are shown in Figure 3.6.7; the plot on the right shows the stratification resulting from these two simulations at the end of 5 hours, and compares them with the measurement data. The figure plots, as a function of the height  $z$ , temperature averaged over 2m x 2m horizontal planar sections (parallel to the X-Y plane). The stratification resulting from simulations using grid G1 shows a discontinuous transition at  $z = 4\text{m}$ , while from that using grid G2 shows a uniform temperature for  $z < 5\text{m}$ . The figure also plots the experimental data; the simulations using grids G1 and G2 did not capture the observed stratification, while the results obtained using grid G3 compares well with observations. Furthermore, the transient response of the temperature field in simulations using the coarser grids G1 and G2 showed abrupt discontinuities in time, while the response was smooth using the grid G3.

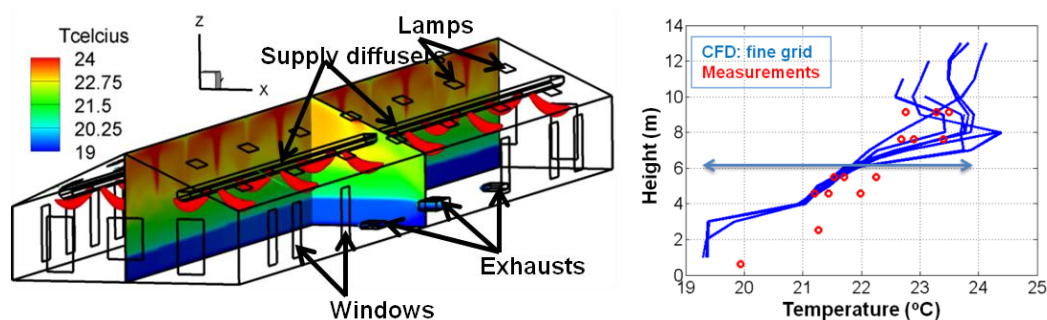


Figure 3.6.7: (Left) Temperature contours along vertical slices and iso-surfaces of the  $z$ -component of the velocity field, for a winter simulation, depicting an adverse stratification with colder temperature near the floor. (Right) Stratification during heating, computed using G3. Measurement data is shown in circles.

### 3.6.5.4 Drill-deck HVAC Retrofits: Displacement Ventilation (Cooling)

In the presence of the baseline HVAC terminal units described so far, the air in the space can be approximated as well-mixed (thermally) when cooling load dominates, but that approximation breaks down when the system operates in the heating mode. We now consider low-energy retrofits to this system. We first consider the cooling scenario, and retrofit the system with displacement vents supplying air directly to the occupied zone. This retrofit could be practically achieved at a reasonable cost by additional duct-work. As compared to the baseline system supplying air through overhead diffusers, in the DV system, cool air is supplied through vents at the floor-level at a much smaller velocity (and hence, smaller Reynolds number); thus, the resulting physics is expected to be different. The modeling procedure is developed to capture most of this physics in a relatively low-dimensional system, also useful for control design.

The model of the new system is shown in Figure 3.6.8 and consists of six diffusers, each of dimensions 1m x 1.25m, equi-spaced along the length of the drill-deck ( $y$ -axis). Numerical grids were generated and refined till convergence was achieved with 564,855 nodes. All the boundary conditions, except those at the supply air ducts, were the same as those in Table 3.6.1 for the baseline simulations.



**Steady-state calculation.** The model reduction procedure results in low-order models that capture the dynamics of perturbations to a baseline steady state. Thus, we first need to compute a baseline steady state. For this purpose, the boundary conditions at the supply vents were fixed at a normal velocity of 0.2 m/s and a temperature of 18 degrees C, while the ambient air temperature was fixed at 27 deg C. The resulting model has these boundary conditions as inputs, and allows perturbations about these baseline values. These conditions correspond to a low-load condition, allowing the controller to modulate the inputs, when the loads increase. The temperature field corresponding to this steady state is shown in Figure 3.6.8 along two vertical slices, and exhibits significant stratification. Thus, lumped models are not sufficient to represent the thermal-airflow dynamics of this system.

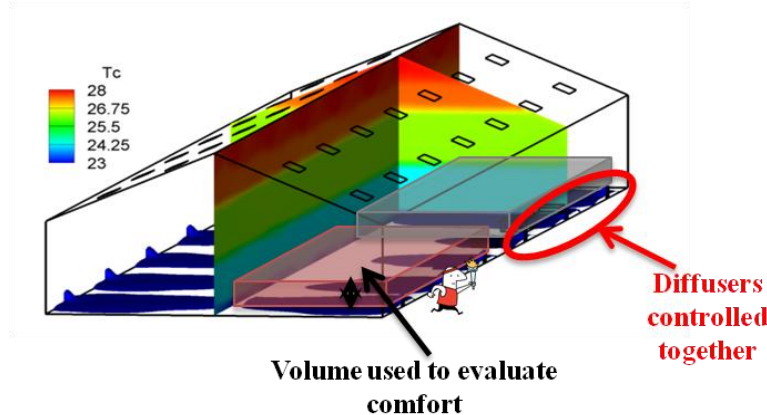


Figure 3.6.8: Retrofits using displacement vents, running along the length of the drill-deck. Six equi-spaced vents, of dimension 1m x 1.25m, are provided along the walls perpendicular to the x-axis. The figure also illustrates the volumes used to define occupant comfort. Finally, the slices of temperature contours at a steady state along two vertical planes illustrate significant temperature stratification along the height.

**Inputs and outputs.** The model reduction procedure starts with a linear input-output system of the form given by equations (8-10) in Appendix B.1; the inputs and outputs of this system are illustrated in Figure 3.6.9. The inputs, which consist of both controls and disturbances, are:

1. Control inputs: velocity and humidity of air supplied through DVs
2. Disturbance inputs:
  - a. Ambient air temperature
  - b. Heat gains from solar radiation,
  - c. Sensible and latent loads due to occupants

The displacement vents are divided into two groups together for control, each supplying the north and south zones, as shown in Figure 3.6.9; thus, six vents in the region lying within  $y = (0,69)$  have the same control inputs, while the six vents in the region lying within  $y = (69,138)$  have the same inputs as well.

The outputs of the system are:

1. Temperature, averaged over the volumes in the occupied region, shown in Figure 3.6.9, ranging vertically from 0.5m to 2m; these are referred to as the North (N) and South (S) volumes in the rest of this section.
2. Humidity ratio, averaged over the same volumes.

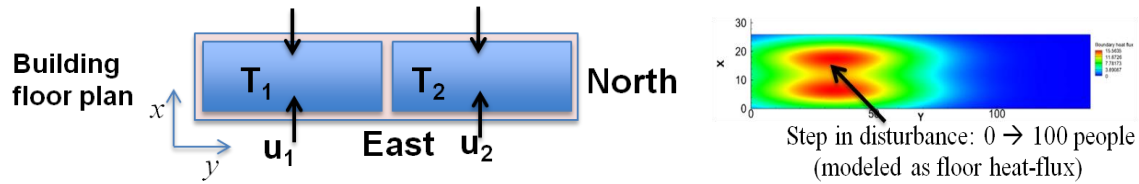


Figure 3.6.9: (Left) Floor-plan of the building, illustrating the two occupied zones (blue rectangles, north and south) used to define a comfort metric, and the two controls  $u_1$  and  $u_2$ , each representing either the supply flow rate or supply air humidity to a set of six diffusers (arrows, north and south). (Right) Model of the disturbance due to solar radiation or occupants flux; both are modeled as heat-fluxes through the floor, with contours shown in the top figure.

**Step responses for model reduction.** The next step in model reduction is to compute an impulse response of the system to all the inputs. Since it's difficult to subject boundary conditions in a CFD solver to impulses, instead, we compute step responses. Then, time-differences are used to compute the impulse responses from the step responses.

The step responses to the control input are shown in Figure 3.6.10; both, the outputs of the full and the reduced systems are plotted in the figures. The two control inputs, supply velocity and supply air humidity are stepped to enable them to handle greater sensible and latent loads, respectively. The velocity of supply air through the diffusers on the North portion of the building is increased from the baseline value of 0.2m/s to a higher 0.4m/s; as a result, the average temperature in the occupied zones drop by about 1 deg C (Figure 3.6.10). Next, the humidity ration of the air supplied through the diffusers on the North is changed from 10 g/kg of vapor/dry air to a lower 8 g/kg; as a result, the average relative humidity in the occupied volume on the North end drops by about 5%, while that on the south end remains relatively unchanged.

In order to capture the effect of disturbances, we model the load due to solar radiation as a heat-flux through the floor, as shown in Figure 3.6.9. The assumption is similar to that in energy simulation tools, where the solar radiation is assumed to first impact the floor and affects other surfaces through subsequent reflection from the floor. For simplicity, the sensible load from occupants is modeled similarly as a heat-flux through the floor, while the latent load from occupants is modeled as a water-vapor source, distributed uniformly through the lower portion of the occupied zones, ranging in height from 0.5m to 1.5m. The temperature and humidity responses to a step change in occupants (from 0 to 100 people, in the North portion) are shown in Figure 3.6.11. Each occupant is assumed to contribute 150W of sensible load and 225W of latent load, corresponding to an elevated activity level. The average temperature and relative humidity of the occupied zone volume in the North end rise by approximately 1 deg C and 5%, respectively, and remain relatively unchanged for the South end. Finally, a response to the change in ambient temperature is computed as well.

The responses of the system to step changes in the inputs on the South portion of the building are not explicitly computed, but assumed to be similar and symmetric to the responses to the inputs on the North portion of the building.

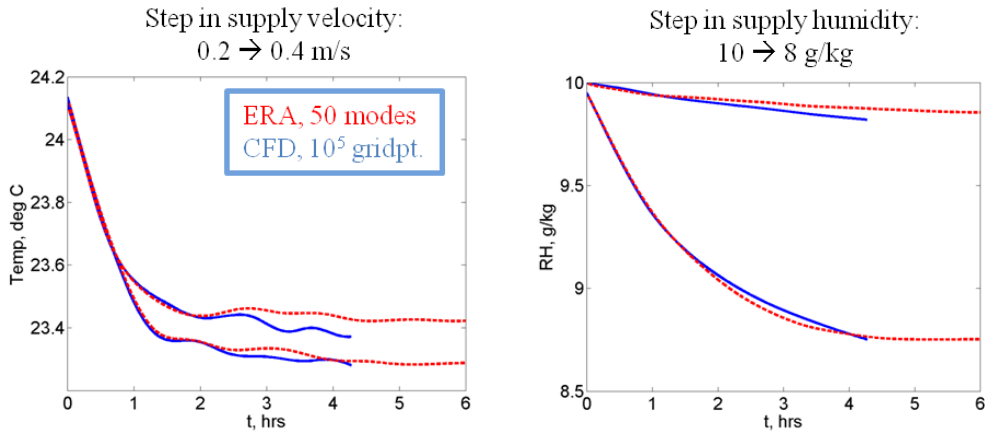


Figure 3.6.10: Outputs of the system to step changes in the supply velocity (left) and supply air humidity (right). The curves show the filtered CFD responses (blue) and a 50-mode ERA model prediction (red, dashed lines). The inputs are stepped from their baseline values over 15 minutes, starting at  $t=0$ .

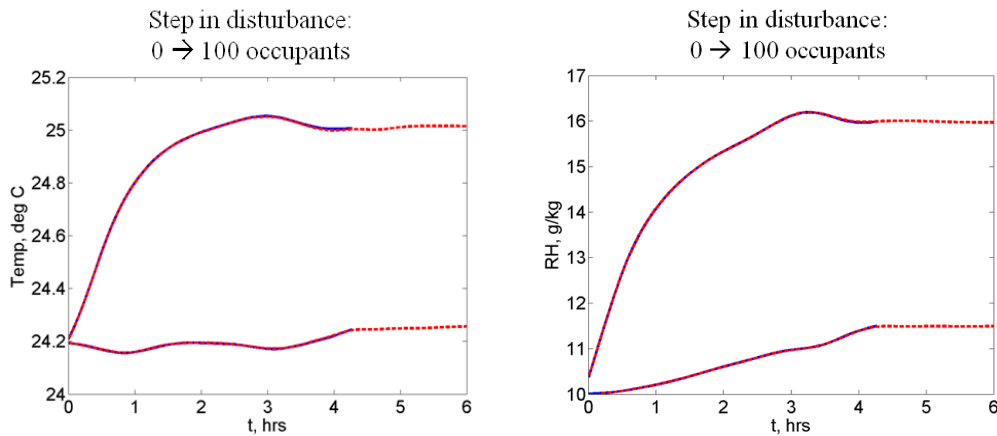


Figure 3.6.11: The response of the system to a step change in occupants from 0 to 100 in the southern zone (left); each occupant is assumed contribute 100W of sensible load and 200W of latent load. The latent load is modeled as a vapor source, uniformly distributed over the occupied volume.

**Reduced-order model using ERA.** The next steps involve stacking up the resulting outputs in a Hankel matrix, computing its singular valued decomposition (SVD), and using the SVD factors in combination with the Hankel matrix to compute a transformed model using ERA. The singular values obtained from SVD approximate the Hankel singular values (HSVs), which represent the controllability and observability of the system. If only few modes are controllable or observable, the HSVs decay rapidly and provide a basis of truncating the resulting model. If the original system is stable, the resulting model is guaranteed to be stable (unlike in POD) and is balanced in the input-output sense. In this case, a 50-mode model turns out to be sufficient to capture the original dynamics. The resulting model has 4 control inputs (velocity and humidity of air, N and S), 5 disturbance inputs (solar radiation and occupants, N and S; ambient air temperature), and 4 outputs (volume averaged temperature and humidity, N and S). As shown in Figure 3.6.10 and Figure 3.6.11, the step responses of a 50-mode model accurately reconstruct the CFD step responses.

**Control design and implementation.** Next, we construct realistic disturbances, and design controllers to reject those. The disturbances from solar radiation are computed from TMY3 Chicago-weather file, for a period of 24 hours in July. The disturbances from occupants are constructed from a schedule obtained from a calibrated EnergyPlus model, developed in another part of this project (section 3.3). The floor-flux resulting from these disturbances is shown in Figure 3.6.12.

The model is used to develop an optimal controller, assuming known future disturbances, and an observer is developed to reconstruct the model states. The cost function is similar to that in equation (7), with the weights  $Q = qI$  and  $R = rI$ . The resulting observer-based feedback controller is implemented in Fluent using user-defined functions (UDFs), and is found to maintain the zone set points. The results are shown in Figure 3.6.12; with the control turned off, the temperature of the occupied zone rises by about 2 deg C, which is suppressed when the control is turned on. Moreover, the model accurately predicts the CFD response, even for disturbances larger in magnitude as compared to those used to develop the model.

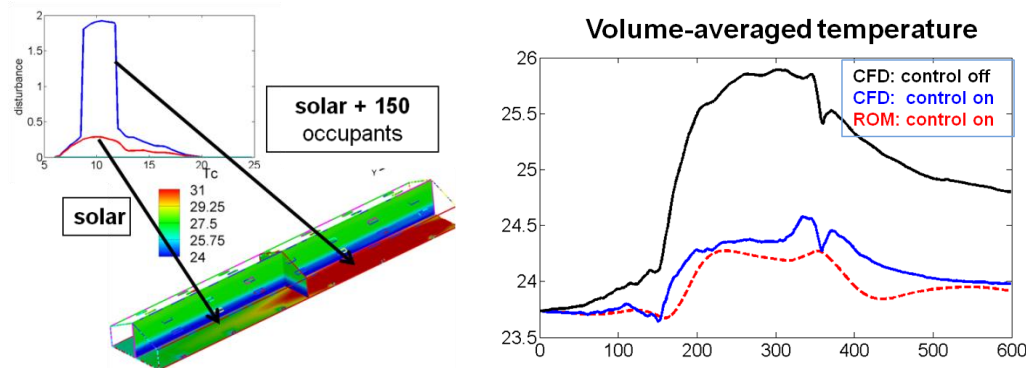


Figure 3.6.12: Realistic disturbances from solar radiation and occupants, shown in the left plot. The right plot shows the system responses, with and without control.

**Estimated energy savings.** The main advantage of displacement ventilation (DV) is the reduction of load by providing cooling energy only to a portion of the room (occupied region). The advantage is even greater in zones with high ceilings, such as the drill-deck.

In order to estimate savings, the low-order model is used to compute energy consumption for a period of 3 months (a similar computation in CFD would take several years of computational time, on similar processors). It is compared to the energy consumption in the baseline system consisting of overhead diffusers. The model of the baseline system was that developed in EnergyPlus, which was outlined in section 3.3, and it treats the air in the rooms as well-mixed. The assumption is reasonable for a cooling scenario, since the temperature in the zone is uniform, as seen in Figure 3.6.3. For comparison, the same disturbances are used in the two systems: ambient temperature and solar radiation is obtained from TMY3 weather data set, while occupants schedules are obtained from an EnergyPlus model calibrated against metered data. Further, the controllers in the two models are tuned to maintain the same zone temperatures, indicating similar comfort levels.

Figure 3.6.13 shows a comparison of the zone temperatures served by the two systems; the larger fluctuations in the zone served by DV are during the periods where the ambient temperature or

the supply air velocity undergoes large deviations from their values at “steady” state. Recall, the ERA model is applicable only in a linear neighborhood of the baseline values used for the various inputs. The figure also shows a comparison of the mass flow rate of the air supplied by the two systems; it can be seen that DV requires lower amount of supply air for larger periods of time, thus resulting in fan power savings. The power consumed by the supply and return fans in the two systems are computed using the following fan curves:

where, the subscript *design* is used to indicate the design values. Also, the chiller loads to provide are computed in the two cases, assuming a same constant minimum supply of outdoor air for ventilation. Thus, the chiller load is given by

where,  $f_a$  is the fraction of ambient air,  $T_a$  and  $T_r$  are the ambient, supply, and return air temperature respectively, and  $\dot{V}_s$  is the supply air flow rate. The resulting estimates of fan energies and chiller loads are listed in Table 3.6.2, and indicate approximately 15% savings in the fan powers and a 40% reduction in the chiller load.

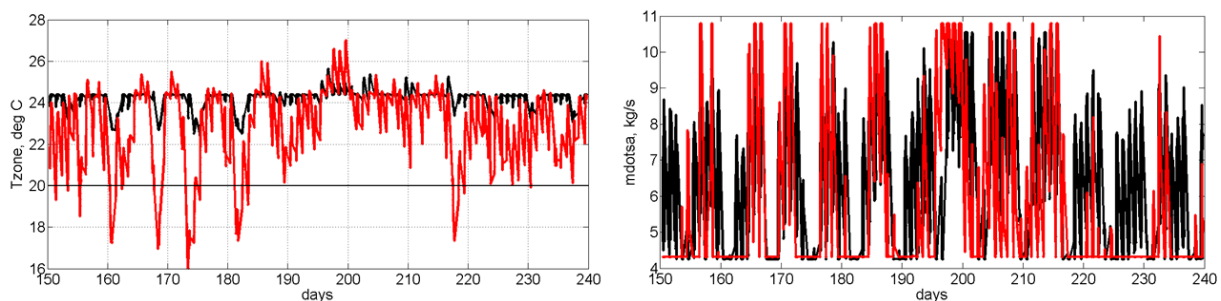


Figure 3.6.13(a): (Left) Zone temperatures in the systems served by overhead diffusers (black) and displacement ventilation (red). (Right) Mass flow rate of air supplied by the two systems; in both cases, the minimum flow is constrained by the same outdoor air (ventilation) requirement.

Component Energy (MW-hr)	Baseline (overhead supply)	Low-energy (DV)	% savings
Supply fan power	7.1	6.2	14.0
Return fan power	2.5	2.1	16.0
Chiller load	78.5	47.6	39.4

Table 3.6.2: Estimated of energy savings in different HVAC components, over with a baseline system modeled in EnergyPlus, for a period of 3 months (June-August).

Finally, Figure 3.6.13(b) provides an estimate of how the above energy savings translate to savings at the whole building level; the figure provides energy consumption using the current baseline system. The figure shows that chiller and fans together consume 60% of the annual energy, for the whole building. Of the various AHUs, the ones (AHU 1 and 2) serving the drill-deck consume 91% of the energy. If we assume that the energy consumed by the chiller to serve the required cooling to the drill-deck is proportional to the fan energy, the chiller energy consumed to maintain the comfort in the drill-deck is around 31% of the whole building energy. Thus, the reduction of chiller load by 39% translates to 12.5% energy savings at the whole building level, by using DV. Of course, actual savings would be higher if DV was

used in all the zones and not just the drill-deck. Further, the 15% savings in fan energy translates to 3% savings at the whole building level. The total energy savings by just using DV are thus 15% for the cooling mode operation.

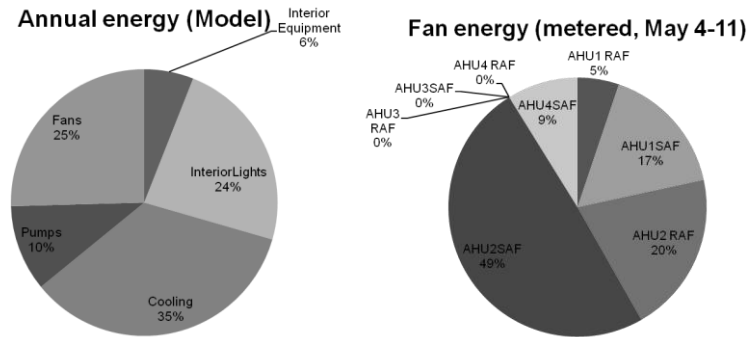


Figure 3.6.13(b): Whole building energy consumption. (Left) Energy consumption by components, obtained from a model calibrated against measurement data. (Right) Energy consumed by fans, obtained from measurements during a week in May. The drill-deck is served by AHU 1 and 2, which consume more than 90% of the total fan energy.

**Proportional-Integral (PI) control.** The standard practice in buildings control design is to use a proportional-integral (PI) control, since, it's straightforward to design and implement. However, the controller tuning is typically done on the field while commissioning, which can be very expensive. Alternatively, building models could be used to tune the controllers, but the typical lumped models are accurate only for forced-air systems (e.g., overhead diffusers). The models developed using the proposed technique would be useful for controller tuning, especially in low-energy systems.

In this section, we compare the proposed optimal control design with the simple PI control. For that purpose, we first briefly explain our procedure of designing the PI controller. In the DV system, our control inputs are (the perturbations from the steady states of,) the supply air velocity ( $u_1$ ) and the supply air humidity ( $u_2$ ), while our outputs are (again, perturbations from the steady states of,) the zone-averaged temperature ( $y_1$ ) and humidity ( $y_2$ ). So, we prescribe the following forms of the controls:

We choose various control gains and, for each control gain, we compute the closed-loop response of the low-order model, for a given disturbance over a period of 8 hours. The disturbance chosen is from a design day, and consists of a combination of occupant schedule and solar radiation. For each simulation, we then compute the norm of the error (deviation from the set points) and the control effort, defined as:

Similarly, we also develop the optimal controllers, varying the weights  $Q$  and  $R$  in the cost function defined by equation (7). A plot of the error vs. cost, for both the control designs, is shown in Figure 3.6.14; each data-point in the figure corresponds to an 8-hour closed-loop simulation for a set of chosen control gains. Note that the PI controller results in a similar error, but at a much lower cost as compared to the optimal control design. However, we also note that the PI control has a lot more variation in cost, for a prescribed error, and thus less robust. Finally, we note that,



at a minimum, the resulting low-order models, can also guide the choice of PI control gains, by avoiding expensive field experiments.

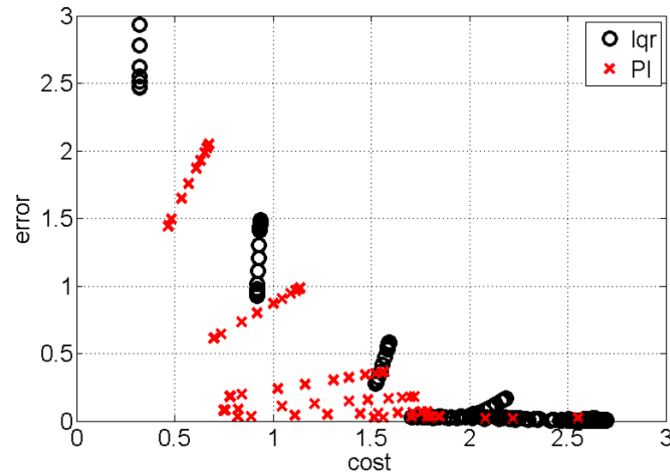


Figure 3.6.14: Comparison of the proposed LQR control design vs. the currently practiced PI control design. Shown is the time-integral of the square error (deviation from the set-point) vs. that of cost. Each point in the plot is obtained from a 6-hour simulation using the same disturbance profile, but with different control gains. For a given error (say, error=0.2), the PI controller shows a wider variation in the potential cost as compared to LQR.

### 3.6.5.5 Drill-deck HVAC Retrofits: Radiant heated floors and DV (heating)

We now consider retrofits for the winter operation, when heating loads dominate. The retrofits considered are a radiant floor, for heating and DV, for ventilation. These retrofits are chosen partially from a practical point of view: the same DV vents that are proposed to supply cool air in summer could be used to provide ventilation air during winter. The radiant system also provides a case-study with potentially different physics as compared to DV, due to much smaller supply air velocity, and thus, a much smaller Reynolds number.

Numerical grids were generated using Airpak, and one with 50,000 nodes was used for all simulations, which is much coarser than the previous study; the current study was restricted to this due to time limitation. The boundary conditions are again similar to those used in Table 3.6.1, except that the floor-heat flux can now be controlled as an additional input, and are summarized in Table 3.6.3.

Boundary	Momentum boundary condition	Energy boundary condition	Species (water-vapor) boundary condition
Radiant Floor	No-slip	Specified heat-flux = $2.5 \text{ W/m}^2$	Zero normal gradient
DV vents (total area = $15 \text{ m}^2$ )	Velocity magnitude = $0.075 \text{ m/s}$	Supply temperature = $20 \text{ deg C}$ (neutral, for ventilation)	Supply air humidity ratio = $5 \text{ g/kg}$ of vapor/dry air

Table 3.6.3: Boundary conditions for the drill-deck retrofitted with radiant heated floor and DV.

**Steady state calculation.** As before, the first step in model reduction is to compute a steady state, at a low-load operating point. For that, in addition to the boundary conditions listed in Ta-



ble 3.6.3, we assumed the ambient air temperature to be 0 deg C, and the number of occupants in the drill-deck to be 40, distributed uniformly in the region. The resulting steady state, shown in Figure 3.6.15, indicates that air in the zone is well-mixed (exhibiting a Rayleigh-Benard like flow pattern) as opposed to the steady stratification obtained for the cooling operation. Thus, we expect the energy savings estimates to be lower as compared to the cooling mode operation. However, due to a radiant heating system, the comfort metric is the radiant surface temperature, and is typically higher than the zone air temperature. Thus, energy savings could be achieved by lowering the temperature set-points.

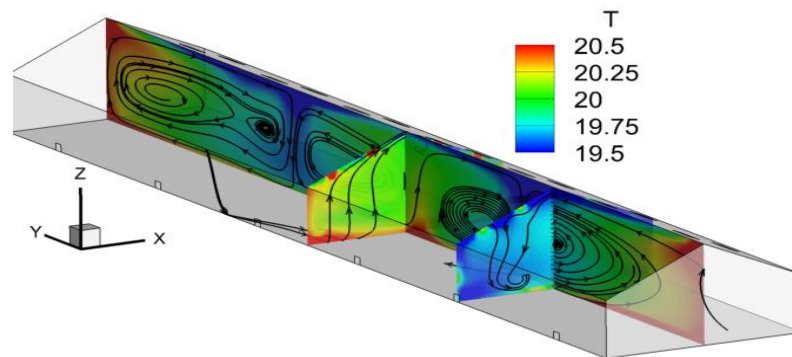


Figure 3.6.15: Temperature contours at a steady state, in the drill-deck retrofitted for a heating mode operation. The contours are shown along two vertical planes, and illustrate that air is well-mixed in the zone for the heating operation, and the velocity contours indicate a Rayleigh-Benard like airflow pattern.

**Reduced-order model using ERA.** We now define the inputs and outputs of the system, which are required for developing the reduced-order model. The control inputs are:

1. Floor heat-flux (for heating); the North and South halves of the floor are assumed to have separate control inputs.
2. Velocity of air supplied through DV (for ventilation); again, the vents in the North and South portions are assumed to be controlled separately.

The disturbance inputs are the same as those used in section 3.6.5.4; they are the ambient air temperature, solar heat-flux impinging on the floor, and the sensible and latent gains from occupants, modeled as sources of heat and humidity. The outputs are also considered to be the same as those used in section 3.6.5.4, that is, the occupied zone averaged temperature and humidity ratio. The humidity of supply air is not actively controlled, but the measured humidity is assumed to serve as a proxy for occupancy sensor, and is used to control the amount of supply air (providing ventilation).

Next, a set of CFD simulations is performed, computing responses to a step change in all the (North-end) inputs, one at a time. The step inputs are:

1. Floor-flux (southern-half) is stepped from  $2.5 \text{ W/m}^2$  to  $7.5 \text{ W/m}^2$ .
2. Supply air velocity is stepped from  $0.075 \text{ m/s}$  to  $0.125 \text{ m/s}$ .
3. Ambient air temperature is stepped from  $0 \text{ deg C}$  to  $-3 \text{ deg C}$ .
4. Number of occupants is stepped from 50 to 200; each occupant contributes 100W of sensible load (modeled as floor-flux) and 200W of latent load (modeled as a volumetric source of water-vapor).
5. Solar flux is stepped from  $2.5 \text{ W/m}^2$  to  $7.5 \text{ W/m}^2$ .

The resulting outputs are then assembled into the Hankel matrix, whose SVD factors are then used to compute a low-order model. A 50-mode model compares well with the full simulations, and some of the comparisons are summarized in Figure 3.6.16.

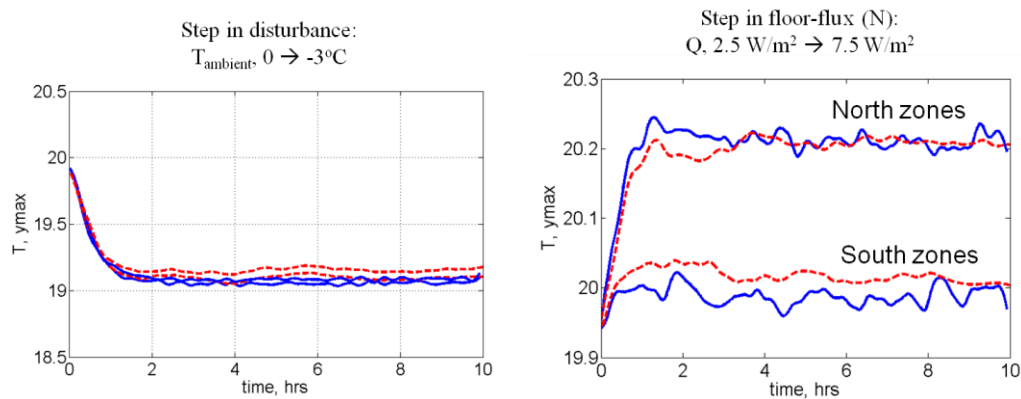


Figure 3.6.16: Outputs of the system to step changes in the floor-flux (left) and ambient air temperature (right). The curves show the filtered CFD responses (blue) and a 50-mode ERA model prediction (red, dashed lines). The inputs are stepped from their baseline values over 15 minutes, starting at  $t=0$ .

**Control design and implementation.** The reduced-order model is used to design controllers that assume a future knowledge of disturbances. The feedback controller is implemented in Fluent, and the results are shown in

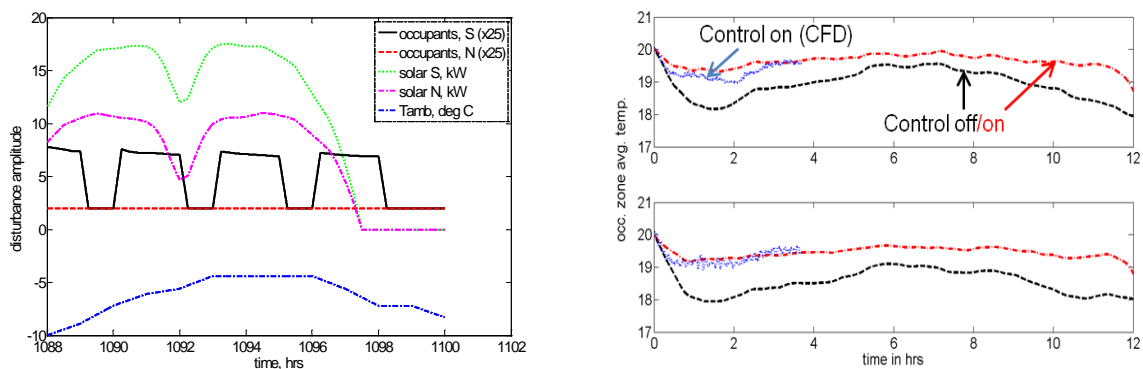


Figure 3.6.17.

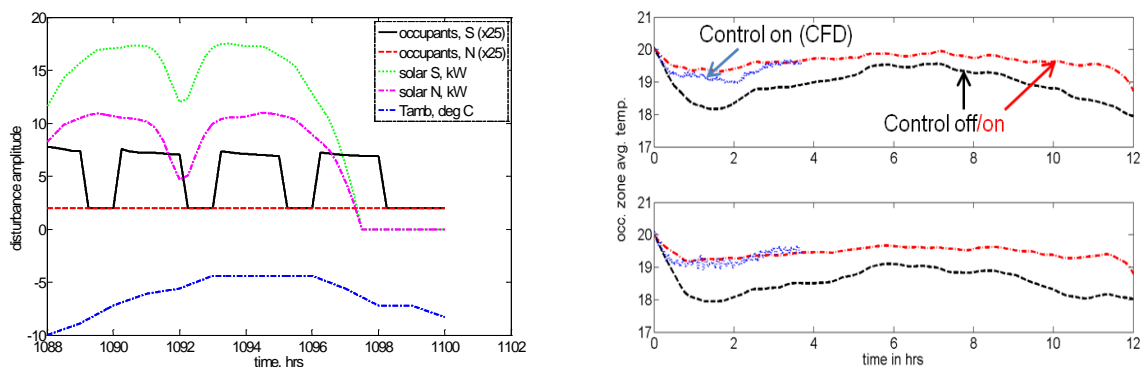


Figure 3.6.17: Realistic disturbances from changes in the ambient air temperature and occupancy, shown in the left plot. The right plot shows the system responses, with and without control.

**Estimated energy savings.** As we noted earlier, the radiant heating system is not characterized by spatial temperature stratification, but the physics is dominated by buoyancy. The main advantage of the radiant floor system is that it provides additional comfort at the same dry-bulb temperature, due to radiant effects, and allows a lowering of temperature set-points, which allows a reduction in energy consumption.

As for the cooling-dominated case, the low-order model developed using ERA is used to compute energy consumption for a period of 2 months. Again, it is compared to the energy consumption in the baseline system (modeled in EnergyPlus) consisting of overhead diffusers. Recall, that the EnergyPlus model treats air in the rooms as well-mixed; from our experimental (section 3.6.5.3) data, this assumption breaks for a heating-dominated operation, and the zonal air is characterized by an adverse stratification. For a more accurate comparison, it would be required to develop an ERA-based model of the baseline case (served by overhead diffusers) as well; however, the project timeline was too short to complete this part of the study. We provide an estimate of energy savings computed using the EnergyPlus model, however, we expect the actual savings to be higher.

Again, for comparison, the same disturbances are used in the two systems: ambient temperature and solar radiation is obtained from TMY3 weather data set, while occupants schedules are obtained from an EnergyPlus model calibrated against metered data. Further, the controllers in the two models are tuned to maintain the similar comfort levels; the set-point in the system served by radiant heating and DV is reduced by 2 deg C to account for increased comfort.

Figure 3.6.18 shows a comparison of the zone temperatures served by the two systems. The figure also shows a comparison of the mass flow rate of the air supplied by the two systems; since the advanced system only supplies air for ventilation, the flow rate required is much lower. The energy consumed by fans is again computed using performance curves, as for the cooling case-study. In addition, the heating loads (sensible) are computed in the two cases, with an assumption that the baseline uses a constant minimum supply of outdoor air for ventilation. Thus, the total heating load in the baseline is computed the same way as the total cooling load. The heating load in the advance system is computed by simply integrating in time, the heat flux through the radiant floors.

The resulting estimates of fan energies and heating loads are listed in Table 3.6.4, and indicate approximately 40% savings in the fan powers and a smaller 5% reduction in the overall heating load. We note that an additional component, namely a water pump, is required to supply heated water to the radiant floors, and would consume additional energy. However, the computation of this energy would require an additional model of this component, and was beyond the scope of this effort. We note that the reduced-order models developed using this method could easily be integrated with an existing energy simulation tool such as TrnSys, and the entire analysis presented in this section could be easily reproduced using its component libraries.

Component Energy (MW-hr)	Baseline (over-head supply)	Low-energy (Radiant floors + DV)	% savings
--------------------------	-----------------------------	----------------------------------	-----------

Heating load: sensible	49.5	18.7	62.2
Heating load: ventilation	135.9	156.6	-15.2
Overall heating load	185.4	175.3	5.4
Supply fan power	9.3	5.6	39.8
Return fan power	3.2	2.0	37.5

Table 3.6.4: Estimated of energy savings in different HVAC components, over with a baseline system modeled in EnergyPlus, for a period of 2 months (January and February).

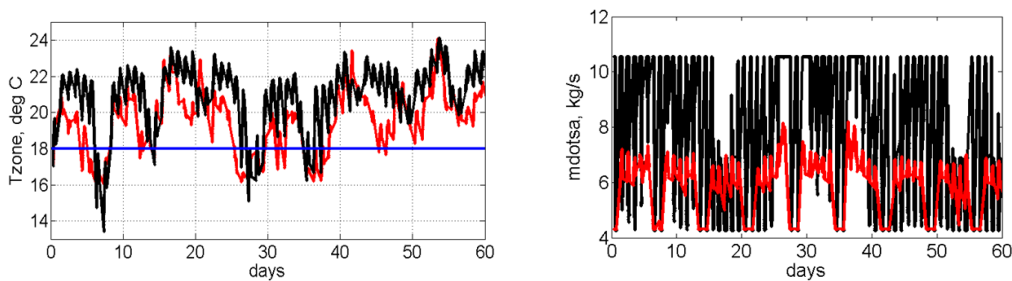


Figure 3.6.18: (Left) Zone temperatures in the systems heated using overhead diffusers (black) and using radiant floors (red). (Right) Mass flow rate of air supplied by the two systems; in both cases, the minimum flow is constrained by the same minimum ventilation requirement; the low-energy system has considerably lower supply air flow rate, due to primary heating by the radiant floors.

### 3.6.5.6 Conference Room HVAC Retrofits: DV (cooling)

Here we consider design and control of a Displacement Ventilation (DV) system for a model of a conference room in the Atlantic Fleet Great Lakes facility (see Figure 3.6.19). In this section, we focus on maintaining temperature and humidity levels in the presence of (sensible and latent) disturbances induced by occupants. It should be noted that the DV system does not model the actual installed cooling system, but the proposed retrofitted system.

The model of the conference room is shown in Figure 3.6.19, and consists for four DV inlets at the floor-level, a ceiling exhaust, two ceiling lamps, two windows, and a central table modeling the largest current furniture. The boundary conditions at these boundaries are detailed in Table 3.6.5, for a cooling mode operation.

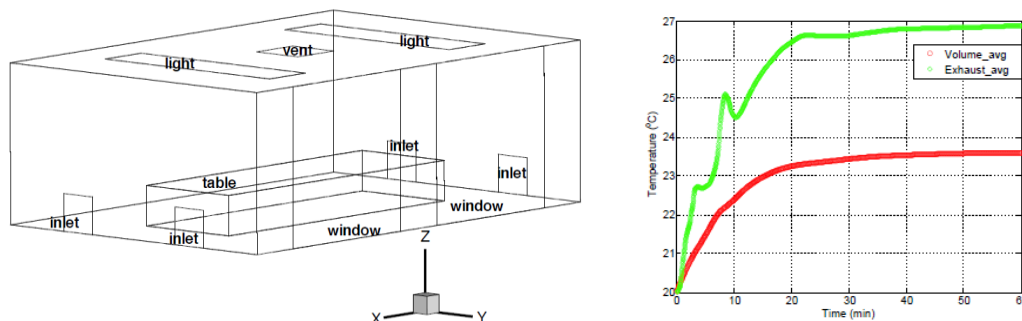


Figure 3.6.19: Conference Room Geometry, illustrating the boundary conditions. On the right is shown an initial transient response of the volume-averaged and exhaust temperature, starting from a uniform initial condition. The flow evolved to a “steady” state, with minimal fluctuations on temperature or velocity fields.

Boundaries	Momentum boundary conditions	Energy boundary conditions	Species boundary conditions
Inlet vents (four, each 0.49 m <sup>2</sup> )	Parabolic profile; mean velocity = 0.07 m/s	Supply temperature = 20 deg C	Supply humidity ratio = 10g/kg
Outlet: ceiling-centered	Pressure = 0	-	-
Lights (two, each 4m <sup>2</sup> )	No-slip	100 W/m <sup>2</sup>	Zero gradient
Walls	No-slip	Adiabatic	Zero gradient
Windows	No-slip	Iso-thermal	Zero gradient
Table	No-slip	Specified heat flux	Zero gradient

Table 3.6.5: Boundary conditions for the conference room; cooling mode operation.

**ERA Model.** For purposes of control design, we opted for a model wherein the fluid is a mixture of air and water vapor. To this end we identified three occupied zones around the table (see Figure 3.6.19). The regions above and on the max-y side of the table have distributed water vapor sources at 0.008 gm/m<sup>3</sup>/s and distributed energy sources at 12.0 W/m<sup>3</sup>, whereas in the region on the min y side of the table the values are 0.015 gm/m<sup>3</sup>/s and 22.5 W/m<sup>3</sup>. These values reflect occupancy by about six people. The boundary conditions are as above, except that the inlet fluid contains water vapor at 10.0 g/kg mass fraction.

The flow field was initialized to zero velocity and a uniform temperature of 25 deg C, and Fluent was run on a grid of 200,000 points, with a time step of 2.0 seconds for  $0 < t < 2400$ s. We specified certain flow “monitors”, including the area-averaged temperature at the outlet duct-outlet. As seen in Figure 3.6.19, the volume-averaged temperature (red) initially decreases (due to in-flow air at 21 deg C) and approaches 22.5 deg C. The average-outflow temperature (blue) initially increases (heating), then decreases (supply air) before beginning a slow oscillatory increase. By  $t = 2400$ s the outflow temperature is nearly constant at 26.5 deg C. A “snapshot” of the temperature/flow field at  $t = 2400$  s is shown in Figure 3.6.19. The flow is not truly steady; regions of cooler/warmer air are entrained alternately in the outflow producing the oscillation observed in Figure 3.6.19. This data was averaged from  $t = 2400$  to  $t = 3000$  seconds to produce an ersatz steady flow solution.

ERA data was generated by monitoring three output variables:

1. sensed temperature on the max  $x$  wall,
2. controlled H<sub>2</sub>O-mass fraction in the region above table,
3. controlled temperature in the region above the table;

while, four inputs were subjected to step-like changes:

1. Inlet air velocity - (two) inlets on max  $x$  wall,
2. Inlet air temperature - (two) inlets on max  $x$  wall,
3. Inlet air moisture (mass fraction) - (two) inlets on max  $x$  wall,
4. Disturbance - distributed sensible and latent load.

	dv <sub>ctl</sub>	T <sub>ctl</sub>	h2o <sub>ctl</sub>	dstrb
h2o <sub>abv</sub>	a (16)	a	a	a
T <sub>max_x</sub>	b (28)	b	c (28)	b
T <sub>abv</sub>	b	b	d (16)	b

Table 3.6.6: Input-output decomposition

Rather than constructing a single state-space model for the four-input, three-output system, we grouped the input/output pairs into four subsystems as shown in Table 3.6.6. We believe that this decomposition method is easier to manage than applying various weights to the 4 inputs and 3 outputs for the full system. The composite  $(16 + 28 + 28 + 16)$  88<sup>th</sup> order system was assembled as:

$$\mathbf{x} = [x_a; x_b; x_c; x_d], \quad \mathbf{A} = \begin{pmatrix} A_a & 0 & 0 & 0 \\ 0 & A_b & 0 & 0 \\ 0 & 0 & A_c & 0 \\ 0 & 0 & 0 & A_d \end{pmatrix}$$

$$\mathbf{B} = \begin{pmatrix} B_a(:,1) & B_a(:,2) & B_a(:,3) & B_a(:,4) \\ B_b(:,1) & B_b(:,2) & 0 & B_b(:,3) \\ 0 & 0 & B_c(:,1) & 0 \\ 0 & 0 & B_d(:,1) & 0 \end{pmatrix}, \quad \mathbf{C} = \begin{pmatrix} C_a & 0 & 0 & 0 \\ 0 & C_b(1,:) & C_c & 0 \\ 0 & C_b(2,:) & 0 & C_d \end{pmatrix}.$$

Several data/model comparisons are shown in the Figures 3.6.20 and 3.6.21. Whereas the fit-to-data is good, note that the composite model is of rather high-order (88); this is much higher than typical POD models.

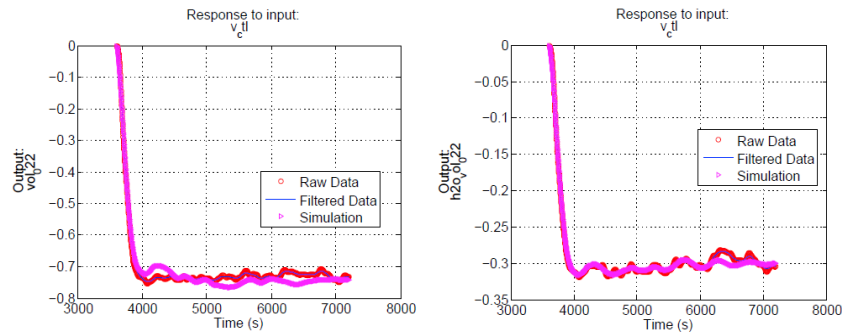


Figure 3.6.20: Responses of the system to a step change in the supply velocity. Both the temperature and humidity drop with increasing supply; an 88-mode model accurately predicts the response of the full system.

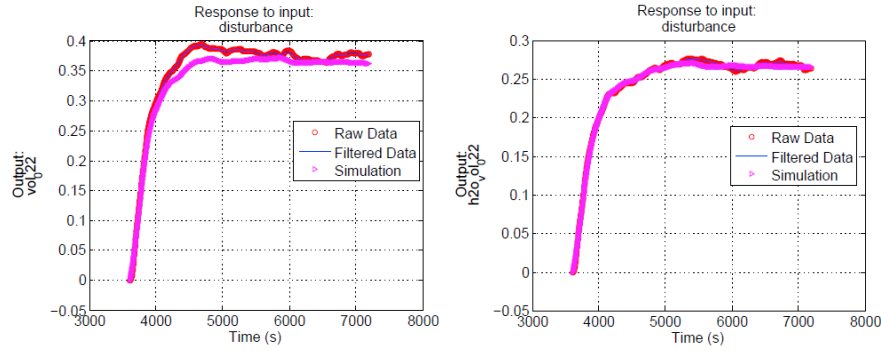


Figure 3.6.21: Responses to a step in the disturbance inputs; plots similar to those shown in Figure 3.6.20

**H<sub>2</sub> Control Design.** The structure of the H<sub>2</sub> control problem has been described in Appendix D.2. In the present case we identify three controls ( $u$ ): (a) inlet air velocity, (b) inlet air temperature, (c) inlet air moisture (mass fraction) and a single input disturbance ( $w$ ) – distributed sensible and latent loads (plus sensor noise terms). For outputs ( $y$ ), we identify two sensors (a) temperature on max  $x$  wall, (b) H<sub>2</sub>O mass fraction in region above table; and two controlled outputs ( $z$ ): (a) H<sub>2</sub>O mass fraction in region above table, (b) temperature in region above the table.

Since we have single disturbance, we include an 89<sup>th</sup> state with dynamics:

$$\dot{d}(t) = -\frac{1}{\tau}d(t), \quad \tau = 10^4 \text{ (s)}.$$

The resulting dynamic compensator is an 89<sup>th</sup> order system with two inputs (the H<sub>2</sub>O mass fraction in the region above table, and the temperature on max  $x$  wall) and three outputs (the controls -  $u$ ). A Simulink diagram of the closed-loop system is shown in Figure 3.6.22. The (3) gains on the left-side of the figure reflect units conversion of the input quantities to engineering units; the values are dictated by the step inputs used in generating the ERA data. The controller output was augmented with a 4<sup>th</sup> row to read-out the last controller state ( $d$ ); this characterizes the (estimated) magnitude of the disturbance.

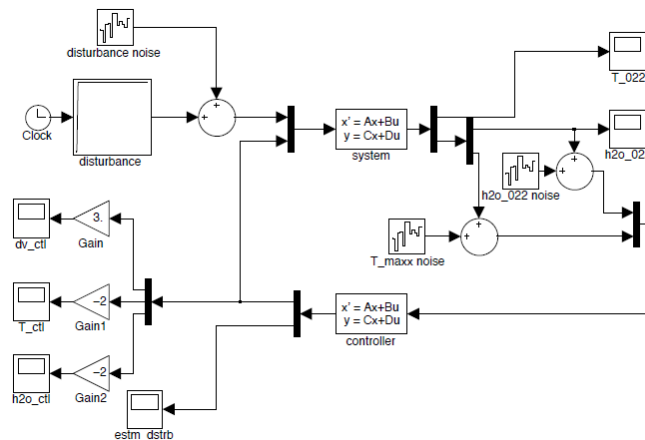


Figure 3.6.22: Simulink diagram of the closed-loop conference room cooling.



**Closed-loop Simulation.** The controller was implemented as a discrete-time system with a time-step of 2 seconds, and coupled to the Fluent simulation. The simulation was started from a steady condition, and after 10 seconds the controller was turned on. At 60 seconds, the disturbance began and was ramped to its full value over an additional 60 seconds and then maintained. The disturbance simulated three additional people entering the room. Specifically, in the regions above and on the max y side of the table the distributed water-vapor sources begin at  $0.008 \text{ gm/m}^3/\text{s}$  and increased to  $0.012 \text{ gm/m}^3/\text{s}$  and the distributed energy sources begin at  $12.0 \text{ W/m}^3$  and increase to  $18.0 \text{ W/m}^3$ . In the region on the min y side of the table the water vapor begins at  $0.015 \text{ gm/m}^3/\text{s}$  and increase to  $0.0225 \text{ gm/m}^3/\text{s}$ , while the energy source begins at  $22.5 \text{ W/m}^3$  and increases to  $33.75 \text{ W/m}^3$ . These values simulate an occupancy change from six to nine people.

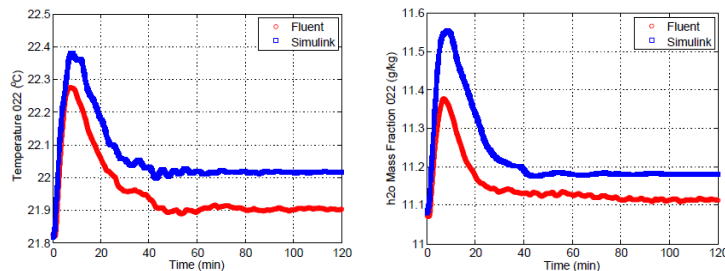


Figure 3.6.23(a): Controlled temperature and humidity responses.

The complete (120 minute) responses of the temperature and the water vapor responses for zone 022 are shown in Figure 3.6.23(a). Recall that these are the controlled quantities in our H2 design formulation (that is, these are the quantities we wish to make insensitive to the disturbance). The Simulink predictions seem to over-predict the responses. The disturbance induces a net increase in temperature of about  $0.10 \text{ deg C}$  and a small increase in  $\text{H}_2\text{O}$  mass fraction (less than  $0.03 \text{ g/kg}$ ). This amounts to about a  $0.1\%$  increase in relative humidity. The control activity for these cases is shown in Figure 3.6.23(b) (blue). The control predictions from the Fluent and Simulink simulations are reasonably close.

An H2 control design requires the analyst to select various weights, including weights on the control components. In neighboring optimal control the weights are implied by the Hessian of the (Lagrange) cost-functional with respect to the control. In our application, an appropriate choice for this functional would characterize the power usage by the controls. Here we selected several different weighting to study their effect. The results presented in Figure 3.6.23(b) (red) are based on control with relative weights 8:1:1, on the three inputs in the following order: supply air velocity, temperature and humidity; this choice would make sense if the control of supply air velocity were more expensive than the supply temperature and humidity. We compare these responses with the responses from a second closed-loop design with relative control weights 1:8:8.

As seen, with the second weight (blue), the controlled-temperature excursions are slightly smaller (note the scale). With higher weights on the inlet temperature control and the inlet  $\text{h}_2\text{o}$  vapor control the latter case uses practically no control on inlet temperature and much less inlet  $\text{h}_2\text{o}$  control. In contrast, the decreased penalty weight on inlet velocity results in considerable increase in use of that control. As noted above, the choice of these control weights should be informed by the energy cost of control use.

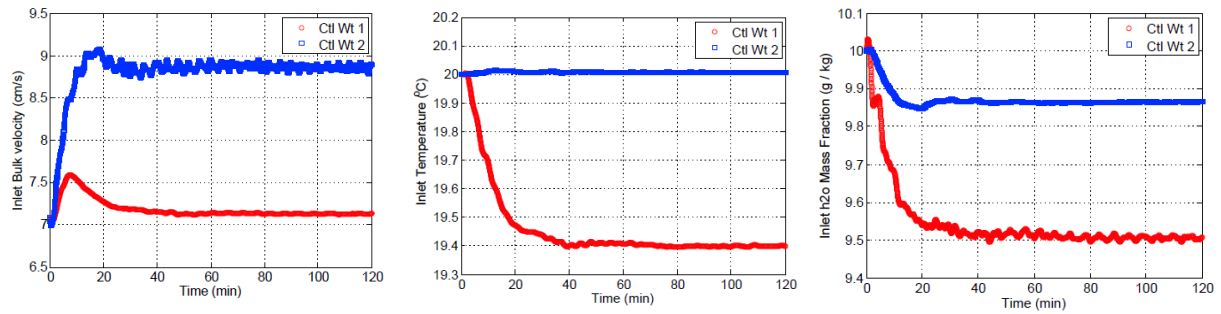


Figure 3.6.23(b): Control inputs, for two different choices of gain, chosen such that the weights on the temperature and humidity control are 8-times larger (blue) or 8-times smaller (red) than that on the velocity input.

### 3.6.5.6 Conference Room HVAC Retrofits: Radiant floors and DV (heating)

Here we consider design and control of a heating/ventilation (HV) system for a model of a conference room in the Atlantic Fleet Great Lakes facility (see Figure D.8). The HV system consists of displacement ventilation and radiant floor heating. In this section, we focus on maintaining temperature and humidity levels in the presence of a disturbance induced by a change in the temperature on the interior window surface. It should be noted that the HV system does not model the actual installed system. The various boundary conditions are listed in Table 3.6.7.

The disturbances are assumed to be the sensible and latent heat gains from occupants, and modeled as volumetric sources of energy and water-vapor. The region above the table has distributed water vapor sources at  $0.008 \text{ gm/m}^3/\text{s}$  and distributed energy sources at  $12.0 \text{ W/m}^3$ , whereas in the regions on the min y and max y sides of the table the values are  $0.004 \text{ gm/m}^3/\text{s}$  and  $6.0 \text{ W/m}^3$ . These values reflect occupancy by about four people. Fluent was run to a near steady-state; Figure 3.6.24 displays transient responses for volume-averaged and exhaust temperatures (left) and several level-surfaces of water mass-fraction at the near steady condition (right). Note that the relatively cool window/max y wall induces a locally higher concentration of water vapor.

Boundaries	Momentum boundary conditions	Energy boundary conditions	Species boundary conditions
Heated floor	No-slip	Specified heat-flux, $1.5 \text{ W/m}^2$	Zero gradient
Inlet vents (four, each $0.49 \text{ m}^2$ )	Parabolic profile; mean velocity = $0.015 \text{ m/s}$	Supply temperature = $20 \text{ deg C}$	Supply humidity ratio = $5\text{g/kg}$
Outlet: ceiling-centered	Pressure = 0	-	-
Lights (two, each $4\text{m}^2$ )	No-slip	$100 \text{ W/m}^2$	Zero gradient
Wall: max-y	No-slip	Iso-thermal, $12 \text{ deg C}$	Zero gradient
Walls: min-y, min-x and max-x	No-slip	Iso-thermal, $17 \text{ deg C}$	Zero gradient
Windows	No-slip	Iso-thermal, $10 \text{ deg C}$	Zero gradient

Table	No-slip	Specified heat flux	Zero gradient
-------	---------	---------------------	---------------

Table 3.6.7: Boundary conditions for the conference room, for a heating-mode operation

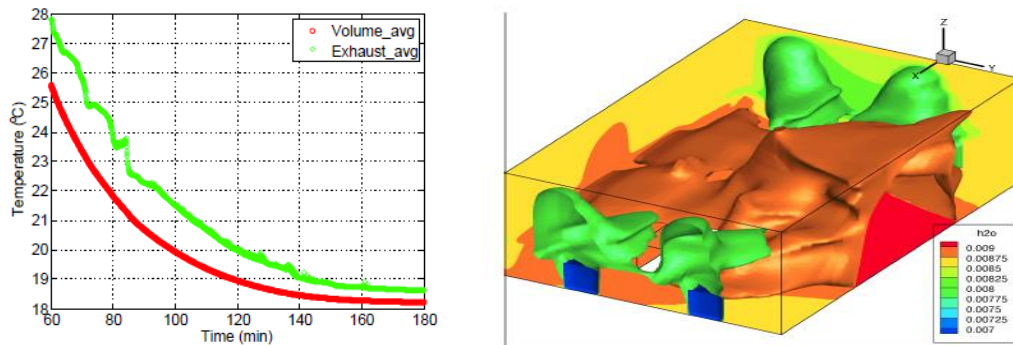


Figure 3.6.24: Startup temperature transients (left) and steady h2o field (right)

**ERA Model.** ERA data was generated by monitoring three output variables:

1. controlled h2o mass fraction in the region above table,
  2. sensed temperature on the max-x wall,
  3. controlled temperature in the region above the table;
- while two inputs were subjected to step-like changes:
1. Heat flux on the floor,
  2. Disturbance - window surface temperature

We used an ERA procedure to construct a 24th order model of the two-input, three-output system. Several data/model comparisons are shown in Figure 3.6.25.

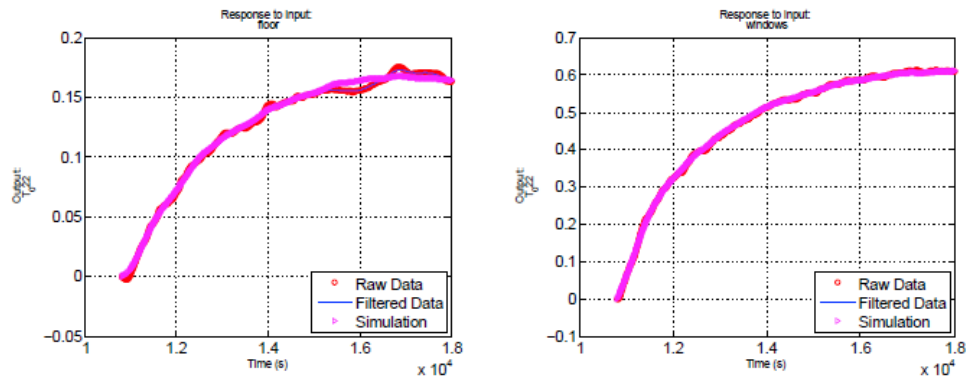


Figure 3.6.25: Response of the volume-averaged temperature to a step in the floor flux (left) and window temperature (right).

**H2 Control Design.** The structure of the H2 control problem has been described previously (Sunil: we need a pointer). In the present case we identify: a single control (u) - the floor thermal flux; a single input disturbance (w) - window interior temperature (plus sensor noise terms); two sensed outputs (y):

1. temperature on max x wall,
  2. h2o mass fraction in region above table;
- and two controlled outputs (z):
1. h2o mass fraction in region above table,

2. temperature in region above the table.

Since we have single disturbance, we include a 25<sup>th</sup> state with dynamics:

$$\dot{d}(t) = -\frac{1}{\tau}d(t), \quad \tau = 10^4 \text{ (s)} .$$

The resulting dynamic compensator is a 25<sup>th</sup> order system with two inputs (the h2o mass fraction in the region above table, and the temperature on max x wall) and a single output (the controlled floor thermal flux - u).

**Closed-loop Simulation.** The controller was implemented as a discrete-time system with a time-step of 5.0 seconds, and coupled to the Fluent simulation. The simulation was started from a nominal steady condition and after 10 seconds the controller was turned on. At 60 seconds, the disturbance began and was ramped to its full value (-2°C) over an additional 60 seconds, maintained for 7200 seconds, then ramped back to zero over another 60 seconds. The disturbance simulated a drop of 2°C in the interior surface temperature of the windows. Figure 3.6.25 displays the time history of the estimated disturbance. This is an internal state in the controller and we include it to show that the controller is marginally successful at identifying the disturbance input. Note however, that after an initial close match say about 10 minutes the Fluent and Simulink predictions diverge with a peak discrepancy of about 0.7°C. The Simulink model is closer to the actual disturbance, indicating that the ERA model and the Fluent simulation differ. The feedback control (floor flux) is shown in Figure 3.6.26. Here again, there is an initial period of close tracking with a divergence at about 10 minutes. The peak difference is about 1.5W/m<sup>2</sup>. Figure 3.6.27 displays the temperature and the water vapor responses for zone 022. Recall that these are the controlled quantities in our H2 design formulation (that is, these are the quantities we wish to make insensitive to the disturbance). Observe that the Fluent and the Simulink temperature predictions initially track, but differ by about 0.7°C. Similarly, the h2o mass fraction predictions differ by up to 0.032 g/kg.

**Energy Performance.** During the simulated three hour period the controlled system used about 430 Watt-hours of energy while maintaining the temperature within 0.3°C and the relative humidity within 3-4%.

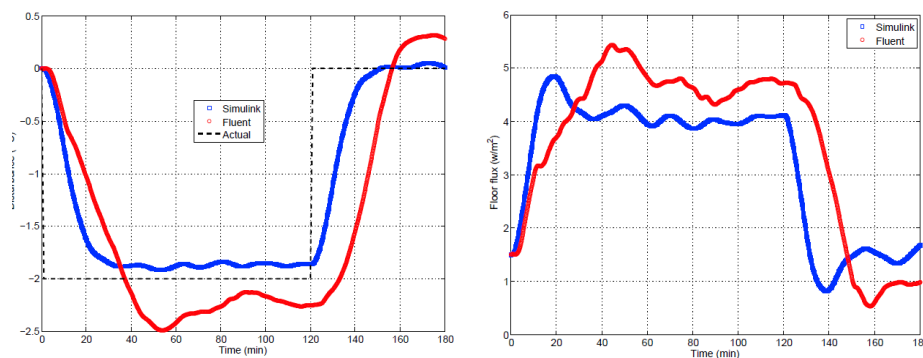


Figure 3.6.26: (Left) Actual and estimated disturbances, representing a step change in the window temperature. (Right) The radiant floor heat-flux, required to maintain the zonal set-points; both, inputs predicted by the model and those in the full are plotted.

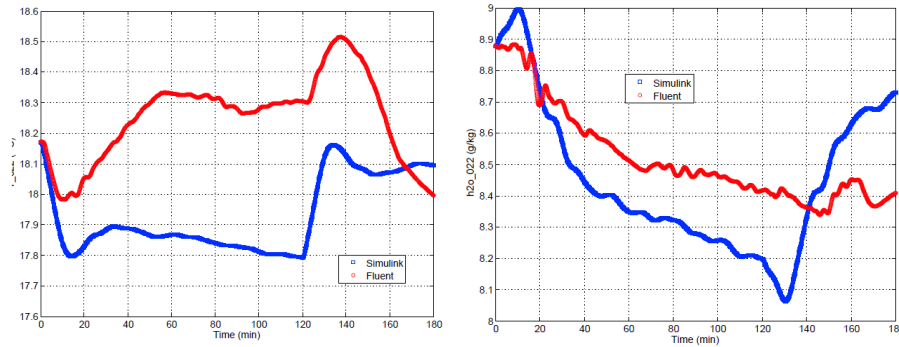


Figure 3.6.27: Responses of the closed-loop system, in the reduced and full-order systems.

### 3.6.6 Summary and Next Steps

In this part of the project, we demonstrated a technique for developing control-oriented low-order models of airflow in indoor spaces. These models are essential to accurately capture the dynamics of airflow, especially in zones equipped with low-energy consumption HVAC terminal units. The modeling procedure shown here requires data from CFD simulations, but could be substituted with data from field experiments. We also presented a method for developing controller based on these models, to maintain comfort in an indoor building environment with disturbances, which may or may not be known a-priori. The model reduction and control design techniques were demonstrated using two zones in a DoD building, at different spatial scales: one, a small conference room, and second, a larger gymnasium-like space. Through closed-loop CFD simulation, it was demonstrated that the resulting controller is capable of rejecting heat gains from solar radiation and occupants; moreover, the models accurately predicted the response of the full-order system. In addition, the models were (or can be) useful to:

1. Estimate energy consumption, and hence evaluate energy savings in low-energy systems. The same calculation would be infeasible with CFD due to computational expense.
2. Rapidly evaluate trade-offs between cost and comfort, by tuning controller gains. The method could do away with expensive controller tuning via onsite experiments.
3. Models could be integrated into whole building simulation tools such as TrnSys or Modelica, for an accurate representation of zonal airflow.

In this work, the CFD simulations were validated against field measurements, for a baseline case served by overhead diffusers. However, validation of systems served by low-energy systems such as DV or radiant floors was not possible due to lack of such cases in the chosen DoD buildings. The next steps would be to validate the CFD simulations of the low-energy systems, develop model-based controllers, implement these experimentally and test the performance.

## 4. References

Ahuja, S. and Rowley, C. W. 2010 Feedback control of unstable steady states of flow past a flat plate using reduced-order estimators. *J. Fluid Mech.* 645, 447–478.

Aimdyn GoSUM Software, 2011, “Global optimization, sensitivity and uncertainty in models (GoSUM).” Available from: <http://aimdyn.com>.

ASHRAE Standard 62.1-2004 Atlanta, GA: American Society of Heating, Refrigerating and Air-Conditioning Engineers.

*ASHRAE Handbook, HVAC & Equipment*. (2008). American Society of Heating, Refrigerating and Air-Conditioning Engineers, Inc.

Bagheri, S., Brandt, L. and Henningson, D. S. 2009 Input–output analysis, model reduction and control of the flat-plate boundary layer. *J. Fluid Mech.* 620, 263–298.

Barbagallo, A., Sipp, D. and Schmid, P. J. 2009 Closed-loop control of open cavity model using reduced-order models. *J. Fluid Mech.* 641, 1–50.

Bensoussan, A., Da Prato, G. , Delfour, M. C. , and Mitter, S. K. 2007 Representation and Control of Infinite Dimensional Systems. *Systems & Control: Foundations & Applications*. Birkhauser, 2<sup>nd</sup> edition.

Bertsekas, D. P. 1999 Nonlinear programming. Athena Scientific.

Bertsekas, D. P. 2005 Dynamic Programming and Optimal Control, 3rd edition, vol. 1. Athena Scientific.

Borggaard, J. T., Burns, J. A., Cliff, E. M. and Zietsman, L. 2009a A PDE approach to optimization and control of high performance buildings. In *Proceedings of the Oberwolfach Workshop on Numerical Techniques for Optimization Problems with PDE Constraints* (ed. M. Heinkenschloss, R. H. W. Hoppe & V. Schulz), pp. 205–208.

Borggaard, J. T., Burns, J. A., Surana, A. and Zietsman, L. 2009b Control, estimation and optimization of energy efficient buildings. In *Proceedings of IEEE American Control Conference*. St. Louis, Missouri, USA.

Braun, E. J., & Zhong, Z. (2003). *Development and evaluation of night ventilation precooling algorithm*. California Energy Commission.

Brohus, H., Heiselberg, P., Hesselholt, A., and Rasmussen, H., 2009a. Application of Partial Safety Factors in Building Energy Performance Assessment. In: *Eleventh International IBPSA Conference*, July 27-30., 1014–1021.

Brohus, H., Heiselberg, P., Simonsen, A., and Sorensen, K., 2009b. Uncertainty of energy consumption assessment of domestic buildings. In: *Eleventh International IBPSA Conference*, 1022–1029.

Burhenne, S., Jacob, D., and Henze, G. 2011, Sampling based on Sobol' sequences for Monte Carlo techniques applied to building simulations, *Proceedings of IBPSA BUILDSIM*, Australia.

Burns, J. A. and King, B. B. 1994 Optimal sensor location for robust control of distributed parameter systems. In *Proceedings of the 33<sup>rd</sup> IEEE Conference on Decision and Control*, pages 3967-3972.

Burns, J. A., King, B. B. and Ou, Y. R. 1995 Computational approach to sensor/actuator location for feedback control of fluid flow systems. In *Proceedings of SPIE*, volume 2494, page 60.

Burns, J. A., King, B. B., Rubio, A. D. and Zietsman, L.. 2002 Functional gain computations for feedback control of a thermal uid. In *Proc. 3<sup>rd</sup> AIAA Theoretical Fluid Mechanics Meeting*, number AIAA 2002-2992.



- Campolongo, F., Cariboni, J., and Saltelli, A., 2007. An effective screening design for sensitivity analysis of large models. *Environmental Modelling and Software*, 22, 1509–1518.
- Capozzoli, A., Mechri, H., and Corrado, V., 2009. Impacts of Architectural Design choices on building energy performance, applications of uncertainty and sensitivity analysis. In: Eleventh International IBPSA Conference, July., 1000–1007.
- Clarke, J., Yeneske, P., and Pinney, A., The Harmonization of thermal properties of building materials. , 1990. , Technical report, Building Environmental performance analysis club, Building research Establishment, Watford, UK.
- Conn, A., Scheinberg, K., and Vicente, L., 2009, Introduction to derivative-free optimization. Society of Industrial and Applied Mathematics.
- Corrado, V. and Mechri, H., 2009. Uncertainty and sensitivity analysis for building energy rating. *Journal of building physics*, 33 (2), 125–156.
- C’ostola, D., Blocken, B., Ohba, M., and Hensen, J., 2010. Uncertainty in airflow rate calculations due to the use of surface-averaged pressure coefficients. *Energy and Buildings*, 42, 881–888.
- Crawley, D.B., Pedersen, C.O., Lawrie, L.K., and Winkelmann, F.C., 2000. EnergyPlus: Energy Simulation Program. *ASHRAE Journal*, 42, 49–56. Crawley, D.B., Pedersen, C.O., Lawrie, L.K., and Winkelmann, F.C., 2000. EnergyPlus: Energy Simulation Program. *ASHRAE Journal*, 42, 49–56.
- Department of Defense, MIL-STD-1629A, “Procedures for Performing A Failure Mode, Effects and Criticality Analysis” Washington DC, November 24, 1980.
- Deru, M., K. Field, D. Studer, K. Benne, B. Griffith, P Torcellini, M. Halverson, D. Winiarski, B. Liu, M. Rosenberg, J. Huang, M. Yazdanian, and D. Crawley. 2009. “DOE Commercial Building Research Benchmarks for Commercial Buildings.” Technical Report, Washington, DC: U.S. Department of Energy, Energy Efficiency and Renewable Energy, Office of Building Technologies
- Deru, M., et al., DOE Commercial Building Research Benchmarks for Commercial Buildings. , 2009. , Technical report, Washington, DC: U.S. Department of Energy, Energy Efficiency and Renewable Energy, Office of Building Technologies.
- DesignBuilder, 2010. Design Builder Building Simulation [online]. Gloucestershire, UK: Design-Builder Software Ltd.. Available from: <http://www.designbuilder.co.uk/> [Accessed 19 July 2010].
- de Wit, S. and Augenbroe, G., 2002. Analysis of uncertainty in building design evaluations and its implications. *Energy and Buildings*, 34, 951–958.
- Diakaki, C., Grigoroudis, E., and Kolokotsa, D., 2008, “Towards a multiobjective optimization approach for improving energy efficiency in buildings,” *Energy and Buildings*, vol. 40, p. 1747–1754.
- Dominguez-Munoz, F., Anderson, B., Cejudo-Lopez, J., and Carrillo-Andres, A., 2009. Uncertainty in the thermal conductivity of insulation materials. In: Eleventh International IBPSA Conference, 1008–1013.



Djuric, N., Novakovic, V., Holst, J., and Mitrovic, Z., 2007, "Optimization of energy consumption in buildings with hydronic heating systems considering thermal comfort by use of computer-based tools," *Energy and Buildings*, vol. 39, pp. 471–477.

*Efficient Windows*. (n.d.). Retrieved from <http://www.efficientwindows.org>

Eisenhower, B., O'Neill, Z., Fonoberov, V. A., and Mezic, I., 2011a, "Uncertainty and sensitivity decomposition of building energy models," *Journal of Building Performance Simulation*, Available Online, In Press.

Eisenhower, B., O'Neill, Z., Narayanan, S., Fonoberov, V. A., and Mezic, I., 2011c, A comparative study on uncertainty propagation in high performance building design. *Proceedings of IBP-SA BUILDSIM*, Australia.

Ellis, P., Griffith, B., Long, N., Torcellini, P., and Crawley, D., 2006, "Automated multivariate optimization tool for energy analysis," in *Proceedings of the Second National IBPSA-USA Conference*, Cambridge, MA, pp. 42–48.

ESTCP, 2010. Automated Continuous Commissioning of Commercial Buildings. Department of Defense Environmental Security Technology Certification Program Project EW-200929.

Fanger, P. O., 1970, "Thermal comfort," Danish Technical Press.

Firth, S., Lomas, K., and Wright, A., 2010. Targeted household energy-efficiency measures using sensitivity analysis. *Building Research and Information*, 38 (1), 25–41.

Fumo, N., Mago, P., and Luck, R., 2010. Methodology to estimate building energy consumption using EnergyPlus Benchmark Models. *Energy and Buildings*, In Press, Corrected Proof.

*Efficient Windows*. Retrieved from <http://www.efficientwindows.org>

Griffith, B. T. 2002 Incorporating nodal and zonal room air models into building energy calculation procedures. Master's thesis, Massachusetts Institute of Technology.

Griffith, B., Long, N., Torcellini, P., & Judkoff, R. (2008). *Methodology for Modeling Building Energy Performance across the Commercial Sector*. NREL/TP-550-41956.

Gugercin, S. 2005 An iterative rational Krylov algorithm (IRKA) for optimal H2 model reduction. In *Householder Symposium XVI*, Seven Springs Mountain Resort, PA, USA.

Hampton, R. D., Knospe, C. R. and Townsend, M. A. 1996 A practical solution to the deterministic nonhomogeneous lqr problem. *Transactions of the ASME* 118, 354–360.

Heiselberg, P., et al., 2009. Application of Sensitivity Analysis in Design of Sustainable Buildings. *Renewable Energy*, 34, 2030–2036.

Hogberg, M., Bewley, T. R. and Henningson, D. S. 2003 Linear feedback control and estimation of transition in plane channel flow. *J. Fluid Mech.* 481, 149–175.

Hughes, T. J. R. and Cliffs, E. 1987 *The finite element method: linear static and dynamic finite element analysis*. Prentice-Hall.

Hunt, G. R., & Linden, P. F. (1999). The fluid mechanics of natural ventilation-displacement ventilation by buoyancy-driven flows assisted by wind. *Building and Environment*, 34 , 707-720.

- Ilak, M. and Rowley, C. W. 2008 Modeling of transitional channel flow using balanced proper orthogonal decomposition. *Phys. Fluids* 20 (034103).
- Juang, J.-N. and Pappa, R. S. 1985 An eigensystem realization algorithm for modal parameter identification and model reduction. *J. Guid. Contr. Dyn.* 8 (5), 620–627.
- Kampf, J., Wetter, M., and Robinson, D., 2010 “A comparison of global optimization algorithms with standard benchmark functions and real-world applications using EnergyPlus,” *Journal of Building Performance Simulation*, vol. 3, pp. 103–120.
- Kobayashi, N. and Chen, Q. 2003 Floor-supply displacement ventilation in a small office. *Indoor and Built Environment* 12 (4), 281–292.
- Kundu, P. K. 1990 *Fluid Mechanics*. New York: Elsevier.
- Lam, J., Wan, K., and Yang, L., 2008. Sensitivity analysis and energy conservation measures implications. *Energy Conversion and Management*, 49, 3170–3177.
- LeDigabel, S., 2011, “Nomad: Nonlinear optimization with the MADS algorithm,” *ACM Transactions on Mathematical Software*, vol. 37, no. 4, pp. 1–15.
- Lee, K. S., Jiang, Z. and Chen, Q. 2009 Air distribution effectiveness with stratified air distribution systems. *ASHRAE Transactions* 115 (2).
- Li, G. and Rabitz, H., 2006. Ratio Control variate method for efficiently determining high-dimensional model representations. *Journal of Computational Chemistry*, 27, 1112–1118.
- Li, G., et al., 2002. Global uncertainty assessments by high dimensional model representations (HDMR). *Chemical Engineering Science*, 57, 4445–4460.
- Lions, J.-L. 1971 *Optimal Control of Systems Governed by Partial Differential Equations*. Springer-Verlag, Berlin.
- Lomas, K.J. and Eppel, H., 1992. Sensitivity Analysis Techniques for Building Thermal Simulation Programs. *Energy and Buildings*, 19, 21–44.
- Lumley, J. L. 1970 *Stochastic Tools in Turbulence*. New York: Academic Press.
- Ma, Z., Ahuja, S. and Rowley, C. W. 2010a Reduced order models for control of fluids using the Eigensystem Realization Algorithm. *Theor. Comput. Fluid Dyn.* in press, DOI: 10.1007/s00162–010–0184–8.
- Ma, Z., Rowley, C. W. and Tadmor, G. 2010b Snapshot-based balanced truncation for linear time-periodic systems. *IEEE Trans. Automat. Contr.* 55 (2), 469–473.
- Macdonald, I., 2002. Quantifying the effects of uncertainty in building simulation. Thesis (PhD). University of Strathclyde, Department of Mechanical Engineering.
- Macdonald, I., 2009. Comparison of sampling techniques on the performance of Monte Carlo based sensitivity analysis. In: *Eleventh International IBPSA Conference*, 992–999.
- Mara, T. and Tarantola, S., 2008. Application of Global Sensitivity Analysis of Model Output to Building Thermal Simulations. *Building Simulation*, 1, 290–302.
- Moon, H., 2005. Assessing Mold Risks in Buildings under Uncertainty. Thesis (PhD). Georgia Institute of Technology.

- O'Neill, Z. D., Eisenhower, B., Yuan, S., Bailey, T., Narayanan, S., and Fonoberov, V., 2011, "Modeling and calibration of energy models for a DoD building," ASHRAE Transactions, vol. 117, no. 2.
- Rahni, N., Ramdani, N., Candau, Y., and Dalicieux, P., 1997. Application of group screening to dynamic building energy simulation models. *Journal of Statistical Computation and Simulation*, 57 (1), 285–304.
- Renardy, M. and Rogers, R. C. 1993 *An introduction to partial differential equations*. New York, NY: Springer-Verlag.
- Rowley, C. W. 2005 Model reduction for fluids using balanced proper orthogonal decomposition. *Int. J. Bifurcation Chaos* 15 (3), 997–1013.
- Rowley, C. W., Colonius, T. and Murray, R. M. 2004 Model reduction for compressible flows using POD and Galerkin projection. *Phys. D* 189 (1–2), 115–129.
- Saltelli, A., Chan, K., and Scott, E.M., 2000. *Sensitivity Analysis*. Wiley. Saltelli, A., et al., 2010. *Global Sensitivity Analysis, The primer*. Wiley. Simlab, 2010. Simlab: A professional tool for model developers, scientists and professionals, to learn, use and exploit uncertainty and sensitivity analysis techniques [online]. European Commission: Unit of Econometrics and Applied Statistics of the Joint Research Centre. Available at: <http://simlab.jrc.ec.europa.eu/> [Accessed 4 May 2010].
- Scholkopf, B. and Smola A., 2002, *Learning with Kernels*. The MIT Press.
- Smola, A. and Scholkopf, B., 2004. A tutorial on support vector regression. *Statistics and Computing*, 14, 199–222.
- Sobol', I., 2001. Global sensitivity indices for nonlinear mathematical models and their Monte Carlo estimates. *Mathematics and computers in simulation*, 55, 271–280.
- Sobol, I. and Kucherenko, S., 2009. Derivative based global sensitivity measures and their link with global sensitivity indices. *Mathematics and Computers in Simulation*, 79, 3009–3017.
- Soratana, K. and Marriott, J., 2010. Increasing Innovation in Home Energy Efficiency: Monte Carlo Simulation of Potential Improvements. *Energy and Buildings*, 42 (6), 828–833.
- Spitler, J., Fisher, D., and Zietlow, D., 1989. A Primer on the Use of Influence Coefficients in Building Simulation. *Building Simulation '89 Transactions*, 299–304.
- Struck, C., Hensen, J., and Kotek, P., 2009. On the Application of Uncertainty and Sensitivity Analysis with Abstract Building Performance Simulation Tools. *Journal of Building Physics*, 33 (1), 5–27.
- Surana, A., Hariharan, N., Narayanan, S. and Banaszuk, A. 2008 Reduced order modeling for contaminant transport and mixing in building systems: A case study using dynamical systems techniques. In *Proceedings of the ACC*, Seattle, WA.
- Surana, A., Sahai, T. and Banaszuk, A. "Iterative methods for scalable uncertainty quantification in complex networks", to appear in *Special Issues of Journal of Uncertainty Quantification*, 2012.

Thornton, B., et al., Technical Support Document: 50 Design Technology Packages for Medium Office Buildings, 2009. Technical report PNNL-18774, Pacific Northwest National Laboratory, Richland, WA.

Zhang, Y., 2009. "Parallel" EnergyPlus and the Development of a Parametric Analysis Tool. In: Eleventh International IBPSA Conference, July 27-30.

Ziehn, T. and Tomlin, A.S., 2009. GUI-HDMR -A software tool for global sensitivity analysis of complex models. *Environmental Modelling and Software*, 24, 775–785.

Wachter, A. and Biegler, L. T., 2006, "On the implementation of a primal dual interior point filter line search algorithm for large-scale nonlinear programming," *Mathematical Programming*, vol. 106, no. 1, pp. 25–57.

Wetter, M., 2001, "A generic optimization program," in *Proceedings of the Seventh International IBPSA Conference*, Rio de Janeiro, Brazil, pp. 601–608.

Wetter, M., and Wright, J., 2003, "A comparison of deterministic and probabilistic algorithms for nonsmooth simulation-based optimization," *Building and Environment*, vol. 39.

Wetter, M. and Wright, J., 2003b, "Comparison of a generalized pattern search and a genetic algorithm optimization method," in *Proceedings of the Eighth International IBPSA Conference*, Eindhoven, Netherlands, pp. 1401–1408.

Wetter, M., and Polak, E., 2004, "A convergent optimization method using pattern search algorithms with adaptive precision simulation," *Building Services Engineering Research and Technology*, vol. 25, no. 4, pp. 327–338.

## APPENDIX A

### Building Load and Energy Performance Model

A building load and energy performance model was created to calculate the annual energy consumption of the buildings in the DOD real property database. The model was designed to quickly perform an 8760 hour annual load and energy calculation from the limited building data in the DOD database plus the characteristics estimated from CBECS equivalent buildings. The model assumptions were as follows:

- The building could be represented by a single, well mixed zone (i.e. single inside air temperature node).
- The thermal capacitance of building structure and furnishings could be represented by a single lumped mass.
- Wall surface temperatures were assumed to be uniform and therefore that heat transfer processes are 1-D.
- The combination of direct and diffuse solar radiation heat gains and convective heat gains to exterior surfaces can be represented by the interaction of the wall with an effective sol-air temperature.
- The sol-air temperature method allows wall and roof conduction processes to be modeled using the ASHRAE Radiant Time Series (RTS) method, which accounts for the thermal resistance and capacitance effects of exterior surfaces.
- The building heating/cooling load can be calculated from a quasi-steady energy balance on the zone air node as follows:

$$\dot{Q}_{LOAD} = \dot{Q}_{People,sensible} + \dot{Q}_{Equip,sensible} + \dot{Q}_{Fenestration} \left( T_{Sol-Air}, \dot{Q}_{Solar\ Radiation}, T_{Zone} \right) + \sum_{All\ Surfaces} \dot{Q}_{Conduction} \left( T_{Sol-Air}, T_{Zone} \right) + \dot{Q}_{Infiltration} \left( T_{Outside\ Air}, T_{Zone} \right) + \dot{Q}_{Internal\ Mass} \left( T_{Zone}, T_{Internal\ Mass} \right)$$

- Sensible heat gain due to people is calculated based on standard per occupant values of defined in the ASHRAE Handbook of Fundamentals.
- Equipment (plug loads) are calculated by summing the peak energy consumption of each equipment type modified by the hourly use schedule over all equipment of each type [Griffith et al. 2008].
- Window and skylight fenestration gains are calculated, from the direct and diffuse solar radiation incident on the window area modified by the solar heat gain coefficient [Griffith et al. 2008].
- Infiltration heat gains or losses are calculated from the enthalpy gain or loss due to an exchange of outdoor and indoor air due to infiltration. The infiltration rate is based on standard ASHRAE values of 0.1 cfm/sf(wall), 0.3 cfm/sf(wall), and 0.7 cfm/sf(wall), for tight, average and leaky buildings respectively [Griffith et al. 2008].
- Heat conduction through the walls and roof of the building was calculated using the ASHRAE radiant time series method. This accounts for the time lag of heat pulses through a surface due to thermal capacitance effects. The tabulated RTS values in the ASHRAE Handbook were used by mapping the building wall thermal properties to the Handbook construction with the closest match.

- The wall heat flux due to conduction is calculated from a time history of surface temperature and surface fluxes. The total surface heat flux equals sum of product of surface heat input history terms and conduction time factors.

### HVAC and Central Plant Model and Assumptions

HVAC system and central plant performance was calculated using the hourly load data to drive the system response. In keeping with the simplicity of the building load model, the air side of the primary HVAC system was modeled as a single loop serving the single building thermal zone as shown in Figure A.1 below. Chilled water, hot water and condenser water were also modeled as single loops. The conditions around the HVAC air loop, needed to compute the heating and cooling coil loads and the airflow rate required to meet the building load were determined by performing an energy and mass balance across each component around the loop. The mixed air conservation equations are shown below, as an example:

$$\begin{aligned}\dot{m}_{MIXED} &= \dot{m}_{OA} + \dot{m}_{RECIRC} \\ W_{MIXED} &= \frac{\dot{m}_{OA} W_{OA} + \dot{m}_{RECIRC} W_{RECIRC}}{\dot{m}_{OA} + \dot{m}_{RECIRC}} \\ h_{MIXED} &= \frac{\dot{m}_{OA} h_{OA} \left( \epsilon_{OA}, W_{OA} \right) + \dot{m}_{RECIRC} h_{RECIRC} \left( \epsilon_{RECIRC}, W_{RECIRC} \right)}{\dot{m}_{OA} + \dot{m}_{RECIRC}}\end{aligned}$$

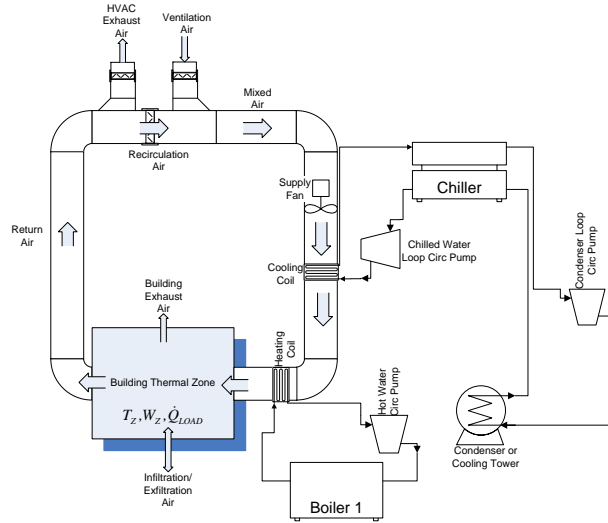


Figure A.1 Air and water loop schematic for the building, HVAC air and central plant model

Detailed coil performance calculations were avoided by assuming that the coils would be sized correctly and controlled to meet the desired setpoint temperature and, in the case of the cooling coil, relative humidity. The cooling coil load is thus given as follows:

$$\begin{aligned}\dot{m}_{Cool\ Coil, Leaving} &= \dot{m}_{Cool\ Coil, Entering} \\ W_{Cool\ Coil, Leaving} &= f_w \left( \epsilon_{Cool\ Coil, Leaving}, RH_{Cool\ Coil, Leaving} (=95\%) \right) \\ \dot{Q}_{Cool\ Coil} &= \dot{m}_{MIXED} \left( \epsilon_{Cool\ Coil, Leaving} - h_{MIXED} \right) \\ \text{where; } h_{Cool\ Coil, Leaving} &= f_h \left( \epsilon_{Cool\ Coil, Leaving}, RH_{Cool\ Coil, Leaving} (=95\%) \right)\end{aligned}$$

Following a similar procedure for the heating/reheat coil, and proceeding around the air loop, the required zone flow rate and the zone humidity ratio are calculated from:

$$\dot{m}_{SUPPLY} = \frac{\dot{Q}_{LOAD}}{\rho_{AIR} C_{p,AIR} (T_{ZONE} - T_{SUPPLY})}$$

$$\dot{m}_{RETURN} = \dot{m}_{SUPPLY}$$

$$W_{ZONE} = \frac{\dot{m}_{SUPPLY} W_{SUPPLY} + \dot{m}_{Infiltration} W_{Infiltration}}{\dot{m}_{RETURN} + \dot{m}_{ZONEEXHAUST}}$$

The energy consumption of components on the chilled water, hot water, and condenser water loops, such as chillers, boilers, and cooling towers are calculated using simple constant efficiency relationships to the coil loads, as in the case of pumps and chillers as shown below:

- Pump Flow rate

$$\dot{V}_{CHW PUMP} = \frac{\dot{Q}_{CoolCoil}}{\rho_{H2O} C_{H2O} \Delta T_{CHW}}$$

- Pump Power

$$\dot{Q}_{CHW PUMP} = \frac{\dot{V}_{CHW PUMP} \Delta P_{CHW PUMP}}{\eta_{Im pellerCHW PUMP} \eta_{MOTORCHW PUMP}}$$

- Chiller Power

$$\dot{Q}_{CHILLER} = \frac{\dot{Q}_{CoolCoil} + \frac{\dot{Q}_{CHW PUMP}}{\eta_{MOTORCHW PUMP}}}{COP_{CHILLER}}$$

Similar relationships were derived and used for boiler energy, heating loop pump energy, cooling tower energy, and condenser loop pump energy.

## Low Energy Design Principles and Models

In this section we describe various low energy design principles, or energy conservation measures (ECMs), and our approach to modeling them. These measures have been categorized based on how they affect the building: Lighting and equipment, Envelope, HVAC terminal side and HVAC supply side (see Table 3.1.1 for the list of measures in each category).

- **Lighting and Equipment Retrofits**

Table A.2: Lighting and Equipment Retrofits

Principle	Description	Modeling
<b>Light Scheduling (Baseline)</b>	Light switching based on building usage	Use ASHRAE lighting schedules based on CBECS Primary Usage
<b>Occupancy Sensors</b>	Light switching based on occupancy detection	5% reduction in installed lighting power
<b>Daylight Based Dimming</b>	Use of daylighting to reduce area to be lit by artificial light in occupied hours	Use perimeter depth upto 15ft (including window area correction factor) for area daylite and modulate schedule daylite based on available sky illumination
<b>Upgraded Lighting</b>	Use of T5/CFL/LED lighting fixtures to reduce lighting power density	Use 80% of ASHRAE recommendations for Lighting Power Density upgraded values
<b>Plug Load Control (Baseline)</b>	Plug loads based on occupancy schedule	Use ASHRAE occupancy schedules based on CBECS Primary Usage
<b>Efficient Equipment</b>	Use of Energy Star efficient equipment (computers, servers, printers, refrigerators, vending machines, case registers etc)	10% reduction in installed equipment power
<b>Light Shelves</b>	Horizontal light-reflecting overhangs that allows daylight to penetrate deep into a building.	Increase the perimeter depth upto 25 ft + daylight based dimming
<b>Added daylight</b>	Use of Skylights & Solartubes	Increase Area Daylite: Top Floor=75% , Penultimate Floor=50% +daylight based dimming



## • Envelope Retrofits

Table A.3: Envelope Related Retrofits

Principle	Description	Modeling
<b>Weatherization</b>	Measures to reduce convective heat flow through building envelope	Reduce leakage rate to 0.1 cfm/sqft (Default 0.3 cfm/sqft)
<b>Trees</b>	Planting trees nearby to reduce fenestration and wall conduction load (applicable only to 1 storey buildings)	Reduction in SHGC and absorption coefficient based on season : •Summer: 50% reduction in SHGC •Winter: 10% reduction in SHGC (similar changes in absorption coefficient)
<b>Cool Roof</b>	A roofing system that can deliver high solar reflectance and high thermal emittance	50% reduction in Global horizontal irradiance (affecting the roof conduction load)
<b>Upgraded Windows</b>	Efficient windows based on CBECS climate zone	Use upgraded SHGC, Visible Transmittance and U-factor
<b>Upgraded Insulation</b>	Use insulation in wall cavity, to wall exterior., or to wall interior. Layer of insulation on roof exterior..	Use ASHRAE recommendation + 2 inches XPS (R10) on walls and 4 inches XPS (R20) on roof, to obtain upgraded RTS coefficients
<b>Green Roof</b>	Roof system that is partially or completely covered with vegetation planted over a waterproofing membrane	Use ASHRAE recommendation + 1ft soil layer on roof to obtain upgraded RTS coefficients. Assume roof OAT=OAWBT (when OAT>Tin)
<b>Active External Shading</b>	Overhangs to reduce fenestration and wall conduction load (only for multiple storey buildings)	Reduction in SHGC & absorption coefficient based on season Effective only in summer period: •60% reduction in SHGC (for early morning, evening and nighttime) •30 % reduction in SHGC (during daytime between 10am and 5pm) (similar changes in absorption coefficient)

## • Terminal HVAC Retrofits

Table A.5: HVAC Terminal Side Retrofits

Principle	Description	Modeling
<b>Air Side Economizer (Baseline)</b>	Use of outside air when OAT < Treturn to provide free cooling	•100% OA if Tsupply<Tout<Tin •OA throttled proportionally from supply airflow rate to MinOA when Tpreheat<Tout<Tsupply •MinOA when Tout<Tpreheat
<b>Fan assisted Night Ventilation for Pre-Cooling</b>	Use of existing fans to draw in nighttime outside air (under favorable conditions) to precool internal structure	Purge (at 1cfm/sqft) in nighttime unoccupied hours when •Tout< Tin, HRout < HRin •Internal Structure Temp > HSP
<b>Proper Space Setpoints</b>	Use recommended values for the setpoints	Adjust setpoints: CSP+1, CSB+2, HSP-1, HSB-2 (Baseline: CSP=24C, CSB=33C; HSP=21C, HSB=13C)
<b>Supply Air Temp Reset</b>	Adjusting cold deck leaving air temp to minimize reheat	Increase cold deck temp (upto 65F) when MinOA exceeds airflow rate required at design cold deck temp.
<b>Static Reset</b>	Reduce fan static pressure until VAV box requiring most pressure is fully open	5% reduction in CentralFanPower
<b>Water Side Economizer</b>	Cooling tower to provide chilled water to air handlers when outside air WBT is favorable	WBT<=50F, for distributed systems e.g. fancoils (Used only in conjunction with DOAS),
<b>DCV</b>	Adjust outside air cfm based on occupancy schedule	Use ASHRAE standard for MinOA requirements
<b>Displacement Ventilation + Radiant Cooling/Heating</b>	Use chilled ceiling/beams+radiant floors +DV for generating buoyancy driven airflow to provide conditioning in occupied space	Adjust Setpoints: CSP+2, CSB+2, HSP-2, HSB-2 50% reduction in CentralFanPower & ZoneFanPower
<b>Under Floor Air Ventilation (UFAD)</b>	Deliver conditioned air to a relatively large no of supply air locations, often in close proximity to occupants	Adjust setpoints: CSP+1, CSB+1, HSP-1, HSB-1 75% reduction in CentralFanPower & ZoneFanPower
<b>Personal Air Supply/Temp Control</b>	Incorporate occupant thermal/comfort preferences management at individual level	Adjust setpoints: CSP+2, CSB+2, HSP-2, HSB-2 (supersedes proper space setpoints)

- **HVAC Supply Retrofit**

Table A.6: HVAC Supply Side Retrofits

Principle	Description	Modeling
<b>Conversion from constant volume to variable flow with VFD</b>	Install variable frequency drives (VFDs) on the supply and return air fans	10% reduction in CentralFanPower
<b>Chiller Plant Optimization</b>	Optimizing operational sequence by introducing appropriate controls	5% increase in COPCoolEquip
<b>Optimized Pumping</b>	Optimizing pump scheduling & VFDs for improved water distribution efficiency	37% reduction in pump power
<b>Tankless Water Heating</b>	Heat water directly without the use of a storage tank (thereby avoiding the standby heat losses)	10% increase in COPWaterHeat
<b>Two Stage Absorption Chillers</b>	Improves energy efficiency of absorption by recovering in 2 <sup>nd</sup> stage some of the heat normally rejected to cooling tower circuit	20% increase in COPCoolEquip (when single stage absorber is present)
<b>Condensing Boiler</b>	Extract additional (latent) heat by condensing water vapor in the waste gases	10% increase in COPHeatEquip
<b>GSHP</b>	Hybrid systems: GSHP with an auxiliary heating or cooling system	•33% increase in Condenser Loop Pump power to account for additional head of GHX •COPCoolEquip=8, COPHeatEquip=4, with adjustments based on thermal load imbalance
<b>Daytime Natural Ventilation</b>	Use buoyancy driven NV flow under favorable conditions to meet daytime ventilation and conditioning requirements	Physics Based
<b>Night-time NV for Pre-Cooling</b>	Use of NV to draw in outside air (under favorable conditions) in nighttime to precool the internal structure: which serve as a heat sink during the daytime hours, reducing the mechanical cooling required	Physics Based
<b>Energy Recovery</b>	Use of heat wheels for extracting heat and moisture between exhaust air stream and inlet air stream	Energy & mass balance
<b>Indirect Evaporative Cooling</b>	Remove sensible energy from the air stream with a water to air heat exchanger	Based on ASHRAE Handbook
<b>Direct Evaporative Cooling</b>	Remove sensible energy from air stream adiabatically by directly adding moisture to it	Based on ASHRAE Handbook
<b>Solar Water Heating and Waste Heat</b>	Solar panels to heat service hot water & use excess heat for space heating or desiccant regeneration	Sized to 50% total roof area, 50% absorption efficiency, assume fixed azimuth=latitude & south facing orientation
<b>Desiccant Dehumidification</b>	Use of enthalpy wheel for dehumidification by using waste solar heat (used only when excess solar heating available)	Energy & mass balance
<b>DOAS</b>	Supplies conditioned minimum ventilation air at space neutral temperature	Energy & mass balance (Used in conjunction with Displacement ventilation+Radiant heating/cooling system)

## Comparison of Stock Tool Calculation Results with Reported CBECS Data

The current official CBECS database was compiled in 2003 from owner/occupier reported survey data containing information about the physical characteristics and energy use of 5129 buildings distributed across the United States. The building data can be further subdivided into 9 distinct climate zones and 20 classifications of primary building activity.

Since the CBECS database is used by the stock tool to populate building simulation default parameters for the buildings in the DOD RPAD and for individual buildings, it is important to understand the energy use characteristics of the buildings in the CBECS database and how well the stock tool results represent those characteristics.

In figure A.3, the total annual energy use of all the buildings in the CBECS database is 15.8 TWh of which, the components in order of largest to smallest are heating, electric use for all functions other than heating or cooling (i.e. fans, pumps, plug loads, lights, refrigeration, etc.), and cooling.

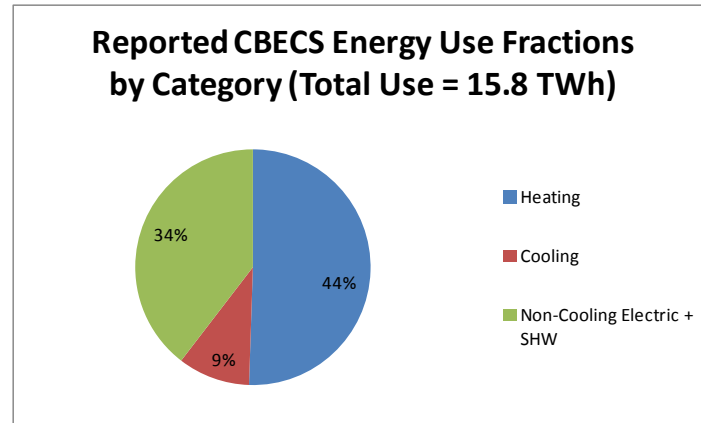


Figure A.3: CBECS total site reported energy use and component fractional use

In contrast, the stock tool predicts total site energy use for the CBECS building stock of 11.6 TWh (27% less than the reported value) and from largest fraction to smallest fraction the energy use components are electric (as defined above), heating, and cooling. These results are shown in Figure A.4 below:

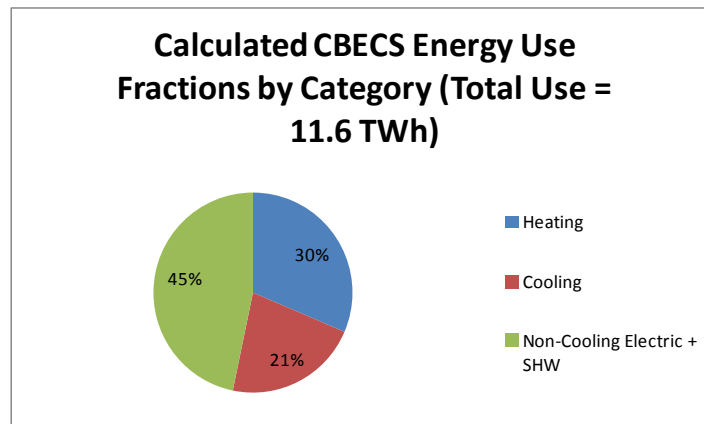


Figure A.4: Stock tool total site reported energy use and component fractional use

The data used to create Figures A.3 and A.4 is compared directly in Figure A.5, which shows that reported and calculated electric use matches within 4% but that total cooling is over-predicted by 100% and total heating is under-predicted by 50%. These differences are shown in Figure A.6. There are several possible causes for the discrepancies, some or all of which likely play a role in the differences in energy use that are observed in the results. The possible causes, in no particular order, include:

- **Input error:** Translation of the CBECS data fields to usable simulation input involves extrapolation and estimation based on the NREL procedure, which may result in the simulated building having significantly different characteristics than the actual building. It is likely that this represents a significant source of error since the stock tool has produced much more accurate results when detailed building information is known.
- **Single well-mixed zone building model assumption:** Treating the building as a single well-mixed zone will have the effect of increasing the cooling energy consumption and decreasing the heating energy consumption compared to the actual building being modeled. In the single zone model, core cooling loads are distributed to the perimeter where they can reduce the heating load due to conduction heat loss through the building envelope.
- **Equipment part load performance:** In the stock tool, all equipment performance with a single constant figure of merit, e.g. COP for chillers and heat pumps and efficiency for boilers and furnaces. In practice, this will tend to underestimate the efficiency of chillers and overestimate the efficiency of heating equipment. The COP used to simulate cooling equipment was the full-load value at design conditions. However, at low load conditions when the outside air temperature is typically lower than the design value, the chiller can operate more efficiently lowering energy consumption compared to the value expected based on the nominal COP. Using SEER or IPLV values in place of the design COP would improve the results, but would not be as accurate as using a COP that varies with the temperature returned from the condenser or cooling tower. In addition, heating equipment efficiency is reduced from the nominal value by partial loading and cycling on/off. Improved accuracy in predicting heating equipment energy consumption could be achieved by implementing part load performance models of the heating equipment in the stock tool.

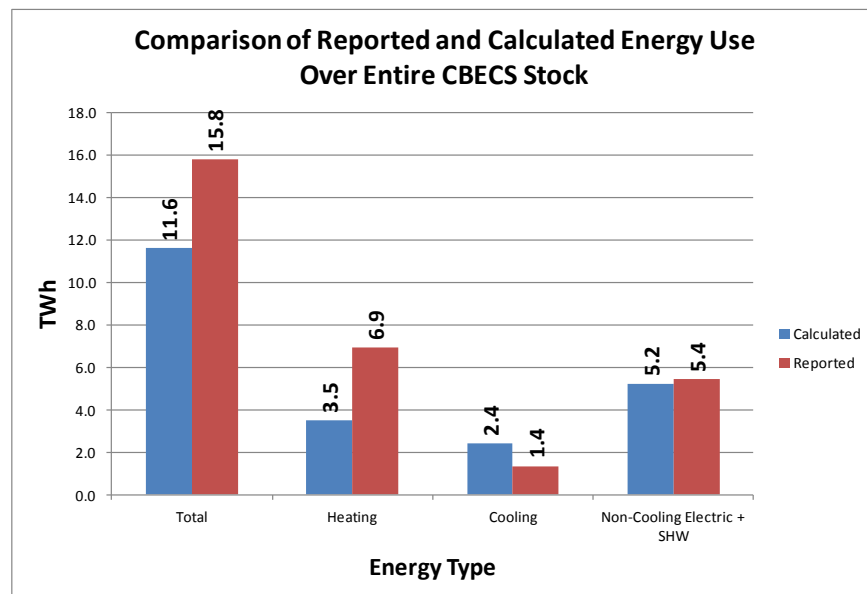


Figure A.5: Comparison of reported and stock tool energy use

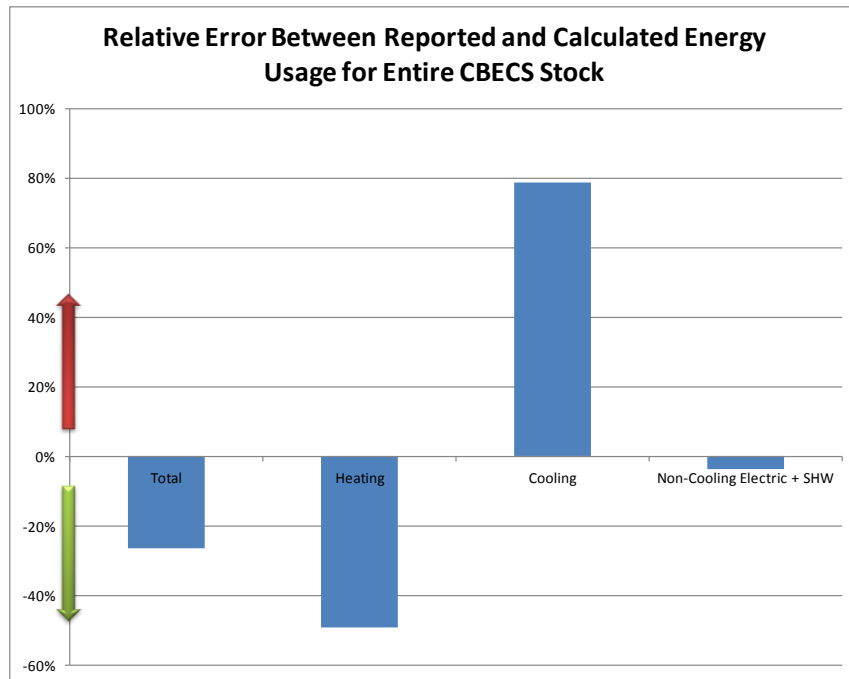


Figure A.6: Differences in stock tool calculated and CBECS reported energy use for CBECS building stock

The accuracy of the screening tool model was further evaluated by plotting calculated versus reported electric energy use and total energy use intensity over the 5129 buildings in the CBECS database. Ideally, there should be a one-to-one correlation between the two numbers and, consequently all the data points should lie on a single straight line when plotted against each other. In Figure A.7, the electric use intensity shows that the correlation is roughly one-to-one, but with a lot of scatter indicating that the model is both under predicting and over predicting electric energy use compared to the reported values. The comparison of total calculated and reported energy use intensities, shown in Figure A.8, indicates significantly more scatter. However, for these CBECS building cases, the simulation inputs represent a high level approximation of each building; simulation inputs must be populated from the information reported in the database and estimated using rules of thumb derived from the NREL procedure. In addition, the model used TMY3 weather data from the closest available location. The scatter in the CBECS results compared to the very good match between the two spot checked buildings is probably reasonable given the likely magnitude of error between the input parameters that accurately represent each CBECS building, but are unknowable, and the imputed input parameters that were derived to provide a data set sufficient to run the energy model.

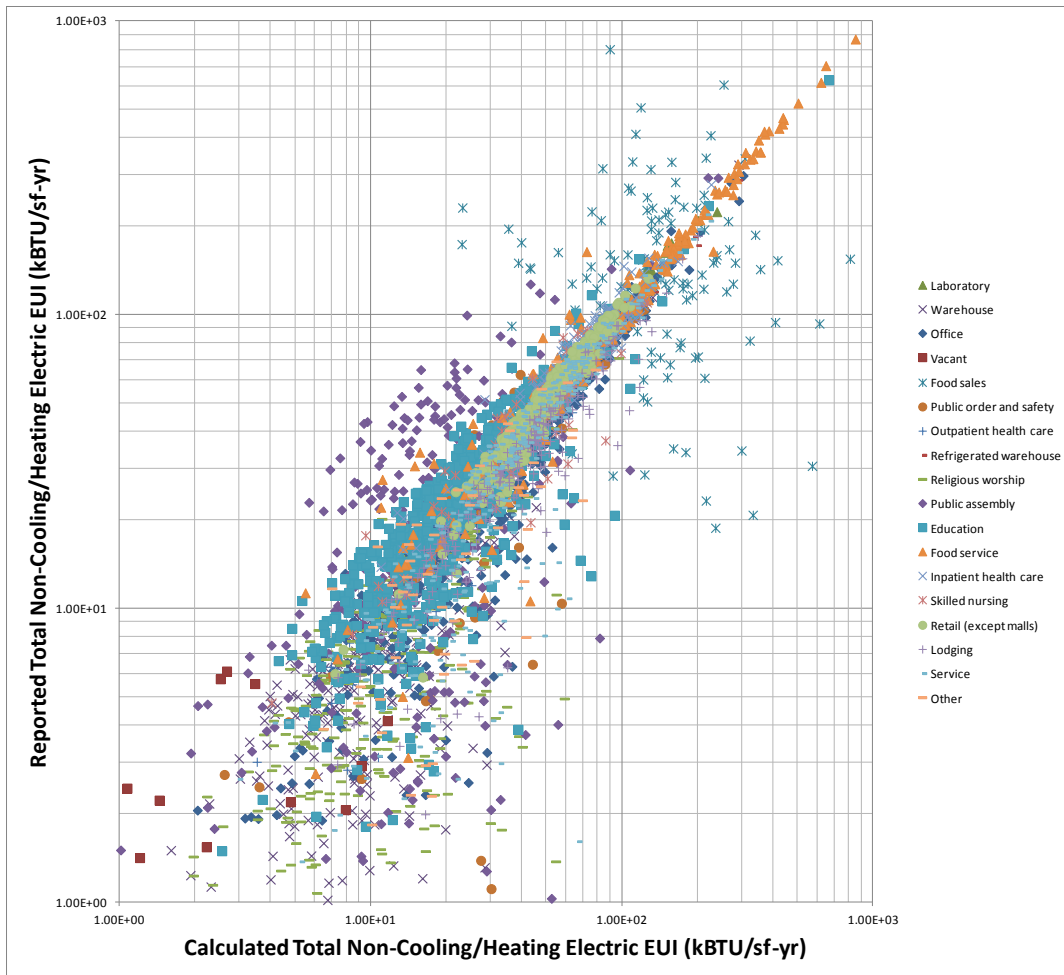


Figure A.7: Reported vs. computed electricity EUI for buildings in the CBECS database

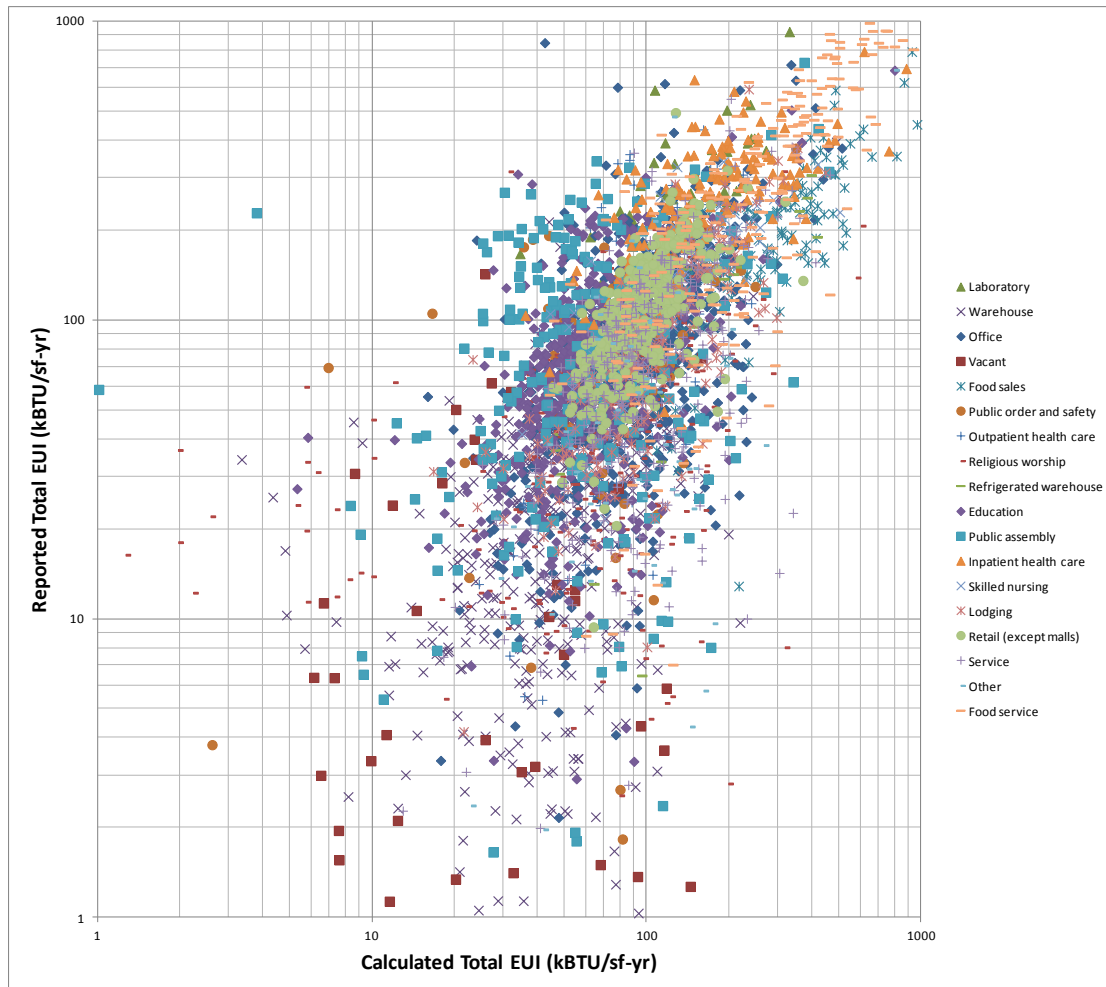


Figure A.8: Reported vs. computed EUI for buildings in the CBECS database

Another way to analyze the CBECS data is to see how much variance there is in reported energy consumption for a single building use type in a single climate zone. Figure A.9 shows the normalized standard deviation,  $\sigma$ , in total energy consumption reported at the level of a building use type and climate zone (the ratio of standard deviation of reported EUI to the mean EUI for that building type and climate zone). For a Gaussian distribution, the mean,  $\mu$ ,  $\pm \sigma$  contains approximately 68% of the data points, and  $\mu$ ,  $\pm 2\sigma$  contains approximately 95% of the data points. The larger the value of  $\sigma$ , the more widely distributed the data, and for the CBECS data, the less likely it is that any single building within the intersection of an activity type and a climate zone can be assumed to be representative of all the buildings within that intersection. However, as shown in Figure A.9 the CBECS building EUI data shows significant scatter for most of the building activity type and climate zone categories. At least some of the problem may be due to having insufficient samples for some activity/climate zone categories, meaning that the mean EUI for a category is not close to any of the actual building EUIs. In addition, since the EUI's for the CBECS buildings are computed from self-reported energy consumption numbers, it is not clear how much error may have been introduced in the energy consumption of individual buildings by inconsistent reporting standards and methods.



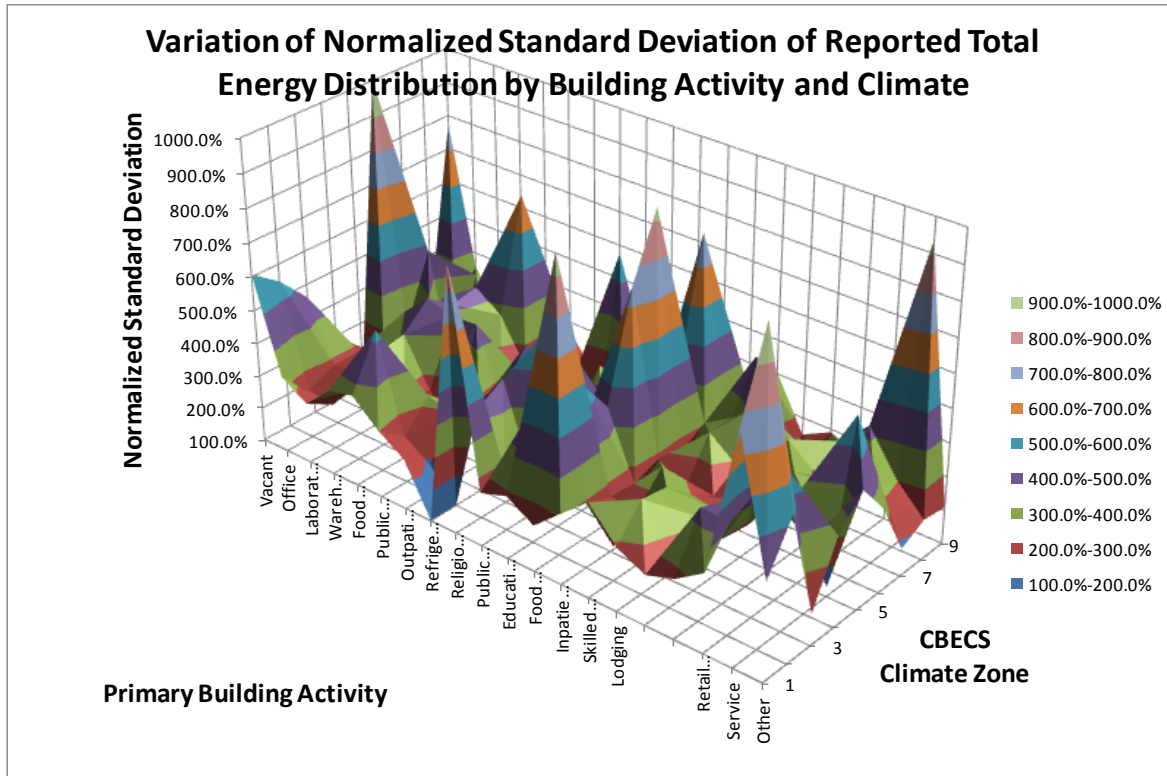


Figure A.9: Normalized standard deviation of CBECS reported total energy consumption values

In Figure A.10, the normalized error between the calculated and reported energy consumption for all CBECS buildings is shown. The peak of the distribution is offset by -15% from the expected value of 0% and 5.5% of the buildings fall in this error band. Because the distribution is skewed in the positive direction the mean error between the prediction and the reported energy use over all CBECS buildings is 16% and 68% of the buildings will fall in an error range of -46% to +80%. Therefore, on an aggregate basis, the stock tool calculated results can be said to represent the total energy use of the CBECS building stock quite well.

The comparison is even better for non-space heating/cooling electric energy, as shown in Figure A.11 and, in which, the mean error is 11% with  $\sigma = \pm 32\%$ . This close agreement was somewhat expected as the simulation is calibrated to the reported lighting and plug electric consumption.

Figures A.12 and A.13 show the EUI error distributions for cooling and heating energy consumptions respectively. In both cases, the peaks of the distributions are within  $\pm 20\%$  of the desired value of 0%, but the average errors and standard deviations are significantly larger than for total energy or electric due to the reasons previously outlined

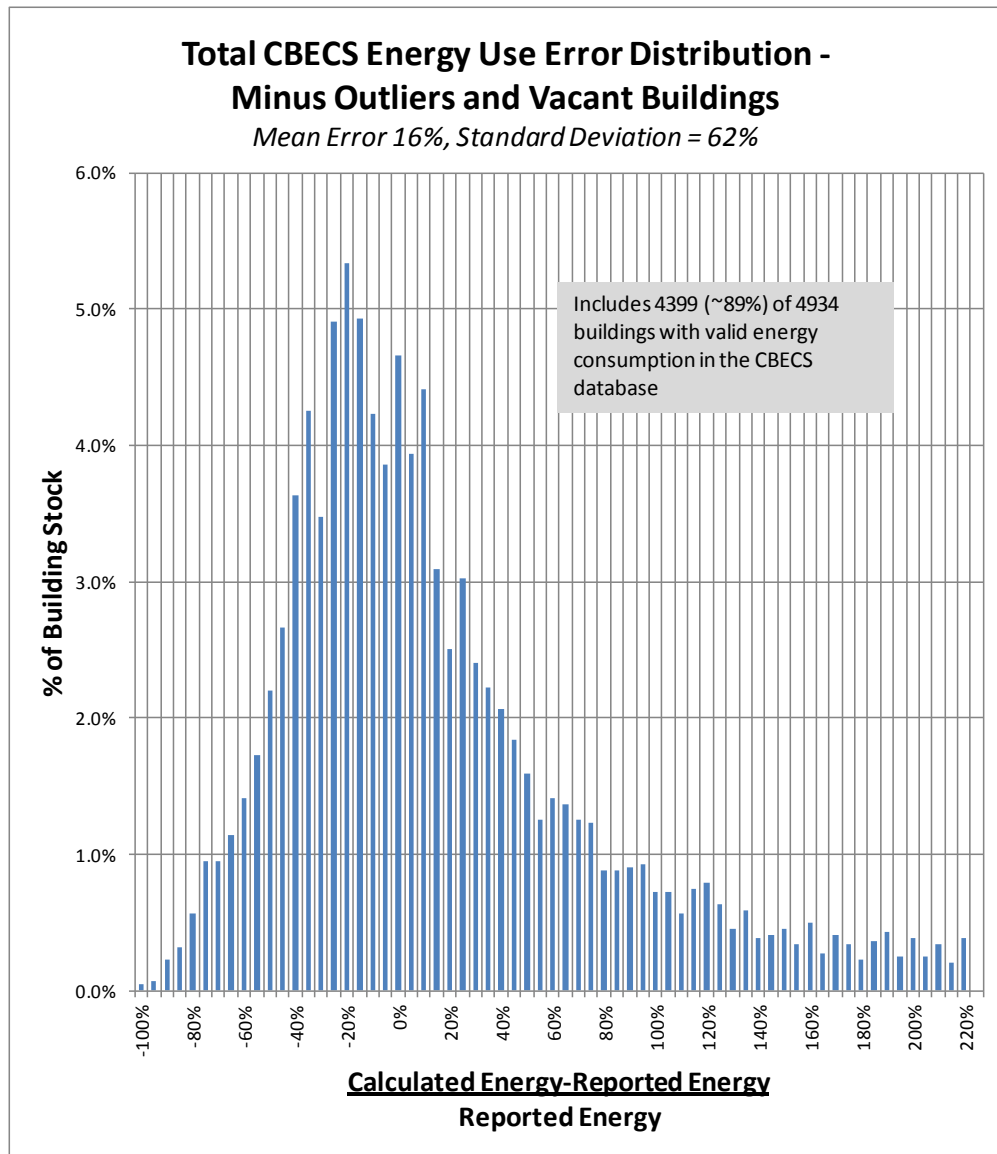


Figure A.10: Distribution of error in total energy consumption between reported and calculated values

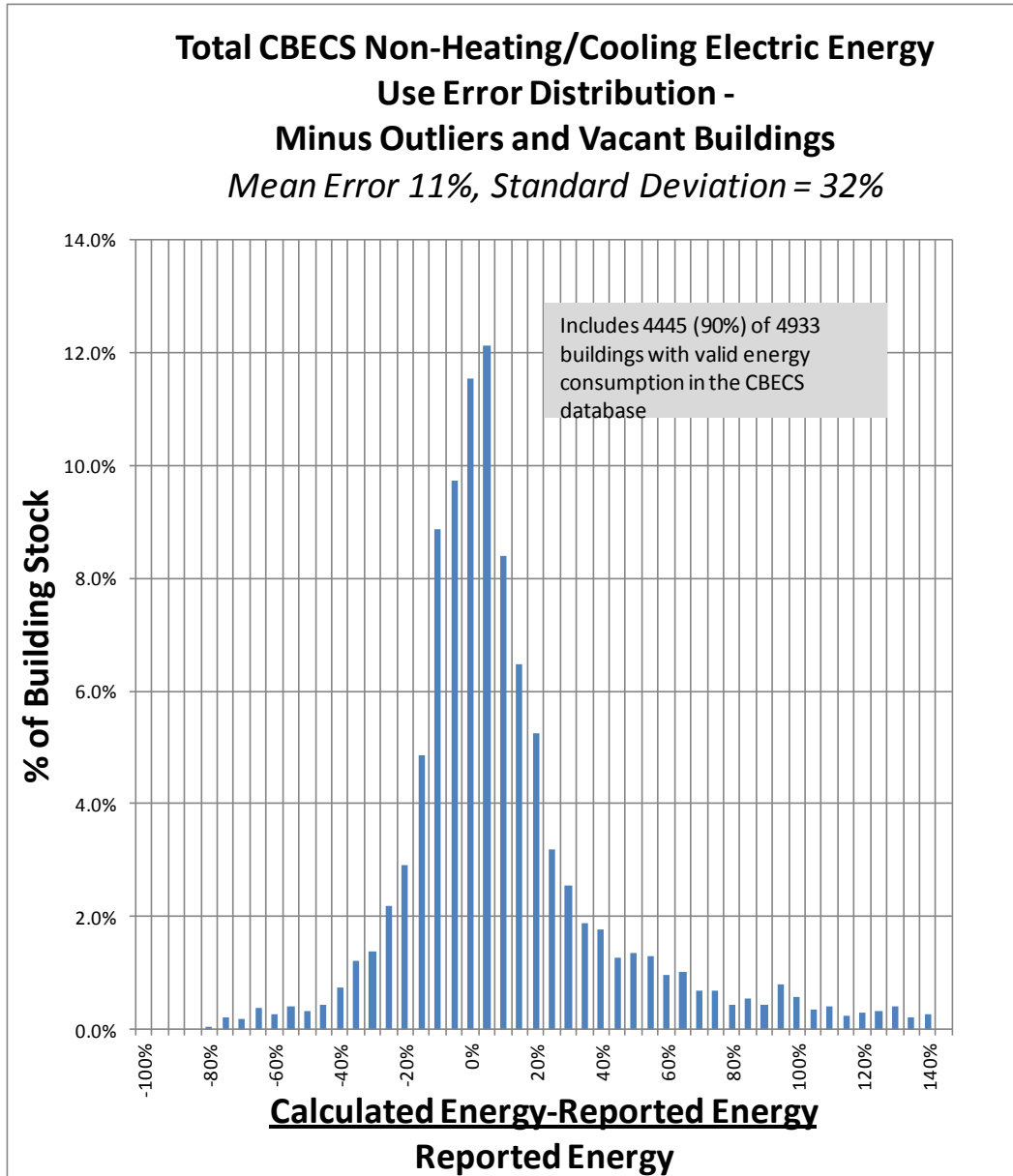


Figure A.11: Distribution of error in non-heating/cooling energy consumption between reported and calculated values

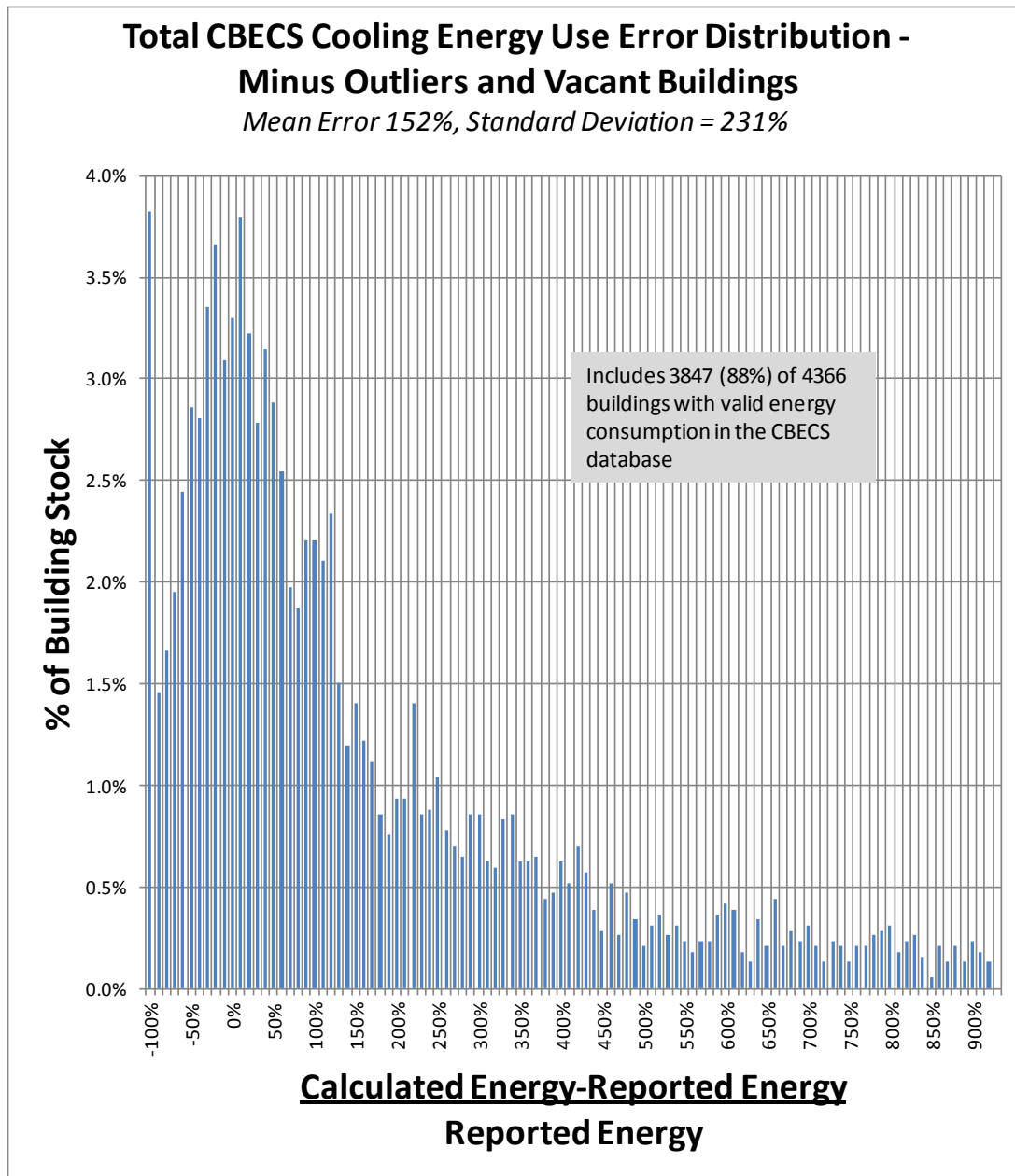


Figure A.12: Distribution of error in cooling energy consumption between reported and calculated values

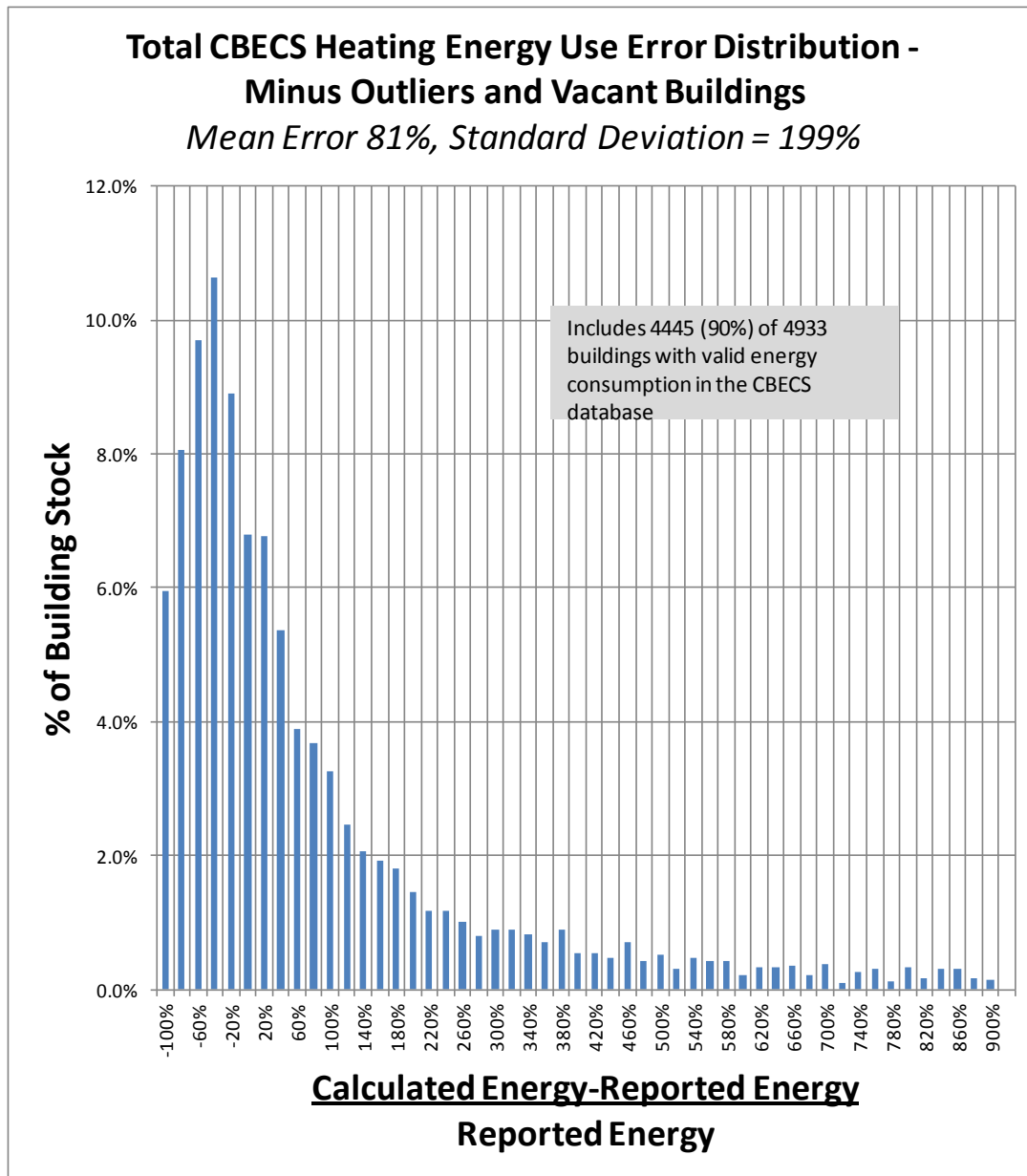


Figure A.13: Distribution of error in heating energy consumption between reported and calculated values

## APPENDIX B: Whole Building Energy Performance Simulations

### Whole Building Simulation Tool Selection

In the following, we provide criteria and guidelines for the assessment of simulation tools for low energy (high performance) building systems. The criteria are organized into three groups. The first group outlines physical concepts that the tool necessarily needs to capture. These concepts are specific to building systems models. The second group characterizes usage traits of the modeling tools. The third group discusses the ability to perform advanced analysis once a build-

ing is modeled within a specific framework. Our effort is to assess at least five different whole building system modeling packages (EnergyPlus, TRNSYS, Modelica , IDA, and ESpr). For each software package the following criteria will be considered.

**Available Low Energy Concepts:** This section describes the available component libraries of each tool. When a concept is not available as a prepackaged library, the ability to implement the concept should be discussed (how hard it is to add the concept to the tool). There are so many low energy concepts, and we are focusing the concepts in the scope of the ESCTP project. For example, power generation will not be a part of the assessment though power generation plays a very important role in the demand-supply equation in low energy buildings.

**Site:** Most simulation tools use a typical mean year weather data. This data includes solar and wind information. For low energy buildings, it is useful to know the variance in the weather data, so that the technologies incorporated allow for low energy building at all conditions. In addition, ground and water temperatures are necessary information because technologies like geothermal systems or thermal storage make use of earth/water as heat source/sink.

**Building Envelope:** The technologies considered under this category are those that are most commonly used for passive solar construction, those that allow for using the natural environment for conditioning the building to the extent possible, allow for shifting the energy load on a daily or a seasonal cycle, and depending on the climate, enhancing or reducing solar loads. Power generating technologies that interface with the envelope are also considered. Examples include: thermal mass, phase change materials, double façade ventilation, Trombe wall, underground thermal storage, sun room, green roof, radiant barrier, electrochromic windows, evaporative cooling with windows, operable windows.

**Lighting:** Most important lighting technology for low energy buildings is daylight and the related dimming controls. In addition, passive technologies like light shelves that allow for transferring light to the interiors are also considered. Examples of technologies employed include: light shelf, light well, daylight dimming (with lumens into consideration from lighting).

**Airflow:** Allowing for natural ventilation is one of the important ways to reduce the need for cooling. Technologies (systems and control strategies) allowing for natural ventilation in conjunction with HVAC systems will be considered. Examples include: natural ventilation and hybrid ventilation.

**HVAC:** HVAC systems are critical parts of low energy buildings. The most important aspect is the right-sizing of these systems and using them at the highest efficiency level as possible. Given that the HVAC systems available in the marketplace evolve continuously, it is very important to have a tool which has the flexibility to model different HVAC components and control strategies. Terminal unit types included are: underfloor air distribution (UFAD), displacement ventilation (DV), low temperature radiant heated floor, low temperature radiant hydronic system (cooled floor and walls), variable refrigerant flow (VRF), water-to-water heat pump, water-to-air heat pump, chilled beam/chilled ceiling, humidity control (liquid and solid dessicant), low-exergy cooling (solar absorption chiller, free cooling), ground heat exchanger HX (pond HX, ground surface HX, ground vertical borehole HX, standing column well HX), thermal storage (ice storage, stratified chilled water storage tank, stratified hot water storage tank), miscellaneous (ground source heat pump, heat recovery/Enthalpy wheel,

heat reclaim, nighttime fresh air purge cycle to reduce ventilation load at peak occupancy, pre-cooling to reduce peak demand on cooling plant, demand controlled ventilation)

**Controls:** We need to include supervisory control strategies that span single/multiple systems. The dynamics of how the control works (PID loops, the time for the fluid flow from system to room, leakage through closed dampers, etc.) will also be included in the assessment. Another aspect to consider would be the time step used for simulation. This will depend on the type of control strategy to be simulated.

**Domestic Water Heating:** Technologies that help in reduction of water usage and allow for using waste heat will be considered.

**Efficiency, Usability and Development Issues:** The following section addresses usage concerns including everything that is involved before the model is completed (developing the model, interaction with the software distributor, etc.) as well specifics about the general performance of the simulation tool. There will be an attempt to model a standard building using each of the tools and many of the criteria below will be evaluated during this process.

**Ease of Model Creation:** The time and manpower needed to generate a building will be a metric of the usefulness of the tool. The learning curve should be addressed for someone who is not familiar with the tool and this should be further characterized with the complexity of the building which is to be modeled. Creation of building geometry and building energy and control systems will be evaluated separately. With the introduction of BIM (building information modeling) concept, creation of building geometry model will become easier for new buildings. However, this is still a big issue for large amount of existing buildings.

**Flexibility of Model Enhancement and Extension:** When a concept is not available as a prepackaged library, the ability to implement the concept should be discussed (how hard it is to add the concept to the tool). Is the tool's structure flexible or modular for integration of new module?

**Simulation Turnaround Time:** A simple quantitative comparison regarding the amount of time for a standard simulation of one year/month of weather data. We also will assess the stability of solver. For example, numerically solving for initial conditions and time trajectories of building systems in Modelica can sometimes pose difficulties for solvers in Dymola.

**Prediction Accuracy:** We should assess the accuracy in some way. For example, is the tool complied with ASHRAE Standard 140-2007 (Standard Method of Test for the Evaluation of Building Energy Analysis Computer Programs)? What is the uncertainty of model? Is there any uncertainty study available?

**Calibration of Models:** Is there any calibration procedure available? Since different tool has different inputs and parameters and uses different methods to capture the physics, each tool probably will have some unique requirements for the calibration.

**User Support:** Where do we go for help, who helps us when we are stuck? Also, a qualitative understanding of how active the software tool is. Is it dying out or are there many people using it currently. How useful is the user manual? Is there any detailed guideline for the developer?

**Software Development:** Similar to the above topic but more focused on the company rather than the public. Is the company hiring or firing? Is it a dying tool? Are they tackling new challenges and updating the software to keep it current? Is it state of the art (with respect to building systems *and* with respect to dynamics / controls analysis)?



**Ability to Perform Advanced Analysis:** We intend to perform more than just the standard time-domain simulation using these tools. In this section we discuss the tools flexibility and ability to help with some of these advanced concepts.

**Time Scales Captured:** Some of the new concepts that we will investigate have time scales which may be different than what is typically analyzed in these tool packages. For instance there is a wide disparity between the relevant time scales of natural convection and thermal storage and the computational structure of the tool must be able to handle this.

**Accessibility of States:** Accessing state information is vital for advanced analysis including structural decomposition. Is the tool a black box?

**Linearization:** Linearized models of the dynamics will be needed for structural analysis as well as control design. Will the software provide these linear approximations and at different operating points?

**Steady State Calculation:** Can the software calculate steady-state operating points without exhaustive time simulation?

**Matlab/Simulink Interface:** Can / Has the software tool ever been interfaced to Matlab or Simulink? Has it been interfaced to any other tool for optimization or other purposes?

**Real Time Simulation:** Can the model be executed in real time or faster? Has the simulation tool ever been used in a Hardware in the Loop setting?

**Co-Simulation Capability:** Can this software easily be interfaced with other software? Can this software exchange data with other software? For example, there is a prototype to use E+ for geometry and TRNSYS for HVAC equipments.

## Whole Building Simulation Tool Assessment

The task focused on assessing the suitability of available energy simulation tools to the project. Selection criteria listed earlier are used to evaluate tools such as EnergyPlus, TRNSYS and Dymola/Modelica. A medium-sized office building from DOE benchmarks was modeled in EnergyPlus and TRNSYS. Low energy systems including radiant heating, ground source heat pump and chilled beams were modeled and analyzed. While the tools provide consistent energy performance predictions, TRNSYS enables the required flexible use of component models and controls.

### EnergyPlus Modeling

EnergyPlus is a whole-building simulation program developed by the U.S. Department of Energy (Crawley et al., 2000). It models heating, cooling, lighting, and ventilating processes, as well as water usage in buildings, and includes many innovative simulation capabilities such as time steps of less than one hour, modular systems, multizone airflow, thermal comfort, water use, and natural ventilation. An EnergyPlus model takes as input a description of the building (e.g., geometry, materials, roof type, window type, shading geometry, location, orientation), its usage and internal heat loads (as a scheduled function of time), and the HVAC equipment and system description (e.g., chiller performance, air and water loop specifications), and then computes the energy flows, zonal temperatures, airflows, and comfort levels on sub-hourly intervals for periods of days to years.

The two models that are used in this study originate from the United States Department of

Energy (DOE) EnergyPlus Benchmark Model Suite (Deru et al. 2009). The DOE benchmark model suite contains 15 models that represent the majority of commercial building stock in the United States (70% of the commercial building stock). The models are then organized so that each one of them can be simulated at one of 16 different locations in the US (using local typical meteorological year (TMY) weather data for each of these locations). Each model is also organized by construction type; new construction, existing construction - post 1980, and existing construction - pre 1980.

In this study, we chose a new construction medium office building located in Las Vegas, Nevada as baseline case because of the hot and dry summers and cool winters. This medium office building has three floors and approximately 5000 m<sup>2</sup> (50,000 ft<sup>2</sup>) of floor area. The entire building is conditioned and the total energy per total building area is about 425 [MJ/m<sup>2</sup>]. The building is a rectangular cube (aspect ratio 1.5), with 33% window to wall ratio, and is zoned with 5 zones per floor (one central zone and one zone for each perimeter side of the building). This baseline model can be downloaded directly from DOE website<sup>1</sup>. The rendered geometry generated by Sketchup is shown in the Figure B.1.

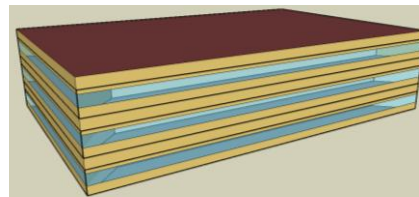


Figure B.1 Rendered Geometry for DOE Medium Office Building

This building has one boiler which serves three air handling units as well as VAV reheat coils for each of the 15 occupied zones. Cooling is supplied by three packaged air conditioning units, one for each floor. Load and usage schedules are based on ASHRAE guidelines (ASHRAE Standard 62.1-2004, 90.1-2004). Figures B.2 and B.3 shows schematic ductwork and controls for air and water loops for this building.

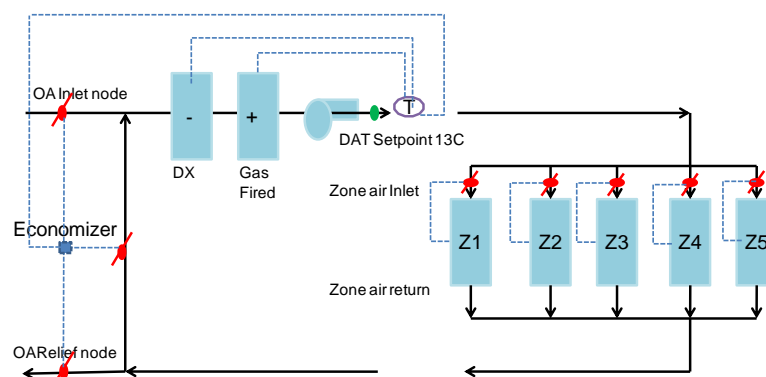


Figure B.2 Schematic Ductwork and Controls for Air Loop in DOE Medium Office Building

<sup>1</sup> [http://www1.eere.energy.gov/buildings/commercial\\_initiative/reference\\_buildings.html](http://www1.eere.energy.gov/buildings/commercial_initiative/reference_buildings.html)

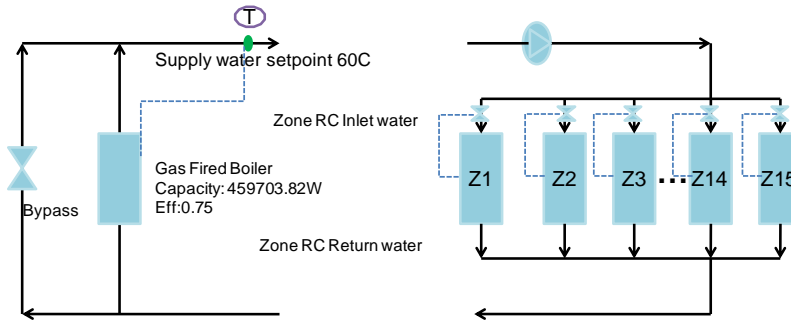


Figure B.3 Schematic Ductwork and Controls for Water Loop in DOE Medium Office Building

As a comparison, a high performance version of this building was also constructed in EnergyPlus. The specifics for this design were taken from a technical report from the Pacific Northwest National Lab (Thornton et al. 2009). Increased performance in this building was obtained by improvements in both the envelop as well as energy the equipment within the building (including scheduling). For the envelope, the insulation was enhanced in both the walls (R13 to R20.5) and in the roof (R15 to R25) without changing its thermal capacity. For additional heat rejection, the solar reflectance of the roof was increased from 0.23 to 0.69. Because the building was designed based on standards for Las Vegas, high efficiency windows were already specified in DOE benchmarking case, and there was no change between the baseline and high performance models. However, in the high performance model, overhang shading was added with a projection factor of 0.5. The electrical loads were also decreased in the high performance building. The interior lighting power density was decreased from  $10.8 \text{ W/m}^2$  to  $8.1 \text{ W/m}^2$  with occupancy sensor control. For the perimeter zones, lighting is dimmed down based on sensed natural daylight. Exterior lighting (building façade) power allowances was reduced by 37.5% and the exterior lights were turned off between 6am and 12pm. On top of the lighting changes, the plug load density was also decreased from  $8.07$  to  $5.92 \text{ W/m}^2$ .

To reduce the amount of energy consumed by the heating and cooling equipment, a ground source heat pump (GSHP) was incorporated into the design. This heat pump supplies hot water for radiant floor heating and cold water for active chilled beam cooling. In the high performance building, a dedicated outside air system for ventilation was also implemented. Figure B.4 shows the schematic diagram for the HVAC system used in the proposed high performance building. The schematic ductwork and controls for air loop is illustrated in Figure B.5.

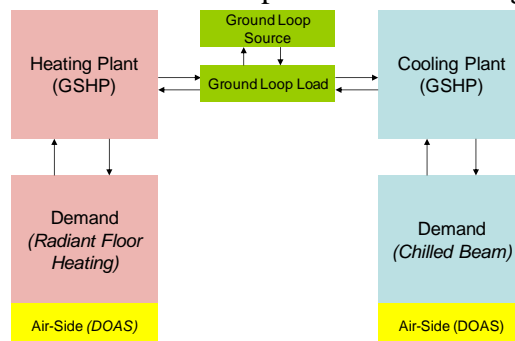


Figure B. 4 HVAC System Schematic Diagram for High Performance Building

With the performance enhancements to both the envelope and equipment, the energy usage index (EUI) shown in Figure B.6 was reduced by about 42.40% (from 40.75 to 23.75 [KBTU/sf/yr]). In addition to the reduction of energy, the building was more comfortable as modeled. Table B.1 and Figure B.7 show the electricity end use breakdown comparisons between two cases. The zone hours not comfortable in either winter or summer clothes as calculated by EnergyPlus was reduced by 73% in the high performance model.

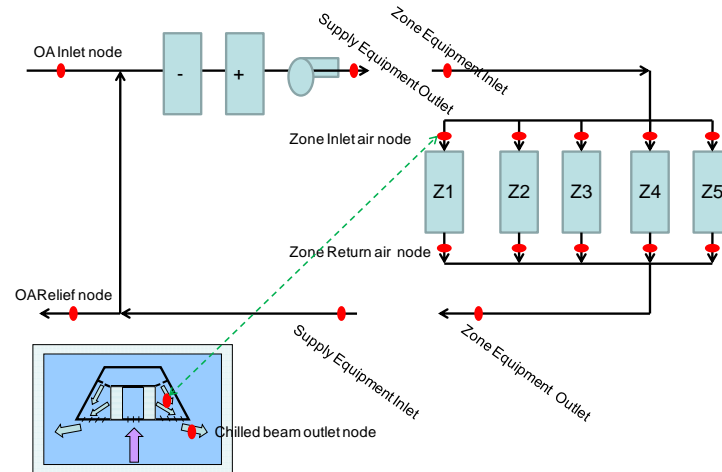


Figure B.5 Schematic Ductwork and Controls for Air Loop in High Performance Building

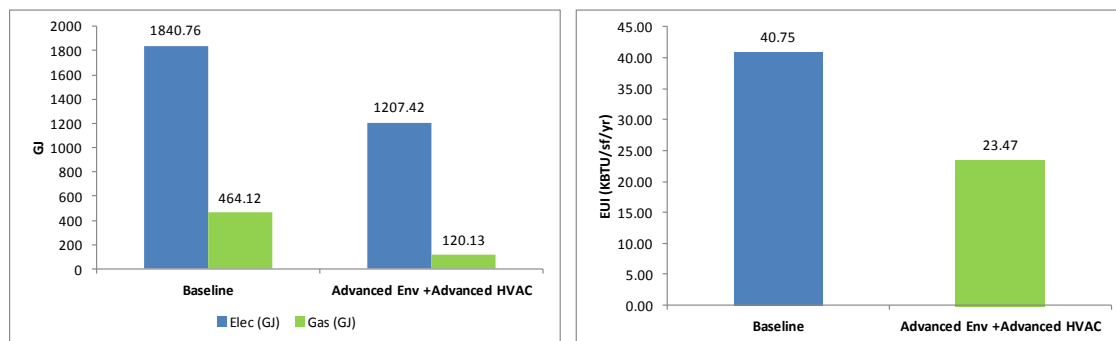


Figure B.6 Energy Consumption Comparisons between DOE Baseline Case and High Performance Case

Table B. 1 Electricity End Use Breakdown

Electricity (GJ)	Baseline	High Performance Case
Heating	0	32.69
Cooling	318.93	216.32
Interior Lighting	552.57	260.6
Exterior Lighting	42.89	9
Interior Equipment	806.04	554.47
Fans	119.51	56.61
Pumps	0.82	77.73
sum	1840.76	1207.42

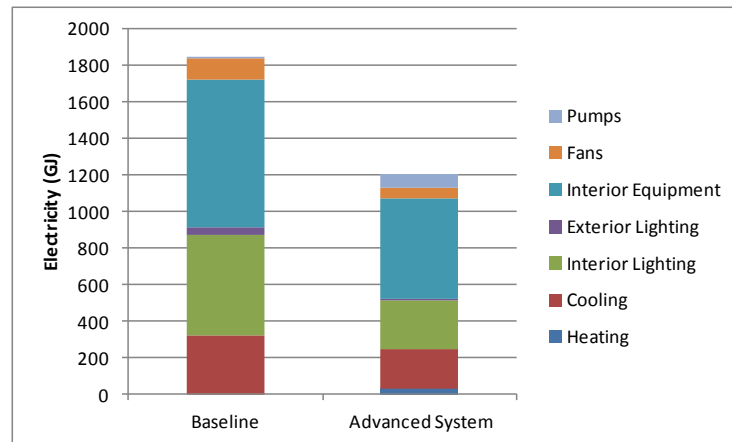


Figure B.7 Electricity End Use Breakdown Comparisons

## APPENDIX C: Uncertainty and Sensitivity Decomposition of Building Energy Models

### Problem formulation

#### *C.1 Uncertainty and Sensitivity Analysis*

Uncertainty analysis is used to quantify how uncertainties in parameters of a given building energy model influence the conclusions that are made and hence quantify confidence intervals of the output (Moon, 2005, and deWit and Augenbroe, 2002). Sensitivity analysis further investigates these uncertain intervals to determine which parameters are driving variation the most (Saltelli et al, 2000, Macdonald, 2002, Mara et al, 2008, and Struck et al 2009). In order to quantitatively capture these characteristics, a sampling within a given parameter range is typically performed and many simulations performed. From this data, statistical analysis is performed on the output to quantify information associated with output uncertainty. Algorithms are then executed to calculate sensitivity indices which rank-order parameters according to their criticality on variance of the output variables. In order to calculate the sensitivity indices, a meta-model (a model of the energy model) is derived. These methods are discussed briefly below and more detail in (Eisenhower et al., 2011a and Eisenhower et al., 2011c).

To characterize the model in an uncertain region around its nominal specification, a range is chosen and parameter samples are chosen within this range. The range that is chosen is on the order of 25% of the nominal value and the distribution type that has been chosen is uniform if the parameter is nonzero and exponential when the parameter value is zero. There does exist literature that describes accepted ranges for some parameters in a building. Since these studies are fragmented, and because we are varying thousands of parameters, we have not utilized this information. The strategy is to use generic input distributions to identify which parameters are critical and then use specific distributions from literature to study this smaller subset in more detail. Historically, a Monte Carlo-based method is used to generate the samples (Macdonald, 2009). To obtain faster convergence we utilize a deterministic sampling procedure that has convergence bounds that are faster than Monte Carlo methods (Burhenne et al., 2011). For a model with 1000-2000 parameters, we are able to get sufficient convergence from about 5000-6500 model samples (all parameters are varied concurrently for this approach).

Immediately after the data is generated from the sampling procedure, statistical analysis is performed on the output. Typical outputs that are chosen are annual or peak energy consumption (at the facility level and at sub-meters) or averaged thermal comfort in occupied zones. Average values or standard deviations are considered as well as the coefficient of variation (COV) which is the standard deviation divided by the mean. This quantity is often studied when variables that have significantly different means are investigated. All of these statistical quantities quantify expected performance bounds of the building when aspects of its design, construction, or operation are uncertain.

To further the analysis, a meta-model is generated from the data generated during the sampling procedure. To do this, a machine learning technique (support vector regression with Gaussian kernels (Scholkopf and Smola, 2002, Smola and Scholkopf 2009)) is used to fit an analytic model to the data. This is needed because the building energy models (in their current state) act as black boxes and access to the equations is limited. An analytic version of this model, which is accurate for the range of expected uncertainty in the parameters, offers much more freedom in analysis (e.g. for calculating sensitivity indices, model reduction, or for optimization).

Once a meta-model is calculated from the original model, sensitivity analysis is performed. Historically, analysis of variance (ANOVA) based methods are used to calculate dominant influences on variance in output data (Mara and Tarantola, 2008, Brohus et al., 2009a, Capozzoli et al., 2009). These methods calculate first order influences (one parameter only) as well as combinatorial influences from multiple parameters on the output variance. Unfortunately, most of the available codes are not numerically efficient enough to handle thousands of parameters that we seek to investigate in this study. To overcome this, we generated numerically efficient techniques to perform these calculations. In addition to this, the ANOVA methods analyze the variance within the data, which does not always contain all of the pertinent information (sometimes important behavior of the model is not captured only by the variance). Due to this, methods have also been derived to calculate sensitivity indices based on derivative estimates of the output data (Sobol and Kucherenko, 2009).

The meta-model that is generated has the same dimension as the full energy model (e.g. EnergyPlus or TRNSYS) and therefore model reduction is often desired for more manageable analysis. That is, if the full energy model has 2050 uncertain parameters and 8 informative outputs, the meta-model will have the same input-output dimensions. Model reduction can be performed by omitting some of the input data and asking the regression algorithm to find the best fit using only key input parameters. These key input parameters can be chosen based on some intuition (e.g. by choosing all envelope, or all scheduling parameters), but this often results in a meta-model that is not fit very well. It is more useful to select the most influential parameters (say top 1-10%) to use for the model fit. This is easily performed once the sensitivity indices are calculated and rank-ordered. This model reduction technique is particularly useful when performing optimization as it is not often that a building designer or manager has the ability to alter all parameters of the building to obtain an optimal design and operation approach.

### ***C2 Sensitivity Decomposition***

Sensitivity analysis typically investigates input-output relations between uncertain parameters and outputs of a model (e.g. a full building energy model) and the decomposition method we developed seeks to better understand what happens in between. For example, envelope parameters of a building may be varied to investigate how they influence the total energy used in a building. Studying the input-output behavior of building system models is insightful, but more information can be gained by decomposing the path in which uncertainty passes through the dynamics of the model. For example, the energy consumed by a building may be derived from a combination of many different HVAC subsystems. It is insightful to identify which of these subsystems contribute most to the uncertainty at the building level. In particular, it is useful to have this type of information when trying to calibrate the model to better fit data, or to design optimizing controllers, or to identify design approaches that increase the robustness of the building. We are unaware of any previous attempts to perform this type of analysis on a building energy model.

### ***C3 Meta-model based optimization***

Building systems have competitive design and operation objectives, on the one hand, it is essential to minimize design, construction, and operation costs, while on the other hand comfort and productivity of the occupants is an essential constraint of the building in design or operation. Optimal thermal comfort may be achieved by advanced designs that carefully consider the environment in which a building is exposed to (weather, people, etc.), or by conditioning occupied areas of the building with mechanical equipment. Both of these approaches incur costs on the building owner or tenant and need to be implemented carefully to minimize costs.

Multi-objective optimization is a design approach that considers multiple criteria like those in which buildings are exposed to, and seeks optimal design and operation scenarios that balance these concerns (Ellis et al., 2006, Wetter, 2001). Numerical optimization has been performed on building energy models in the past to some extent, while these studies typically investigate only tens of optimization parameters (out of typically 1000's present in an energy model) (Djuric, et al, 2007, Kampf et al, 2010, and Diakaki et al, 2008). One of the reasons that past efforts only study a limited set of parameters is due to the mathematical properties of typical energy models and the simulation time required to evaluate proposed optimal designs.

The mathematical properties of building energy models are typically hidden in thousands of lines of commercial source code and therefore no analytic representation of the function (or its derivatives) is available. In addition to this, the cost function surface of these models is often discontinuous when varying the optimization parameters (Wetter, 2003b). Because of this, derivative-free optimization methods are typically used – which are not very efficient when large numbers of optimization parameters are studied (Conn et al., 2009).

In this work, we use uncertainty and sensitivity analysis and meta-modeling to alleviate some of these concerns. In creating the meta-model, we have an analytic representation of the building energy model that is accurate in an acceptable range of parameter variation. Because of this, optimization algorithms that leverage local derivatives can be used which accelerates the process and provides a means to study much larger numbers of parameters (1000's). The uncertainty and sensitivity analysis is used to select the best suited parameters to use for the optimization process. Details of this procedure are available in (Eisenhower, 2011b).



#### ***C4 Energy model calibration***

Building energy models have been thoroughly refined over the years and the equations within them accurately capture reality when the model is constructed appropriately. Unfortunately, when an energy model is initially created, its prediction capabilities are not very accurate. To increase the accuracy of the model, it may be calibrated using sensor data from the actual building if it has been built by modifying parameters of the building energy model to drive the prediction of the model closer to reality.

In this part of the work, we use the uncertainty and sensitivity analysis, in conjunction with the meta-model based optimization to provide a means for automatic calibration of a baseline energy model of a building. The uncertainty and sensitivity analysis is used to identify which are the most influential parameters in the building energy model to use for the calibration procedure. Once this has been performed, a cost function that considers the difference between sensor values and model prediction is developed and meta-model based optimization is performed to adjust a subset of the parameters (e.g. 20 of the total 2000) to drive this difference to zero. This project was in conjunction with the ESTCP project SI-0929 Automated Continuous Commissioning of Commercial Buildings and therefore the presentation here is brief.

#### ***C5 Case Study 1 – DOE Benchmark Building Models***

The objective of this study was to quantify and compare the influence of uncertainty on two different building designs; a standard code compliant building, and the same building redesigned with high performance design elements (efficient envelope and less energy intensive sub-system equipment). We present input-output sensitivity analysis which illustrates which parameter type influences the uncertainty in the consumption of energy in the building model the most. Past efforts to perform sensitivity and uncertainty analysis have focused on tens of parameters at a time. In this study, we increase the size of analysis by two orders of magnitude (by studying the influence of about 900 parameters), which is much more comprehensive than previous studies of similar models. Key conclusions are that the most sensitive parameters of the model are for building operation (i.e. scheduling), and a low energy building design with well integrated envelope and equipment systems is more robust to parameter variations than a conventional design that does not explicitly address sub-system interactions. The analysis is performed on two different EnergyPlus models but the technique can be performed using almost any building simulation tool.

**Models:** The two models that are compared in this study originate from the United States Department of Energy (DOE) EnergyPlus Benchmark Model Suite (Deru et al., 2009). The DOE benchmark model suite contains 15 models that represent the majority of commercial building stock in the United States (70% of the commercial building stock). The models are then organized so that each one of them can be simulated at one of 16 different locations in the US (using local typical meteorological year (TMY) weather data for each of these locations). Each model is also organized by construction type; new construction, existing construction -post 1980, and existing construction -pre 1980. Previous work has been performed using these models including (Fumo et al., 2010) where reduced models were generated from this benchmark suite for prediction purposes.

The model studied in this paper is a new construction medium office building located in Las Vegas, Nevada. We chose this location because of the hot and dry summers and cool winters (relatively extreme in both the summer and winter). This medium office building has three floors and

approximately 5000 m<sup>2</sup> (54k ft<sup>2</sup>) of floor area. The entire building is conditioned and the total energy per total building area is about 425 [MJ/m<sup>2</sup>]. The building is a rectangular cube (aspect ratio 1.5), with 33% window to wall ratio, and is zoned with 5 zones per floor (one central zone and one zone for each perimeter side of the building). Throughout this paper we will call the model of this building the nominal model.

The building has one boiler which serves variable air volume (VAV) reheat coils for each of the 15 occupied zones, and heating in the air handling units (AHUs) is provided by a gas furnace. Cooling is supplied by three packaged air conditioning units, one for each floor. Load and usage schedules are based on ASHRAE guidelines (e.g., ASHRAE Standard 62.1-2004, 90.1-2004) and other literature from national labs.

As a comparison, a high performance version of this building was constructed in Energy-Plus. The specifics for this design were taken from a technical report from the Pacific Northwest National Lab (Thornton et al., 2009). Increased performance was obtained by improvements in both the envelope as well as equipment within the building (including scheduling).

For the envelope, the insulation was enhanced in both the walls (R13 to R20.5) and in the roof (R15 to R25) without changing its thermal capacity. To reduce the impact of solar radiation, the solar reflectance of the roof was increased from 0.23 to 0.69. Since the nominal building was designed based on standards for Las Vegas, high efficiency windows were already specified, and there was no change between the nominal and high performance models. However, in the high performance model, overhang shading was added with a projection factor of 0.5.

To reduce the amount of energy consumed by the heating and cooling equipment, a ground source heat pump (GSHP) was incorporated into the design. This GSHP supplies hot water for radiant floor heating and cold water for active chilled beam cooling. In the high performance building, a dedicated outside air system for ventilation was also implemented.

The electrical loads were also decreased in the high performance building. The interior lighting power density was reduced from 10.8 W/m<sup>2</sup> to 8.1 W/m<sup>2</sup>. Interior lighting schedules (usage fraction) were changed to consider occupancy-based sensor control. For the perimeter zones, lighting is dimmed based on sensed natural daylight. Exterior lighting power allowances were reduced by 37.5%, and the exterior lights were turned off between 12am and 12pm. In addition to the lighting changes, the plug load density was also decreased from 8.07 to 5.92 W/m<sup>2</sup>.

With the performance enhancements to both the envelope and equipment, the energy intensity of the building was reduced by about 41% (from 463 to 273 [MJ/m<sup>2</sup>]). In addition to the reduction of energy, the building was more comfortable as modeled. The zone hours not comfortable in either winter or summer clothes as calculated by EnergyPlus was reduced by 73% in the high performance model. Table C.1 presents a usage comparison for subsystems in the nominal and high performance models.

Table C. 1. Electricity usage comparison, nominal versus high performance model.

Electricity (GJ)	Nominal	High Performance Case
Heating	0	32.69
Cooling	318.93	216.32
Interior Lighting	552.57	260.6
Exterior Lighting	42.89	9.00
Interior Equipment	806.04	554.47
Fans	119.51	56.61
Pumps	0.82	77.73
Sum	1840.76	1207.42

**Parameter Variation and Simulation:** In each model, almost every numeric parameter was varied to capture the quantitative influence of its variation on energy use in the building. The exceptions were in the parameters related to equipment performance curve coefficients, and parameters that describe solution methods (e.g. auto-sizing, or method of calculating infiltration). Because of the different building designs, the models had a different number of parameters (746 for the nominal model, while the high performance building had 947). To present the results, we have selected 10 different groups as shown in Table C. 2 to characterize these parameters. All of these parameters were varied by  $\pm 25\%$  of their nominal value. Many of the parameters were constrained; for instance, fractional parameters with a nominal of 0.9 would be varied between 0.72 and 1.0. The heating and cooling setpoints had to be limited to 6.5% variation because otherwise they would overlap, which created conflict in the dual-setpoint management. All parameters were varied concurrently using a quasi-random approach. In this way, 5000 model realizations were created which were ultimately parallelized and simulated on a 184-CPU Linux cluster using EnergyPlus build 3.1.0.027. It was found that 5000 realizations (EnergyPlus models with different input files) were more than enough to gain good convergence results on the statistics of the output variables. EnergyPlus has the ability to output many different metered variables from the energy simulation. From the outputs that are available, 7 different outputs were chosen for analysis as shown in Table C. 3. These outputs are related to building energy consumption, including electricity and gas from the facility level, to subsystems such as pumps, equipment, and lights. Annual total energy consumption and peak demand (hourly peak in one year) were two metrics used in this study. We chose these outputs because the profiles of these outputs clearly reflect the building performance and energy end-use pattern. Outputs 1 and 2 are facility-wide consumption variables, and because of this, more attention will be paid to these two quantities in this section.

**Uncertainty Analysis:** The simulations were performed on the realizations of both models and the statistics of the outputs were calculated. In Figure C.1, standard deviation for each output in Table C.3 is presented for both the nominal model and the high performance model. From observing the standard deviations, we find that in general, with the modification of the envelope, equipment, and schedules in the high performance building, less uncertainty passes through the model from the input parameters to the consumption outputs (when compared to the nominal design). We also find that the uncertainty in peak usage (the simulated hour with highest magnitude consumption) is much less than in the annual consumption. This can be explained by the idealized control systems within the model, which attempt to keep process variables within a certain controlled range. It should be noted that the total consumption of the high performance building is less than the nominal building, and this should be accounted for when considering the uncertainty. To accommodate for this difference, the coefficient of variation (CV) for each of the outputs of both models is presented. The CV is just the standard deviation divided by the mean,

which allows a comparison of distributions from dissimilar sources (which consume drastically different amounts of energy). The plot of the CV for each of the outputs of both models is presented in Figure C.2. For brevity, the entire distributions for only two of the outputs are illustrated in Figure C.3. The distributions for all of the other outputs look fairly similar to these two example plots. Figure C.3 shows that a low energy building design with well integrated envelope and equipment is more robust to parameter variations than a conventional design that does not explicitly address sub-system interactions.

Table C.2 Parameter group types.

Number	Type	Examples
1	Heating source	Gas-fired furnace (efficiency), boiler (capacity, efficiency), ground source heat pump (rated heating capacity, rated heating power consumption, rated load/source side flow rate), ground heat exchanger (depth, number of boreholes etc.)
2	Cooling source	DX coil (COP, sensible heat ratio) , ground source heat pump (rated cooling capacity, rated cooling power consumption, rated load/source side flow rate etc)
3	AHU	(AHU SAT setpoint, outside air fraction schedule, etc.)
4	Primary Mover: Air loop	fans (efficiency, pressure rise, etc.)
5	Primary Mover: Water loop	pumps (rated flow rate, rated head, rated power consumption, etc.)
6	Terminal unit	VAV boxes (maximum air flow rate, minimum air flow fraction, etc.), radiant heating floor (hydronic tube inside diameter, heating control throttle range etc.), chilled beam (supply air flow rate, maximum total chilled water flow rate, beam length, number of beam etc.)
7	Zone external	Building envelope (material thermal properties such as conductivity, density, and specific heat, window thermal and optic properties, etc.), outdoor conditions (ground temperature, ground reflectance, etc.)
8	Zone internal	Internal heat gains design level (lighting load, number of people, people activity level, etc.), schedules
9	Zone setpoint	Zone temperature setpoint (space cooling and heating setpoints)
10	Sizing parameter	Size factor, design parameters for zones, system and plant (zone cooling design supply air temperature, loop design temperature difference etc.)

Table C.3 Consumption outputs chosen for the analysis.

Number	Name
1*	Facility Gas [J]
2*	Facility Electricity [J]
3	Heating [J]
4	Cooling [J]
5	Pump Electricity [J]
6	Interior Lights [J]
7	Interior Equipment [J]

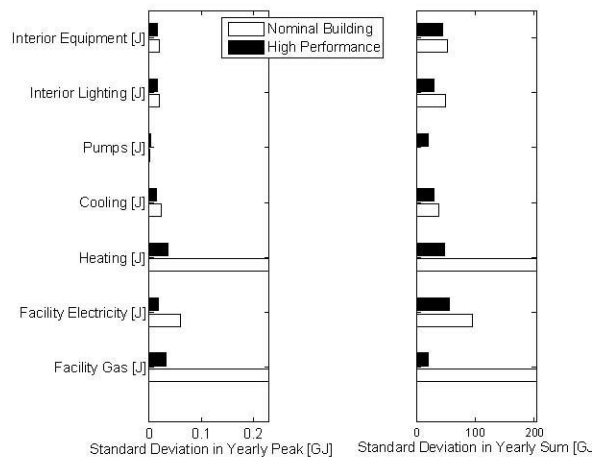


Figure C.1 Standard deviation for the seven outputs of the two models (nominal model and high performance design).

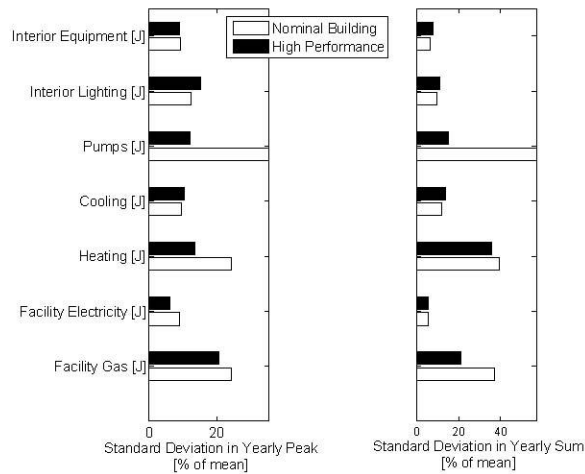


Figure C.2 Coefficient of variation for the seven outputs of the two models (nominal model and high performance design).

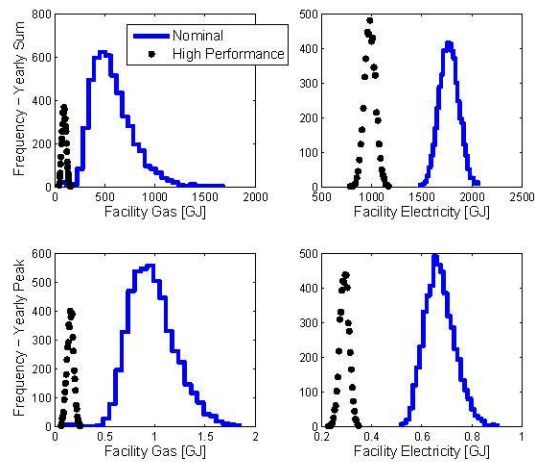


Figure C.3 Example histograms of the two main facility wide outputs.

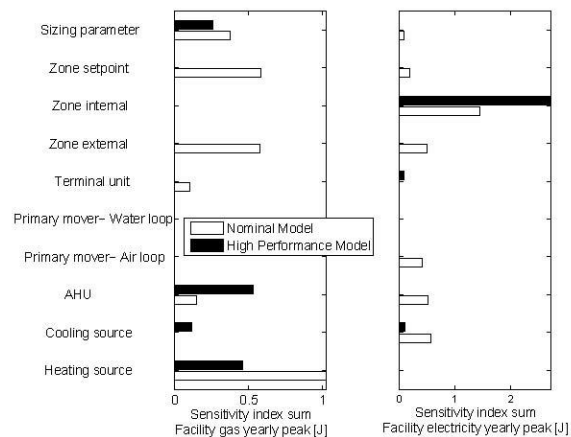


Figure C.4 Aggregated influence coefficients for yearly peak energy consumption (nominal and high performance models)

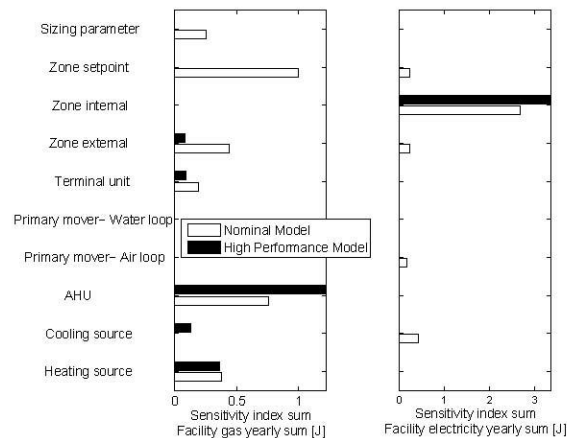


Figure C.5 Aggregated influence coefficients for yearly sum energy consumption (nominal and high performance models)

**Parameter Sensitivity:** After gaining insight into how uncertainty in parameter inputs influences the uncertainty in the outputs, we now proceed to calculate the sensitivity indices which identify which parameters influence the variance of the output the most. Figures C.4 and C.5 illustrate the aggregated total sensitivity coefficients for the 10 parameter groups described in Table C.2. To generate these numbers, the total sensitivity for each of the parameters was calculated. If the influence coefficient was less than 0.08, it was considered negligible and ignored. We came up with this number by observing a cutoff in the number of influential parameters vs. the influence coefficient amplitude. All parameters with an influence coefficient greater than this were then collected into their respective parameter type (as in Table C.2). For the nominal model, 55 of 746 (7.4%) were found to be important, while 63 of the 947 (6.7%) were found to be important for the high performance model. Once collected, the total sensitivities for each parameter type were then added to generate a single number for the aggregated total sensitivity between a parameter group type and an output type. It should be noted that since we are using derivative based sensitivities (Equation 1), the summation may be larger than 1.0. It is clear from Figures C.4 and C.5 that the model of the high performance has different parameter sensitivities compared to the no-

minimal design. Below we go through each parameter type and describe which specific parameters are most influential.

**TRNSYS Analysis:** Similar analysis was performed using a second modeling tool to better understand how uncertainty and sensitivity analysis can be performed using TRNSYS. In order to do this, the nominal model (which was downloaded from the DOE website in EnergyPlus format) was re-created in the TRNSYS modeling language. Again, all of the parameters were selected as uncertain and 5000 simulations were performed. Below in Figure C.6 and C.7 the sum of the influence coefficients is presented from the various outputs of the model.

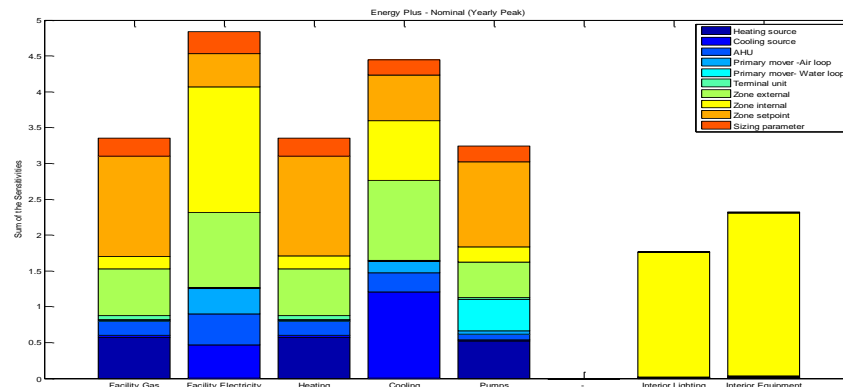


Figure C.6 Sum of the total influence coefficients for peak consumption in the TRNSYS model

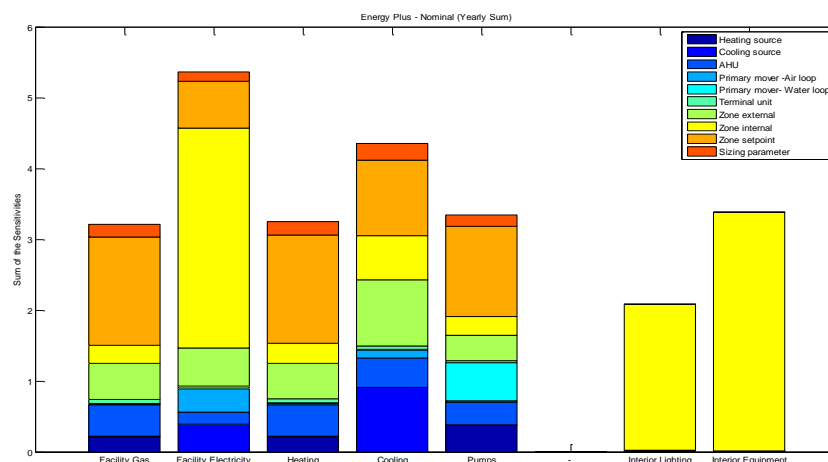


Figure C.7 Sum of the influence coefficients for annual consumption in the TRNSYS model.

When performing the uncertainty and sensitivity analysis, there was not a direct quantitative comparison made because some components of the DOE benchmark model were not directly available in the TRNSYS libraries. However, the behavior of the two models was qualitatively similar. Future efforts on this project will include more usage of the TRNSYS modeling tool.

**Summary:** In this part of the project, we performed uncertainty and sensitivity analysis on two similar building designs. The first design was a standard medium sized office building, while the second design is the same building with high performance features added (better envelope and



more efficient equipment). In both models, almost all parameters were considered uncertain (700-900), and thousands of simulations were performed to quantify how this uncertainty influences the predicted energy consumption. It was found that the high performance building is more robust to parameter uncertainty due to better specification of the envelope and the equipment, while considering their interactions carefully during design. It was also found that zone loads (lighting, plug loads, etc.) are dominant parameters for propagating uncertainty to the output. This is more noticeable in the high performance model due to the energy efficient envelope that manages external loads very well and leaves the system more sensitive to internal loads.

## APPENDIX D: Reduced-Order Modeling and Control Design for Low Energy Building Systems

### D.1 Model Reduction Techniques

In this appendix, we briefly describe the model reduction techniques used in this project, namely the eigensystem realization algorithm (ERA) and the proper orthogonal decomposition (POD).

#### D.1.1 Eigensystem Realization Algorithm (ERA)

Eigensystem realization algorithm (ERA) is a method for model reduction of discrete-time, stable, linear time-invariant systems of the form

$$x_{k+1} = Ax_k + Bu_k \quad (8)$$

$$y_k = Cx_k, \quad (9)$$

where, in the context of the paper one can think of (8, 9) as being obtained from a spatio-temporal discretization of the linearized Boussinesq equations, with an explicit control term (such as a localized body force). The discretization timestep  $dt$  is assumed to be a constant, and the index  $k$  is used to represent time  $t = k dt$ . ERA begins by computing the impulse response of (8, 9), and the resulting outputs  $y_k$  can be compactly described by the Markov parameters as  $y_k = CA^k B$ , where  $y_k$  is a matrix with elements  $y_{ij}$  which represent the  $i^{th}$  output from an impulse on the  $j^{th}$  input. The Markov parameters are sampled every timestep:

$$(y_0 \ y_1 \ y_2 \ \dots \ y_{m_c+m_o}) = (CB \ CAB \ CA^2B \ \dots \ CA^{m_c+m_o}B), \quad (10)$$

and these outputs are used to assemble the Hankel matrix  $H$  as follows:

$$H = \begin{pmatrix} y_0 & y_1 & \dots & y_{m_c} \\ y_1 & y_2 & \dots & y_{m_c+1} \\ \vdots & \vdots & \ddots & \vdots \\ y_{m_o} & y_{m_o+1} & \dots & y_{m_c+m_o} \end{pmatrix} \quad (11)$$

The reduced-order model is obtained by computing the SVD of  $H = U\Sigma V^*$ . Let  $U_r$  and  $V_r$  be the leading columns of  $U$  and  $V$ , and  $\Sigma_r$  contain the leading  $r$  rows and columns of  $\Sigma$ , then the reduced model of (8, 9) is given by

$$a_{k+1} = A_r a_k + B_r u_k, \quad (12)$$

$$y_k = C_r a_k \quad \text{where,} \quad (13)$$

$$A_r = (\Sigma_r^{-\frac{1}{2}} U_r^*) H_1 (V_r \Sigma_r^{-\frac{1}{2}}), \quad B_r = (\Sigma_r^{-\frac{1}{2}} U_r^*) \text{Col}_{\text{first}}(H), \quad C_r = \text{Row}_{\text{first}}(H) (V_r \Sigma_r^{-\frac{1}{2}}). \quad (14)$$

In the above expressions,  $\text{Col}_{\text{first}}(H)$  and  $\text{Row}_{\text{first}}(H)$  represent the first block column and row of  $H$  (11) respectively and  $H_I$  is obtained by deleting the first block column of  $H$  and appending a block column at the end.

### D.1.2 Proper Orthogonal Decomposition (POD)

Proper orthogonal decomposition (POD) is a method for obtaining an energetically optimal basis for a given dataset. In our setting we have spatially varying fields (e.g.,  $T(\mathbf{Z})$ ;  $\mathbf{v}(\mathbf{Z})$ ) representing spatially distributed properties of interest (e.g. temperature, velocity). Based on experiments (numerical in our case) we have a finite collection of such field data. For example,  $T^i(\mathbf{Z}) = T(t_i; \mathbf{Z})$  arising from the numerical solution of a boundary-value problem at times  $t_i$ ;  $i = 1, 2, \dots, N$ . The goal of the POD process is to produce a linearly independent set of basis functions that efficiently represent the collection  $\{T^i(\mathbf{Z}), i = 1, 2, \dots, N\}$ .

The POD process is naturally set in a Hilbert space ( $H$ ) with inner-product  $\langle \cdot, \cdot \rangle_H$  and norm  $\|u\|^2 = \langle u, u \rangle_H$ . We suppose we have a collection of data functions  $U = \{u_1, u_2, \dots, u_N\}$ . For the 1<sup>st</sup> POD vector we seek a unit vector  $\phi^1$  to maximize

$$\sum_i \langle u_i, \phi^1 \rangle^2. \quad (25)$$

To motivate this problem, note that the error in approximating the element  $u_i$  in our data collection by the vector  $\phi^1$  is given by

$$e^i \triangleq u_i - \langle u_i, \phi^1 \rangle \phi^1, \text{ and that } \|e^i\|^2 = \|u_i\|^2 - \langle u_i, \phi^1 \rangle^2.$$

Thus, a solution of (25) minimizes the sum of the (squared) error norms.

It is possible to continue in this way to compute additional POD vectors (e.g.,  $\phi^2$ , etc). In practice, one computes coefficient vectors  $\beta$  as eigenvectors  $R\beta = \beta\Lambda$ , where  $R$  is the correlation matrix

–  $R_{ij} = \langle u_i, u_j \rangle$ . The POD vectors are assembled as  $\Phi = [\phi^1, \phi^2, \dots, \phi^N]$ . The eigenvalues in the diagonal array  $\Lambda$  are ordered with  $\lambda_1 \geq \lambda_2 \geq \dots \geq \lambda_N \geq 0$ . Thus, the eigenvector associated with  $\lambda_1$  represents the most energetic POD basis vector, followed by  $\lambda_2$ , and so on. A reduced-order model is then obtained by Galerkin projection, that is, by projecting the dynamics onto the (low-dimensional) subspace spanned by the POD vectors.

**Temperature Evolution POD Model:** In this work, we assume that the velocity field remains frozen, while the variation of temperature field is governed by an advective-diffusive equation. That is, we freeze the velocity field at the ‘steady’ value from an initial transient run, and assume the following PDE model:

$$\frac{\partial T(t, \vec{x})}{\partial t} + \vec{v}(\vec{x}) \cdot \nabla T(t, \vec{x}) = \frac{1}{\rho C_p} \nabla \cdot (k \nabla T(t, \vec{x})) \quad (40)$$

where  $\mathbf{v}(\mathbf{x})$  is the frozen velocity field as noted above. We admit three potential inputs on the actively heated/cooled surfaces, with the boundary conditions of the form

A proposed form for a reduced model is

$$T(t, \vec{x}) = T^{\text{ss}}(\vec{x}) + \sum_j z_j(t) \Phi^j(\vec{x}) \triangleq T^{\text{ss}}(\vec{x}) + \tilde{T}(t, \vec{x}). \quad (41)$$

Here,  $T_{ss}(x)$  is the steady solution as noted above, and the  $\Phi^j(x)$  are (real-valued) POD functions described earlier. The perturbation term is also a solution of the equation of the form (40), with  $T$  replaced by  $T_{ss}$ , with boundary conditions at the heated/cooled surfaces given by  $q = u_\ell(t)$ . From the weak form of (40), the reduced-order model is:

$$M \dot{z}(t) + D z(t) = K z(t) + \sum_{\ell} B_{\ell} u_{\ell}(t), \quad (42)$$

$$\text{where } M = \int_{\Omega} \Phi^j \Phi^j, \quad D = \int_{\Omega} (v(\vec{x}) \cdot \nabla \Phi^j) \Phi^j, \quad K = -\frac{1}{\rho C_p} \int_{\Omega} k \nabla \Phi^j \cdot \nabla \Phi^j, \quad (43)$$

$$\text{and } B_{\ell} = \frac{1}{\rho C_p} \int_{\Gamma_{\ell}} \Phi^j. \quad (44)$$

## D.2 Control Design

The reduced-order models obtained using the techniques described in Section D.1 result in standard state-space equations, either in discrete or continuous time setting, with the control and disturbance terms explicitly appearing in the governing dynamics. We now describe techniques to develop controllers that reject a known disturbance, while minimizing a user-defined cost function. The disturbance is first assumed to be known over a future time-horizon, and the assumption is later relaxed to consider disturbances known only at the current time.

### D.2.1 Optimal Control for Discrete-Time Systems with Known Future Disturbance

In this section, we consider an inhomogeneous LQR problem, for rejection of a disturbance known over a future time-horizon. Consider the following linear system obtained, for instance, by numerical discretization of the weak form (24):

$$x_{k+1} = Ax_k + Bu_k + Dd_k, \quad (26)$$

$$s_k = C_1 x_k, \quad (27)$$

$$z_k = C_2 x_k, \quad (28)$$

where the index  $k$  represents the time-instant  $t_k = k \, dt$ . The outputs  $s_k$  are considered to be the outputs that represent sensor measurements, while the outputs  $z_k$  are considered to be the outputs that represent quantities of interest for control, such as the average temperature in the occupied region of a room, and are used to define a cost function. The objective is to find a control law  $u_k$  such that the output  $z_k$  tracks a reference trajectory  $r_k$ , while minimizing a quadratic cost function of the form:

$$J(z_k, u_k) = \frac{1}{2} \left[ \sum_{k=0}^{N-1} ((z_k - r_k)^T Q (z_k - r_k) + u_k^T R u_k) + (z_N - r_N)^T Q (z_N - r_N) \right], \quad (29)$$

where,  $Q > 0$ ,  $R > 0$  are positive-definite weighing matrices. Note that due to the disturbance term  $d_k$  appearing in (26), this is not a standard LQR problem; see Bertsekas (2005). The solution to this problem in continuous time setting has been considered, for instance, in Hampton et al. (1996). We are not aware of any known solution approach in literature for the discrete-time setting considered here. We solve this problem below using the method of constrained Lagrangian. Using Lagrange multipliers  $\lambda_k$  for the constraints (26), the Lagrangian can be expressed as

$$L(x_k, u_k) = J(x_k, u_k) + \sum_{k=0}^{N-1} \lambda_{k+1}^T (Ax_k + Bu_k + Dd_k - x_{k+1}), \quad (30)$$

leading to the following Kuhn-Tucker optimality conditions (Bertsekas, 1999)

$$\lambda_k = A^T \lambda_{k+1} - C_2^T Q(r_k - C_2 x_k), \quad \text{with } \lambda_N = -C_2^T Q(r_N - C_2 x_N), \quad (31)$$

$$u_k = -R^{-1} B^T \lambda_{k+1}, \quad (32)$$

for  $k = 0, 1, \dots, N-1$ . To obtain the control law  $u_k$  in closed form, we use the notion of backward sweeping to express the Lagrange multipliers as

$$\lambda_k = P_k x_k + n_k, \quad k = 0, 1, \dots, N-1. \quad (33)$$

Further manipulations result in the following recursion relations for  $P_k$  and  $n_k$

$$P_k = A^T P_{k+1} A - A^T P_{k+1} B (R + B^T P_{k+1} B)^{-1} B^T P_{k+1} A + C_2^T Q C_2 \quad (34)$$

$$n_k = -A^T P_{k+1} B (R + B^T P_{k+1} B)^{-1} B^T (P_{k+1} D d_k + n_{k+1}) + A^T P_{k+1} D d_k + A^T n_{k+1} - C_2^T Q r_k \quad (35)$$

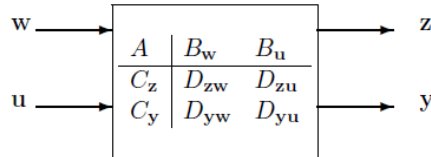
with the terminal conditions  $P_N = 0$  and  $n_N = 0$ . If the disturbance  $d_k$  is known over the horizon  $k = 0, 1, \dots, N$ , recursions (34,35) can be solved for  $P_k, n_k, k = 0, 1, \dots, N-1$  and the control law computed using

$$u_k = -R^{-1} B^T (P_k x_k + n_k) = K_k^{fb} x_k + u_k^{ff}, \quad (36)$$

where,  $K_{fb}$  is the feedback gain and  $u_k^{ff}$  is the feed-forward term incorporating the knowledge of the disturbance  $d_k$ . Note that, when the entire state  $x_k$  is not accessible for control, but only sensor measurements  $s_k$  given by (27) are available, one can design an appropriate observer (e.g., Kalman filter) for the system (26, 27) to obtain an estimate of the state to be used in place of  $x_k$  in the expression (36).

### D.2.2 Robust Control Design for Unknown Future Disturbances

The canonical  $H_2$  control problem is depicted as:



The input signal  $w$  is envisioned as a disturbance and includes measurement noise terms; the input signal  $u$  is the control. The output signal  $z$  characterizes the quantities we wish to moderate; the output  $y$  are sensed variables. The objective is to define a (internally stable) feedback from  $y$  to  $u$  so that the closed-loop system displays acceptably small variations in  $z$  under disturbances from  $w$ .

**Conduction Example.** To illustrate an important result we consider a one-dimensional conduction example wherein the body is insulated at each end and subject to a disturbance (internal heat source) near one end (say left). The control is an internal heat source near the middle of the body

and the sensed output is the temperature in this middle region. The objective is so maintain an average temperature in the body.

The disturbance is envisioned as a step in the internal source at the left end. Improved control response can be achieved by augmenting the plant model with a model of the disturbance. In the present case the disturbance is modeled as a constant; the added state satisfies  $\dot{d} = 0$ . However, since the  $H_2$  synthesis procedure requires a detectable system, it's necessary to add another sensor near the disturbance location (left end). The details are omitted here.

Figure D.1 (a,b) displays the sensor time histories for a particular realization with a unit step in the disturbance heat load at time  $t = 10$ . Figure D.1(c,d) displays the control input and the average temperature over a central region of the body.

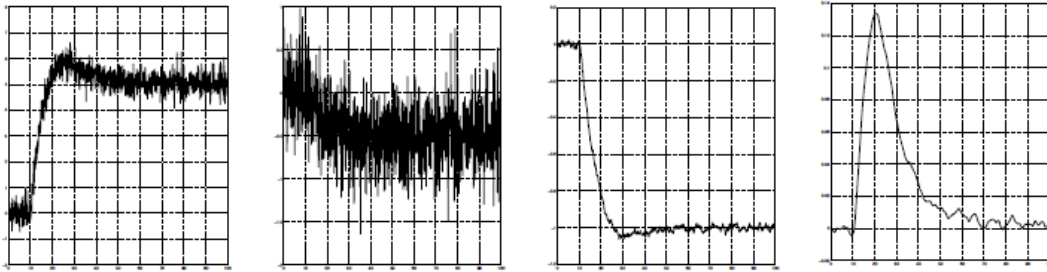


Figure D.1: (a,b) Sensed temperatures: T1, Tmid, (c) Control flux and (d) Tcore

### D.3 Case Study 1: DOE Benchmark Building Model

The first case-study undertaken in this work uses a DOE EnergyPlus benchmark model, which is a middle-sized office building shown in Figure D.2. The purpose of this study was to qualitatively assess the robustness of the flow fields in presence of candidate low-energy HVAC systems. In particular, we considered two different candidate systems: (a) active chilled beams and (b) passive chilled ceilings, with displacement vents (DV). The system was subjected to external disturbance from solar radiation.

Specifically, we considered one peripheral room facing West (number 4 in Figure D.2b), with dimensions 33.3m x 6m x 2.74m. The room has a window running all along the exterior (West-facing) wall, and covers the middle-third along the vertical dimension, with the transmitted solar heat flux on a summer design day as shown in Figure D.2c.

In the early part of the project, we explored the simulation software ANSYS AIRPAK for modeling airflow in buildings. The advantages of this tool are that it is tailored for building simulations, with capabilities to develop models, generate grids, solve and post-process solutions. It has an extensive library of building components such as walls, fans, diffusers, heat sources, people, and many others. The solver used by this tool is FLUENT, but the only a small fraction of the capabilities of FLUENT are available. For instance, the boundary conditions can be either temporally or spatially varying, but not both; user-defined outputs, such as local area or volume averages cannot be accessed; solar load model is not accurate with certain radiation models. The

main disadvantage of AIRPAK is that it does not allow closed-loop control implementation, which FLUENT does via user-defined functions (UDFs).

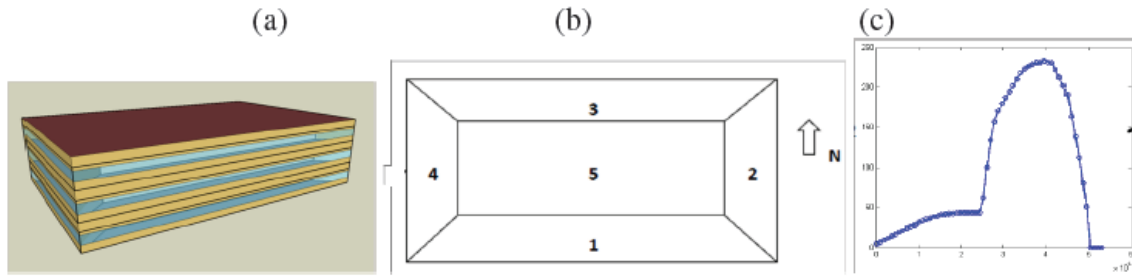


Figure D.2: DOE Energyplus benchmark model: (a) 3-D geometry (b) Plan/top view. (c) Solar heat flux (in  $\text{W/m}^2$ ) transmitted through the window facing West, for one design day in summer.

The boundary conditions (supply air conditions, and internal and solar heat gains) for numerical simulations were setup consistent to the corresponding EnergyPlus simulations. The boundary conditions common to the two low-energy systems considered in this work are summarized in Table D.1. The solar load is considered to be time-varying and is shown in Figure D.2c. Numerical simulations were performed over the same time-interval and the resulting flow-fields at times corresponding to low and high solar loads were compared to assess robustness to this disturbance.

Boundary	Momentum boundary condition	Energy boundary condition
Walls, floor and ceiling	No-slip	Isothermal, 29 deg C
Internal loads (floor-mats)	No-slip	$106 \text{ W/m}^2$
Windows (west-facing)	No-slip	Time-varying heat-flux, Figure D.2c
Exhaust	$p=0$	-

Table D.1: Boundary conditions for one room in the DOE medium-office building approximated using inputs from EnergyPlus simulations.

The results are summarized in the following. We first consider a system equipped with active chilled beams. The supply air velocity through the chilled beams was  $1.12 \text{ m/s}$ , while the temperature of the supply air was varied from  $17^\circ\text{C}$  at low solar load to  $14^\circ\text{C}$  at peak solar load.

**Active Chilled Beam CFD Model.** In active chilled beams (a cartoon is shown in Figure D.3), primary or ventilation air is supplied at a high velocity through nozzles, which creates a low-pressure region near the central core. This induces the room air into the central portion of the beam, which is circulated with cold water through pipes. The room air passes over this central region, cools down, and mixes with the supplied air, and the mixed air is supplied to the room. The detailed modeling of this beam is expensive in CFD, so we use a simpler model that results in a flow that retains the coarse features of the physical beam. The model, shown in Figure D.3, consists of two inclined channels that represent the supply of mixed air, and a central region that removes air out of the domain and represents the central inducing part of the beam. The boundary conditions specified are the air velocity and temperature at the exit of the two channels and at the central portion of the beam. For our study, the two channels were inclined at an angle of  $30^\circ$



degrees to the horizontal, and the supply air velocity through the channel was 1.12 m/s, while the velocity of the fluid outgoing through the central portion was 0.43m/s (assuming that the ratio of induced air to the supply air is 2.5). The temperature of the supply air was varied from 17°C at low solar load to 14°C at peak solar load (shown in Figure D.3c).



Figure D.3: Schematic of a chilled beam (left). Model used in CFD (right), showing supply ducts and a return duct, which models the airflow induced by a low-pressure region formed near the central part of the beam.

With these conditions, the relevant non-dimensional quantities, namely the Reynolds number ( $Re$ ) and the Grashof number ( $Gr$ ) are:  $Re = UL/\nu = 1.3 \times 10^5$ ,  $Gr = g\beta TL^3/\nu^2 = 8 \times 10^8$ . The ratio  $Gr/Re^2 = 0.4 \ll 1$  implies that forced convection dominates.

The locations of the active chilled beams and the exhausts in the room are shown in Figure D.4, along with the temperature contours and projected streamlines on different vertical slices, taken along the two central planes, under the chilled beam, and under an exhaust. For comparison, plots of the streamlines on a central plane, perpendicular to the  $z$ -axis, are also shown, at low and high values of the solar heat flux. The plots show that the flow-field is dominated by a pair of vortices, rotating about a direction parallel to the  $z$ -axis. It is seen that this pair of vortices persists even at higher solar load, and the flow-field pattern is robust to this disturbance.

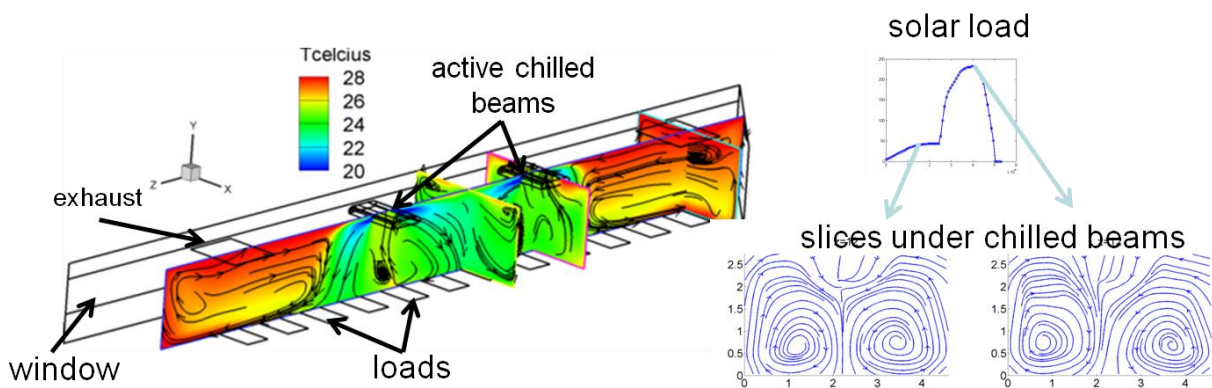


Figure D.4: Flow and temperature fields in a room equipped with active chilled beams. The plots show the temperature fields and projected streamlines at a few vertical cross-sections. The slices on the right show velocity streamlines on the central slice, perpendicular to the  $z$ -axis. The counter-rotating vortices persist in the presence of solar radiation.

**Passive beams and DV.** Next, we consider the room equipped with a passive chilled beam and displacement ventilation (DV). In this system, the DV provides ventilation air and handles a portion of the cooling load ( $< 40$ - $60$  W/m<sup>2</sup>), while the chilled beam handles the remaining loads; for cases where the load is small enough, only DV can suffice. The model of this system is shown in



Figure D.5, which shows a passive beam over the central portion of the ceiling, and four DVs on the wall across from the window. The chilled beam is modeled as a negative heat flux surface that is varied from 140W/m<sup>2</sup> at low solar load condition to 210W/m<sup>2</sup> at the peak of solar load. The displacement vents supply air at 20 deg. C and a constant velocity of 0.05m/s. For this case, the non-dimensional quantities are:  $Re = 7 \times 10^3$ ,  $Gr = 8 \times 10^8$ . Since  $Gr/Re^2 = 16 \gg 1$ , the flow is dominated by natural convection, and is thus expected to be less robust to disturbances.

The temperature contours and streamlines on vertical sections – two central sections, one each through the DV and exhaust – are also shown in Figure D.5; the plots are similar to those in Figure D.4. These show significant temperature stratification away from the central portion, which is exploited in DV to reduce energy costs. The figure also shows the streamlines on a central plane at times corresponding to low and high solar loads. The flow is again dominated by two counter-rotating vortices, rotating about a direction parallel to the X-axis. However, the separatrix between the two vortices is shifted towards the window at low solar condition, as compared to the active chilled beam case, where the separatrix is midway along the Z-direction. It is also seen that, at high solar load conditions, this separatrix is pushed farther away from the window towards the opposite wall; there is also a significant roll-up of the vortex closer to the window. Thus, the flow-field is less robust to the solar disturbance.

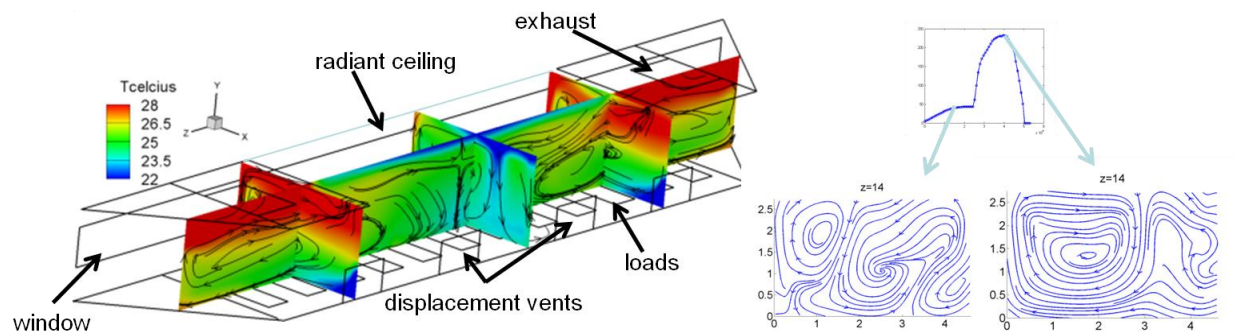


Figure D.5: Flow and temperature fields in the presence of a passive radiant ceiling and displacement ventilation. The slices on the right show velocity streamlines on the central slice, perpendicular to the z-axis. The streamlines considerably drift away from the window when subject to solar radiation.

In both the cases, we also computed POD modes, using the transient data-set over the period shown in figure 3.52c, with varying solar load. In both cases, it was observed that around 10-20 POD modes captured more than 90% of the energy and thus the flow was inherently low-dimensional. A reduced-order model was also developed by projecting the governing Boussinesq equations onto the computed POD modes; however, the model, truncated at various different orders, was unstable. This is a problem of the POD/Galerkin procedure, which does not guarantee stability of the resulting models. The model could still be used in conjunction with sensor measurements to develop an extended Kalman filter, as in Surana et al. (2008).

#### D.4 Case Study 2: Room with Displacement Ventilation and Chilled Ceiling

In this section, we consider a simple case-study to illustrate the application of the model reduction and control design tool-chain. We consider dynamics of airflow in a room, shown schemati-

cally in figure 3.58, with the domain of interest  $D$  being the region defined by  $X = [-2, 2]$ ,  $Y = [0, 3]$ ,  $Z = [-2, 2]$ . The room is considered to be equipped with a displacement vent that supplies air near the floor and a chilled ceiling that provides radiant and convective cooling. The vent is on the boundary  $X = -2$  and defined by the region  $Z = [-2, 2]$  and  $Y = [0, 0.6]$ . As described in the introduction, such a system relies on thermal stratification to provide occupant comfort while reducing energy consumption. The boundary conditions for (1-3) are as follows:

1. Inlet velocity and temperature specified at the displacement vent
2. Chilled ceiling, modeled as a cooling source with a uniformly distributed flux  $u(t)$  which can be controlled
3. Internal load due to occupants and equipment, represented as a floor-mat with a uniformly distributed heat flux  $d(t)$  and represents the disturbance
4. The remaining boundary of  $D$  is assumed to be adiabatic.

#### D.4.1 Problem definition

The problem considered here is that, given the knowledge of the disturbance over a future time horizon, determine a minimal control effort (i.e. flux through the chilled ceiling), that maintains stable stratification. Furthermore, we assume that localized temperature measurements are available at some given locations on the walls (say, from thermostats), which can be used in designing a control law for disturbance rejection. Later, we also consider a control design problem, which does not assume the knowledge of this future disturbance.

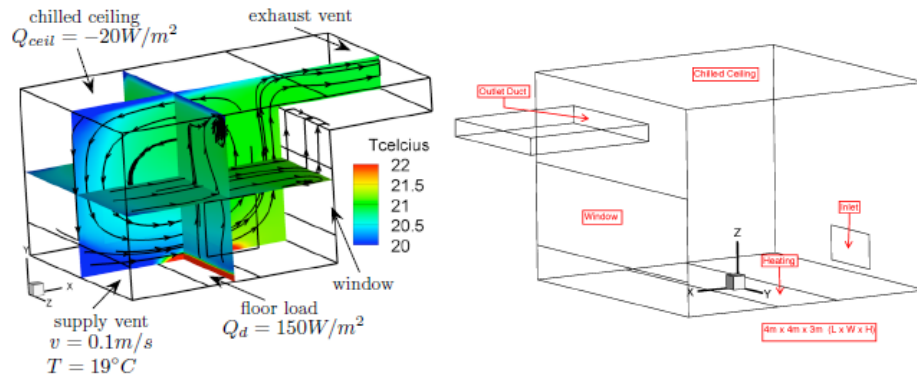


Figure D.6: Room equipped with a displacement vent, a chilled ceiling, a window and an internal load modeled as a floor-mat, with the boundary conditions as shown in the figure. The slices represent the steady-state temperature field and projected stream-lines, obtained from a FLUENT simulation. The right plot shows a slightly modified geometry used (by Virginia Tech) for developing POD/Galerkin model.

The problem described above can be more formally stated as follows: for a known floor disturbance  $d(t)$ ;  $0 < t < T_f$ , determine a control input  $u(t)$  that maintains the average temperature in a specified region  $D_o$  of the room at a desired value  $T_{avg}$  while minimizing the control effort or equivalently, energy consumption. This trade-off can be represented as a quadratic cost functional:

$$J(u, T) = \int_0^{T_f} q(\bar{T}(t) - \bar{T}_{avg})^2 + ru^2(t) dt, \quad (37)$$

where  $q$  and  $r$  are given positive constants, and  $T$  represents the average of  $T(X,Y,Z)$  over the region  $D_o$ . Here, we think of  $T_{avg}$  as being the desired average temperature in a room or a set-point.

#### D.4.2 Simulation details

The room geometry and the mesh are generated using ANSYS AIRPAK. The maximum grid size is limited to 0.2m, 0.15m and 0.2m along the X, Y and Z axes respectively, leading to 66,205 mesh points in the domain  $D$  comprising the room. A constant integration time-step of 2 seconds is used for all the simulations. To obtain nominal operating conditions for the room, we use constant heat flux values for the boundary conditions, and an initial condition with zero velocity and a uniform temperature of 24 deg C. The fluxes are obtained by simple energy balance calculation, so that the chilled ceiling can compensate for roughly 50% of the heat input through the floor-mat. Under these conditions, the flow settles to a steady state, as shown in Figure D.6.

The optimal-control problem described above is intractable for dimensions larger than  $10^3$ ; hence, we develop reduced-order models of the full dynamics and use the same for control design.

#### D.4.3 Reduced Order Modeling

##### (a) Reduced-Order Model using ERA

We use a model reduction technique called Eigensystem Realization Algorithm (ERA), to develop low-order models of the airflow linearized about the above computed steady state. This method is described in detail in Appendix B, and here we illustrate the application of the algorithm to this simple problem.

The methods obtained models of an input-output system, and results in a model that is input-output balanced; i.e., the most controllable modes in the reduced system are the same as the most observable modes. Thus, we first need to define the outputs, and they are as follows:

1. Sensed outputs  $s_k$ , are the temperatures averaged over two regions on the walls  $Z = -2$  and  $Z = 2$  (the walls to the left and right of the supply vent), bounded by  $Z = [-0.25, 0.25]$  and  $Y = [0.25, 0.75]$ . This output is used for feedback control.
2. Controlled output  $z_k$  is the volume average of temperature  $T(Z, t)$  field over the occupied region  $D_o = [-1.5, 1.5] \times [0.25, 1.25] \times [-1.5, 1.5]$ . This output is used as a measure of comfort, and is used in the cost function (29).

The control input  $u_k$  is the chilled ceiling flux, perturbed about its steady-state value of  $-20\text{W/m}^2$ , while the disturbance  $d_k$  is the floor flux, perturbed about its steady-state value of  $150\text{W/m}^2$ . Similarly, the outputs defined in (9) are the perturbations from their steady states. The ERA-based model reduction requires computation of the impulse responses of the original system. The data resulting from these responses is analyzed, as described in the algorithm, and a low-dimensional model is computed that retains that the most controllable and observable modes.

Since it is difficult to numerically subject a black-box simulator like FLUENT to an impulsive input, we alternatively compute the step response. The step response is obtained by gradually changing the boundary inputs (fluxes at chilled ceiling and floor-mat) from their nominal value linearly to a perturbed value over 30 time-steps (i.e, 1 minute of simulation time). If the step-

response of (8, 9) is denoted by  $y_k^{step}$ , where  $k$  denotes the time-index, the corresponding step response is then computed using

$$y_k = y_{k+1}^{step} - y_k^{step}. \quad (39)$$

The outputs above are then used in the steps outlined in Appendix B.1 to obtain a transformed system, and a low-order model with 10 modes, is obtained by truncating the system on the basis of the Hankel singular values, which represent the controllability and observability of the system. The performance of the model is tested against the data from the original step-responses. A comparison is shown in Figure D.7, which shows that the model accurately predicts the controlled output  $z_k$ .

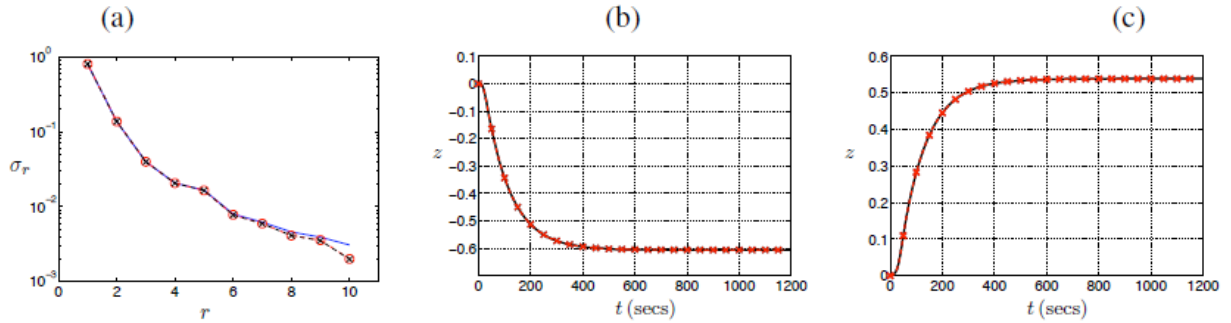


Figure D.7: (a) Hankel singular values of the system in a log-scale; these decay sharply, indicating that the system is low-dimensional. These also quantify the approximation error and provide a guideline for truncation. Response of the full system (black, solid line) and a 10-mode reduced-order model (red, dashed line, crosses) to (b) -10W/m<sup>2</sup> step in the chilled ceiling flux (c) 40W/m<sup>2</sup> step in the floor-mat flux. Plots compare the controlled outputs  $z_k$ , that is, perturbations from the steady state temperature averaged over the occupied region  $D_o$ .

### (b) Reduced-Order Model Using POD/Galerkin Method

We now describe model reduction of this system using the POD/Galerkin approach. The basic geometry of our problem is shown in Figure D.6, slightly modified from the one considered in the previous subsection. Based on data from certain Fluent simulations we construct a low-order dynamic model for control design.

**Start-Up Transient to “Steady State”:** The flow field was initialized to zero velocity and a uniform temperature of 21°C, and Fluent was run on a grid of ~100,000 points, with a time step of 2.0 seconds for  $0 \leq t \leq 5400$ s. As seen in Figure 3.60 (left), the volume-averaged temperature initially rises (due to net heating) and approaches 24.5 deg C. Whereas, the volume-averaged temperature seems to approach a steady value, the average-outflow temperature (right) clearly exhibits a residual oscillation of about 0.5 deg C. A ‘snapshot’ of the temperature flow field at  $t = 5400$  s is shown in Figure 3.60. It can be seen that the induced flow moves up the wall; a portion is vented out through the duct. The flow is not truly steady; regions of cooler/warmer air are entrained alternately in the outflow producing the oscillation observed in Figure D.8 (right). The data from  $t=5400$ s to  $t=5700$ s was averaged to produce an ersatz steady flow solution.

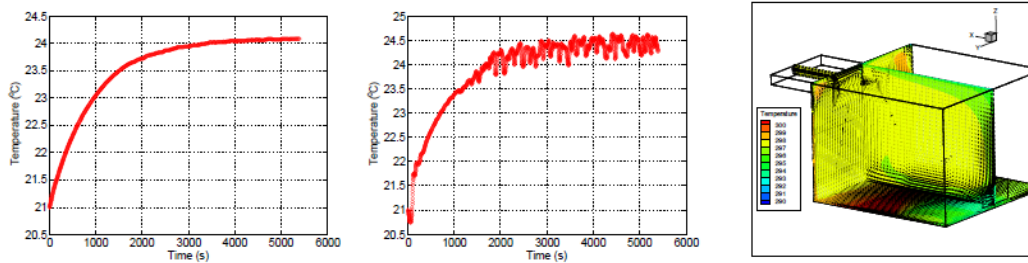


Figure D.8: Startup transient for volume-averaged temperature (left), outflow temperature (center) and the temperature field at  $t = 5400s$  (right).

**Impulse Response:** The first ‘snapshot’ data for a POD-based dynamic model was produced by the response to an impulsive change in the temperature field (only). This was achieved by changing the temperature field to a uniform value of  $301.15^\circ K$ , while retaining the velocity field from the steady solution at  $t = 5400s$ . Using this field as an initial condition, a subsequent simulation was ran on the time interval  $[5400, 6600]$ , saving data every 6 seconds (200 snapshots). In Figure D.9 the volume-averaged temperature is seen to relax from  $T = 28^\circ C$  to  $T = 25.2^\circ C$  in the twenty minutes of simulated response.

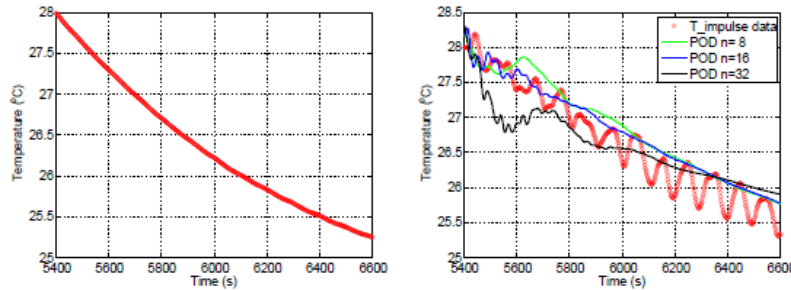


Figure D.9: Volume-averaged temperature; relaxation from  $T = 28^\circ C$  (left). Reduced-order model prediction of the outflow-averaged temperature (right).

To account for the effects of the inputs (control and disturbance), we ran FLUENT simulations, while varying each input using the following time-varying function (uniform in space):

$$Q_{input}(t) = Q_s + Q_{mag} \sin \left( 2\pi \frac{(t - 5400s)^2}{(600s)^2} \right) \quad (W/m^2) .$$

Note that this is a linear chirp with the frequency varying from 0 at  $t = 5400s$  to  $2\pi/600s$  at  $t = 6000s$ . In the above equation,  $Q_s$  is the value of the inputs used to compute the steady state;  $-20 W/m^2$  for the chilled ceiling,  $15 W/m^2$  for the floor disturbance, and zero for the window disturbance. Also,  $Q_{mag}$  is the magnitude of the chirp disturbance, and the values for the ceiling, floor and window fluxes are 4, 15 and  $10 W/m^2$ , respectively. For all the simulations, the startup flow field from  $t=5400s$  was used as an initial condition. The solution was run on the interval  $t=5400s$  to  $t=6000s$  and the temperature field saved every 6 seconds. These 100 temperature field snapshots from each impulse response were combined with the 200 snapshots from the state-impulse response, and the combined set of snapshots used to develop the POD/Galerkin model. Shown in Figure D.10 are the applied ceiling, floor and window fluxes and the corresponding responses of



the volume-averaged temperature are shown in Figure D.11. There is an expected lag in all the responses: the peak applied flux occurs at  $t = 5700$ s, whereas the peak temperature appears slightly after 5800s.

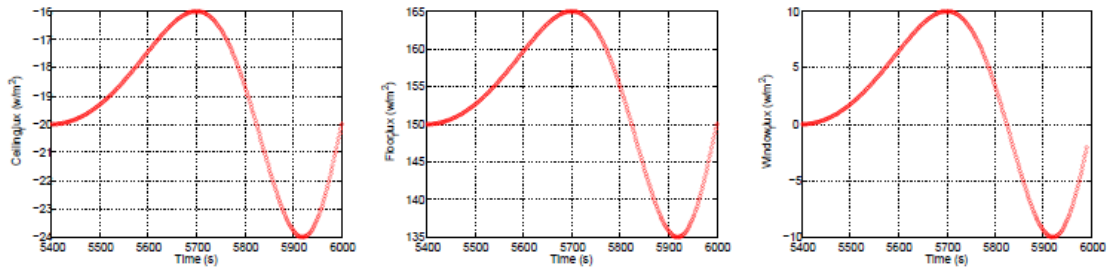


Figure D.10: Applied input fluxes at the ceiling (left), floor (center) and the window (right).

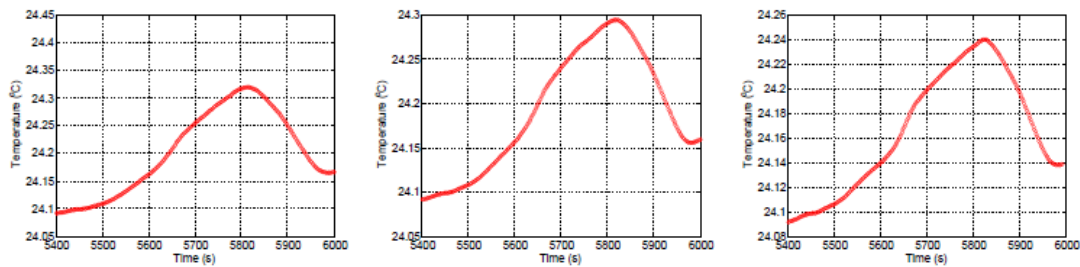


Figure D.11: Responses of the volume-averaged temperature to the inputs shown in Figure 3.62.

**POD Basis:** For  $\Phi^j$  we compute POD modes of the perturbed data-set,  $T(t, x) - T^{ss}(x)$ , for the FLUENT responses described in an earlier section: using the 200 snapshots from the state impulse response and 100 snapshots from each of the responses to the chirp inputs. The steady solution  $T^{ss}$  was approximated by averaging temperature fields from the start-up solutions on the interval [5400, 5700] as described in earlier section. The resulting steady-state temperature field is similar to that shown in Figure D.8. The first two POD basis vectors are shown in Figure 3.64. In the first POD mode, we see (along the  $x = 0$ , back wall) a temperature gradient from the cool ceiling to the warmer floor. Note the scale is quite compressed; the maximum difference is less than 0.3 deg C. The second mode is curiously anti-symmetric about the  $y=0$  plane. The problem data would suggest only symmetric temperature fields. The FLUENT solutions do, however, display anti-symmetric elements. The cumulative energy in the first  $k$  modes is shown in Figure D.12. Note that eight modes recover more than 98.5% of the ‘energy’ in the first 100 modes.

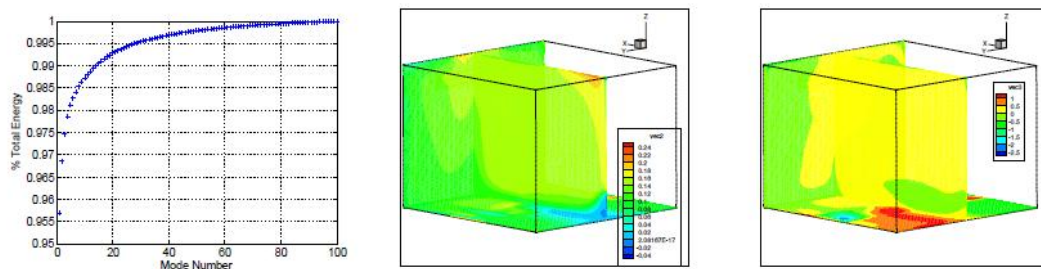


Figure D.12: Cumulative POD energy (left), first (center) and second (right) POD modes

**Reduced-Order Model:** A reduced-order model can be obtained by using the computed POD basis in (42, 43, 44), and the resulting dynamics can be reduced to normal form

$$\dot{z}(t) = A z(t) + \sum_{\ell} \hat{B}_{\ell} u_{\ell}(t), \quad \text{where} \quad A = M^{-1}(K - D) \quad \text{and} \quad \hat{B}_{\ell} = M^{-1} B_{\ell}.$$

The resulting model can be used for control design using techniques described in earlier sections. To test the performance of the resulting modes, we first compare results from FLUENT simulations (i.e. data) with simulations based on our POD models. Unfortunately, at this time we have only a single interesting scalar quantity from the FLUENT simulations. Specifically, we recorded the spatially averaged temperature over the region of the room-to-duct interface. As a complication, this surface is composed of 1,082 triangles in our FEM grid; some are highly skewed.

Recall that the first data set we discussed was generated by impulsively setting the temperature field of the  $t = 5400$ s solution to a uniform 28 deg C, and recording the relaxation response. For the POD model, it is necessary to approximate this initial condition by projecting the difference  $301.15 \text{ deg K} - T_{ss}(x)$  onto the span of the POD basis. In Figure D.13, we display the predicted time histories of the outflow-averaged temperatures for FLUENT and for POD models with  $n = 8, 16$ , and  $32$ . At best we can claim qualitative agreement.

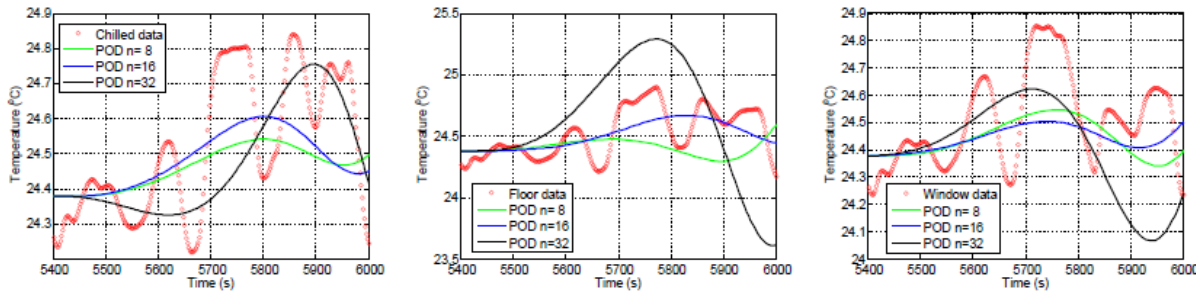


Figure D.13: Predicted outflow average temperatures, in response to the perturbed (a) ceiling (b) floor and (c) window fluxes. Initial condition used is  $T(5400, x) = T_{ss}(x)$ .

The other data-sets that we discussed, were generated starting at the nominal  $t = 5400$ s and perturbing the boundary fluxes (chilled ceiling, floor and window) with a linear chirp input of different magnitudes. In Figure D.14, we display the predicted time histories of the outlet temperatures for FLUENT and for POD models with  $n = 8, 16$ , and  $32$ . In Figure D.13, the initial condition is  $T(5400+, x) = T_{ss}(x)$  so that the reduced model has  $z_n(5400) = 0$ . In Figure D.14, the initial condition is the  $t = 5400$ s solution for the startup problem section, and the difference  $T_{\text{startup}}(5400, x) - T_{ss}(x)$  was projected onto the span of the POD basis to obtain the model initial condition.



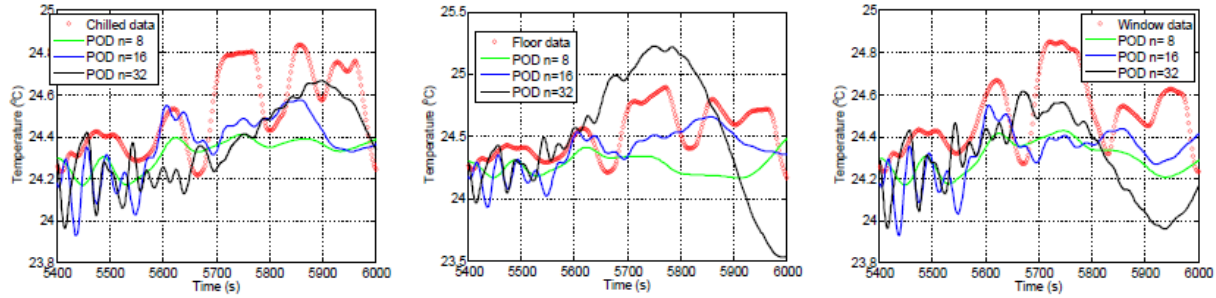


Figure D.14: Predicted outflow average temperatures, in response to the perturbed (a) ceiling (b) floor and (c) window fluxes. Initial condition used is  $T(5400; x) = T_{\text{startup}}(5400; x)$ .

#### D.4.4 Controller Design and Performance

The reduced model derived using ERA is used to develop a controller that rejects a floor disturbance known over a time horizon  $(0, T_f)$ . The floor disturbance is considered to be of the form shown in Figure D.16a. In the absence of the control, the average temperature in the room rises by about 4 deg C, as shown in the resulting flow-field in the Figure D.16b. The control design approach, described in appendix C, is used to develop a controller that suppresses the deviations of the averaged temperature from its steady-state value. We define  $Q = qI$  (where  $I$  is the identity) in the cost function (29) and consider different values of  $q$ , while fixing  $R = 1$ . We use Kalman filter as a reduced-order observer for state estimation based on the two temperature measurements to compute the feedback term in the control law (36). The resulting observer-based control is implemented in FLUENT using user-defined functions (UDFs) to test its performance in the full CFD simulation; a schematic is shown in Figure D.15. The results are shown in Figure D.17 for  $q = 5$  and  $q = 50$ , where it is evident that the controller suppresses the deviation of the temperature from its steady value, thus maintaining occupant comfort. For the larger value of  $q = 50$ , the controller completely suppresses the effect of the disturbance, but the required control effort is almost twice as large as that required using  $q = 5$ .

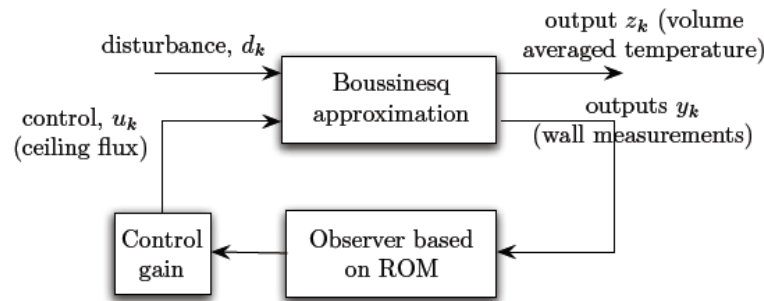


Figure D.15: Schematic of controller implementation in the full simulation.

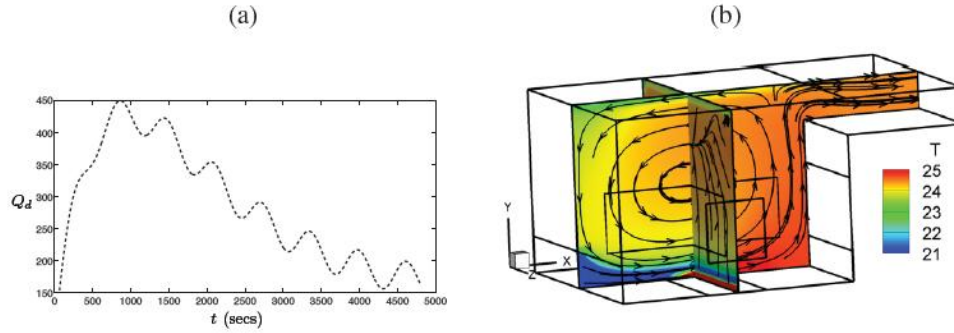


Figure D.16: (a) Disturbance input (floor heat flux, in W/m<sup>2</sup>) as a function of time, and (b) the flow-field resulting when the disturbance reaches its maximum value.

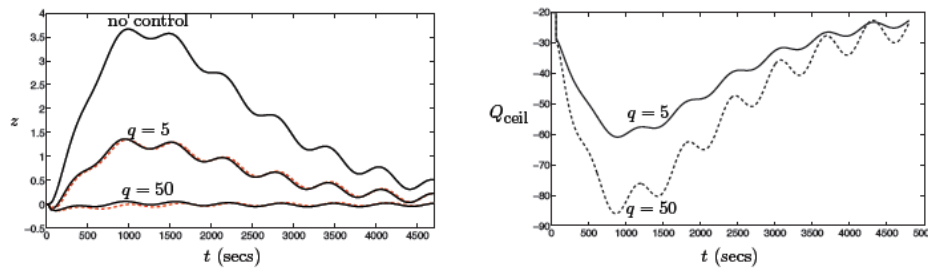


Figure D.17: (a) The controlled outputs  $z_k$  (temperature, averaged over the occupied zone), in the presence of the disturbance shown in Figure D.16a, for different control gains obtained using  $q = 5, 50$ . Also shown is the response when the control is off. The response of the full simulation (black, solid line) is compared with the observer reconstruction (red, dashed line). (b) Control inputs (chilled ceiling flux in W/m<sup>2</sup>) required to reject the disturbance, for the two control gains.

## D.5 Functional gains for sensor and actuator placement

Linear feedback control operators for distributed parameter systems can be represented as an integral of the state against a kernel function. These kernels are known as functional gains (Lions, 1971; Bensoussan, et al., 2007). In many examples, the structure of these functional gains has been used to guide the location of actuators and sensors (Burns et al., 1994, 95, 2002). As a first step in understanding whether or not these techniques can be brought to bear on a complex control design problem such as those considered in this research, we computed feedback functional gains for a simplified version of our problem, where the velocity field was frozen and the control was applied to the inlet temperature in the room.

As a first approach, we attempted to directly calculate the functional gains corresponding to a linear quadratic regulator problem, where the control objective was minimizing the  $L^2$ -norm of the deviation of the temperature from a desired fixed value. The traditional approach for approximating these functional gains would require the (dense) solution to full-rank Riccati equation of order 200,000. This is well beyond the capabilities of modern algorithms. However, we could exploit the fact that we have only one control input (temperature of the incoming air at the 4 vents) to compute the functional gains using specialized software. The gains for this case are given in Figure D.18. As we see, the support of the feedback gains are largest around the inlets and highlight the fact that for convection dominated flows, getting the inflow temperature correct eventually controls the temperature throughout the space. We note that in earlier case studies,

with unrealistically low Reynolds number flows and coarse meshes, these gains were very useful in providing spatial information about the control (Borggaard et al., 2009).

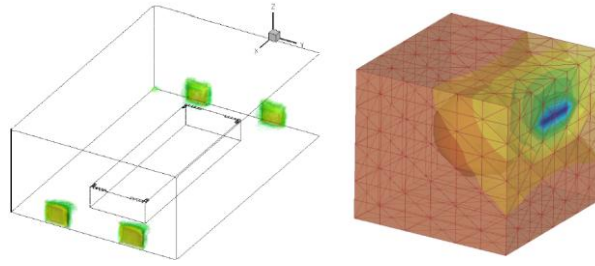


Figure D.18: (Left) Functional Gain for  $Re=4800$ ; advection field. (Right) Functional Gain for  $Re=100$ .

### D.5.1 Reduce, then control

The computational cost of solving the large Riccati equations required in the previous section motivated us to consider reduce-then-control approaches. In other words, we build reduced-order models for the system, then use these models to design control laws. However, to obtain spatial representations of the control law (functional gains), we needed to consider projection-based model reduction methods. In this case, we developed large linear systems corresponding to finite element discretization to the advection-diffusion equations considered in the previous section, but computed left and right projections based on optimal  $H_2$  interpolatory model reduction (Gugercin, 2005). For example, our original finite element system has the form:

$$E\dot{x} = Ax + Bu, \quad y = Cx$$

where,  $B$  represents both inputs and disturbances to the system and  $C$  provides both controlled output and system measurements. The sparse matrices  $E$  and  $A$  represent the finite element mass matrix and discretization of the advection-diffusion equation and are typically large (200,000 in this example). The input and output vectors  $u$  and  $y$  have relatively small numbers (2 in our example). The corresponding transfer function from inputs to outputs has the form:

$$G(s) = C(sE - A)^{-1}B.$$

Thus, we seek a reduced-order model of the form,

$$G_r(s) = C_r(sE_r - A_r)^{-1}B_r,$$

that matches the input-output behavior of the full-order finite element system as well as possible. Specifically, Gugercin's IRKA algorithm approximates:

$$\min_{\dim(G_r)=r} \|G - G_r\|_{H_2}$$

$$E_r = W^T E V, \quad A_r = W^T A V, \quad B_r = W^T B, \quad \text{and} \quad C_r = C V.$$

The solution to this problem solves a set of tangential interpolation conditions. The Iterative Rational Krylov Algorithm (IRKA) is an iterative algorithm that produces better interpolation points and tangential interpolation directions. The tangential directions can be used to construct the projection matrices from the full-order system to the reduced-order system. Having access to  $V$  allows us to reconstruct functional gain approximations in this reduce-then-control approach.

As a test case, we consider the indoor-air environment in the Great Lakes conference room with four inlets, one return vent and thermal loads provided by two windows, two overhead lights and occupants (see Figure 3.6.19). We use the Fluent CFD software package to perform simulations

of the indoor-air velocity, temperature and moisture. We assume adiabatic boundary conditions on all surfaces except the inlets, windows and lights. We simulated the indoor-airflow in this room with varying inlet temperature, occupant loads, as well as solar and lighting loads for thirty minutes. Occupant loads are modeled using a source term equivalent to 75W/person sitting around the conference table.

### D.5.2 Finite Element Model of Convection/Diffusion

We constructed a finite element model for thermal energy transfer in an indoor environment based on a convection/diffusion model with frozen velocity field  $v$ ,

$$\frac{\partial T}{\partial t} + \nabla \cdot \nabla T = \frac{1}{\text{RePr}} \Delta T + Bu,$$

where  $B$  represents control and disturbance inputs. A finite element discretization of this equation led to a high-order state-space model in the form with  $n = 202140$  degrees of freedom. The states  $x$  correspond to nodal values of the temperature, the matrix  $E$  corresponds to the finite element mass matrix,  $A$  is the finite element approximation of the convection and diffusion operators,  $B$  represents two inputs

- (1) the temperature of the inflow air at all four vents, and
- (2) a disturbance caused by occupancy around the conference table,

whereas, the discretized output operator  $C$  corresponds to:

- (1) the temperature at a sensor location on the max  $x$  wall,
- (2) and the average temperature in an occupied volume around the table,

The system has  $n = 202140$  degrees of freedom; yet 2 inputs and 2 outputs. We reduce the order to  $r = 30$  using IRKA.

### D.5.3 Functional Gain Calculations

Both model reduction approaches produced reduced-order models that showed excellent tracking of the input-output behavior of the original system. However, when the full-order system and the projections  $Wr$  and  $Vr$  are available, we can analyze the structure of the control law in the full-order system. To demonstrate this, we solved the LQR control problem: minimize  $[C(T)^T]_2 [C(T)]_2$  by controlling the temperature at the inlets. Using a reduce-then-control approach, we obtained a feedback functional gain shown in Figure D.1. It is well known that this gain can be used to identify good locations for locating temperature sensors. However, in this case it is also interesting to see that the gain captures information about the windows and the lights, even though they are not explicitly included in the convection-diffusion model. The fact that these sources affected the (frozen) velocity field is enough to affect the structure of the gains.

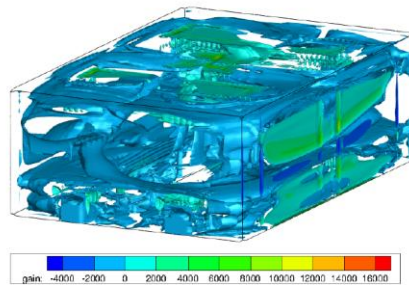


Figure D.19: Feedback functional gain.

## APPENDIX E: List of Scientific/Technical Publications Resulting From Project

Borggaard, J., Ahuja, S., Burns, J.A., Cliff, E.M. & Surana, A. “A Comparison of Model Reduction Approaches for Feedback Control Design of Thermal Flows in Buildings”, presented at 63<sup>rd</sup> Annual Meeting of APS Division of Fluid Dynamics, Long Beach, CA, Nov. 2010.

Burns, J.A. & Rautenberg, C. “Galerkin Type Algorithms for Optimal Sensor Placement”, in Proceedings of the 49<sup>th</sup> IEEE Conference on Decision and Control, Atlanta, GA, December 2010

Burns, J.A., Cliff, E.M., Rautenberg, C. & Zietsman, L. “Optimal Sensor Design for Estimation and Optimization of PDE Systems”, in Proceedings of the 2010 American Control Conference, Baltimore, MD, June 2010

“A Systems Approach to Increase DoD Building Energy Efficiency”, Poster Presentation at *Partners in Environmental Technology Technical Symposium & Workshop*, Nov. 30-Dec. 2, Washington DC, 2010.

Narayanan, S. “A Systems Approach to Achieving and Sustaining Energy Efficiency in DoD Facilities”, presented at *Partners in Environmental Technology Technical Symposium & Workshop*, Nov. 30-Dec. 2, Washington DC, 2010.

Ahuja, S. “Reduced-order Models for Control of Building Airflow”, Invited Presentation at *SIAM Conference on Applications of Dynamical Systems*, May 22-26, 2011, Snowbird, Utah

Eisenhower, B. “Uncertainty and Sensitivity Analysis In Building Energy Models”, Invited Presentation at *SIAM Conference on Applications of Dynamical Systems*, May 22-26, 2011, Snowbird, Utah

O'Neill, B. “Modeling and Calibration of Building Energy Models for a DoD Building”, Invited Presentation at *ASHRAE Energy Modeling Conference*, Apr. 5, 2011, Atlanta, GA

O'Neill, Z.D., Eisenhower, B., Yuan, S., Bailey, T., Narayanan, S. & Fonoberov, V. “Modeling and Calibration of Energy Models for a DoD Building”, in Proceedings of *ASHRAE 2011 Annual Meeting*, June 25-29, 2011, Montreal, Canada.

Ahuja, S., Surana, A. & Cliff, E.M. “Reduced-order Models for Control of Building Indoor Environment”, in *Proceedings of the 2011 American Control Conference*, San Francisco, CA, June 2011.

Eisenhower, B., O'Neill, Z.D., Fonoberov, V. & Mezić, I. “Uncertainty and Sensitivity Decomposition of Building Energy Models”, *Journal of Building Performance Simulation*, pp. 1-14, 2011

“A Systems Approach to Increase DoD Building Energy Efficiency”, Poster Presentation to be done at *Partners in Environmental Technology Technical Symposium & Workshop*, Nov. 30-Dec. 2, Washington DC, 2011.

Eisenhower, B., O'Neill, Z.D., Narayanan, S., Fonoberov, V. & Mezić, I. “A Methodology for Meta-Model Based Optimization in Building Energy Models”, *Energy and Buildings*, Vol. 47, pp. 292-301, 2012

Eisenhower, B., O'Neill, Z.D., Narayanan, S., Fonoberov, V. & Mezić, I. "Impact of High Performance Building Design on Uncertainty Propagation in Building Energy Models", in Proceedings of *Building Simulation 2011: 12<sup>th</sup> International Conference of the International Building Performance Simulation Association*, Nov. 11-16, 2011, Sydney, Australia.

Surana, A., Taylor, R., Narayanan, S. & Otto, K., "Rapid Assessment of Deep Retrofit System Solutions to Improve Energy Efficiency in DoD Installations and Buildings", to be presented at *2<sup>nd</sup> International High Performance Buildings Conference*, Purdue University, July 16-19, 2012.